Resource Allocation, User Association, and User Scheduling for OFDMA-based Cellular Networks

by

Shahida Jabeen

A thesis
presented to the University of Waterloo
in fulfillment of the
thesis requirement for the degree of
Doctor of Philosophy
in
Electrical and Computer Engineering

Waterloo, Ontario, Canada, 2019

Examining Committee Membership

The following served on the Examining Committee for this thesis. The decision of the Examining Committee is by majority vote.

External Examiner:	Chadi Assi Professor, Concordia Institute for Information Systems Engineering, Concordia University
Supervisor:	Pin-Han Ho Professor, Dept. of Electrical and Computer Engineering, University of Waterloo
Internal Member:	Amir Keyvan Khandani Professor, Dept. of Electrical and Computer Engineering, University of Waterloo
Internal Member:	Patrick Mitran Associate Professor, Dept. of Electrical and Computer Engineering, University of Waterloo
Internal-External Member:	Henry Wolkowicz Professor, Dept. of Combinatorics and Optimization, University of Waterloo

This thesis consists of material all of which I authored or co-authored: see Statement of Contributions included in the thesis. This is a true copy of the thesis, including any required final revisions, as accepted by my examiners.

I understand that my thesis may be made electronically available to the public.

Statement of Contribution

The contents presented in Chapter 3 were written in collaboration with Professor Catherine Rosenberg, while the contents in Chapter 6 were co-authored with a Post-Doctoral Fellow Syed Hassan Raza Naqvi. The rest of this thesis contains original content and was authored under the supervision of Professor Pin-Han Ho.

Abstract

Current advances in wireless communication are driven by an increased demand for more data and bandwidth, mainly due to the development of new mobile platforms and applications. Ever since then the network operators are overwhelmed by the rapid increase in mobile user subscriptions and the amount of average data volume per subscription, which is primarily fueled by more viewing of data-intensive content. Furthermore, according to the statistics, the ratio of downlink and uplink data traffic demands have changed drastically as they are observed to be significantly asymmetric even over small time periods.

In recent years, different solutions, based on topological and architectural innovations of the conventional cellular networks, have been proposed to address the issues related to the increasing data requirements and uplink/downlink traffic asymmetries. The most trivial solution is to scale the network capacity through network densification, i.e., by bringing the network nodes closer to each other through efficient spectrum sharing techniques. The resulting dense networks, also known as heterogeneous networks, can address the growing need for capacity, coverage, and uplink/downlink traffic flexibility in wireless networks by deploying numerous low power base stations overlaying the existing macro cellular coverage. However, there is a need to analyze the interplay of different network processes within these heterogeneous networks, which has not been studied in detail due to its complexity.

In the first part of this thesis, we analyze the performance of the most fundamental network process, i.e., the user scheduling process and understand its interplay with other network processes, which is more challenging in a heterogeneous network setting. Since, we need to propose a global optimization framework that allows us to obtain the throughput performance of a heterogeneous network when the network processes are optimized jointly. This is viable under a fixed network setting, where the parameters like the channel gains and the number of users are fixed and assumed to be known. Using this framework, we have been able to study different choices of resource allocation, which has allowed us to provide a number of important engineering insights on the throughput performance of different traffic scenarios and the resource allocation schemes.

The heterogeneous networks are often characterized by complex user dynamics and interference patterns, which are known to present difficulties in their design and performance

evaluation under conventional solution techniques, hence, it is expected that by centralizing some of the network processes common to many nodes, such as coordination between nodes, it will be easier to achieve significant performance gains. In the next part of this thesis, we centralize the control of the underlying network processes through Centralized Radio Access Networks (C-RAN), to meet the high data requirements as well as the asymmetric traffic demands in a centralized manner. We analyze both large-scale centralized solutions and the light-weight distributed solutions to obtain practical insights on how to design and operate future heterogeneous networks.

The last part of this thesis focuses on understanding the impact of front-haul infrastructure's capacity limitation on the underlying network processes. Most of the existing studies assume an ideal front-haul, however, in practice this assumption needs to be revisited as front-haul considerations are critical in C-RANs due to the economic considerations. In this study, we propose a framework for joint user scheduling under LAN cable based front-haul limitations, to show how this limitation has a fundamental impact on the user scheduling process. Using results from the joint framework, we show that simple heuristics can be used to obtain good throughput performance with relatively very low complexity/overhead.

Acknowledgements

I would like to thank everyone who made this thesis possible.

Dedication

I dedicate this thesis to my parents, Dr. Muhammad Hussain (Late) and Mrs. Tahira Nasreen (Late), my husband, Shahrukh Athar, and my daughter, Maryam Athar.

Table of Contents

List of Tables

List of Figures

Abbreviations

2G Second Generation 3

3G Third Generation 3

4G Fourth Generation 3

5G Fifth Generation 4, 10

BB Baseband 110

BBU Baseband Unit 10, 54

BS Base Station 5, 21

C-RAN Centralized-Radio Access Network 5, 10, 53, 54

CCD Co-channel Deployment 7, 20, 77

CSI Channel State Information 17, 23

CUD Coupled Uplink and Downlink 8

DAU Distributed Antenna Unit 15, 107

DL Downlink 6

DUD Decoupled Uplink and Downlink 8, 19

EVM Error Vector Magnitude 119

FD Full Duplex 14, 20

FDD Frequency Division Duplexing 27, 58, 62, 77

FEXT Far-end Crosstalk 110

GM Geometric Mean 30

GP Geometric Programming 23, 34, 108, 121, 123, 148

HetNet Heterogeneous Cellular Network 5

ICI Inter-cell Interference 7, 17, 23

IoT Internet-Of-Things 1, 6, 77

LAN Local Area Network 15, 107

LoC LTE over Cable 107

LTE Long Term Evolution 18, 107

LTE-NR Long Term Evolution New Radio Access Technology 4

MBS Macro Base Station 5, 18

MCS Modulation and Coding Schemes 18, 21, 22, 70

MIMO Multiple Input Multiple Output 4, 17, 106

MINLP Mixed Integer Non-Linear Programming 79, 88, 108

MU-MIMO Multi-user MIMO 4, 106

NR New Radio 107

OD Orthogonal Deployment 7, 20

OFDM Orthogonal Frequency-Division Multiplexing 7

OFDMA Orthogonal Frequency-Division Multiple Access 7

PBS Pico Base Station 5

PF Proportional Fairness 16, 29

PRB Physical Resource Block 9

PSD Partially Shared Deployment 7, 20

RAN Radio Access Networks 3, 4

RAT Radio Access technology 5, 143

RATs Radio Access technologies 10

RF Radio Frequency 107, 110

RRM Radio Resource Management 5, 106

RRU Remote Radio Unit 10, 54

SC Small Cell 5, 18, 106, 107, 112

SINR Signal-to-Noise-Ratio 22, 25

SRS Sounding Reference Symbol 63

TDD Time Division Duplexing 27, 58, 62, 77

UE User Equipment 24

UL Uplink 6

Wi-Fi Wireless Fidelity 4

Chapter 1

Introduction

1.1 Overview

Cellular network providers have been experiencing tremendous growth in data traffic demands since the last decade. According to the statistics reported by Ericsson [1], the demand for more data has been increasing rapidly since 2012, driven by the development of new mobile communication platforms, such as, android phones and tablets. Ever since then the network operators are overwhelmed by the rapid increase in smartphone subscriptions and the amount of average data volume per subscription, which is primarily fueled by more viewing of video content. As a consequence, a huge amount of Internet traffic is originated or terminated at one of these communication devices. It has been noted that the uplink data traffic is increasing drastically along with the overall traffic demand. Perhaps the reason behind this expeditious increase in uplink traffic is the emergence of new mobile applications and Internet usage scenarios, such as, the ones that have emerged with interactive gaming, social media, cloud storage, and, nonetheless, with Internet-Of-Things (IoT). It is expected that the ratio of uplink to downlink data will increase significantly in the next few years as reported by [1, 2]. The recent trends have been shown in Fig. 1.1, which demonstrates the total global monthly data and voice traffic from 2012 to 2017, along with the year-on-year percentage change for mobile data traffic.

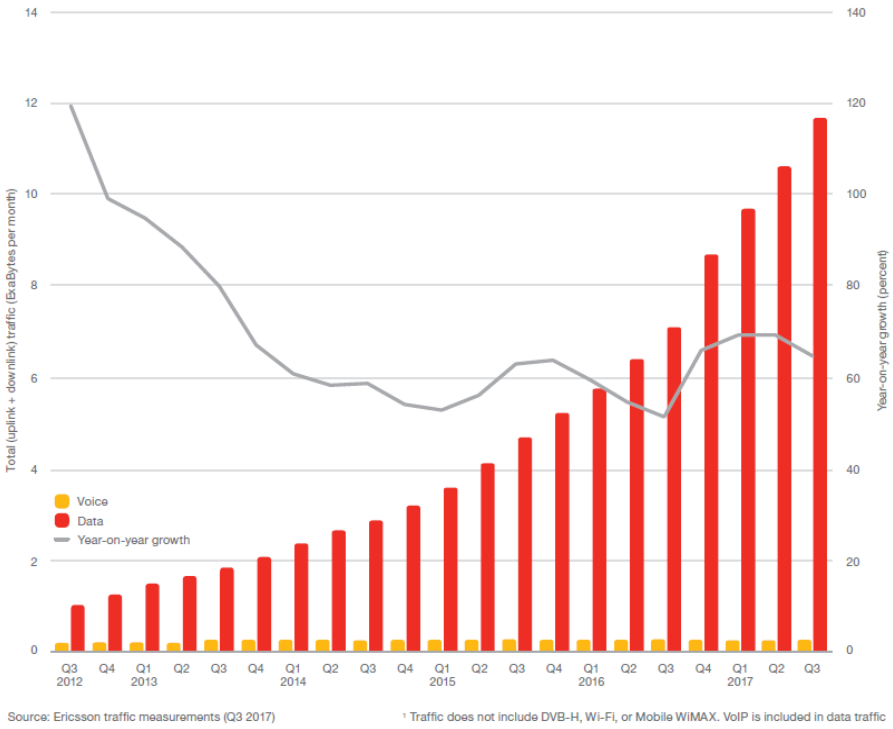

Figure 1.1: Total (uplink+downlink) traffic per month[1].

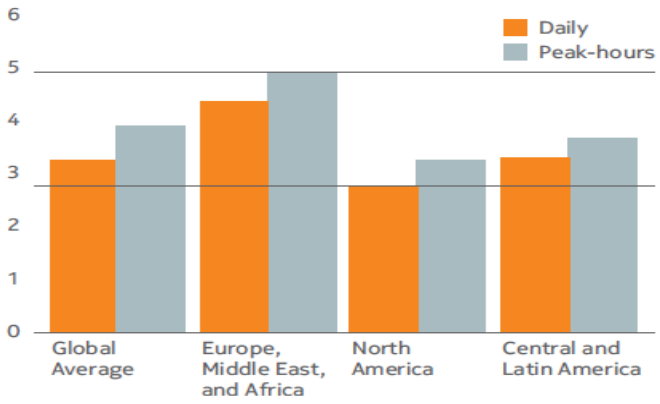

Figure 1.2: Downlink to uplink usage ratios [3].

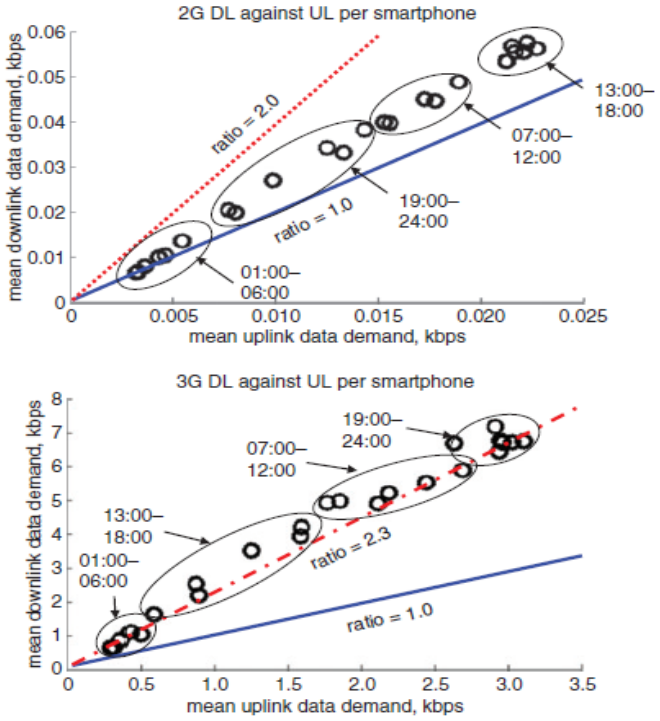

Figure 1.3: Smartphone usage over 2G and 3G RANs: plot of downlink against uplink data demand for different times of the day [4].

According to the statistics reported by Nokia Solutions and Networks, given in Fig. 1.2, the actual uplink to downlink ratio in North America was 1:2.37 in 2013, which means the downlink traffic was 70% of the total. This shows that globally, with given traffic usage, the uplink to downlink ratio was 1:3.29; which is fairly asymmetric. In addition, according to the statistics based on a few million smart phone users, which were reported by [4], the downlink and uplink data demands were observed to be significantly asymmetric over small time periods across different RANs. Note that the current data demand over 2G networks remains largely symmetric with strong temporal variations, whereas the demand over 3G or Fourth Generation (4G) is asymmetric with surprisingly weak temporal variations as shown in Fig. 1.3.

In recent years, different solutions, based on topological and architectural innovations of the current cellular networks, have been proposed to address the issues related to the increasing data requirements and asymmetries. Most of these solutions are designed for LTE based cellular networks while recognizing that the Fifth Generation (5G) cellular networks will aggregate other RANs, for example, Wireless Fidelity (Wi-Fi) and Long Term Evolution New Radio Access Technology (LTE-NR). In a broader sense, the current trends in LTE based wireless networks are:

1. To add more spectrum, which is indeed available due to some recent policy-level decisions, especially at higher frequencies (e.g., mmWave bands). The communication technologies in these bands are promising, but are still far from mature, and are not expected to be mainstream any soon. In addition, the mmWave bands have a very short range that makes them impenetrable through building walls, nonetheless, they can not be used for access links, especially in urban areas where the cellular data usage is enormous.

2. To enhance the spectral efficiency of the currently available spectrum by using Multiple Input Multiple Output (MIMO) antennas or other related solutions which are based on enhanced physical layer techniques. Note that these MIMO antennas are used on a large scale (also known as "Massive MIMO"), to further enhance the spectral efficiency of the underlying cellular network, nonetheless, at the cost of distributed signal processing operations that require strict synchronization/alignment of the cellular users with the MIMO antennas. Further, Multi-user MIMO (MU-MIMO) have been proposed for wireless communication, which adds multiple access (multi-user) capabilities to MIMO by leveraging multiple users as spatially distributed transmission resources, at the cost of somewhat more expensive signal processing operations. In comparison, conventional, or single-user MIMO considers only local multiple antennas to serve each user.

3. To enhance the performance of the available spectrum through network densification, which has gathered much interest, both in industry [5], [6] as well as academia; where, the performance of the existing cellular network (also known as a homogeneous

network) is further enhanced by bringing the network nodes closer to each other with the help of different spectrum sharing strategies.

4. To centralize the control of the underlying RRM processes by using Centralized-Radio Access Networks (C-RANs). It is expected that by centralizing some of the functions common to many nodes, such as coordination between nodes, it will be easier to achieve significant performance gains. However, the challenges are numerous since centralizing some of the RRM functions will make them much more complex to solve.

The above mentioned trends have brought a paradigm shift in the way the Radio Resource Management (RRM) processes have been run in the past. For example, the network operators now want to deliver more with less, e.g., more network throughput and better Quality-of-Service with less energy for any of the underlying Radio Access technology (RAT). It is expected that network densification along with the centralized control of the underlying RRM processes will meet the future data traffic demands by bringing greater spatial reuse opportunities along with efficient spectrum sharing between different network nodes.

1.2 Heterogeneous Networks

The capacity of the homogeneous networks can be expanded by overlaying low power Base Stations (BSs) to complement the existing Macro Base Station (MBS) based infrastructure, *i.e.*, also called a *macro cell*. A Pico Base Station (PBS) is an example of these low power BSs and it differs from an MBS in terms of coverage size, transmit power, form-factor and the way the data back-hauling is performed. These low power BSs are simply referred as Small Cells (SCs), which can be connected to the MBSs via wired back-haul or wireless front-haul links. The deployment of these SCs can effectively reduce the traffic load on the MBSs, also termed as *macro-offloading*. Typically, an operator will place SCs at strategic points to improve the performance of users, i.e., at cell-edge and/or within a hotspot, while keeping the cost of infrastructure as low as possible. This network, also known as a Heterogeneous Cellular Network (HetNet), improves the spectral efficiency and the cell-edge coverage of the existing homogeneous network.

The paradigm shift in the amount and ratio of uplink and downlink traffic has brought a plethora of new technological and operational challenges, which require fundamental changes in different network processes, such as, resource allocation, user association, user scheduling, and interference management. Most of the research so far on RRM has focused on the downlink, the uplink has received considerably less attention than the downlink because it was felt that the traffic was mostly to rather than from the devices, and because of the fact that the downlink is much easier to study.

With the emergence of the IoT and with the realization that users are creating and uploading more of their own content from wireless devices, the uplink is becoming more important. Nonetheless, addressing the research problems on the uplink are complicated but critical, which is the main reason why the existing HetNet based solutions are designed to optimize the performance of downlink traffic only. Given the unprecedented growth in uplink data traffic, both Downlink (DL) and Uplink (UL) performance needs to be analyzed together and the associated network processes that are designed for the downlink traffic only needs to be revisited for the uplink traffic. This is necessary, because, for instance if a user association rule is based on the DL performance only then it might not be optimal for the UL and the same can be said about resource allocation.

To the best of our knowledge, no study has been done so far to investigate different network processes for both UL and DL using a similar framework. In effect, the standpoint of the UL has been neglected, perhaps due to the complex interplay of these network processes on the UL. We need to analyze them from the UL's perspective before deciding what to do, *i.e.*, 1) we do nothing (if the *DL-centric* processes are good enough for the UL), 2) we can use *UL-centric* processes (if they are good enough for the DL), 3) we can propose processes that jointly optimize the performance on the DL and the UL, or 4) we can use different processes for the uplink and downlink traffic. From an engineering point of view, it is highly desirable to study these processes for both DL and UL under a given framework. The ability to model them using a similar framework would enable us to perform a comparative study of different deployment choices in a HetNet.

Next, we describe these network processes one-by-one to develop an understanding of the underlying challenges.

1.2.1 Resource Allocation (RA)

Resource allocation process is responsible for allocating different resources to different BSs in a HetNet. The communication band in Orthogonal Frequency-Division Multiplexing (OFDM) based HetNets is divided into a set of Orthogonal Frequency-Division Multiple Access (OFDMA) sub-channels that are equally spaced in frequency, where OFDMA adds multiple access capabilities to OFDM. The set of sub-channels allocated to a BS can be (fully or partially or non) overlapping with the subsets allocated to other BSs (also known as Co-channel Deployment (CCD), Partially Shared Deployment (PSD), and Orthogonal Deployment (OD), respectively). In TDD-based HetNets, at a given time the communication channel can either be allocated to the UL or the DL. Therefore, the fraction of the time the channel is allocated to the UL or the DL can be considered as another resource that can be allocated to each BS in a HetNet. Once the resources are allocated to all BSs, they can schedule their users independently. Typically, the changes in the RA parameters are rare, therefore, it is a slowly varying process.

Resource allocation within a macro cell, in the presence of SCs, yields numerous technical challenges, notably due to the presence of intra-cell interference. Over the last few years, multiple resource allocation schemes, such as CCD, OD, and PSD, have been proposed for limiting the intra-cell as well as the Inter-cell Interference (ICI) on the DL of a HetNet. In these schemes, the resources were allocated by choosing RA parameters based on the downlink traffic only. An optimal choice of these parameters would yield optimal performance on the DL, but the performance might not be optimal for the UL. It is therefore necessary to tune these RA parameters to achieve acceptable (if not optimal) performance on the uplink along with the downlink, however, achieving acceptable performance on the uplink is not trivial. In fact, it would be interesting to answer the key questions, which have not been answered yet, such as: *What would be an optimal resource allocation scheme on the uplink? What is the impact of DL-centric resource allocation schemes on the uplink performance? What is the impact of UL-centric resource allocation schemes on the downlink performance?.*

The RA process in a macro cell along with the underlying scheduler is simplified under static FDD or TDD based spectrum sharing techniques. Mainly because, the interfering macro cells are synchronized, the RA/US process can be decoupled into an UL-only and DL-only process. Nonetheless, such a strategy deals with either UL-only or DL-only traffic and cannot be extended for flexible HetNets, where the UL and DL resources are allocated jointly based on the prevailing traffic demands. Ideally, the RA should be employed in each macro cell by allocating the PRBs locally/independently when the ratio of UL to DL traffic is varying significantly from one cell to the other. However, this is possible only if the interference from other cells could be measured exactly. In the case that the inter-cell interference cannot be measured exactly, the performance of a local RA scheme could be far from the optimal one, consequently, the flexible spectrum sharing techniques could not be employed locally and independently in a multi-cell network.

1.2.2 User Association (UA)

Given a resource allocation scheme, a user association process defines a set of rules for assigning a user, upon its arrival or at a re-association event, to one or multiple BSs. A good user association rule should take into account both uplink and downlink performance. Many DL-centric UA rules for HetNets have been proposed in the literature that perform better than the UA rules that were designed for homogeneous networks. However, given some inherent differences between the uplink and the downlink traffic flows, it is not clear whether these DL-centric UA rules will perform well on the uplink. Therefore, it is necessary to propose UL-centric UA rules and compare their performance with the existing DL-centric UA rules. In this context, the key research questions are: *What are the performance gains on the uplink (if any) in using UL-centric rules over DL-centric rules?*. We can develop UA rules in which a user can associate differently on the uplink and on the downlink, these are called Decoupled Uplink and Downlink (DUD) UA rules, but we need to answer the following: *What are the performance gains (if any) in using DUD UA rules over the Coupled Uplink and Downlink (CUD) ones?*.

1.2.3 User Scheduling (US)

User scheduling process (within each BS) is responsible for allocating Physical Resource Blocks (PRBs)[1] to the associated users when the RA scheme and the set of UAs are known and fixed. The US process is also responsible for allocating power to the PRBs. Typically, the power budget of a BS (i.e., on the DL) is considerably larger than that of a user (i.e, on the uplink), therefore, the US process on the downlink can be simplified by spreading the BS power equally among all sub-channels and then allocating all sub-channels to a user for the duration of one or more sub-frames, this type of US is called *time-based* US. Due to power limitations, this type of US cannot be used on the uplink. Hence, either a subset of sub-channels (instead of all sub-channels of a BS) are allocated to a user (i.e., *channel-based* US) or a subset of PRBs are allocated to a user (i.e, *PRB-based* US) for the duration of a frame.

The user scheduling process on the uplink depends on the interference which is coming from the users scheduled by other BSs. Since, these users are distributed randomly, the uplink interference at a BS may vary significantly from one sub-channel to another (if US is time-based) or from one PRB to another (for PRB-based US). Nonetheless, the uplink interference cannot be computed exactly unless the user scheduling process (within a BS) knows the global information of the users that are associated with other BSs and also their exact schedules. It is important to realize that this global information cannot be provided to the user scheduling process beforehand because of a loop: the user schedules depend on uplink interference, which in turn depends on user schedules from other BSs.

The user scheduling process can be made *local*[2] on the downlink because interference estimation can be made exact as the interferers are the other BSs transmitting on the same sub-channels. This estimation can be simplified if all BSs distribute power equally among the sub-channels allocated to them at all times[3]. In contrast, the user scheduling process on the uplink cannot be made local (to each BS) because interference depends on both the transmit power and the channel gains from users scheduled by other BSs. As a result, the

[1]For time synchronization, data is transmitted through frames that are equally spaced in time and each frame contain multiple sub-frames, where each PRB corresponds to one sub-channel for one sub-frame.

[2]We use the word "local" for user scheduling within a BS.

[3]Note that the location and channel gains from each BS can be known beforehand.

optimal user scheduling problem on the uplink is a complex problem and we refer to it as a *global user scheduling problem*[4].

1.2.4 Complex Interplay of Network Processes

The interplay of network processes on the uplink is more complex than on the downlink. The resource allocation process is responsible for sharing resources among the BSs, while the user scheduling process (in each BS) is responsible for the sharing of BS resources among the users associated with that BS, hence, it is linked to the user association process. User association is about selecting a BS for a user that will deliver good performance, where performance is a function of user scheduling. The user scheduling process is the basic building block of a cellular network on which all other network processes are built, but it is highly dependent on uplink interference. This is the reason why the interplay of these network processes has only been studied from a DL-centric perspective. The resource allocation, user association and user scheduling schemes that have been designed for the downlink might be very inefficient for the uplink. Also, we need to consider the trade-offs by finding user associations that are acceptable on both uplink and downlink, in addition to the schemes that allow devices to associate differently. In the same way, the resource allocation process needs to be revisited.

1.2.5 HetNets under C-RAN Deployment

The emerging 5G cellular networks will integrate different Radio Access technologies (RATs) by deploying a large number of C-RANs to satisfy the diversified bandwidth and latency requirements. Unlike the existing HetNets, where each node (e.g., Macro/Pico BS, Relay, etc.) performs baseband processing at the local cell site, a C-RAN aims to free radio access units from baseband processing. Essentially, a C-RAN consists of three fundamental components: (i) the distributed Remote Radio Units (RRUs) at the cell site, (ii) the centralized Baseband Unit (BBU) pool, and (iii) the high-bandwidth low-latency front-haul links to connect RRUs and the BBU pool.

[4]We use the word "global" for user scheduling within a multi-cell system.

Although, C-RAN appears to be nothing more than the centralization of BBUs, centralization is a prerequisite for many technologies that are difficult to implement in traditional architectures; especially joint processing and cooperative communication, which is viable in a C-RAN context only. The centralized baseband processing/scheduling in the BBUs allows for dynamic cell re-configuration. In addition, the co-located BBUs can be utilized to perform complex coordinated tasks for enhancing the performance of the aforementioned network processes. Moreover, the lightweight RRUs yield easier deployment of different types of cells, while reducing the energy consumption of each site; they can cooperate flexibly and seamlessly to improve the spectral efficiency and the capacity of the underlying radio network. In addition, C-RAN enables all user-related signal processing tasks, such as the ones required for MIMO antennas, to be carried out at a central unit with greater computational power than conventional processors. This is particularly important in terms of resource management, as C-RAN can jointly manage the radio resources via the front-hauls yielding a potentially high performance gain.

However, the challenges come along with the advantages: full-scale coordination leads to high computational overhead in the BBU pool especially for large-scale networks; real-time user scheduling, resource allocation for flexible HetNets, and high-bandwidth front-haul links are important to achieve the reliable connection and mapping between the BBU and the RRUs. Note that a C-RAN only focuses on the radio link interfaces and cannot solve the problems emerging in the core network or the higher layer protocols.

1.3 Contributions

In this thesis, we will focus on both downlink and uplink, and will study the HetNet from a throughput performance point of view. Our contributions can be summarized as follows. A more detailed summary of contributions are presented in the beginning of each chapter.

1.3.1 User Scheduling in a Multi-Cell Network

As discussed earlier, there is a need to formulate a global user scheduling problem that allows us to study and compare different US schemes for both uplink and downlink transmissions under the same framework. Such a framework should allow us to find a globally optimal US solution that can reduce cross-cell interference and maximize the spectral efficiency of a multi-cell network. Note that finding the globally optimal solution is highly challenging, but necessary to benchmark and gain insights on how to design good online schedulers for both UL and DL.

Our main contributions in this context can be summarized as follows:

1. We formulate a joint US problem for a multi-cell network that is intractable because of the large number of binary and continuous variables. We are interested in solving this problem to deal with the ICI exactly and also to compute an offline benchmark. We transform this problem into a tractable upper bound US problem, which is obtained by using the continuous rate function and removing all integer variables by a smart transformation. Nonetheless, the resulting problem is non-linear and non-convex in nature and solving such problems is NP-hard.

2. We convexify the upper bound problem and show that its optimal solution can be mapped to a feasible solution of the joint optimal problem with a small gap, *i.e.*, verified via extensive simulations.

3. Using the above framework, we design local user schedulers and find that their performance is far from the optimal. Indeed, the interference coordination is the key in finding optimal schedules within each macro cell.

1.3.2 User Scheduling and RRU Association under C-RAN Deployment

In this thesis, we investigate a joint US and UA process for OFDMA based radio networks under the C-RAN setting. Since the RRUs are in co-channel for accessing the underlying radio spectrum, the exact interference estimation/measurement on both UL and the DL is critical to the US and UA processes that critically determine the overall network throughput. Note that the exact interference can only be computed based on the full knowledge of the cross channel gains, power allocations, and channel allocations for all the users associated with other RRUs. Such dynamic system states can only be obtained via *inter-BBU coordination* under the C-RAN architecture; where, all BBUs are physically co-located and can share dynamic states with each other in real time. Our main goal is to study the joint US and UA process while considering full inter-BBU coordination in order to find the maximum performance gains that could be achieved under the considered network setting.

Our main contributions in this context are summarized as follows:

1. We provide a complete formulation for the joint US and UA problem where inter-BBU interference coordination is considered. This problem is intractable in its exact form, because it deals with very large number of binary and continuous optimization variables. Hence, we introduce an upper bound problem that can yield reasonable upper bound solutions for the original joint problem. The upper bound problem is further convexified and the corresponding optimal solutions are mapped to the feasible solution space of the original joint problem using a simple method.

2. We further develop heuristic based algorithms to obtain efficient solutions for the joint US and UA problem, on both UL and DL, via a divide-and-conquer approach. The numerical simulations demonstrate that the proposed heuristic based algorithms yield quasi-optimal solutions for the original joint US and UA problems under different network settings.

1.3.3 Resource Allocation for Flexible HetNets

As discussed earlier, the emergence of flexible FDD/TDD and in-band Full Duplex (FD) communications has complicated the RA process, mainly due to the complex UL-to-DL and DL-to-UL interference scenarios. Although, the performance gains of different RA schemes have been studied extensively for DL of a static FDD/TDD based network, they need to be revisited for flexible FDD/TDD; where, the UL performance is significantly vulnerable due to the strong DL-to-UL interference scenarios. In this thesis, we investigate the optimal RA performance for flexible FDD based multi-cell multi-tier networks as finding optimal performance is necessary to benchmark the performance of existing RA schemes, but not trivial due to the high complexity of solving a joint RA and US problem; mostly due to the fact that the formulated joint RA problem considers all types of interferences, including (i) *inter-cell inter-link interference* and (ii) *intra-cell inter-link interference*. Note that we do not consider *self-interference* which exists in a FD network.

Our main contributions in this context are summarized as follows:

1. We formulate a joint RA and US problem for a multi-tier network that allocates proportionally fair user schedules by considering both UL and DL transmissions. Solving this problem was challenging, but we converted it into a tractable problem which can be solved efficiently, where the tractable problem is used to obtain benchmark solutions to analyze the usefulness of different RA schemes for flexible FDD/TDD based HetNets.

2. We demonstrate the efficacy of Reverse-FDD and Static-FDD based spectrum sharing techniques through extensive network simulations with different UL and DL traffic scenarios.

1.3.4 Cable based Front-hauls for C-RANs

We introduce a novel distributed antenna access architecture for achieving a cost-effective solution of 5G indoor service provisioning. The proposed architecture takes advantage of multi-pair Local Area Network (LAN) cables to support simultaneous transmission of multiple baseband and intermediate frequency (IF) signals between the RRU and each Distributed Antenna Unit (DAU), so as to meet the massive antenna requirements and overcome the non-line-of-sight nature of the indoor environment with extremely low cost.

Our main contributions in this context are summarized as follows:

1. We propose a joint optimization framework for mapping 5G signals from each DAU to the LAN cable, this is also referred to as Multi-pair Air-to-Cable (MP-A2C) mapping problem. Based on the given DAU architecture, we introduce an optimal MP-A2C scheduler for mapping the antenna signals on the sub-channels of a multi-pair cable (*i.e.*, CAT-5 cable).

2. We transform the MP-A2C optimization problem into a tractable problem, which can be solved efficiently for evaluating the performance of any MP-A2C scheduler, and propose heuristic-based schedulers for solving the MP-A2C problem in real-time.

Thesis Organization:

The rest of the thesis is organized as follows. Chapter 2 presents a summary of the related work. In Chapter 3, we present the optimization model for a multi-cell network that allows us to characterize the optimal network performance when the user schedules are jointly optimized across multiple cells. We use this model to compare the performance of local user scheduling schemes for both UL and DL transmissions. In Chapter 4, we study the joint UA and UA problem in the context of a C-RAN and propose efficient heuristic based solutions that can be used in real-time. In Chapter 5, we use a similar framework to investigate the performance of existing RA schemes for flexible HetNet deployment. In Chapter 6, we focus on the wired front-haul deployment for C-RANs and present two different LTE-over-Cable architectures. Chapter 7 presents the summary and a list of some extensions of this thesis work.

Chapter 2

Literature Survey

In this chapter, we provide an overview of the relevant literature on user scheduling, resource allocation, and user association in cellular networks. In addition to providing a context to our research, we present our view on the limitations of the existing work, and how we approach to address them in this thesis.

2.1 User Scheduling

2.1.1 Single-cell vs Multi-cell Analysis

User scheduling in a single-cell network is a well-studied problem, on both uplink and downlink, and numerous scheduling policies have been proposed so far in this context. The notion of fairness has also been used to maximize the throughput of the worst user, *i.e.*, dedicating more resources to them, by using different utility maximization problems; where, the utility is a function of user data rates that ensure more fairness. For instance, to provide Proportional Fairness (PF), the logarithm of the user data rates has been used as a utility function, in [7, 8], which can be used to achieve PF among the users. Nonetheless, PF cannot be achieved without considering a global user scheduling problem encompassing the users of the entire network, which may have more than one macro cells operating over the given spectrum (also called *multi-cell networks*).

The uplink US process in a multi-cell network is fundamentally different and much more complex than the DL one, mainly because the UL interference strongly depends on the US decisions of the neighboring cells, while the DL interference does not necessarily depends on US. Note that the interference on the DL is created by the BSs whose positions are known and they transmit all the time, hence, the interference can be computed exactly under fixed transmit power assumptions, as discussed in [9–11]; however, these assumptions significantly limit the potential performance gains. In contrast, the interference on the UL is created by users whose transmissions may vary from time to time, therefore, the UL interference cannot be computed exactly beforehand. This is the reason why most of the existing US schemes, mainly on the UL [12–15] are based on a single-cell analysis with (or without) an estimate of ICI.

To the best of our knowledge, only a very few studies consider exact ICI, for example, the authors in [16] propose an algorithm for predicting ICI along with an UL scheduler; where, the schedules are computed by exchanging US information between different BSs while considering perfect Channel State Information (CSI). A joint interference avoidance and US scheme has been proposed in [17] that does not require BS-coordination, but uses probabilistic analysis over the received interference levels. A coordinated UL scheduling problem has been presented in [18], where the joint US problem across multiple-cells has been decoupled into multiple local US and power allocation problems (*i.e.*, one per macro cell) that are not globally optimal. Similarly, a heuristic based uplink US solution has been proposed in [19] that also does not guarantee global optimality.

The benefits of BS-coordination across a multi-cell network have been examined in [20] for interference mitigation. The proposed scheme optimizes the user schedule, transmit and receive beamforming vectors (*i.e.*, required for MIMO), and transmit power jointly, while taking into consideration both the inter-cell and intra-cell interferences, and the fairness among the users. System-level simulation results have been shown in [20], which demonstrate that BS-coordination can significantly improve the overall network throughput as compared to the conventional network design with fixed transmit power and no BS-coordination. However, these user scheduling schemes with ICI considerations, either rely on perfect BS-coordination and/or heuristics on ICI for computing the schedules that need to be validated under a realistic multi-cell network scenario.

2.1.2 User Scheduling with Discrete Rates

Due to high variations in channel gains, scheduling in Long Term Evolution (LTE) is performed along with an underlying mechanism, which dynamically adjusts the rate while maintaining the transmit power at a constant level, to compensate for channel variations, *i.e.*, called *rate adaptation*. Scheduling with rate adaptation is suitable for packet-data traffic where a fixed rate is not required as long as the (long-term) average rate is above a certain threshold [21]. The existing user scheduling schemes, such as, [12–20], make use of the classical Shannon's capacity (or some formula derived from it) to model the rate adaption process in LTE. However, in practical LTE networks, only a discrete set of rates are achievable due to a fixed number of Modulation and Coding Schemess (MCSs). The aforementioned user scheduling algorithms, which indeed use a set of discrete MCSs, have mainly focused on the downlink, e.g., [9, 10], while a very few studies have taken up the uplink US problem, such as, [11]. In this thesis, we assume that the LTE network under consideration uses an adaptive MCS with discrete rates, such as the ones give in [22–24]. Note that using a discrete set of MCSs will significantly change (as well as complicate) the design of the UL and DL US schemes.

2.2 User Association

User Association is a well-studied problem on the downlink of a HetNet, where different UA rules have been proposed in the literature. For a given RA scheme, the problem of user association arises whenever a user can connect to more than one BS (i.e., when there is an overlapping coverage). In homogeneous networks, UA is not as critical as in HetNets, since, it is typically based on maximum signal-to-interference and noise ratio (SINR) rule; where a user upon arrival associates with the BS who offers the highest downlink SINR. In HetNets, the problem of UA is more complicated due to the inherent differences between the MBS and the SCs. Therefore, new UA rules have been envisaged to split the users between the MBS and SCs more efficiently and fairly. One example of such downlink-based UA rules is cell range expansion (CRE), in which a user at the time of association adds a positive biasing parameter to the SINR from the SCs and, as long as the *biased SINR* value

is greater than the actual SINR from the MBS, it keeps associated with the SC. With CRE, the SC's downlink coverage area is virtually expanded and hence more users are off-loaded from the MBS to the SCs. Another similar downlink-based UA rule introduced in [9] is the small-cell first (SCF) rule. Under SCF, the users are offloaded to the SCs as long as the received downlink SINR from the SC is greater than a pre-determined threshold, which needs to be configured precisely for the underlying RA scheme and user traffic. Another simple UA rule, proposed in [25], is range extension (RE), where a user associates with the BS with the lowest path-loss.

The aforementioned UA rules mainly rely on the physical-layer measurements from the user and can be easily implemented without any computational complexity. However, these rules have been proposed by considering the performance on the downlink only and might result in a very sub-optimal performance on the uplink. A good user association rule should take into account the performance on both uplink and downlink. Given the inherent differences between the uplink and the downlink, it is not clear whether these DL-centric UA rules for HetNets will perform well on the uplink. If the DL-centric rules do not perform well on the uplink, then either new UA rules incorporating fairness among the downlink and the uplink users should be proposed or new devices should be introduced in which a user can associate differently on the uplink than on the downlink (DUD UA rules).

We classify the relevant literature on UA into two groups: Coupled UA rules (CUD) and decoupled UA rules (DUD). In [26], the authors study a joint uplink and downlink coupled UA problem, using a single-cell analysis that maximizes the total energy efficiency of the network. The formulated problem is non-convex, hence they propose a heuristic-based algorithm, without considering any optimal scheme, which associates the users in an energy-efficient way. In [27], the authors propose a UA framework for backhaul-limited HetNets, showing how different backhaul topologies and capacity limitations affect the performance of coupled user associations. The authors in [28] present a decoupled UA rule, where the downlink association is based on the downlink received power, while the uplink association is based on the minimum pathloss rule. The authors of [29, 30] study the capacity and throughput gains brought by decoupled UA using stochastic geometry. None of these studies consider a multi-cell network with exact inter-cell interference, hence,

these solutions might not reflect the actual performance gains. In this thesis, we study the network-wide optimal UA rules in a multi-cell network with exact interference on both uplink and downlink.

2.3 Resource Allocation

Resource allocation is a well-studied problem on the downlink of a heterogeneous cellular network. Resource allocation (on both uplink and downlink), in the presence of SCs, yields numerous technical challenges, notably due to the presence of intra-cell interference. Over the last few years, multiple resource allocation schemes for the downlink, such as CCD, OD, and PSD, have been proposed for limiting the interference on the downlink.

In the aforementioned RA schemes, the resources are allocated by choosing parameters based on downlink performance. An optimal choice of these parameters would yield optimal downlink performance, but they may or may not be optimal for the uplink. It is therefore necessary to tune these parameters to achieve acceptable (if not optimal) performance on the uplink along with the downlink; however, achieving acceptable performance on the uplink is not trivial. To quantify the performance of different resource allocation schemes for HetNets, we need to consider the performance on the uplink along with the downlink. To the best of our knowledge, a comprehensive model for comparative assessment of the resource allocation schemes, for both uplink and downlink, with the joint consideration of other important network processes (including user association and user scheduling) is missing in the literature.

Further, as discussed earlier, the emergence of flexible FDD/TDD and in-band FD communication has complicated the RA process, mainly due to the complex UL-to-DL and DL-to-UL interference scenarios. Although, the performance gains of different RA schemes have been studied extensively for DL of a static FDD/TDD based network, they need to be revisited for flexible FDD/TDD; where, the UL performance is significantly vulnerable due to the strong DL-to-UL interference scenarios.

Chapter 3

User Scheduling in a Multi-Cell Network

3.1 Introduction

In Chapter 1, we presented a number of important network processes, namely resource allocation, user association, and user scheduling, which need to be optimized properly as they greatly impact the throughput performance of the underlying cellular network. We also discussed that these network processes have a complex interplay, especially on the UL, that has not been clearly analyzed before in a multi-cell context.

Our Objective:

In this chapter[1], we investigate the most fundamental network process, *i.e.*, the user scheduling process, which critically schedule the users that are associated with each BS in the network. We attempt at solving the global user scheduling problem for both UL and DL transmissions in order to find the optimal performance under a given set of MCSs with exact power allocations, channel gains, and intra/inter cell interference. We consider

[1]Some of the results in this chapter were published in [31] and [32].

a joint optimization framework with full inter-BS coordination, which is used for computing benchmark solutions to compare the throughput gains that are achievable under the considered local US scenarios for both UL and DL. Our main goals for this chapter are listed as follows:

1. To formulate and solve a global user scheduling problem with full-coordination for both UL and DL, which can be used as an offline benchmark for multi-cell networks.
2. To characterize the performance of simple local user scheduling schemes for both UL and DL, that do not require any inter-BS coordination.
3. To compare the performance of the considered local user scheduling schemes on both UL and DL with their respective benchmarks, *i.e.*, the globally optimal schedules.

3.1.1 Need for a Global Optimization Framework

We discussed, in Chapter 2, that a global optimization framework is crucial for analyzing the user scheduling process for both UL and DL traffic under a multi-cell deployment scenario; where, we assume that all BSs are in co-channel for accessing the underlying radio spectrum. This framework is essential for comparing the performance of the *local* US processes, *i.e.*, one per BS. Note that the exact interference estimation/measurement on both UL and DL is critical for each local US process (within a BS) as it critically determines the local throughput of the users associated with that BS, which in turn impacts the overall throughput of the multi-cell network. However, we will explain it later that the exact interference can only be computed using a global optimization framework, which is based on the full knowledge of the cross channel gains, power allocations, and channel allocations for the users associated with all BSs in the entire network.

3.1.2 Existing User Scheduling Schemes

The global US problem in OFDMA networks with multiple macro/micro cells has not been studied extensively, primarily due to the difficulty in calculating the exact Signal-to-Noise-Ratio (SINR) and MCS. Note that computing the exact SINR and MCS is difficult as it

highly depends on the underlying association/scheduling decisions and the transmit power levels of the users scheduled by the neighboring BSs through the interference term in its denominator. In general, the exact interference cannot be computed by a local US process without inter-BS coordination. However, the DL interference could be measured precisely at the expense of some performance degradations when the power is equally spread over the underlying channel [9, 10]. On the other hand, the ICI on the UL is created by users from other cells whose transmissions vary with time, therefore, it cannot be computed exactly in advance.

To the best of our knowledge, only a few studies have taken into account the exact interference, SINR, and the MCS, such as, [9, 11, 22]. Most of the existing studies have bypassed the interference problem by resorting to a single-cell analysis [12–15], which can obviously deviate from the real scenario; they do not consider the exact MCS and ICI in the design of their schedulers, hence, their performance needs to be validated under a multi-cell scenario. In contrast, some of the studies do consider the exact interference in the design of their schedulers, for example, [16] introduced an algorithm for predicting UL interference at a local scheduler by assuming perfect CSI, where the schedules are computed locally by exchanging only the US information among adjacent BSs. Similarly, [17] introduced a local scheduler with interference avoidance via a probabilistic analysis.

A related work on joint UL scheduling has been presented in [18], where the global user scheduling problem has been decoupled into a local scheduling and power allocation problem that is unable to provide globally optimal schedules. Some heuristic based solutions have also been used for UL scheduling problem including opportunistic approaches, such as the ones discussed in [19]. A counterpart research work was given in [24], where a relaxed *signomial programming* problem was formulated by using a novel power-fractionizing mechanism. However, the relaxed problem has to be convexized via a series of tractable Geometric Programming (GP) problems that can converge to a local optimum, which not only takes excessive computation but also leaves some gaps from the true optimal. In addition, the aforementioned studies are different from our approach as they use the Shannon's capacity formula for computing data rates without considering any specific MCS for estimating the transmission rates rather then using the exact rate of the employed MCS.

The rest of this chapter is organized as follows: in Section 3.2, we discuss the user scheduling process in detail. Our system model has been described in Section 3.3, whereas the global optimization framework will be discussed in Section 3.4. The numerical results for the global problem are presented in Section 3.4.2. Section 3.5 is dedicated to the local user scheduling schemes and the corresponding results have been presented in Section 3.5.3.

3.2 User Scheduling with OFDMA

User scheduling (US) has been extensively studied under various RATs in the past decade for both UL and DL, which is a critical process for other network processes that are running on the top, for example, resource allocation and user association. In OFDMA based RATs, the US process is based on allocating OFDM symbols, which are equally spaced in time and frequency domains; where, different set of OFDM symbols can be grouped together to constitute a *sub-channel* in frequency-domain and a *time-slot* in time-domain. One sub-channel in a given time-slot is also known as a *physical resource block* (PRB), which is the smallest unit of resource that can be allocated to a user. Therefore, the US process or a user scheduler, no matter for UL or DL, is also responsible for allocating power and a physical-layer MCS on each PRB of a given *frame*, where each frame is composed of multiple PRBs.

3.2.1 Power and Channel Allocation

The user scheduling process is responsible for allocating power on each PRB of a given OFDM frame. Typically, the power budget of a BS (on the DL) is considerably larger than that of a user (on the UL); therefore, the user scheduling process on the DL could be simplified by spreading a BS's power equally among all PRBs and then allocating all sub-channels to a user for the duration of one or more time-slots, this type of US is called *time-based* US [9, 10]. Since the users (or User Equipments (UEs)) are limited in power, this type of user scheduling cannot be used on the UL, because the users should be allocated sub-channels in proportional with their channel gains. For instance, if the

received UL SINR of a user is significantly lower then allocating more sub-channels to that user would lead to zero rate. Instead, *channel-based* user scheduling is more realistic on the UL, for example, the one discussed in [11], where a subset of sub-channels (instead of all sub-channels of a BS) are allocated to a user. Likewise, a more flexible way of scheduling is to allocate a subset of PRBs to each user for the duration of a frame, which is called *PRB-based* US.

3.2.2 MCS Allocation

Due to high variation in the channel gains, scheduling in OFDMA is performed using an underlying mechanism, called *rate adaptation*, by which the data rate of each user is adjusted based on its exact SINR. Most of the existing US schemes [13–15, 24, 33–35] make use of the classical Shannon's theory for approximating the data rate of each user. However, such an approach does not directly translate into the discrete rates achievable by the given set of MCSs. Further, these US schemes do not consider the mapping of the data rates from the physical layer to the link layer, which is essential for computing the amount of useful data bits being transmitted and received over the duration of each frame, *i.e.*, also known as *Goodput*. Note that each MCS has a coding overhead that cannot be counted as useful data and it significantly varies from one MCS to another.

When assigning a PRB to a user, the scheduler has to decide on a MCS that would be used for physical layer transmission. The purpose of the scheduler is to assign precise coding rates so that it can maximize the goodput over each frame. Note that if the transmit power, number of sub-channels, and the MCS are not chosen properly, the receiver (*i.e.*, either a BS or a user) might not be able to decode and the PRB would be wasted. For computing a precise MCS for each PRB, the scheduler requires accurate estimates of SINR; whereas the SINR depends on the allocated power, channel gain, and the received interference on each PRB. It is important to realize that estimating SINR between a user and its serving BS on the UL is not as simple as on the DL. The interference on the DL is created by BSs whose positions are known and they transmit all the time, but the interference on the UL is created by users whose transmissions may vary from one frame to another, as they may or may not be transmitting over a given frame.

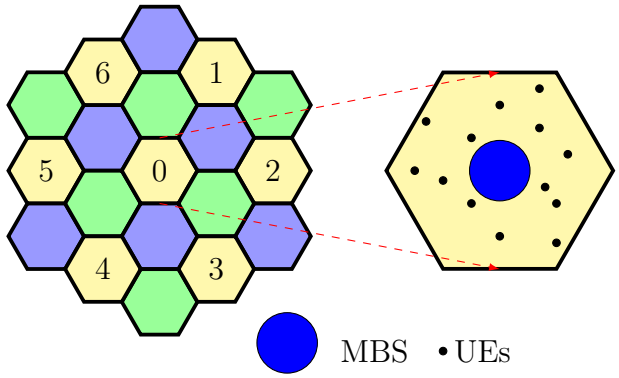

Figure 3.1: System-1: A multi-cell homogeneous system with omni-directional MBSs

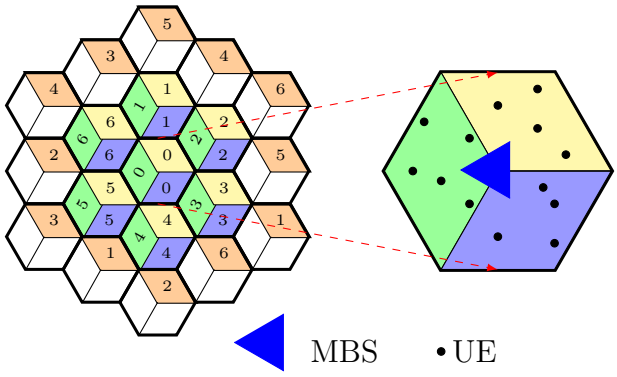

Figure 3.2: System-2: A multi-cell homogeneous system with tri-directional MBSs

In summary, for precise power allocation, sub-channel allocation, and MCS allocation, the user scheduling process needs to know the *global information* from all users that are associated with other BSs; mainly because, the local scheduler within a BS depends on interference which in turn depends on the local schedules generated by other BSs. The resulting problem indeed remains "global" and we will see later in this chapter that the global problem cannot be solved exactly by the local schedulers. Before formulating and solving this problem in detail, we first provide an overview of our system in the next section.

3.3 System Overview

We consider two different systems, i.e., *System-1* and *System-2* (as shown in Fig. 3.1 and Fig. 3.2), with each one of them operating on a set of cells denoted by $\mathscr{K}$. The yellow-coloured cells are using the same spectrum and are a part of the same system, while the adjacent cells that are operating on the same spectrum are coloured with orange. Note that in order to incorporate ICI for the edge cells, a wrap-around technique has been employed as recommended by 3GPP in [36]. The centrally placed MBSs, one per macro cell, are in co-channel with each other; where, each MBS is operating on a set of $\mathscr{C}$ sub-channels to serve a set of randomly distributed user equipments (UEs). To simplify our analysis, we assume that the MBSs and the users are equipped with single antenna each, although the proposed US problem can be extended to the case of multi-antenna MBSs.

Assumption 1: All users are equipped with omni-directional antennas with identical antenna gains and transmit power budget (P_{UE}). The MBSs in System-1 and System-2 have omni-directional and tri-directional antennas, respectively, with identical transmit power budget (P_{MBS}) and unlimited back-haul capacity.

3.3.1 Channel Model

We analyze the global US problem by using a *realization*-based approach [37]; where, the duration of each realization (ω) is considered to be the same as that of a frame, which corresponds to a set of sub-channels and a set of time-slots, denoted by $\mathscr{C}$ and $\mathscr{T}$, respectively. The realization-based approach is simple yet insightful as it can be used to solve a network utility maximization problem over a large number of snap-shots/realizations of the network: a realization ω is defined by a set of UEs who want to transmit or receive data during a frame[2]. For mathematical simplicity, we assume that during each realization the users are either transmitting on the UL or receiving on the DL. Consequently, each realization consists of either a set of UL users (denoted by $U_{UL}(\omega)$) or a set of DL users

[2]We assume that the MBSs are synchronized in terms of the UL and DL frames by using either Time Division Duplexing (TDD) or Frequency Division Duplexing (FDD)

(denoted by $U_{DL}(\omega)$)[3]. The corresponding set of channel gains between all MBS and UE pairs are denoted by $\{G_{u,k}(\omega)\}$ and $\{G_{k,d}(\omega)\}$, respectively. Note that each channel gain (either $G_{u,k}(\omega)$ or $G_{k,d}(\omega)$) depends on:

1. The location of the user resulting in a path-loss between the user and the MBS.
2. The large scale slow fading coefficient between the user and the MBS.

Assumption 2: We assume that the channel exhibits large-scale slow fading characteristics. The coherence time of the channel is greater than the duration of one frame, i.e., the channel gains remain constant within a realization and are equal on all PRBs of a frame, such that, $G_{u,k}(\omega) = G^{c,t}_{u,k}(\omega), \forall u \in U_{UL}(\omega), \forall k \in \mathscr{K}, \forall c \in \mathscr{C}, \forall t \in \mathscr{T}$. Similarly, $G_{k,d}(\omega) = G^{c,t}_{k,d}(\omega), \forall d \in U_{DL}(\omega), \forall k \in \mathscr{K}, \forall c \in \mathscr{C}, \forall t \in \mathscr{T}$

3.3.2 SINR and Link Layer Rates:

For each realization ω, the UL SINR (on PRB (c,t)) from user u to MBS k is defined as follows:

$$\gamma^{c,t}_{u,k}(\omega) := \frac{P^{c,t}_{u,k} \times G_{u,k}(\omega)}{N_0 + I^{c,t}_{u,k}(\omega)}, \quad \forall u, \forall k, \forall c, \forall t \tag{3.1}$$

Similarly, the DL SINR on PRB (c,t) from MBS k to user d is defined as follows:

$$\gamma^{c,t}_{k,d}(\omega) := \frac{P^{c,t}_{k,d} \times G_{k,d}(\omega)}{N_0 + I^{c,t}_{k,d}(\omega)}, \quad \forall k, \forall d, \forall c, \forall t \tag{3.2}$$

Here, $P^{c,t}_{u,k}$ and $P^{c,t}_{k,d}$ are the transmit powers used by MBS k for user u on the UL and user d the DL, respectively; $I^{c,t}_{u,k}$ is the UL interference for user u on PRB (c,t) as seen by MBS k, and $I^{c,t}_{k,d}$ is the DL interference on PRB (c,t) as seen by user d when receiving data from MBS k. Whereas, N_0 is the average noise power that is assumed to be flat across the underlying channel.

[3]Without loss of generality, the users that are transmitting on both UL and DL can be considered as two separate users.

The UL interference for user u, when it is transmitting to MBS k, is defined as follows:

$$I_{u,k}^{c,t} := \sum_{k' \in \mathscr{K}}^{k' \neq k} \sum_{u' \in U_{UL}(\omega)}^{u' \neq u} P_{u',k'}^{c,t} G_{u',k}(\omega), \forall u, \forall k, \forall c, \forall t \tag{3.3}$$

Similarly, the DL interference for user d, when it is receiving from MBS k, is defined as follows:

$$I_{k,d}^{c,t} := \sum_{k' \in \mathscr{K}}^{k' \neq k} \sum_{d' \in U_{DL}(\omega)}^{d' \neq d} P_{k',d'}^{c,t} G_{k',d}(\omega), \forall d, \forall k, \forall c, \forall t \tag{3.4}$$

We consider a piece-wise discrete function $f(.)$, which corresponds to a set of MCSs denoted by $\mathscr{M}$. This function uses a set of pre-defined SINR thresholds (i.e., $\{\beta_m\}$ with $1 \leq m \leq |\mathscr{M}|$) to compute the corresponding link layer coding efficiency (in bits per OFDM symbol) as follows:

$$f(\gamma) := \begin{cases} 0, & 0 \leq \gamma < \beta_1 \\ f(\beta_m), & \beta_m \leq \gamma < \beta_{m+1}, \quad 1 \leq m < |\mathscr{M}| - 1 \\ f(\beta_{max}), & \gamma \geq \beta_{|M|} = \beta_{max} \end{cases} \tag{3.5}$$

The corresponding data rate (in bits per second) on each PRB can be computed as follows by using the exact SINR (γ), $f(\gamma)$, the total number of OFDM symbols (N_S), and the duration of each time-slot (T):

$$Rate(\gamma) := f(\gamma) \times \frac{N_S}{T} \tag{3.6}$$

The SINR remains constant within a PRB, therefore, the rate remains constant across all OFDM symbols of a PRB.

3.4 The Global User Scheduling Problem

We formulate a global US problem for UL, which refers to jointly scheduling the users across the entire system for UL transmissions over the resources available to all BSs. Traditionally, the US problem amounts to finding a schedule for each user, with the goal of optimizing some fairness criterion, often captured by a network-utility function. To incorporate fairness, we use PF as our utility function and maximize the sum of the logarithm

(with base e) of the total link layer coding efficiencies for each user. Maximizing this objective is known to yield a proportional fair throughput allocation [8]. Note that a PF throughput allocation is known to maximize the Geometric Mean (GM) throughput and hence we will use the GM throughput as our performance metric.

We chose proportional fairness as a metric as it is known to strike a good trade-off between fairness and efficiency. We formulate this problem to understand its intractability, where we consider a PRB-based user scheduling problem. Note that a Channel-based US problem can be formulated as a special case of PRB-based US problem. A similar problem for the DL has been formulated in Appendix B.

Assuming that the cell associations (i.e., $z_{u,k}(\omega)$) are given for each realization, where a user can only associate with one cell/MBS, we define the following optimization variables for the global US problem:

- $\boldsymbol{x_{u,k}^{c,t,m}}$ is a binary variable for assigning discrete rates; it is equal to 1 if user u is allocated MCS m by the MBS k on PRB (c,t) and 0 otherwise.
- $\boldsymbol{P_{u,k}^{c,t}}$ is for allocating UL power on PRB (c,t).
- $\boldsymbol{I_{u,k}^{c,t}}$ is for computing UL interference on PRB (c,t) at MBS k for user u.
- $\boldsymbol{\lambda_{u,k}}$ is the total coding rate seen by user u from MBS k

Given a set of macro cells $\mathscr{K}$, a set of sub-channels $\mathscr{C}$, a set of sub-frames $\mathscr{T}$, a network realization ω, a set of user associations $(\{z_{u,k}(\omega)\}_{u\in U_{UL}(\omega),k\in\mathscr{K}})$, and a set of pre-defined SINR thresholds (i.e., $\{\beta_m\}_{m\in\mathscr{M}}$), we define the global US problem as follows:

$$\boldsymbol{P^{UL}_{Global}(\omega)}: \underset{\{x^{c,t,m}_{u,k}\},\{P^{c,t}_{u,k}\},\{I^{c,t}_{u,k}\},\{\lambda_{u,k}\}}{\text{maximize}} \sum_{u\in U_{UL}(\omega)} \log\Big(\sum_{k\in\mathscr{K}} \lambda_{u,k}\Big)$$

subject to:

$$x^{c,t,m}_{u,k} \in \{0,1\}, \qquad \forall u,\forall k,\forall c,\forall t,\forall m \tag{3.7a}$$

$$x^{c,t,m}_{u,k} \le z_{u,k}(\omega), \qquad \forall u,\forall k,\forall c,\forall t,\forall m \tag{3.7b}$$

$$\sum_{u\in U(\omega)}\sum_{m\in\mathscr{M}} x^{c,t,m}_{u,k} \le 1, \qquad \forall k,\forall c,\forall t \tag{3.7c}$$

$$0 \le P^{c,t}_{u,k} \le P_{UE}\sum_{m\in\mathscr{M}} x^{c,t,m}_{u,k}, \qquad \forall u,\forall k,\forall c,\forall t \tag{3.7d}$$

$$\sum_{c\in\mathscr{C}} P^{c,t}_{u,k} \le P_{UE}, \qquad \forall u,\forall k,\forall t \tag{3.7e}$$

$$P^{c,t}_{u,k}G_{u,k}(\omega) \ge x^{c,t,m}_{u,k}\beta_m(N_0 + I^{c,t}_{u,k}), \forall u,\forall k,\forall c,\forall t,\forall m \tag{3.7f}$$

$$I^{c,t}_{u,k} = \sum_{k'\in\mathscr{K}}^{k'\neq k}\sum_{u'\in U(\omega)}^{u'\neq u} P^{c,t}_{u',k'}G_{u',k}(\omega), \qquad \forall u,\forall k,\forall c,\forall t \tag{3.7g}$$

$$\lambda_{u,k} = \sum_{c\in\mathscr{C}}\sum_{t\in\mathscr{T}}\sum_{m\in\mathscr{M}} x^{c,t,m}_{u,k} f(\beta_m), \qquad \forall u,\forall k \tag{3.7h}$$

where, $u \in U_{UL}(\omega), k \in \mathscr{K}, c \in \mathscr{C}, t \in \mathscr{T}, m \in \mathscr{M}$.

Here, the constraints (3.7c) ensures that only one MCS is assigned to a user on each PRB and also that only one user is scheduled on a PRB of each cell. The constraints (3.7d) and (3.7e) are for assigning UL power on each PRB. The sum of the ICI and the coding efficiencies for user u are computed by (3.7g) and (3.7h), respectively.

Note that the bilinear constraints given by (3.7f) compute power for assigning appropriate MCS, however, they can be linearized by using a very large number $\boldsymbol{B}$ as follows:

$$P^{c,t}_{u,k}G_{u,k}(\omega) \ge \beta_m(N_0 + I^{c,t}_{u,k}) - (1 - x^{c,t,m}_{u,k})\boldsymbol{B}, \forall u,\forall k,\forall c,\forall t,\forall m \tag{3.7i}$$

Here, if $x^{c,t,m}_{u,k} = 0$, the inequality (3.7i) is true for all values of $P^{c,t}_{u,k}$ and $I^{c,t}_{u,k}$, since, the right hand side has a very large negative value. On the other hand, if $x^{c,t,m}_{u,k} = 1$, the inequality states that $P^{c,t}_{u,k}G_{u,k}(\omega) \ge \beta_m(N_0 + I^{c,t}_{u,k})$ and this is exactly desired.

The bilinear constraints given by (3.7f) can be replaced by the linear constraints given in (3.7i) to form a large-scale linearly constrained problem, however, solving this problem is still challenging because of the large number of binary and continuous variables. In the next section, we transform this problem into a continuous upper bound problem that can be solved efficiently.

3.4.1 The Upper Bound Problem

We want to transform the system-wide global US problem into a tractable problem that can be solved efficiently. This can be achieved by removing all binary variables from $\boldsymbol{P^{UL}_{Global}}$. Note that the binary variables $x^{c,t,m}_{u,k}$ in $\boldsymbol{P^{UL}_{Global}(\omega)}$ are required for two reasons: (i) they determine the MCS used by user u on PRB (c,t) and (ii) they represent the PRB mappings for each user. We replace the binary variables by introducing the following two techniques:

1. We introduce a continuous upper bound function $g(.)$ to envelop the piece-wise discrete function $f(.)$ (as shown in Fig. 3.3), whereby the binary variables for MCS allocation are no longer needed. The continuous rate function is defined as follows:

$$g(\gamma) := e^{(\log_{10}(e)\log_e(\gamma))}, \quad \epsilon_\gamma \leq \gamma \leq \beta_{max} \tag{3.8}$$

   where, ϵ_γ is a very small positive value and β_{max} is an upper limit on γ.

2. We add new constraints to ensure that two users in each cell do not to transmit on the same PRB, which is required to achieve one-to-one mapping between PRBs and users of each cell.

Note that the upper bound function will over estimate the rates achieved by the users and thereby it may require higher power in selecting the same MCS. For this reason, a lower bound function $h(.)$ to the piece-wise discrete function $f(.)$ (as shown in Fig. 3.3) can be used to find the rates that are achievable in practice, which is defined as follows:

$$h(\gamma) := a - b * e^{-c\gamma}, \quad \epsilon_\gamma \leq \gamma \leq \beta_{max}$$

where, $a = 6.83, b = 6.92, c = -0.023$. Here, ϵ_γ is a very small positive value and β_{max} is an upper limit on γ.

In this thesis, we deal with the upper bound results only, while leaving the lower bound analysis for future extension of this work. For using the upper bound rate function, we need the following additional variables for the upper bound problem:

- $\boldsymbol{\gamma_{u,k}^{c,t}}$ is the SINR seen by user u at MBS k on PRB (c,t)

We formulate the upper bound US problem as follows:

$$\boldsymbol{P_{Global}^{UB-UL}(\omega)}: \underset{\{P_{u,k}^{c,t}\},\{I_{u,k}^{c,t}\},\{\gamma_{u,k}^{c,t}\},\{\lambda_{u,k}\}}{\text{maximize}} \sum_{u\in U_{UL}(\omega)} \log\Big(\sum_{k\in\mathscr{K}} \lambda_{u,k}\Big)$$

subject to:

$$\epsilon_p \le P_{u,k}^{c,t} \le z_{u,k}(\omega)P_{UE} + (1-z_{u,k}(\omega))\epsilon_p, \qquad \forall u,\forall k,\forall c,\forall t \tag{3.9a}$$

$$\sum_{c\in\mathscr{C}} P_{u,k}^{c,t} \le P_{UE}, \qquad \forall u,\forall k,\forall t \tag{3.9b}$$

$$P_{u,k}^{c,t}P_{u',k}^{c,t} \le \epsilon_p, \qquad \forall u,\forall u', u'\neq u,\forall k,\forall c,\forall t \tag{3.9c}$$

$$\epsilon_\gamma \le \gamma_{u,k}^{c,t} \le \beta_{max}, \qquad \forall u,\forall k,\forall c,\forall t \tag{3.9d}$$

$$P_{u,k}^{c,t}G_{u,k}(\omega) \ge \gamma_{u,k}^{c,t}\big(N_0 + I_{u,k}^{c,t}\big), \qquad \forall u,\forall k,\forall c,\forall t \tag{3.9e}$$

$$I_{u,k}^{c,t} = \sum_{k'\in\mathscr{K}}^{k'\neq k}\sum_{u'\in U(\omega)}^{u'\neq u} P_{u',k'}^{c,t}G_{u',k}(\omega), \qquad \forall u,\forall k,\forall c,\forall t \tag{3.9f}$$

$$\lambda_{u,k} = \sum_{c\in\mathscr{C}}\sum_{t\in\mathscr{T}} g(\gamma_{u,k}^{c,t}), \qquad \forall u,\forall k \tag{3.9g}$$

where, $u\in U_{UL}(\omega), k\in\mathscr{K}, c\in\mathscr{C}, t\in\mathscr{T}$.

Here, the bilinear constraints (3.9c) ensure that on each PRB only one user in each cell is transmitting with a considerable amount of power, where ϵ_p and ϵ_γ are very small positive values that depend on the numerical values of P_{UE} and $\gamma_{u,k}^{c,t}$, respectively. The bilinear constraints (3.9e) are for computing SINR on each PRB, while the constraints (3.9f) and (3.9g) are for computing the exact ICI and link layer coding efficiencies, respectively.

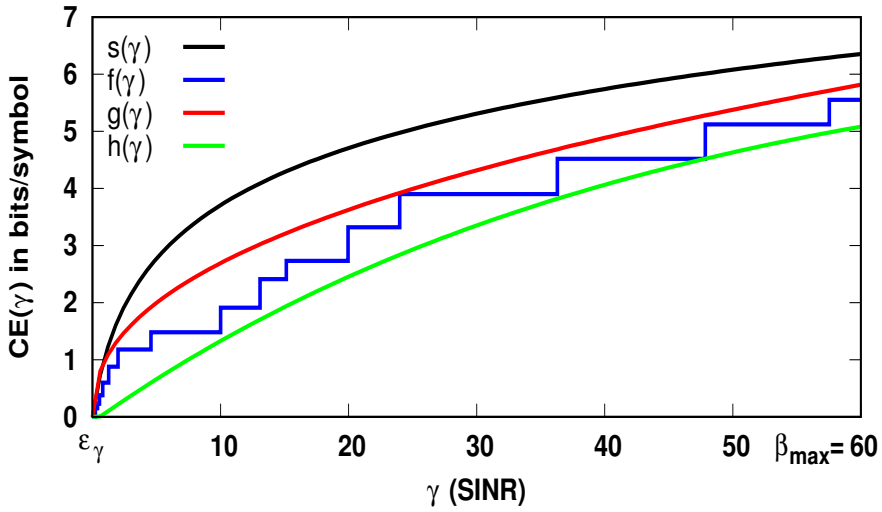

Figure 3.3: Shannon's capacity ($s(\gamma) = \frac{T}{N_S} \times \Delta f \times \log_2(1+\gamma)$) vs. the piece-wise discrete rate function ($f(\gamma)$ with $|\mathscr{M}|$=15 from [22]) and the continuous rate functions ($g(\gamma)$ and $h(\gamma)$).

We ensure that both problems, i.e., $\boldsymbol{P^{UL}_{Global}(\omega)}$ and $\boldsymbol{P^{UB-UL}_{Global}(\omega)}$, share the same solution space for finding their optimal objectives. Since, a feasible solution for the original problem can always be mapped onto a feasible solution for the upper bound problem and vice versa, the objective value of the upper bound problem will always be an upper bound on the objective value of the original problem for any feasible solution.

The upper bound problem ($\boldsymbol{P^{UB-UL}_{Global}(\omega)}$) is non-linear and non-convex in nature that requires extensive computational resources; mainly, due to the presence of bilinear constraints for computing the SINR. However, it can be transformed into an equivalent convex problem by using GP transformation that is described in [38].

Lemma 3.1: $\boldsymbol{P^{UB-UL}_{Global}(\omega)}$ *is an upper bound on* $\boldsymbol{P^{UL}_{Global}(\omega)}$ *and it can be converted into a convex problem.*

Proof: Please see Appendix A.

Computing Feasible Solutions:

In Appendix A, we successfully applied GP to the upper bound problem and converted it into a fairly sparse GP problem ($\boldsymbol{P^{UB-UL'}_{Global}(\omega)}$), which can be solved efficiently through standard interior-point algorithms [38] as each constraint depends on only a modest number of the optimization variables. Consequently, for a given realization ω, an optimal solution for $\boldsymbol{P^{UB-UL'}_{Global}(\omega)}$ can be used to find a feasible solution for the original global US problem $\boldsymbol{P^{UL}_{Global}(\omega)}$ using the method described in Algorithm 1; where, the feasible solution is computed from the optimal SINR values (i.e., $\boldsymbol{\gamma^{*'c,t}_{u,k}(\omega)}$) obtained by solving $\boldsymbol{P^{UB-UL'}_{Global}(\omega)}$. Note that each $\boldsymbol{\gamma^{*'c,t}_{u,k}(\omega)}$ needs to be transformed into the corresponding $\boldsymbol{\gamma^{*c,t}_{u,k}(\omega)}$. As $g(\gamma^{c,t}_{u,k})$ stays greater than or equal to $f(\gamma^{c,t}_{u,k})$, therefore, the optimal objective value of $\boldsymbol{P^{UB-UL'}_{Global}(\omega)}$ will always be greater than or equal to the optimal value for $\boldsymbol{P^{UL}_{Global}(\omega)}$. Nonetheless, the global optimal solution for $\boldsymbol{P^{UL}_{Global}(\omega)}$ lies in-between this feasible solution and the optimal solution obtained by solving $\boldsymbol{P^{UB-UL'}_{Global}(\omega)}$. We will show numerically in Section 3.4.2 that the average gap between these feasible solutions and the upper bound solutions, is small.

Algorithm 1 A Feasible Solution for $\boldsymbol{P^{UL}_{Global}(\omega)}$ using $\boldsymbol{\{\gamma^{*c,t}_{u,k}(\omega)\}_{\forall u,\forall k,\forall c,\forall t}}$

for each $u \in U_{UL}(\omega), k \in \mathscr{K}$ **do**
  for each $c \in \mathscr{C}, t \in \mathscr{T}$ **do**
    $x^{c,t,m}_{u,k} \leftarrow 0$
    for each $m \in \mathscr{M}$ **do**
      if $\gamma^{*c,t}_{u,k}(\omega) \geq \beta_m$ **then** $x^{c,t,m}_{u,k} \leftarrow 1$ **break**
      else $x^{c,t,m}_{u,k} \leftarrow 0$
      end if
    end for
  end for
  $\lambda_{u,k} = \sum_{c\in\mathscr{C}} \sum_{t\in\mathscr{T}} \sum_{m\in\mathscr{M}} x^{c,t,m}_{u,k} f(\beta_m)$
end for

3.4.2 Numerical Results

We evaluate the performance of our proposed upper bound problem by considering two different cell layouts, as shown in Fig. 3.1 and 3.2, with multiple macro cells placed at an inter-site distance (ISD) of $500m$ (i.e., equal to a macro cell radius of $\frac{500}{\sqrt{3}}m$). Each macro cell has one MBS, *i.e.* placed at the center as shown in Fig. 3.1 and 3.2, which is operating on OFDMA-based frames with $|\mathscr{C}| = 30$ sub-channels and $|\mathscr{T}| = 10$ time-slots. The MBSs from the same-colored macro cells are in co-channel with each other, for simplicity, we consider the yellow colored macro cells only with a wrap-around technique to incorporate ICI for the macro cells at the edge (*i.e.*, these macro cells are colored in orange).

Our physical layer parameters are based on the 3GPP evaluation document [5] for LTE, which are also summarized in Table 5.2; where, the channel gains introduced in Section 3.3.1 account for path loss, slow fading, and antenna gains only. The slow fading coefficients are modeled by a log-normal distribution with zero mean and standard deviation equal to $\boldsymbol{\sigma}$. The directivity gain (used for MBSs in cell layout 2 only) is a function of $\boldsymbol{\theta}$, *i.e.*, the angle made by a user (UE) with the broadside direction of the MBS antenna. We consider an adaptive modulation and coding scheme as given in [22] for computing exact link layer rates (*i.e.*, using the function $\boldsymbol{f(.)}$ with $|\mathscr{M}| = 15$), which are required for computing the feasible

Table 3.1: Physical Layer Parameters from [5]

N_S	12×14	T	1ms
Noise Power	-174dBm/Hz	Sub-channel Bandwidth	180kHz
UE Noise Figure	9dB	Penetration Loss	20dB
MBS Noise Figure	5dB	Traffic Model	Full Buffer
UE Antenna Gain	0dBi	P_{UE}	24dBm
Layout 1: MBS Antenna Gain	15dBi	Layout 1: P_{MBS}	46dBm
Layout 2: MBS Antenna Gain	17dBi	Layout 2: $3 \times P_{MBS}$	46dBm
Layout 2: MBS Directivity Gain	$\min(12(\frac{\theta}{70^o})^2, 20)$dB		
Path Loss (dB)	$128.1 + 37.6 \log_{10}(d/1000), d \geq 35m$		

solutions for the global user scheduling problem along with the proposed upper bound solutions. For numerical evaluation, a set of 100 realizations (Ω) have been generated, where each $\omega \in \Omega$ corresponds to the duration of one frame and a set of either UL or DL users, denoted by $U_{UL}(\omega)$ or $U_{DL(\omega)}$, respectively, that are distributed uniformly across all macro cells. We consider the geometric mean (GM) throughput of the UL or DL users, which is equivalent to maximizing our objective function, *i.e.*, $\sum\limits_{u \in U_{UL}(\omega)} \log\big(\sum\limits_{k \in \mathscr{K}} \lambda_{u,k}\big)$ for UL or $\sum\limits_{d \in U_{DL}(\omega)} \log\big(\sum\limits_{k \in \mathscr{K}} \lambda_{k,d}\big)$ for DL, respectively.

The GM throughput (in bits per second) for each realization ω is defined as follows:

$$\begin{aligned} GM^{UL}(\omega) &:= \Bigg(\prod_{u \in U_{UL}(\omega)} \Big(\sum_{k \in \mathscr{K}} \frac{\lambda_{u,k}(\omega) \times N_S}{T \times |\mathscr{T}|}\Big) \Bigg)^{\frac{1}{|U_{UL}(\omega)|}} \\ GM^{DL}(\omega) &:= \Bigg(\prod_{d \in U_{DL}(\omega)} \Big(\sum_{k \in \mathscr{K}} \frac{\lambda_{k,d}(\omega) \times N_S}{T \times |\mathscr{T}|}\Big) \Bigg)^{\frac{1}{|U_{DL}(\omega)|}} \end{aligned} \tag{3.10}$$

where, N_S and T are the total number of OFDM symbols in each PRB and the duration of each time-slot, respectively, for the given frame.

The following performance measures, for each realization ω, have been defined for the UL users, nonetheless, a similar set of performance measures can be defined for the DL users:

- The *Upper bound GM* ($\boldsymbol{GM^{UB-UL}_{Global}(\omega)}$), for the original global user scheduling problem (*i.e.*, $\boldsymbol{P^{UL}_{Global}(\omega)}$), can be computed by solving $\boldsymbol{P^{UB-UL'}_{Global}(\omega)}$ through any non-linear programming solver, such as, SNOPT [39].

- The *Feasible GM* ($\boldsymbol{GM^{FS-UL}_{Global}(\omega)}$), for the original global user scheduling problem (*i.e.*, $\boldsymbol{P^{UL}_{Global}(\omega)}$), can be computed from the upper bound solutions (*i.e.*, from $\boldsymbol{P^{UB-UL'}_{Global}(\omega)}$) by using the method discussed in Algorithm 1.

Table 3.2: System-1: Globally Optimal UL Schedules

$\frac{\lvert U_{UL}(\omega)\rvert}{\lvert\mathscr{K}\rvert}$	$\boldsymbol{GM^{UB-UL}_{Global}(\omega)}$	$\boldsymbol{GM^{FS-UL}_{Global}(\omega)}$	$\boldsymbol{GAP^{UL}_{Global}(\omega)} := \frac{\left(GM^{UB-UL}_{Global}(\omega) - GM^{FS-UL}_{Global}(\omega)\right)\times 100}{GM^{UB-UL}_{Global}(\omega)}$
Average over Ω			
N	Mbps	Mbps	%
5	4.53	4.22	6.94
10	2.31	2.16	6.99
15	1.52	1.41	7.08

Table 3.3: System-1: Globally Optimal DL Schedules

$\frac{\lvert U_{DL}(\omega)\rvert}{\lvert\mathscr{K}\rvert}$	$\boldsymbol{GM^{UB-DL}_{Global}(\omega)}$	$\boldsymbol{GM^{FS-DL}_{Global}(\omega)}$	$\boldsymbol{GAP^{DL}_{Global}(\omega)} := \frac{\left(GM^{UB-DL}_{Global}(\omega) - GM^{FS-DL}_{Global}(\omega)\right)\times 100}{GM^{UB-DL}_{Global}(\omega)}$
Average over Ω			
N	Mbps	Mbps	%
5	4.73	4.37	7.73
10	2.35	2.16	8.09
15	1.59	1.44	9.60

Table 3.4: System-2: Globally Optimal UL Schedules

$\frac{\lvert U_{UL}(\omega)\rvert}{\lvert\mathscr{K}\rvert}$	$\boldsymbol{GM^{UB-UL}_{Global}(\omega)}$	$\boldsymbol{GM^{FS-UL}_{Global}(\omega)}$	$\boldsymbol{GAP^{UL}_{Global}(\omega)} := \frac{\left(GM^{UB-UL}_{Global}(\omega) - GM^{FS-UL}_{Global}(\omega)\right)\times 100}{GM^{UB-UL}_{Global}(\omega)}$
Average over Ω			
N	Mbps	Mbps	%
5	3.99	3.66	8.49
10	2.06	1.90	8.79
15	1.35	1.22	9.92

Table 3.5: System-2: Globally Optimal DL Schedules

$\frac{\lvert U_{DL}(\omega)\rvert}{\lvert\mathscr{K}\rvert}$	$\boldsymbol{GM^{UB-DL}_{Global}(\omega)}$	$\boldsymbol{GM^{FS-DL}_{Global}(\omega)}$	$\boldsymbol{GAP^{DL}_{Global}(\omega)} := \frac{\left(GM^{UB-DL}_{Global}(\omega) - GM^{FS-DL}_{Global}(\omega)\right)\times 100}{GM^{UB-DL}_{Global}(\omega)}$
Average over Ω			
N	Mbps	Mbps	%
5	4.10	3.75	8.72
10	2.08	1.90	8.92
15	1.37	1.24	9.66

A summary of these performance measures for both UL and DL, when averaged over Ω, have been shown in Table 3.2 and 3.3 for System-1 and in Table 3.4 and 3.5 for System-2, respectively. Given an optimal solution for the convex upper bound problem, we can find a feasible solution for the intractable system-wide global problem. Clearly, the average gap between GM^{FS} and GM^{UB} is small on both UL and DL, *i.e.*, less than 10% for different number of users; where, the optimal solution to the intractable system-wide global problem lies in-between the gap. Hence, we have developed a method that delivers a feasible solution to the intractable system-wide global US problem which is very close to the optimal.

3.5 The Local User Scheduling Problem

The proposed global user scheduling problem can be solved in the scenario where a central scheduler has the knowledge of the channel gains to/from all users and it has extensive computational resources. However, in practice the computational resources are very limited and most of the time the user schedulers are employed locally within each BS. To avoid any communication overhead, typically, these user schedulers do not coordinate with each other for scheduling their users.

We will discuss the local US problems for both UL and DL, without assuming any BS-coordination, in order to simplify the system-wide global US problem into multiple decoupled local US problems (*i.e.*, one per BS). Designing these local schedulers to perform efficiently in an on-line fashion is not trivial, especially on the UL, since, the US problem on the UL is more challenging than the DL, *i.e.*, due to various reasons which will be discussed in Section 3.5.1. Specifically, the UL interference pattern strongly depends on the scheduling decisions of the neighboring BSs, which makes the US problem much more complex on the UL. A naive way for scheduling users would be to make the local US decisions on a per-BS basis by assuming that the interference is fixed, but such an approach does not work well because the interference pattern could change drastically when a different user is scheduled on a PRB. Furthermore, simply applying the DL-based local US schemes to the UL, for example the one proposed in [20], would lead to sub-optimal results.

Need for Estimating Interference:

Ideally, scheduling should be local to a BS as it is performed at a very short time scale (typically in milliseconds) and subsequently the system-wide global US problem should be decoupled into multiple independent local schedulers (one per BS). Given that these decoupled local schedulers need to determine their schedules independently without any coordination, they require an estimate/measurement for ICI which could be computed/measured beforehand. However, computing the exact estimate of ICI for decoupling the system-wide global user scheduling problem in a multi-cell system is not possible because of the following reasons:

1. The ICI on the UL is coming from the users that are associated with the BSs in the interfering macro cells and its exact value depends on the power allocations and the channel gains from the users which will get scheduled (by their BSs) on the next frame. Since, these measures depend on the scheduling decisions made by the interfering BSs for their next frames, they cannot be made available beforehand.

2. The ICI on the DL can be computed exactly beforehand as it is created by the BSs whose positions are known and they transmit all the time. Hence, the DL ICI under fixed transmit power assumptions can be measured exactly as discussed in [9–11]. Note that fixing power on each PRB can significantly limit the potential performance gains and if the power is not fixed then the DL US problem becomes similar to the UL problem; where, the only way to compute exact ICI is to solve the system-wide global US problem.

Given the aforementioned reasons, the local US process within each BS, no matter for UL or DL, is somewhat blind with respect to the exact ICI. Nonetheless, if the ICI has to be approximated then the performance of these local schedulers will highly depend on the ICI estimate used by them; since, using a high value would lead to conservative user schedules and a low value would lead to optimistic schedules with higher packet losses. Therefore, the local US solutions based on the estimates of ICI need to be validated as they might lead to sub-optimal solutions as opposed to the ones obtained by solving the system-wide global user scheduling problem from Section 3.4.

State-of-the-Art Interference Measurement:

In practice, the ICI is indeed measured and adjusted by the local schedulers based on the feedback received by them, which is possible only in a closed loop system. In current OFDM-based cellular networks, a user can periodically transmit a sounding reference signal (SRS) on the UL during the last symbol of each time-slot with fixed power, which is typically known beforehand. Thus, each BS can compute a long term average of the channel gains from the users that are associated with the interfering BSs. In contrast, the BSs also transmit a set of reference symbols (on the DL) within each time-slot. These reference symbols are transmitted to facilitate the ICI estimation process on the DL. We use a similar process for computing ICI, however for modeling purposes, we need an open loop estimate which can be validated through simple numerical simulations. Knowing well that if a BS can always decode the data within a frame, its open loop ICI estimate might be overestimating the ICI. Similarly, if the BS is unable to decode properly, the estimator might be underestimating the ICI.

3.5.1 The Uplink Problem

The local US process within each BS needs to make the PRB mapping decisions given an estimate of ICI. More specifically, it determines the number of PRBs allocated to each associated user without considering any inter-BS coordination. Note that the channel gains for each users can be computed locally at each BS through the TDD protocol that results in channel reciprocity. Given an ICI estimate ($\hat{I}$), the corresponding *estimated rates* can be pre-computed by the local schedulers as follows:

$$\hat{R}^{i}_{u,k}(\omega, \hat{I}_k) := i \times f\left(\frac{\frac{P_{UE}}{i} \times G_{u,k}(\omega)}{N_0 + \hat{I}_k}\right), \forall u \in U_{UL_k}(\omega), \forall k \in \mathscr{K}, \forall i \in \{1, ..., |\mathscr{C}|\} \tag{3.11}$$

Here, $U_{UL_k}(\omega)$ denotes the set of UL users that are associated with the BS k[4]. Note that the compensated rates in equation (3.11) are not the exact rates that nonetheless have to be computed with the exact interference. The equal power (EP) allocations have been used to pre-compute these rates for the local US problem, which are not necessarily optimal.

[4]We assume that each macro cell has a local UA process for computing cell associations, *i.e.,* $z_{u,k}(\omega)$.

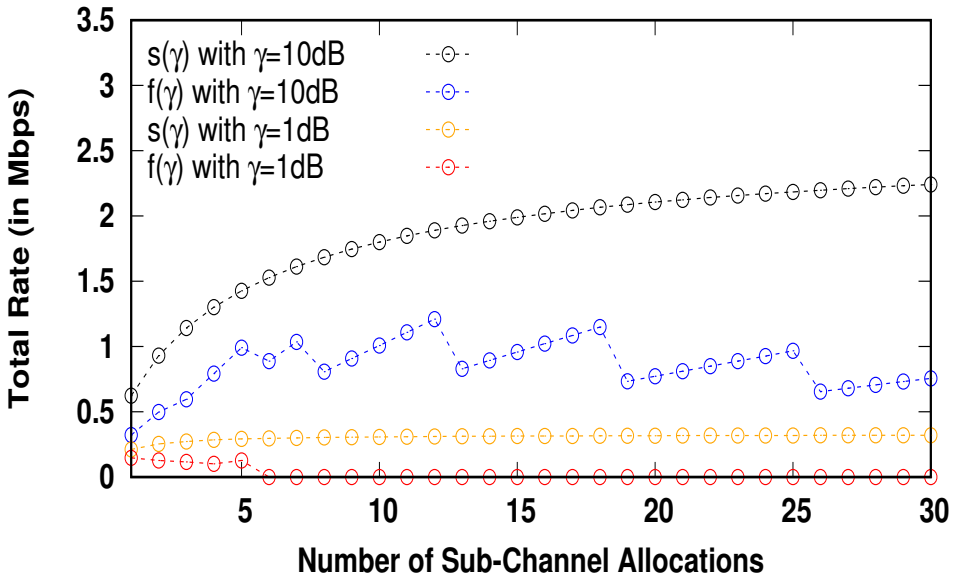

Figure 3.4: Total Rate with received SINR=γ: Shannon's capacity ($s(\gamma) = \Delta f \times \frac{T}{N_S} \times \log_2(1+\gamma)$) vs. the piece-wise discrete rate function ($f(\gamma)$ with $|\mathscr{M}|$=15 from [22])

In fact, we will show numerically in Section 3.5.3 that these compensated rates are far from the optimal and we need to solve the global user scheduling problem in an efficient manner for optimizing the power and the corresponding rates on each PRB. Note that the number of sub-channels allocated to user u should be in proportion to u's channel gain from the MBS. In Fig. 3.4, it has been shown that the total rate received by each user highly depends on the number of sub-channels allocated to that user. The users are limited in power on UL, therefore, if the received UL SINR of a user is significantly low then allocating more sub-channels to that user would lead to zero rate. We can see in Fig. 3.4 that the rates computed using the Shannon's function (*i.e.*, $s(\gamma)$) are far from the actual ones, which are obtained via the set of discrete MCSs (*i.e.*, $f(\gamma)$). Therefore, the number of sub-channel allocations should not be computed using $s(\gamma)$, instead, we need to optimize the number of sub-channel allocations using the discrete rate function $f(\gamma)$.

The following optimization variables are required for the proposed sub-channel allocation problem:

- $\boldsymbol{n^t_{u,k}}$ indicate the number of sub-channels allocated to user u by MBS k during time-slot t.
- $\boldsymbol{s^{i,t}_{u,k}}$ is the sub-channel allocation indicator, which is 1 if user u is allocated i number of sub-channels by MBS k during time-slot t

Given a set of macro cells $\mathscr{K}$, a set of sub-channels $\mathscr{C}$, a set of time-slots $\mathscr{T}$, a network realization ω, a set of user associations $(\{z_{u,k}(\omega)\}_{u\in U_{UL_k}(\omega),k\in\mathscr{K}})$, a set of ICI estimates$(\{\hat{I}_k\}_{k\in\mathscr{K}})$, and a set of pre-computed data rates $(\{\hat{R}^i_{u,k}(\omega,\hat{I}_k)\}_{i\in\{1,...,|\mathscr{C}|\},u\in U_{UL_k}(\omega),k\in\mathscr{K}})$, the optimal sub-channel allocation problem for the MBS k is defined as follows:

$$\boldsymbol{P^{UL}_k(\omega,\hat{I}_k)}: \underset{\{n^t_{u,k}\},\{s^{i,t}_{u,k}\},\{\hat{\lambda}_{u,k}\}}{\text{maximize}} \sum_{u\in U_{UL_k}(\omega)} \log(\hat{\lambda}_{u,k})$$

subject to:

$$s^{i,t}_{u,k} \in \{0,1\}, \qquad \forall i,\forall u,\forall t \tag{3.12a}$$

$$\sum_{i=1}^{|\mathscr{C}|} s^{i,t}_{u,k} \le z_{u,k}(\omega) = 1, \qquad \forall u,\forall t \tag{3.12b}$$

$$\sum_{u\in U_{UL_k}(\omega)} n^t_{u,k} \le |\mathscr{C}|, \tag{3.12c}$$

$$n^t_{u,k} = \sum_{i=1}^{|\mathscr{C}|}(i\times s^{i,t}_{u,k}), \qquad \forall u,\forall t \tag{3.12d}$$

$$\hat{\lambda}_{u,k} = \sum_{t\in\mathscr{T}}\sum_{i=1}^{|\mathscr{C}|}(s^{i,t}_{u,r}\times \hat{R}^i_{u,k}(\omega,\hat{I}_k)), \qquad \forall u \tag{3.12e}$$

where, $\forall i\in\{1,...,|\mathscr{C}|\}, u\in U_{UL_k}(\omega), k\in\mathscr{K}, t\in\mathscr{T}$.

Once the optimal number of sub-channels for each time-slot (*i.e.*, $n^{*t}_{u,k}(\omega)$) have been determined by solving $\boldsymbol{P^{UL}_k(\omega,\hat{I}_k)}$, the local PRBs of each cell k are randomly mapped to the local users using $n^{*t}_{u,k}(\omega)$. Note that the sub-channel allocations obtained by solving

the above problem might create too many failures to decode for some users; therefore, we randomly permute their PRB mappings over different time-slots of a frame to statistically average out the effects of ICI estimation.

3.5.2 The Downlink Problem

Different from the UL case, the DL is not limited in power and also the DL interference is created by the MBSs whose positions are known and they transmit all the time. Therefore, the local US on the DL can be simplified by using equal power (EP) allocations per PRB and the corresponding interference can be pre-computed (for each PRB) as follows:

$$I_{k,d}^{EP}(\omega) := \sum_{k' \in \mathscr{K}}^{k' \neq k} \frac{P_k}{|\mathscr{C}|} \times G_{k',d}(\omega), \quad \forall d \in U_{DL_k}(\omega), \forall k \in \mathscr{K} \tag{3.13}$$

The corresponding EP based compensated rates (on each PRB) can be pre-computed for each user as follows:

$$R_{k,d}(\omega, I_{k,d}^{EP}) := f\left(\frac{\frac{P_k}{|\mathscr{C}|} \times G_{k,d}(\omega)}{N_0 + I_{k,d}^{EP}(\omega)}\right), \quad , \forall d \in U_{DL_k}(\omega), \forall k \in \mathscr{K} \tag{3.14}$$

The following optimization variables are required for the sub-channel allocation problem on the DL:

- $\boldsymbol{n_{k,d}^t}$ indicate the number of sub-channels allocated to user d by MBS k during time-slot t.

Given a set of macro cells $\mathscr{K}$, a set of sub-channels $\mathscr{C}$, a set of time-slots $\mathscr{T}$, a network realization ω, a set of user associations $(\{z_{k,d}(\omega)\}_{d \in U_{DL_k}(\omega), k \in \mathscr{K}})$, a set of equal power (EP) based ICIs $(\{I_{k,d}^{EP}\}_{d \in U_{DL_k}, k \in \mathscr{K}})$, and a set of pre-computed data rates using the EP based ICIs $(\{R_{k,d}(\omega, I_{k,d}^{EP})\}_{d \in U_{DL_k}(\omega), k \in \mathscr{K}})$, the optimal sub-channel allocation problem for the MBS k is defined as follows:

$$\boldsymbol{P_k^{DL}(\omega, \{I_{k,d}^{EP}(\omega)\})}: \underset{\{n_{k,d}^t\},\{\hat{\lambda}_{k,d}\}}{\text{maximize}} \sum_{u \in U_{DL_k}(\omega)} \log\Big(\sum_{k \in \mathscr{K}} \hat{\lambda}_{k,d}\Big)$$

subject to:

$$n_{k,d}^t \leq z_{k,d}(\omega)|\mathscr{C}| = |\mathscr{C}|, \forall d, \forall t \tag{3.15a}$$

$$n_{k,d}^t \in \{0, ..., |\mathscr{C}|\}, \qquad \forall d, \forall t \tag{3.15b}$$

$$\sum_{d \in U_{DL_k}(\omega)} n_{k,d}^t \leq |\mathscr{C}|, \qquad \forall t \tag{3.15c}$$

$$\hat{\lambda}_{k,d} = \sum_{t \in \mathscr{T}} n_{k,d}^t R_{k,d}(\omega), \qquad \forall d \tag{3.15d}$$

where, $d \in U_{DL_k}(\omega), k \in \mathscr{K}, t \in \mathscr{T}$.

Theorem 3.1: *The optimal solution* $\boldsymbol{P_k^{DL}(\omega, \{I_{k,d}^{EP}(\omega)\})}$ *will allocate equal number of PRBs to each user when* $\{n_{k,d}^t\}$ *are relaxed.*

Proof: Please see Appendix C.

Similar to the case for UL, after solving the above problem, we randomly map the local users to the local PRBs of each macro cell. Note that the above problem is an EP based DL scheduler, whose performance can be further improved through optimal power allocations on each PRB. We will show numerically in Section 3.5.3 that the performance of this local scheduler is also far from the optimal.

3.5.3 Performance Evaluation

We evaluate the performance of the local user scheduling schemes, on both UL and DL, using similar simulation settings as the one discussed in Section 3.4.2 and the same set of systems, *i.e.*, shown in Fig. 3.1 and 3.2, have been considered. The physical layer parameters are based on the 3GPP evaluation document [5] for LTE, which are also summarized in Table 5.2. Likewise, a snapshot-based approach has been considered to validate the proposed local schedulers with a set of 100 realizations (Ω), where each realization $\omega \in \Omega$ corresponds to $U(\omega)$ users that are distributed uniformly across all macro cells ($k \in \mathscr{K}$).

Validation of the Local User Schedules on the Uplink:

The exact ICI cannot be measured by the local schedulers on the UL, hence, they need to estimate it as closely as possible for computing the corresponding *Estimated Global GM*. In order to validate the performance of the local user scheduling problem on the UL, we need to find the corresponding *Effective Global GM*, knowing that the solutions obtained via solving the decoupled problems with estimates of ICI would have to be validated with the real ICI. Note that SINRs have been estimated with the estimated ICI, which are required for selected the appropriate MCS (m) for UL transmission. However, a bad estimation might result in decoding errors if the effective SINR (i.e., with the real ICI) on a given PRB is much less than the estimated SINR (i.e., with $\hat{I}_k$ as discussed in Section 3.5.1).

We define a simple *PRB decoding rule* for computing the effective data rates: if the effective SINR is lower than the threshold SINR (*e.g.*, β_m for MCS m), then the receiver will not be able to decode the PRB and we count it as a PRB loss. High losses will impact the *Effective Global GM* of all users. For example, if we assume the ICI to be zero on all PRBs, we can still compute local user schedules within each macro cell, however, the effective data rate seen by each user might be too low with the real ICI.

The proposed UL scheduler can be validated for different numbers of users in different macro cells, however, the validation process in this case will be much more complicated. For simplicity, we assume that the users are distributed uniformly across the network, *i.e.*, $N = \frac{|U(\omega)|}{|\mathscr{K}|}$ and henceforth the same estimate of ICI can be used by all MBSs, *i.e.*, $\hat{I}_k = \hat{I}, \forall k \in \mathscr{K}$. We try all possible values of $\hat{I}$ to find the Effective Global GM throughput when real ICI and the corresponding PRB losses have been considered. Note that a conservative value of $\hat{I}$ might lead to lower PRB losses at the cost of a lower Effective GM, whereas an optimistic estimation can increase it. We consider all possible values of $\hat{I}$ to maximize the Effective GM throughput on the UL, however, in practice this might not be possible for a local scheduler.

Performance Measures:

We compute the following performance measures for each realization ω, where N_S and T are the total number of OFDM symbols in each PRB and the duration of each time-slot, respectively, for the given frame:

1. We consider the geometric mean (GM) throughput of the UL and DL users as determined by the local schedulers, *i.e.*, by solving the local US problems $\boldsymbol{P_k^{UL}(\omega, \hat{I})}$ and $\boldsymbol{P_k^{DL}(\omega, \hat{I}_{k,d}^{EP})}$, respectively. The corresponding *Estimated Global GM* throughput (in bits per second) for each realization ω is defined as follows:

$$\begin{aligned} \hat{GM}^{UL}(\omega, \hat{I}) &:= \left(\prod_{u \in U_{UL}(\omega)} \left(\sum_{k \in \mathscr{K}} \frac{\hat{\lambda}_{u,k}(\omega) \times N_S}{T \times |\mathscr{T}|} \right) \right)^{\frac{1}{|U_{UL}(\omega)|}} \\ \hat{GM}^{DL}(\omega, \{I_{k,d}^{EP}\}) &:= \left(\prod_{d \in U_{DL}(\omega)} \left(\sum_{k \in \mathscr{K}} \frac{\hat{\lambda}_{k,d}(\omega) \times N_S}{T \times |\mathscr{T}|} \right) \right)^{\frac{1}{|U_{DL}(\omega)|}} \end{aligned} \tag{3.16}$$

2. Similarly, we also consider the arithmetic mean (AM) throughput of the UL and DL users by solving the local US problems $\boldsymbol{P_k^{UL}(\omega, \hat{I})}$ and $\boldsymbol{P_k^{DL}(\omega, \hat{I}_{k,d}^{EP})}$, respectively. The corresponding *Estimated Global AM* throughput (in bits per second) for each realization ω is defined as follows:

$$\begin{aligned} \hat{AM}^{UL}(\omega, \hat{I}) &:= \frac{1}{|U_{UL}(\omega)|} \times \left(\sum_{u \in U_{UL}(\omega)} \sum_{k \in \mathscr{K}} \frac{\hat{\lambda}_{u,k}(\omega) \times N_S}{T \times |\mathscr{T}|} \right) \\ \hat{AM}^{DL}(\omega, \{I_{k,d}^{EP}\}) &:= \frac{1}{|U_{DL}(\omega)|} \times \left(\sum_{d \in U_{DL}(\omega)} \sum_{k \in \mathscr{K}} \frac{\hat{\lambda}_{k,d}(\omega) \times N_S}{T \times |\mathscr{T}|} \right) \end{aligned} \tag{3.17}$$

3. The *Effective Global AM/GM* for UL, which can be computed by considering the real ICI with the proposed PRB decoding rule for computing effective AM/GM against each global solution obtained via solving $\boldsymbol{P_k^{UL}(\omega, \hat{I})}, \forall k \in \mathscr{K}$.

4. The *Effective Global AM/GM with ICI-coordination* for UL, which can be computed by re-evaluating the MCS on each PRB according to the real ICI for computing effective AM/GM with ICI-coordination against each global solution obtained via solving $\boldsymbol{P_k^{UL}(\omega, \hat{I})}, \forall k \in \mathscr{K}$.

5. The *Effective Global AM/GM* for DL, which is same as the Estimated Global AM/GM, since, the exact ICI on the DL can be pre-computed exactly when EP based local schedulers are used by all MBSs.

Numerical Results:

The numerical results for the UL are obtained by solving the problem $\boldsymbol{P_k^{UL}(\omega, \hat{I})}, \forall k \in \mathscr{K}$ using a mixed integer programming solver (SCIP [40]), whereas, the results for the DL are obtained analytically with the help of Theorem 3.1, which is described in Section 3.5.2. The global AM/GM throughputs on the UL corresponding to each system have been shown in Fig. 3.5 and 3.6, while the AM/GM throughputs on the DL are shown in Fig. 3.7.

The performance of the proposed local US scheme is almost similar for both systems on the UL as well as the DL, given that System-1 experiences lesser interference than System-2; indeed ICI estimation/measurement is critical for both systems. In both systems, the inter-dependence between the user scheduling processes on the UL (*i.e.*, one per MBS) can be limited by using an estimate for UL ICI and the single-cell-based UL schedulers, such as [12–15], with no ICI considerations (*i.e.*, $\hat{I} = 0$ case), will yield zero GM throughput on the UL. Note that although we see non-zero AM throughput (or sum of the user rates) for $\hat{I} = 0$ case in Fig. 3.5 and 3.6, however, AM throughout does not offer fairness among the users; there are some users with zero rate because the GM throughput is zero at lower values of $\hat{I}$. In contrast, the user scheduling schemes based on worst case ICI, such as the one discussed in [11] with a very large value of $\hat{I}$), will yield higher interference estimates that will lead to a conservative effective AM/GM throughput.

For both systems , it can be seen that the local schedules, no matter on UL or DL, are still far from the optimal with an average gap between 30% to 50% from the globally optimal schedules, which are given in Table 3.2, 3.4, 3.3, and 3.5. In fact, it can be seen in Fig. 3.5 and 3.6 that ICI coordination is indeed useful on UL, even for small values of $\hat{I}$.

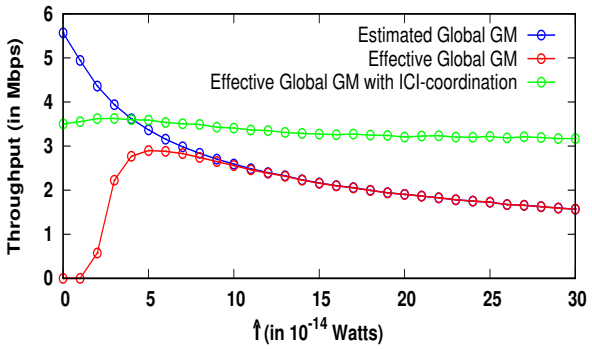

(a) GM with $N = 5$

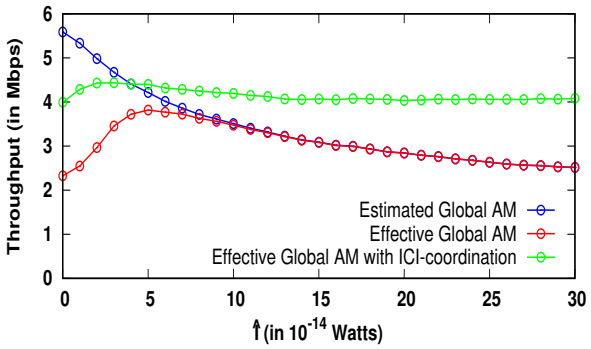

(b) AM with $N = 5$

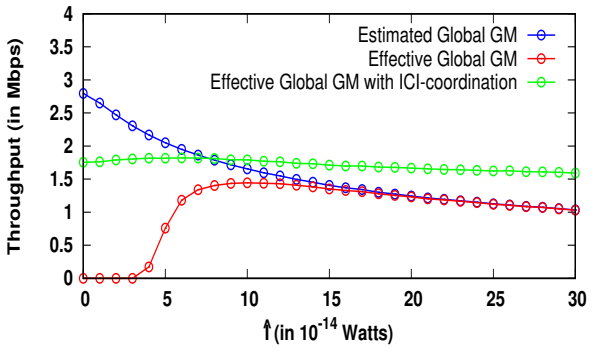

(c) GM with $N = 10$

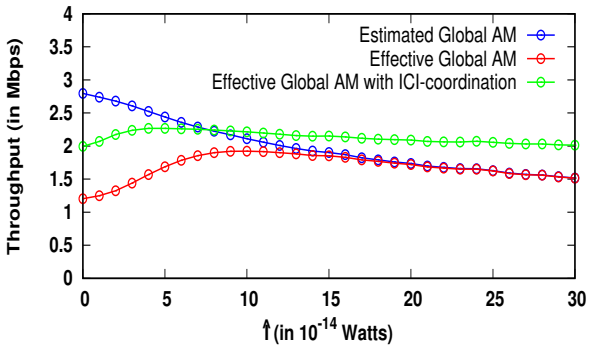

(d) AM with $N = 10$

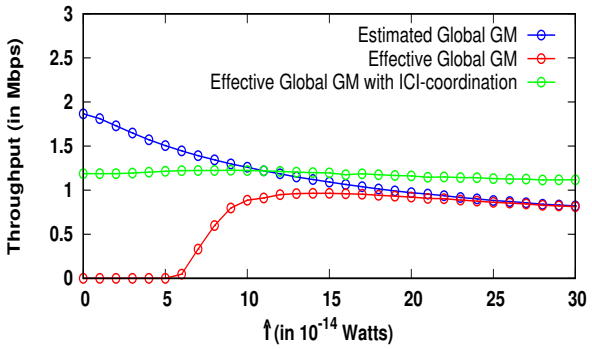

(e) GM with $N = 15$

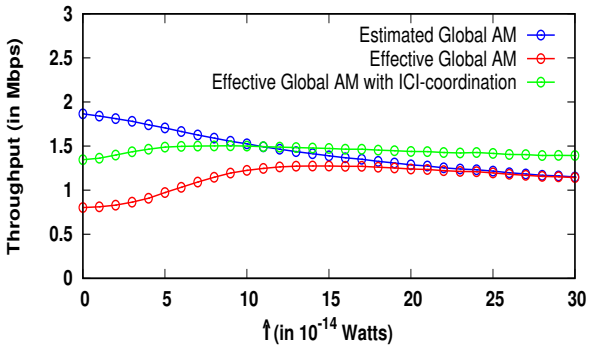

(f) AM with $N = 15$

Figure 3.5: System-1: Average UL throughput over Ω.

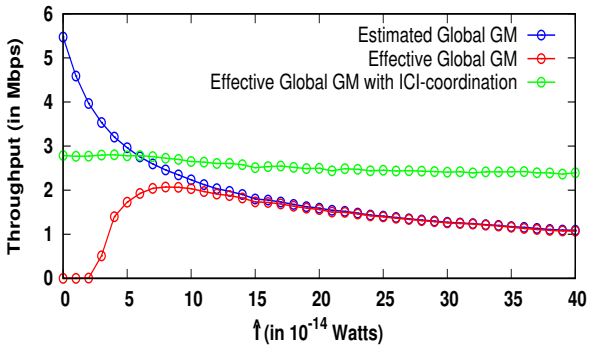

(a) GM with $N = 5$

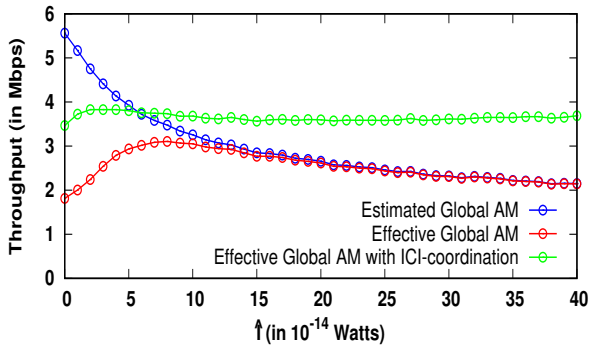

(b) AM with $N = 5$

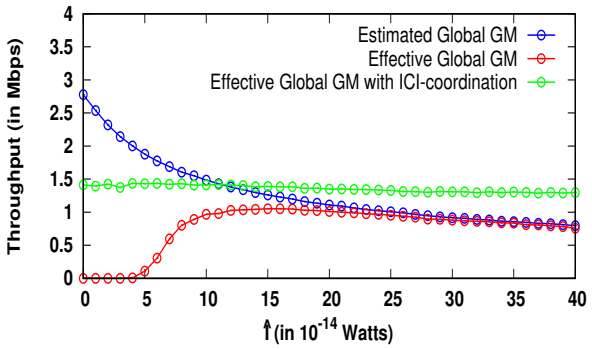

(c) GM with $N = 10$

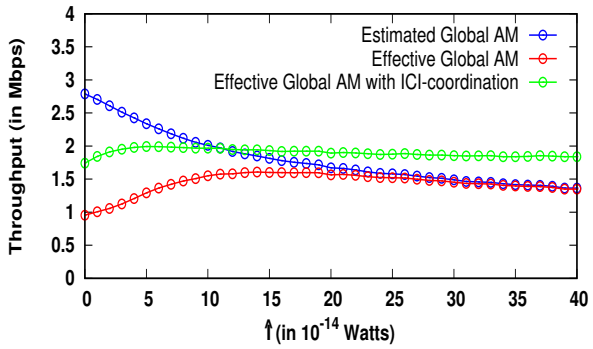

(d) AM with $N = 10$

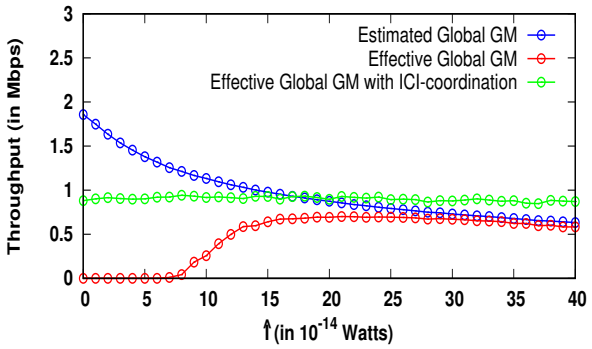

(e) GM with $N = 15$

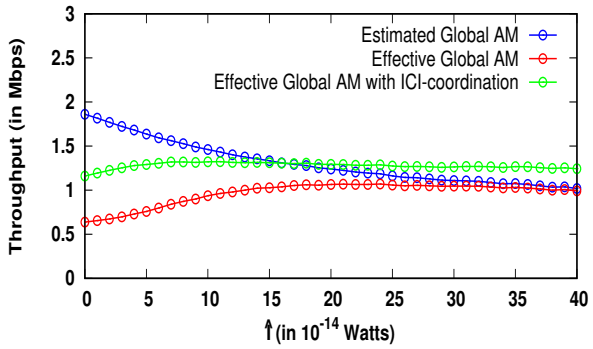

(f) AM with $N = 15$

Figure 3.6: System-2: Average UL throughput over Ω.

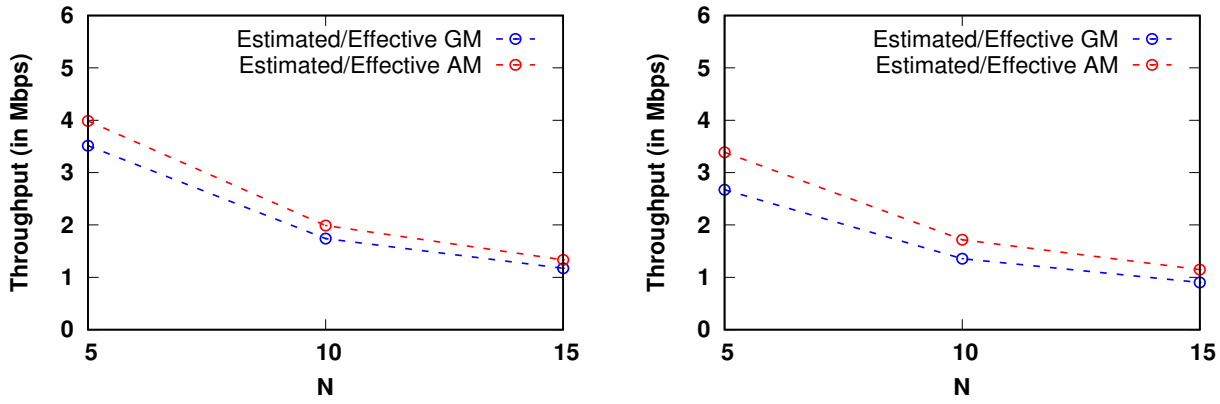

(a) System-1 (b) System-2

Figure 3.7: Average DL throughput over Ω.

In Fig. 3.8, we can see that using the shannon's capacity function $s(\gamma)$, for computing the number of sub-channels on the UL, can significantly lower the data rate received by a user when the discrete set of MCSs (using $f(\gamma)$) have been employed.

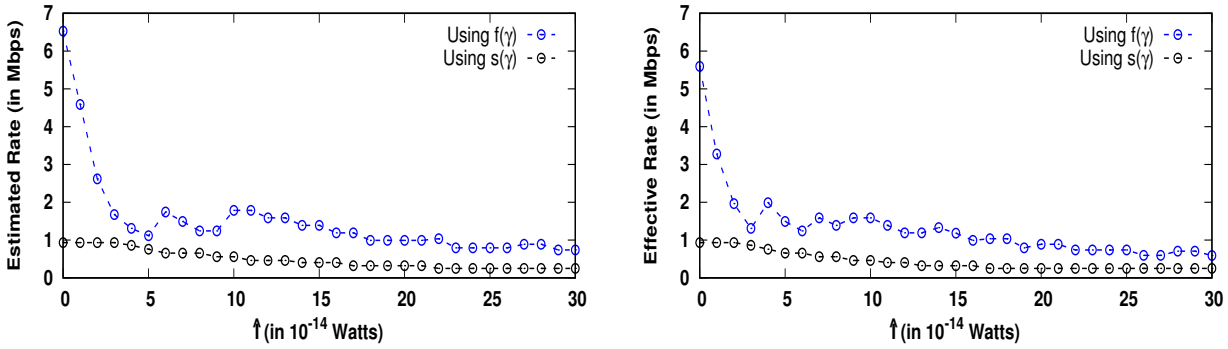

(a) System-1 (b) System-2

Figure 3.8: Uplink Estimated rate for a user (with $N = 5$) when the sub-channel allocation are determined through $s(\gamma)$ as opposed to $f(\gamma)$.

3.6 Conclusions

In this chapter, we formulated an intractable system-wide global user scheduling problem and transformed it into a tractable upper bound problem. This was achieved by replacing the piece-wise discrete rate function with a continuous rate upper bound function. The resulting upper bound problem was transformed into a convex problem via. geometric programming (GP). The optimal solutions for the upper bound problem were mapped into the feasible solutions of the intractable global US problem using a simple method. The average gap between the feasible solutions and the optimal solutions was observed to be tight for different systems, hence, the proposed upper bound problem can be used to obtain reasonable solutions for benchmarking the performance of different user schedulers.

In the later part of this chapter, we explained the inter-dependence of the local user scheduling processes within each macro cell, specifically on the uplink. We elucidated that the user scheduling problem in a multi-cell system is indeed a global problem, which can be decoupled into multiple local user scheduling problems (one per macro cell) by using simple estimates/measurements for inter-cell interference. However, these local problems need to be validated in a multi-cell setting. We validated the performance of these local schedulers through extensive numerical simulations over two different homogeneous systems.

Our results reveal that the schedules obtained through the local user schedulers are far from the ones obtained via solving the original system-wide global user scheduling problem. Further, we found that BS-coordination can be very helpful in improving the performance of these local schedulers. Inspired by the preliminary results obtained via ICI-coordination, we believe that the performance of these local schedulers can be greatly improved under a C-RAN [41] setting, as the exact ICI depends on dynamic system states which can only be obtained by a centralized scheduler.

Chapter 4

User Scheduling and RRU Association under C-RAN Deployment

4.1 Introduction

In Chapter 3, we presented a system-wide global user scheduling problem to benchmark the performance of local user scheduling schemes on uplink and downlink, where the numerical results revealed that the user schedules obtained via solving the local problems were far from the globally optimal ones. Further, we found that ICI-coordination, which is possible only under a C-RAN setting, can be very helpful in improving the performance of these local schedulers. Note that the deployment of C-RANs has been taken as a norm for supporting complex interference scenarios, inter-cell coordination, and cooperative resource sharing. Unlike traditional networks, where each macro/micro cell performs baseband processing at a local site, a C-RAN co-locates all BBUs in a centralized pool. Whereas, each macro/micro cell is equipped with its own RRU that is connected to the BBU pool through a high-bandwidth and low-latency front-haul link.

Centralizing the baseband processing at the BBU pool yields numerous merits. Most importantly, it enables interference coordination that is essential for optimizing the performance of network processes like US and UA; since, the RRUs are in co-channel for accessing the underlying radio spectrum, the centralized BBU pool (with possibly a centralized controller) has to determine optimal RRU associations and user schedules, which are critical for the underlying network as they affect the overall network throughput. Further, with interference coordination, the distributed RRUs can cooperate flexibly and seamlessly to improve the instantaneous network throughput of the underlying radio network by reducing the inter/intra-cell interferences on both UL and DL. Besides this, the lightweight RRUs can be easily deployed and maintained in different types of cells while reducing the energy consumption of each site.

Our Objective:

In this chapter[1], we investigate a joint user scheduling (US) and user association (UA) process for OFDMA based radio networks under the C-RAN setting, where we shall focus on the performance of the radio link interfaces only, while leaving the problems emerging in the core network or the higher layer protocols as a future work. The C-RAN architecture is particularly important in terms of RRM, as it enables a joint management of the radio resources via the front-hauls yielding a potentially higher performance gain. However, the joint processing might lead to a high computational overhead in the BBU pool, especially, for large-scale networks, therefore, an efficient joint US and UA process has to be employed in order to achieve a reliable connection between the RRUs and the users.

In this context, our main goals for this chapter can be summarized as follows:

1. To formulate a joint US and UA process for a multi-cell network, while considering full inter-BBU coordination in order to find the maximum performance gains that could be achieved under the considered network setting. We attempt at solving the joint problem on both UL and DL for finding the optimal performance under a given set of MCSs with exact power allocations, channel gains, and intra/inter cell interferences.

[1]Some of the results in this chapter were published in [32].

2. To find an efficient quasi-optimal solution for the joint US and UA problem, for both UL and DL, and quantify the performance of UL-centric and DL-centric UA schemes.

4.1.1 Existing Literature on C-RANs

Most of the existing work on C-RANs has focused on minimizing the power consumption through coordinated scheduling [42–44]. These studies aim at minimizing the overall energy consumption of the C-RAN architecture subject to the users' data rate requirements without considering any specific MCS. Specifically, [42] analyzed a single massive macro cell without considering any inter-cell interference (ICI) and [44] assumed a number of uncoordinated CRANs surrounding the actual C-RAN under consideration, whereas a single-cell based heterogeneous C-RAN has been discussed in [45] without considering any ICI. A multi-RRU scheduler has been proposed in [43] for energy minimization in a C-RAN by compressing the precoded messages, where a flat ICI value has been considered within each cell; which is not practical, since, a higher ICI value would lead to lower throughput in each cell, while a lower value would result in packet losses.

A similar joint US and power adaptation problem for C-RANs has been solved for a single-cell in [46] by exploiting opportunistic network coding without MCS considerations. An interference-aware UA scheme for a heterogenous C-RAN has been investigated in [47], where the operation state of each BS is controlled by a central controller. The authors first proposed a UA problem which maximizes the users' aggregate utility, but due to high computational complexity of the problem, a distributed heuristic algorithm has been solved to obtain sub-optimal solutions.

To the best of our knowledge, the joint US and RRU association problem for OFDMA based C-RANs with multiple macro/micro cells has not been studied extensively, primarily due to the difficulty in evaluating the exact interference, which makes the problem computationally intractable. Computing exact ICI is difficult, but important as it critically determines SINR (for selecting an appropriate MCS), the RRU associations and scheduling decisions, and the transmit power level on UL/DL. We believe that without considering the exact interference the performance of the aforementioned US or UA schemes is questionable under a multi-cell setting as they might be far from the optimal one.

In this chapter, we propose and solve a joint US and UA problem to obtain globally optimal schedules via interference coordination, which is viable in a C-RAN setting with inter-BBU coordination, in order to benchmark the performance gains. Heuristic based solutions can then be determined to efficiently solve the joint US and UA problem within a C-RAN.

The rest of this chapter is organized as follows: we introduce our C-RAN model in Section 4.2. The joint US and UA problem and its corresponding upper bound problem is introduced in Section 4.3. The heuristic-based UL and DL solutions are presented in Section 4.4 and their efficacy is discussed in Section 4.5.

4.2 C-RAN Model

We consider a C-RAN that consists of a set of RRUs denoted by $\mathscr{R}$, placed at the local cell sites, and their corresponding BBUs (i.e., one for each RRU), that are placed in a centralized BBU pool. The RRUs are in co-channel with each other to serve a set of randomly distributed user equipments (UEs) that are equipped with omni-directional antennas with identical antenna gains and transmit power budget (P_{UE}), whereas all RRUs have unlimited fronthaul capacity with a given transmit power budget ($P_r, r \in \mathscr{R}$). To simplify our analysis, we assume that the RRUs and the users are equipped with single antenna each, although the proposed US and UA problems in this chapter can be extended to the case of multi-antenna RRUs.

4.2.1 Channel Model, SINR, and Link Layer Rates

In this chapter, we assume the same channel model as we did in Chapter 3, *i.e.*, by considering a *realization*-based approach; where, the duration of each realization (ω) was considered to be the same as that of a frame, which corresponds to a set of sub-channels and a set of time-slots, denoted by $\mathscr{C}$ and $\mathscr{T}$, respectively.

A realization ω is defined by a set of UEs who want to transmit or receive data during a frame[2]. For mathematical simplicity, we assume that during each realization the users are either transmitting on the UL or receiving on the DL. Consequently, each realization consists of either a set of UL users (denoted by $U_{UL}(\omega)$) or a set of DL users (denoted by $U_{DL}(\omega)$)[3]. The corresponding set of channel gains between all RRU and UE pairs are denoted by $\{G_{u,r}(\omega)\}$ for UL and $\{G_{r,d}(\omega)\}$ for DL, respectively. The UL SINR (on PRB (c,t)) from user u to RRU r is defined as follows:

$$\gamma_{u,r}^{c,t}(\omega) := \frac{P_{u,r}^{c,t} \times G_{u,r}(\omega)}{N_0 + I_{u,r}^{c,t}(\omega)}, \quad \forall u, \forall r, \forall c, \forall t \tag{4.1}$$

Similarly, the DL SINR on PRB (c,t) from RRU r to user d is defined as follows:

$$\gamma_{r,d}^{c,t}(\omega) := \frac{P_{r,d}^{c,t} \times G_{r,d}(\omega)}{N_0 + I_{r,d}^{c,t}(\omega)}, \quad \forall r, \forall d, \forall c, \forall t \tag{4.2}$$

Here, $P_{u,r}^{c,t}$ and $P_{r,d}^{c,t}$ are the transmit powers used by RRU r for user u on the UL and user d on the DL, respectively; $I_{u,r}^{c,t}$ is the UL interference on PRB (c,t) as seen by RRU r, and $I_{r,d}^{c,t}$ is the DL interference on PRB (c,t) as seen by user d when receiving data from RRU r. Whereas, N_0 is the average noise power that is constant for all PRBs of each RRU.

The UL interference for user u, when it is transmitting to RRU r, is defined as follows:

$$I_{u,r}^{c,t} := \sum_{r' \in \mathscr{R}}^{r' \neq r} \sum_{u' \in U_{UL}(\omega)}^{u' \neq u} P_{u',r'}^{c,t} G_{u',r}(\omega), \forall u, \forall r, \forall c, \forall t \tag{4.3}$$

Similarly, the DL interference for user u, when it is receiving from RRU r, is defined as follows:

$$I_{r,d}^{c,t} := \sum_{r' \in \mathscr{R}}^{r' \neq r} \sum_{d' \in U_{DL}(\omega)}^{d' \neq d} P_{r',d'}^{c,t} G_{r',d}(\omega), \forall r, \forall d, \forall c, \forall t \tag{4.4}$$

[2]We assume that all RRUs of the C-RAN are synchronized in terms of the UL and DL frames by using either TDD or FDD mode

[3]Without loss of generality, the users that are transmitting on both UL and DL can be considered as two separate users.

Due to high variation in channel gains, *rate adaptation* can be used to dynamically adjust the data rate of each user based on its exact SINR. The user schedulers that have been studied in the past make use of the classical Shannon's capacity (i.e., we denote it by $s(.)$) for approximating data rate on each PRB. However, such an approach does not directly translate into the set of achievable discrete rates under the given MCSs (as shown in Fig. 3.3). To overcome this deficiency, we consider a piece-wise discrete function $f(.)$ (as shown in Fig. 3.3) that corresponds to a set of MCSs denoted by $\mathscr{M}$ with pre-defined SINR thresholds (i.e., $\{\beta_m\}$ with $0 \leq m \leq |\mathscr{M}|$) for computing the appropriate coding efficiency (in bits per OFDM symbol).

The corresponding data rate (in bits per second) on each PRB can be computed as follows by using the exact SINR (γ), $f(\gamma)$, the total number of OFDM symbols (N_S), and the duration of each time-slot (T):

$$Rate(\gamma) := f(\gamma) \times \frac{N_S}{T} \tag{4.5}$$

The SINR remains constant within a PRB, therefore, the rate remains constant across all OFDM symbols of a PRB.

4.3 An Upper Bound for Joint US and UA Problem

We formulate an upper bound problem for the joint US and UA problem, similar to the one proposed in Section 3.4.1, by applying two smart transformations: (i) we use a continuous upper bound function $g(.)$ to envelop the piece-wise discrete function $f(.)$ (as shown in Fig. 3.3), whereby the binary variables for MCS allocation are no longer needed and (ii) we add new constraints to ensure that any pair of two users do not to transmit on the same PRB of an RRU and to ensure that a user do not transmit data to more than one RRUs on the same PRB.

The following optimization variables are required for the joint US and UA problem:

- $\boldsymbol{P}_{\boldsymbol{u,r}}^{\boldsymbol{c,t}}$ is for allocating UL power on PRB (c, t).
- $\boldsymbol{I}_{\boldsymbol{u,r}}^{\boldsymbol{c,t}}$ is for computing UL interference on PRB (c, t) at RRU r for user u.

- $\boldsymbol{\gamma_{u,r}^{c,t}}$ is for computing UL SINR on PRB(c,t) at RRU r for user u.
- $\boldsymbol{\lambda_{u,r}}$ is the total coding rate seen by user u from RRU r

4.3.1 The Upper Bound Problem

We use $g(.)$ as a reasonable upper bound on $f(.)$ (as shown in Fig. 3.3) for computing the coding efficiencies (CEs) as follow: $g(\gamma) = e^{(\log_{10}(e)\log_e(\gamma)}, \epsilon_\gamma \leq \gamma \leq \beta_{max}$, where ϵ_γ is a small positive value that acts as a lower bound and β_{max} acts as an upper bound on the SINR, respectively. Given the continuous rate function $g(.)$, we formulate the upper bound problem for joint US and UA on UL as follows; without loss of generality, a similar problem can be formulated for the DL:

$$\boldsymbol{P_{CRAN}^{UB-UL}(\omega)}: \underset{\{P_{u,r}^{c,t}\},\{I_{u,r}^{c,t}\},\{\gamma_{u,r}^{c,t}\},\{\lambda_{u,r}\}}{\text{maximize}} \sum_{u\in U_{UL}(\omega)} \log\Big(\sum_{r\in\mathscr{R}} \lambda_{u,r}\Big)$$

subject to (4.3) and :

$$\epsilon_p \leq P_{u,r}^{c,t} \leq P_{UE}, \qquad \forall u, \forall r, \forall c, \forall t \tag{4.6a}$$

$$\sum_{r\in\mathscr{R}}\sum_{c\in\mathscr{C}} P_{u,r}^{c,t} \leq P_{UE}, \qquad \forall u, \forall t \tag{4.6b}$$

$$P_{u,r}^{c,t} P_{u,r'}^{c,t} \leq \epsilon_p, \qquad \forall u, \forall r, \forall r', r' \neq r, \forall c, \forall t \tag{4.6c}$$

$$P_{u,r}^{c,t} P_{u',r}^{c,t} \leq \epsilon_p, \qquad \forall u, \forall u', u' \neq u, \forall r, \forall c, \forall t \tag{4.6d}$$

$$\epsilon_\gamma \leq \gamma_{u,r}^{c,t} \leq \beta_{max}, \qquad \forall u, \forall r, \forall c, \forall t \tag{4.6e}$$

$$P_{u,r}^{c,t} G_{u,r}(\omega) \geq \gamma_{u,r}^{c,t}\big(N_0 + I_{u,r}^{c,t}\big), \qquad \forall u, \forall r, \forall c, \forall t \tag{4.6f}$$

$$\lambda_{u,r} = \sum_{c\in\mathscr{C}}\sum_{t\in\mathscr{T}} g(\gamma_{u,r}^{c,t}), \qquad \forall u, \forall r \tag{4.6g}$$

where, $u \in U_{UL}(\omega), r \in \mathscr{R}, c \in \mathscr{C}, t \in \mathscr{T}$.

Here, the bilinear constraints (4.6c) ensure that a user cannot transmit to more than one RRUs on a given PRB, while, constraints (4.6d) ensure that on each PRB of an RRU atmost one user can transmit with a considerable amount of power; where, ϵ_p and ϵ_γ are very small positive values that depend on the numerical values of P_{UE} and $\gamma_{u,r}^{c,t}$,

respectively. The bilinear constraints (4.6f) are for computing SINR on each PRB, while the constraints (4.3) and (4.6g) are for computing the exact UL interference and the link layer rates, respectively. Note that this upper bound problem is non-linear and non-convex in nature, however, it can be transformed into an equivalent convex problem by using GP transformation [38]. To avoid verbosity, we omit the proof of GP transformation, which is similar to one discussed in Section 3.4.1. Further, the feasible solutions for the joint US and UA problem, with the original discrete rate function $f(.)$, are computed using a similar methodology as the one defined in Section 3.4.1.

4.4 A Heuristic for Joint US and UA Problem

The proposed joint US and UA problem can be solved in the scenario where a central controller in the BBU pool has the knowledge of the channel gains to/from all users and it has extensive computational resources. However, in practice the computational resources are limited thereby low complexity heuristics for both UL and DL users are required. Proposing heuristic based schedulers are not trivial, especially on the UL, since, the UL problem is more challenging than the DL; mainly because the UL interference pattern strongly depends on the scheduling decisions of the neighboring RRUs. A naive way for scheduling users would be to make the local US decisions on a per-RRU basis by assuming that the interference is fixed, but such an approach does not work well because the interference pattern can drastically change when a different user is scheduled on a PRB.

We propose simple heuristics for solving the joint US and UA problem, for UL as well as DL users, by dividing the joint problem into two smaller problems, namely *Local PRB Mapping Problem* and *Joint Power Allocation Problem*, which can be solved one after the other as follows:

- The **Local PRB Mapping Problem** computes the PRB mapping decisions on an individual RRU basis by assuming that the interference is fixed. More specifically, it determines the number of PRBs allocated to the users associated with each RRU without considering inter-BBU coordination. Once the number of PRBs for each local user has been computed, *PRB Mappings* are determined to find which PRBs

belong to a specific user, i.e., it determines the set $\{y_{u,r}^{c,t}(\omega)\}_{\forall u,\forall r,\forall c,\forall t}$, where $y_{u,r}^{c,t}(\omega) \leq z_{u,r}(\omega)$ and $y_{u,r}^{c,t}(\omega) = 1$ when user u has been allocated PRB(c,t) by RRU r and is 0 otherwise.

- The **Joint Power Allocation Problem** allocates appropriate power and MCS on each PRB based on the exact interference when the set of PRB Mappings, i.e., $\{y_{u,r}^{c,t}(\omega)\}$ is known. Since, we assumed fixed interference pattern while determining the local PRB mappings, the controller in the BBU pool needs to allocate appropriate power, based on the exact interference, by iterating between all PRBs.

Note that the exact interference can only be computed based on the full knowledge of the cross channel gains, power allocations, and channel allocations for all the users associated with other RRUs. Such dynamic system states can only be obtained via *inter-BBU coordination* under the C-RAN architecture; where, all BBUs are physically co-located and can share dynamic states with each other in real time. It is assumed that the local UAs for each RRU and the UL/DL channel gains for user are known to the controller in the BBU pool through inter-BBU coordination, given that each RRU/BBU pair is running a local UA process for computing $z_{u,r}(\omega)$ based on a local UA rule. The channel gains on UL/DL can then be computed locally at each RRU through the TDD or FDD protocol, however, the channel gains for computing exact interference are determined through explicit coordination between the BBUs, which has been discussed in [48] and [49].

4.4.1 Heuristic-based UL Scheduler

The proposed PRB mapping problem for each RRU should determine the number of PRBs allocated to the local users during time-slot t, which is denoted by $\boldsymbol{n_{u,r}^{t}}$. We use an interference *compensation factor* $(\hat{I})$ as an input parameter for computing the following *compensated rates*:

$$\hat{R}_{u,r}^{i}(\omega,\hat{I}) = i \times f\left(\frac{\frac{P_{UE}}{i} \times G_{u,r}(\omega)}{N_0 + \hat{I}}\right), \quad \forall u \in U_{UL_r}(\omega), \forall r \in \mathscr{R}, \forall i \in \{1,...,|\mathscr{C}|\} \tag{4.7}$$

Here, $U_{UL_r}(\omega)$ denotes the set of UL users associated with RRU r using a local UA rule. Note that the compensated rates in equation (4.7) are not the exact rates that nonetheless have to be computed with the exact interference. Moreover, equal power (EP) allocation has been used to pre-compute these rates for the local PRB mapping problem; whereas, the optimal power allocation on each PRB will vary with the exact ICI. We will show numerically in Section 4.5 that these compensated rates are far from the optimal, and as a result we need to solve a joint power allocation problem with inter-BBU coordination for optimizing the rates achieved by the local users of each RRU.

If the interference pattern is assumed to be fixed then the number of sub-channels allocated to the local users (i.e., $\boldsymbol{n^{*t}_{u,r}(\omega) \in \{1, ..., |\mathscr{C}|\}}$) can be determined beforehand by solving the sub-channel allocation problem (*i.e.*, $\boldsymbol{P^{UL}_{k}(\omega, \hat{I}_k)}$) from Section 3.5.1 for each RRU r when $\{z_{u,r}(\omega)\}$ are known. Once the number of PRBs ($n^{*t}_{u,r}(\omega)$) have been determined by solving $\boldsymbol{P^{UL}_{r}(\omega, \hat{I})}$ for each RRU, we compute the set of PRB mappings by randomly allocating the local PRBs to the local users, i.e., $\{y^{c,t}_{u,r}(\omega)\}$, where $\sum_{c=1}^{|\mathscr{C}|} y^{c,t}_{u,r}(\omega) = n^{*t}_{u,r}(\omega), \forall u, \forall r, \forall t$. The local PRB Mappings can be used for computing the initial power and MCS used by the UL users, however, this might result in PRB decoding errors with real interference.

Next, we propose a joint power allocation problem ($\boldsymbol{P^{UL}_{Joint}(\omega, c, t)}$), which yields the optimal power allocations on each PRB(c,t) when the set of PRB Mappings, i.e., $\{y^{c,t}_{u,r}(\omega)\}$ are given. This power allocation problem requires the knowledge of the channel gains from interfering users (i.e., $G_{u',r}(\omega)$) that can be computed at each BBU through the dedicated Sounding Reference Symbols (SRSs) within each PRB. However, this information needs to exchanged through the BBU pool controller for computing the optimal power and MCS on the PRBs of each RRU. The corresponding power allocation problem for PRB(c,t) on UL is defined as follows:

$$\boldsymbol{P^{UL}_{Joint}(\omega, c, t)}: \underset{\{x^{c,t,m}_{u,r}\},\{P^{c,t}_{u,r}\},\{I^{c,t}_{u,r}\},\{\lambda^{c,t}_{u,r}\}}{\text{maximize}} \sum_{u \in U_{UL}(\omega,c,t)} \log\left(\lambda^{c,t}_{u,r}\right)$$

subject to:

$$x^{c,t,m}_{u,r} \in \{0,1\}, \qquad \forall u, \forall r, \forall m \tag{4.8a}$$

$$\sum_{m \in \mathscr{M}} x^{c,t,m}_{u,r} \leq y^{c,t}_{u,r}(\omega) = 1, \qquad \forall u, \forall r \tag{4.8b}$$

$$0 \leq P^{c,t}_{u,r} \leq P^{EP}_{u,r}(\omega) + P^{unused}_{u,r}(\omega), \qquad \forall u, \forall r \tag{4.8c}$$

$$P^{c,t}_{u,r} G_{u,r}(\omega) \geq \beta_m (N_0 + I^{c,t}_{u,r}) - (1 - x^{c,t,m}_{u,r})\boldsymbol{M}, \forall u, \forall r, \forall m \tag{4.8d}$$

$$I^{c,t}_{u,r} = \sum_{r' \in \mathscr{R}}^{r' \neq r} \sum_{u' \in U_{UL}(\omega,c,t)}^{u' \neq u} (P^{c,t}_{u',r'} G_{u',r}(\omega)), \qquad \forall r \tag{4.8e}$$

$$\lambda^{c,t}_{u,r} = \sum_{m \in \mathscr{M}} x^{c,t,m}_{u,r} f(\beta_m), \qquad \forall u, \forall r \tag{4.8f}$$

where, $u \in U_{UL}(\omega, c, t)$, $r \in \mathscr{R}$, and $m \in \mathscr{M}$.

Here, $U_{UL}(\omega, c, t)$ denote the set of UL users that are mapped on PRB (c, t) by their respective RRUs with $|U_{UL}(\omega, c, t)| \leq |\mathscr{R}|$. We divide user u's power equally on each PRB allocated to u, i.e., $P^{EP}_{u,r}(\omega) := \frac{P_{UE}}{n^{*t}_{u,r}(\omega)}$. Since, the power budget is limited on the UL, we also add the unallocated power (i.e., $P^{unused}_{u,r}(\omega)$) that is carried forward from the previous PRBs for user u. The complete heuristic based UL scheduling problem has been summarized in Algorithm 2.

Lemma 4.1: *The problem* $\boldsymbol{P^{UL}_{Joint}(\omega, c, t)}$ *can be transformed into continuous and convex optimization problem using the continuous rate function* $g(.)$.

Proof: Please see Appendix D.

Algorithm 2 The Heuristic-based UL Scheduler

for each $r \in \mathscr{R}$ **do**
  Determine $z_{u,r}(\omega)$ for each user u.
  Solve $\boldsymbol{P_r^{UL}(\omega, \hat{I})}$ to find $n_{u,r}^{*t}(\omega)$.
  Randomly map users in $U_{UL_r}(\omega)$ to PRBs of RRU r.
  Compute $y_{u,r}^{c,t}(\omega)$ for all users in $U_{UL_r}(\omega)$.
  Compute $P_{u,r}^{EP}(\omega) := \frac{P_{UE}}{n_{u,r}^{*t}(\omega)}$ for all users in $U_{UL_r}(\omega)$.
end for
for each $t \in \mathscr{T}$ **do**
  $P_{u,r}^{unused}(\omega) \leftarrow 0$.
  for each $c \in \mathscr{C}$ **do**
    Determine $U_{UL}(\omega, c, t)$.
    Solve $\boldsymbol{P_{Joint}^{UL}(\omega, c, t)}$ to find $P_{u,r}^{*c,t}(\omega)$.
    $P_{u,r}^{unused}(\omega) \leftarrow P_{u,r}^{EP}(\omega) - P_{u,r}^{*c,t}(\omega) + P_{u,r}^{unused}(\omega)$
  end for
end for

4.4.2 Heuristic-based DL Scheduler

Different from the UL case, the local PRB mapping problem on the DL can be simplified by using equal power (EP) allocations per PRB, since, the interference on the DL is created by the RRUs whose positions are known and they transmit all the time [9]. The exact DL interference on each PRB, based on EP allocation can be pre-computed by user u as follows:

$$I_{r,d}^{EP}(\omega) := \sum_{r' \in \mathscr{R}}^{r' \neq r} \frac{P_r}{|\mathscr{C}|} \times G_{r',d}(\omega), \quad \forall r \in \mathscr{R}, \forall d \in U_{DL_r}(\omega) \tag{4.9}$$

The corresponding EP based compensated rates per-PRB can be computed as follows:

$$\hat{R}_{r,d}(\omega) = f\left(\frac{\frac{P_r}{|\mathscr{C}|} \times G_{r,d}(\omega)}{N_0 + I_{r,d}^{EP}(\omega)}\right), \quad \forall r \in \mathscr{R}, \forall d \in U_{DL_r}(\omega) \tag{4.10}$$

Here, $U_{DL_r}(\omega)$ denotes the set of DL users associated with RRU r using a local UA rule. Note that the compensated rates in equation (4.9) are also the exact rates, however, the equal power (EP) allocations have been used to pre-compute these rates for the local PRB mapping problem on the DL; whereas, the optimal power allocation on each PRB will vary with the exact ICI. We will show numerically in Section 4.5 that these compensated rates are far from the optimal, and as a result we need to solve a joint power allocation problem with inter-BBU coordination for optimizing the rates achieved by the local users of each RRU.

If we consider an EP-based interference pattern then we can determine the number of PRBs allocated to each local user during time-slot t (i.e., $\boldsymbol{n^{*t}_{r,d}} \in \{1, ..., |\mathscr{C}|\}$) by using the aforementioned compensated rates and solving the sub-channel allocation problem (*i.e.*, $\boldsymbol{P^{DL}_{k}(\omega, \{I^{EP}_{k,d}(\omega)\})}$) from Section 3.5.2 for each RRU r when $\{z_{r,d}(\omega)\}$ are given. Once the number of PRBs ($n^{*t}_{r,u}(\omega)$) have been determined by solving $\boldsymbol{P^{DL}_{r}(\omega, \{I^{EP}_{r,d}(\omega)\})}$, we randomly map the local users to the local PRBs and compute the resulting set of PRB mappings, i.e, $\{y^{c,t}_{r,d}(\omega)\}$, where $\sum_{c=1}^{|\mathscr{C}|} y^{c,t}_{r,d}(\omega) = n^{*t}_{r,d}(\omega), \forall r, \forall d, \forall t$.

Note that here the power on each sub-channel has been determined through an EP-based DL scheduler, whose performance can be further improved via optimal power allocation on each PRB. We will show numerically in Section 4.5 that the performance of this local scheduler is far from the optimal. As a counter measure, we need to solve a joint power allocation problem with inter-BBU coordination for optimizing the data rates while considering exact interference on the DL. However, the local PRB mappings can be used for computing the initial power and MCS used by the DL users.

Next, we propose a joint power allocation problem ($\boldsymbol{P^{DL}_{Joint}(\omega, c, t)}$), which yields the optimal power allocations on each PRB(c, t) when the set of PRB Mappings, i.e., $\{y^{c,t}_{r,d}(\omega)\}$ are given. This problem also requires the knowledge of the channel gains from interfering RRUs (i.e., $G_{r',d}(\omega)$) that can be shared by the local users through the dedicated DL control channels, which are available within each PRB. This information needs to be further exchanged with the BBU pool controller in order to compute the optimal power and MCS on each PRB.

The corresponding power allocation problem for PRB(c,t) is defined as follows:

$$\boldsymbol{P^{DL}_{Joint}(\omega,c,t)}: \underset{\{x^{c,t,m}_{r,d}\},\{P^{c,t}_{r,d}\},\{I^{c,t}_{r,d}\},\{\lambda^{c,t}_{r,d}\}}{\text{maximize}} \sum_{d\in U_{DL}(\omega,c,t)} \log\left(\lambda^{c,t}_{r,d}\right)$$

subject to:

$$x^{c,t,m}_{r,d} \in \{0,1\}, \qquad \forall r,\forall d,\forall m \tag{4.11a}$$

$$\sum_{m\in\mathscr{M}} x^{c,t,m}_{r,d} \leq y^{c,t}_{r,d}(\omega) = 1, \qquad \forall r,\forall d \tag{4.11b}$$

$$0 \leq P^{c,t}_{r,d} \leq P^{EP}_{RRU}, \qquad \forall r,\forall d \tag{4.11c}$$

$$P^{c,t}_{r,d}G_{r,d}(\omega) \geq \beta_m(N_0 + I^{c,t}_{r,d}) - (1-x^{c,t,m}_{r,d})\boldsymbol{M}, \forall r,\forall d,\forall m \tag{4.11d}$$

$$I^{c,t}_{r,d} = \sum_{r'\in\mathscr{R}}^{r'\neq r} \sum_{d'\in U_{DL}(\omega,c,t)}^{d'\neq d} (P^{c,t}_{r',d'}G_{r',d}(\omega)), \qquad \forall r,\forall d \tag{4.11e}$$

$$\lambda^{c,t}_{r,d} = \sum_{m\in\mathscr{M}} x^{c,t,m}_{r,d} f(\beta_m), \qquad \forall r,\forall d \tag{4.11f}$$

where, $r\in\mathscr{R}$, $d\in U_{DL}(\omega,c,t)$, and $m\in\mathscr{M}$.

Here, $U_{DL}(\omega,c,t)$ denotes the set of users that are mapped on PRB (c,t) by their respective RRUs on the DL with $|U_{DL}(\omega,c,t)| \leq |\mathscr{R}|$. Since the power budget on the DL is significantly larger than the UL, we divide an RRU's power equally on all PRBs, i.e., $P^{EP}_r := \frac{P_r}{|\mathscr{C}|}$, and solve the corresponding power allocation problem in parallel for each PRB(c,t). The proposed heuristic-based DL scheduler has been summarized using Algorithm 3.

Lemma 4.2: *The problem* $\boldsymbol{P^{DL}_{Joint}(\omega,c,t)}$ *can be transformed into continuous and convex optimization problem using the continuous rate function* $g(.)$.

Proof: The problem $\boldsymbol{P^{UL}_{Joint}(\omega,c,t)}$ has been transformed into a convex upper bound problem in Appendix D. A similar approach can be used to transform $\boldsymbol{P^{DL}_{Joint}(\omega,c,t)}$.

Algorithm 3 The Heuristic-based DL Scheduler

for each $r \in \mathscr{R}$ **do**
  Determine $z_{r,d}(\omega)$ for each user d.
  Compute $n^{*t}_{r,d}(\omega) := \frac{|\mathscr{C}|}{|U_{DL_r}(\omega)|}$ for all users in $U_{DL_r}(\omega)$.
  Randomly map users in $U_{DL_r}(\omega)$ to PRBs of RRU r.
  Compute $y^{c,t}_{r,d}(\omega)$ for all users in $U_{DL_r}(\omega)$.
  Compute $P^{EP}_r := \frac{P_r}{|\mathscr{C}|}$.
end for
for each PRB (c,t) **do**
  Determine $U_{DL}(\omega, c, t)$.
  Solve $\boldsymbol{P^{DL}_{Joint}(\omega, c, t)}$.
end for

4.4.3 Computational Complexity

The local PRB mapping problem for UL, i.e., $\boldsymbol{P^{UL}_r(\omega, \hat{I})}$ is an integer problem that can be solved quasi-optimally by using a heuristic based algorithm given in [11] with $\mathcal{O}(|U_{UL_r}(\omega)| \log(|U_{UL_r}(\omega)|) + |\mathscr{C}||U_{UL_r}(\omega)|)$. While, the local PRB mapping problem for DL, i.e., $\boldsymbol{P^{DL}_r(\omega, \{I^{EP}_{r,u}(\omega)\})}$, can be solved optimally by using equal sub-channel allocations. The joint power allocation problems for UL and DL, i.e, $\boldsymbol{P^{DL}_{Joint}(\omega, c, t)}$ and $\boldsymbol{P^{UL}_{Joint}(\omega, c, t)}$, respectively, are small sized mixed integer programs. They can be solved *exactly* to find the optimal power allocations, however, they are transformed into convex problems via the continuous rate function $g(.)$ as described in Lemma 4.1 and Lemma 4.2, respectively. Note that these continuous and convex optimization problems can be solved exactly through interior point methods with a polynomial time complexity [38] that increases linearly with the number of RRUs (since, $|U_{UL/DL}(\omega, c, t)| \leq |\mathscr{R}|$). The number of variables and constraints in the joint problem are equal to $2|\mathscr{R}|$ and $3|\mathscr{R}|$, respectively, therefore, the overall complexity of solving the joint power allocation problem is $\mathcal{O}\big(3|\mathscr{R}| \times (2|\mathscr{R}|)^3\big)$. In the event that the number of RRUs are not significantly large, the proposed heuristic based schedulers can be used for online user scheduling.

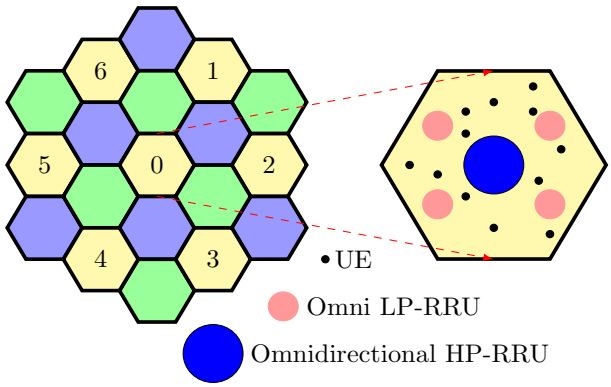

Figure 4.1: Macro cell layout 1

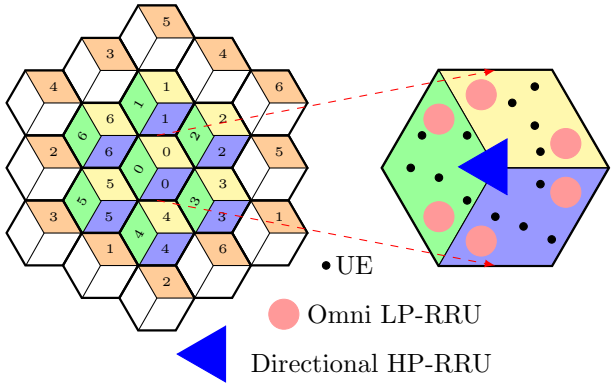

Figure 4.2: Macro cell layout 2

4.5 Performance Evaluation

We evaluate the performance of our proposed heuristic-based schedulers by considering two different layouts with multiple macro cells at an inter-site distance (ISD) of $500m$ (i.e., cell radius is $\frac{500}{\sqrt{3}}m$). Each macro cell, with one high-power (HP-RRU) and multiple low-power (LP-RRU) RRUs as shown in Fig. 4.1 and Fig. 4.2, is operating on OFDMA-based frames with $|\mathscr{C}| = 30$ sub-channels and $|\mathscr{T}| = 10$ time-slots.

The RRUs in the same-colored macro cells are in co-channel with each other, for simplicity, we consider the yellow colored macro cells only with a wrap-around technique to incorporate ICI for the macro cells at the edge (*i.e.*, these macro cells are colored in orange). Our physical layer parameters are based on the 3GPP evaluation document [5] for LTE, which are also summarized in Table 5.2. Note that the channel gains introduced in Section 4.2 account for path loss, slow fading, and antenna gains only, whereas the directivity gain (used for HP-RRUs in Layout 2 only) is a function of θ, i.e., the angle made by a user (UE) with the broadside direction of the RRU antenna. The slow fading coefficients are modeled by log-normal distribution with zero mean and standard deviation equal to σ.

We consider an adaptive MCS as given in [22] for computing exact link rates using the function $f(.)$ with $|\mathscr{M}|= 15$. The performance of the joint US and UA problem along with the proposed heuristic-based solution techniques have been studied for a set of 100 realizations (Ω); where, each $\omega \in \Omega$ corresponds to the duration of one frame and a set of $U_{UL}(\omega)$ UL users and $U_{DL}(\omega)$ users that are distributed uniformly across all cells. We consider the geometric mean (GM) throughput of these users, which is equivalent to maximizing our objective function, i.e., $\sum_{u\in U_{UL}(\omega)} \log\big(\sum_{r\in\mathscr{R}} \lambda_{u,r}\big)$ for UL and $\sum_{d\in U_{DL}(\omega)} \log\big(\sum_{r\in\mathscr{R}} \lambda_{r,d}\big)$ for DL.

The GM throughput (in bits per second) can be computed as follows:

$$\begin{aligned} GM^{UL}(\omega) &:= \Bigg(\prod_{u\in U_{UL}(\omega)} \Big(\sum_{r\in\mathscr{R}} \frac{\lambda_{u,r}\times N_S}{T\times|\mathscr{T}|}\Big)\Bigg)^{\frac{1}{|U_{UL}(\omega)|}} \\ GM^{DL}(\omega) &:= \Bigg(\prod_{d\in U_{DL}(\omega)} \Big(\sum_{r\in\mathscr{R}} \frac{\lambda_{r,d}\times N_S}{T\times|\mathscr{T}|}\Big)\Bigg)^{\frac{1}{|U_{DL}(\omega)|}} \end{aligned} \tag{4.12}$$

where, N_S and T are the total number of OFDM symbols in each PRB and the duration of each time-slot, respectively, for the given frame.

For each realization ω, the following performance measures have been defined for the UL, nonetheless, a similar set of performance measures can be defined for the DL:

- **The *Upper bound GM*** ($GM^{UL}_{UB}(\omega)$), can be computed by solving $\boldsymbol{P^{UB-UL}_{CRAN}(\omega)}$, after GP transformation, using any nonlinear programming solver like SNOPT [39].

Table 4.1: Physical Layer Parameters from [5]

N_S	12×14	T	1ms
Noise Power	-174dBm/Hz	Sub-channel Bandwidth	180KHz
Shadow Fading (σ)	8dB	Penetration Loss	20dB
Traffic Model	Full Buffer	Noise Figure	9dB
UE Antenna Gain	0dBi	LP-RRU Noise Figure	13dB
LP-RRU Antenna Gain	5dBi	HP-RRU Noise Figure	5dB
Layout 1: HP-RRU Antenna Gain		15dBi	
Layout 2: HP-RRU Antenna Gain		17dBi	
Layout 2: RRU Directivity Gain		$\min(12(\frac{\theta}{70^o})^2, 20)$dB	
Path Loss with HP-RRU (dB)		$128.1 + 37.6 \log_{10}(d/1000), d \geq 35m$	
Path Loss with LP-RRU (dB)		$140.7 + 36.7 \log_{10}(d/1000), d \geq 10m$	
P_{UE}	24dBm	P_{LP-RRU}	30dBm
Layout 1: $1 \times P_{HP-RRU}$		46dBm	
Layout 2: $3 \times P_{HP-RRU}$		46dBm	

- **The *Feasible GM*** ($GM^{UL}_{FS}(\omega)$), for the joint US and UA problem considering the actual discrete rate function $f(.)$ [4], can be computed from the upper bound solutions by using a simple method that has been discussed in Algorithm 1.
- **The *Heuristic GM*** ($GM^{UL}_{HS}(\omega)$) can be computed by using the method discussed in Algorithm 2 with any integer programming solver, such as, SCIP [40].

4.5.1 Scenario 1: Joint US and UA for HP-RRUs Only

High-power RRUs generate significant interference for each other, even when they are placed significantly farther from each other, therefore, usually they are placed in separate

[4] To avoid verbosity, we have not defined the original joint US and UA problem in this chapter. However, a similar problem has been defined in Section 3.4.

macro cells. For the sake of simplicity, first we compare the performance of our heuristic-based solutions with HP-RRUs only. In this homogeneous network, the UA (also known as cell association, since, there is only one RRU per cell) is not as critical as in HetNets, since, it can be based on maximum SINR-based rules, where a user upon arrival associates with the BS who offers the highest UL/DL SINR. We assumed the following maximum SINR-based UL-centric and DL-centric cell association rules for our heuristic-based UL and DL schedulers:

$$\begin{aligned} z_{u,r}(\omega) &= \underset{r}{\text{argmax}}\left(\frac{P_{UE} \times G_{u,r}(\omega)}{N_0 + \hat{ICI}_{worst}}\right), \quad \forall u \in U_{UL}(\omega) \\ z_{r,d}(\omega) &= \underset{r}{\text{argmax}}\left(\frac{\frac{P_r}{|\mathscr{C}|} \times G_{r,d}(\omega)}{N_0 + ICI^{EP}_{r,d}(\omega)}\right), \quad \forall d \in U_{DL}(\omega) \end{aligned} \tag{4.13}$$

here, a worst-case ICI (from the users in interfering cells) and an EP-based ICI (from the RRUs in interfering cells) has been used on the UL and the DL, respectively. We studied the performance of the DL-centric rules on the UL and vice versa, by assuming a TDD based setting, where the UL and DL channel gains could be assumed similar due to channel reciprocity conditions. However, we found no significant difference in UL/DL performance.

For completeness, we compare the difference in performance when there is no inter-BBU coordination, which is the case when these HP-RRUs have to perform local scheduling on the UL and DL, while estimating/measuring ICI from other macro cells. The exact ICI cannot be measured by the local schedulers on the UL, hence they need to estimate it as closely as possible for computing the corresponding *Effective GM* (i.e., with $\hat{I}$ as discussed in Section 3.5.1). Similarly, the Effective GM on the DL is computed using the local DL scheduler, which was discussed in Section 3.5.2. It can be seen in Fig. 4.3(a) and 4.3(c) that these local schedules, obtained after choosing proper $\hat{ICI}$, are still far from the optimal. In Fig. 4.3(b) and 4.3(d), it can be seen that the EP based local schedules on the DL are also far from the optimal one with an average gap between 30% to 50%.

The average gap between GM^{UB} and GM^{FS} is quite small for both layouts as shown in Fig. 4.3, which validates our assumption that the local schedulers can benefit from ICI-coordination in a C-RAN setting. For cell layout 1, the average gap between GM^{FS} and GM^{HS} is almost negligible as the frequency re-use factor is 3, that leads to lower ICI,

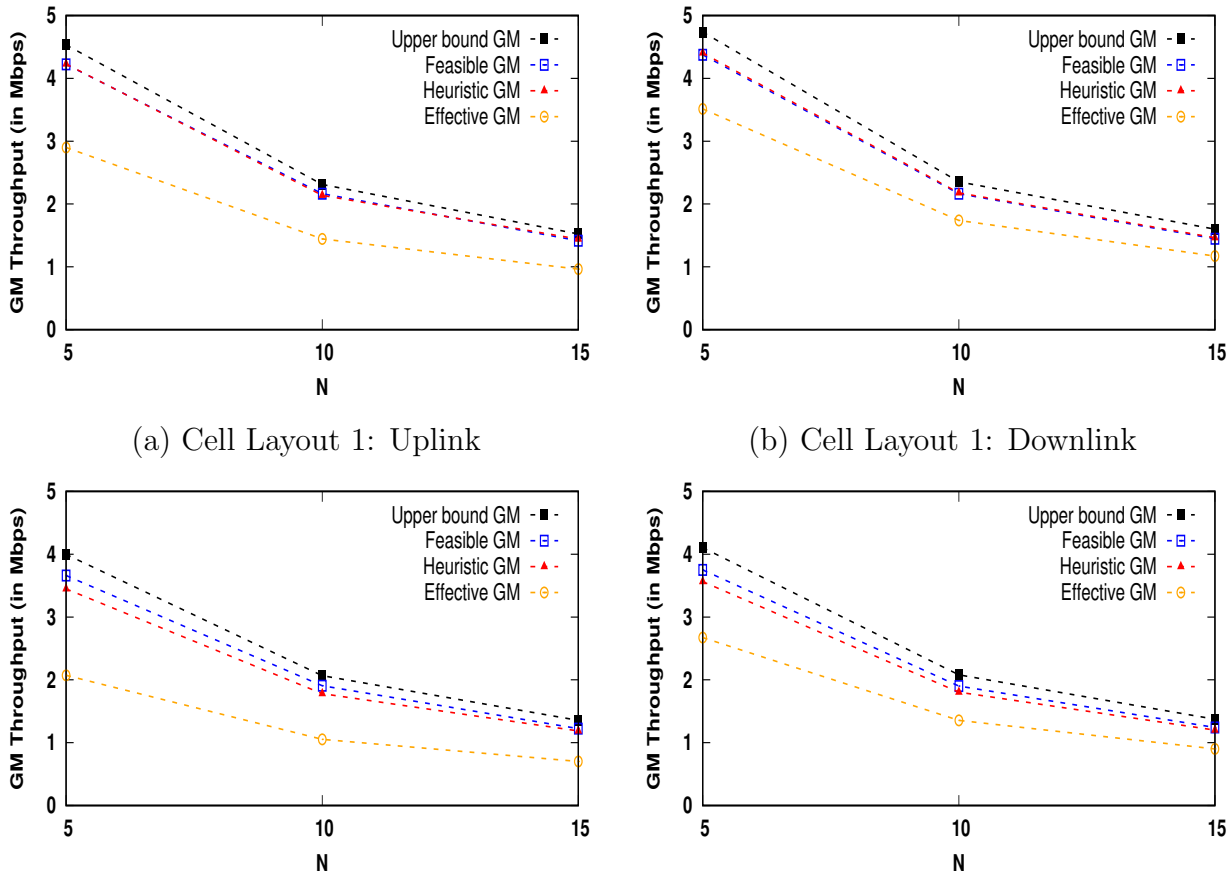

(a) Cell Layout 1: Uplink

(b) Cell Layout 1: Downlink

(c) Cell Layout 2: Uplink

(d) Cell Layout 2: Downlink

Figure 4.3: Scenario 1: Average GM throughput over Ω vs. the average number of users in each macro cell $\left(N = \frac{|U_{UL}(\omega)|}{|\mathscr{R}|} or \frac{|U_{DL}(\omega)|}{|\mathscr{R}|}\right)$.

whereas in cell layout 2 the frequency re-use factor of 1 results in higher ICI, consequently, the average gap between GM^{UB} and GM^{HS} is higher than the one between GM^{UB} and GM^{FS}. This is due to the fact that the proposed heuristics compute PRB mappings at the local RRUs without knowing exact ICI; where, a fixed ICI compensation factor ($\hat{ICI}$) is used for all realizations on the UL and an equal power based ICI (*i.e.*, $ICI_{r,d}^{EP}(\omega)$) has been used for all realizations on the DL.

4.5.2 Scenario 2: Joint US and UA in a Single Macro Cell with One HP-RRU and Multiple LP-RRUs

We also consider the scenario of a single macro cell based C-RAN, where one HP-RRU is placed in the middle with a few LP-RRUs around it, which are in co-channel with the HP-RRU. The interfering macro cells are assumed to be operating independently without any coordination, therefore, the local schedulers on both UL and DL have to estimate ICI generated by the LP-RRUs as well as the HP-RRUs from the neighboring macro cells. The exact ICI cannot be measured by the local schedulers on the UL, hence, we consider a worst case ICI estimate (i.e., $\hat{ICI}_{worst}$ at each RRU) from the users associated with other RRUs in the interfering macro cells; this is necessary to avoid packet losses and also to reduce the complexity of the joint US and UA problem. An equal power (EP) based DL ICI (i.e., $ICI_{r,d}^{EP}(\omega)$) has been considered from the RRUs of the interfering macro cells. We use a fixed estimate of intra-cell UL interference ($\hat{I}$) from the users in the same macro cell and an EP based intra-cell DL interference (i.e., $I_{r,d}^{EP}(\omega)$) from other RRUs within the macro cell under consideration. The local UL-centric and DL-centric UA rules for the heuristic-based schedulers are defined as follows:

$$\begin{aligned} z_{u,r}(\omega) &= \underset{r}{\operatorname{argmax}}\left(\frac{P_{UE} \times G_{u,r}(\omega)}{N_0 + \hat{I} + \hat{ICI}_{worst}}\right), && \forall u \in U_{UL}(\omega) \\ z_{r,d}(\omega) &= \underset{r}{\operatorname{argmax}}\left(\frac{\frac{P_r}{|\mathscr{C}|} \times G_{r,d}(\omega)}{N_0 + I_{r,d}^{EP}(\omega) + ICI_{r,d}^{EP}(\omega)}\right), && \forall d \in U_{DL}(\omega) \end{aligned} \tag{4.14}$$

Note that the optimal GM throughput lies between GM^{UB} and GM^{FS}, which is shown in Fig. 4.4 for both layouts under the heterogeneous C-RAN setting (i.e., Scenario 2). Our heuristic based algorithm, i.e., denoted by GM^{HS}, performs better than GM^{FS} in almost all of the network realizations. The performance of GM^{HS} can be further improved by using multi-RRU association (also known as dual connectivity), which accounts for the large gap between GM^{UB} and GM^{HS} with lower number of users (i.e., $N = 5$). Specifically, the UL performance can be further improved by exploiting multi-user association as the intra-cell interference is lower as compared to the case of DL. We also see that the DL-centric UA rules are sub-optimal for the UL performance and vice versa, when UL and DL channel gains are similar, which is indeed the case in TDD-based systems.

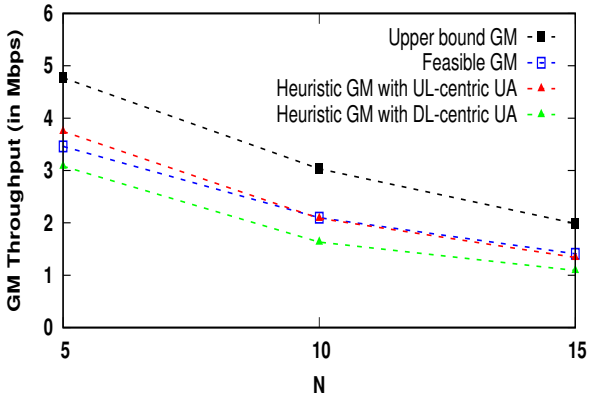

(a) Cell Layout 1: Uplink

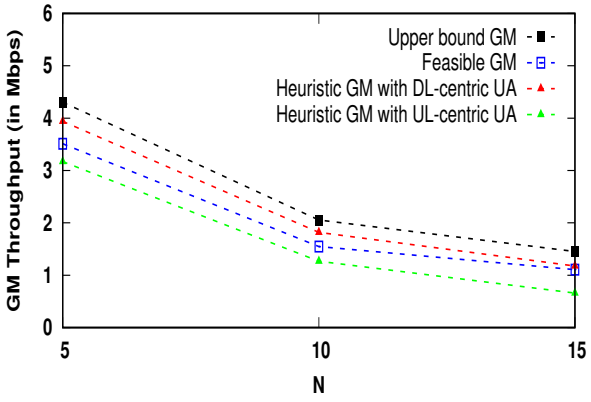

(b) Cell Layout 1: Downlink

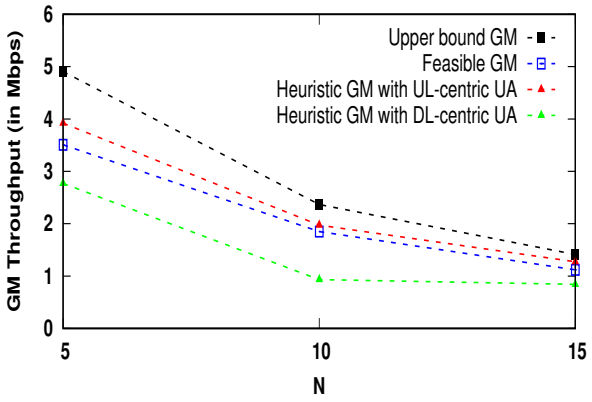

(c) Cell Layout 2: Uplink

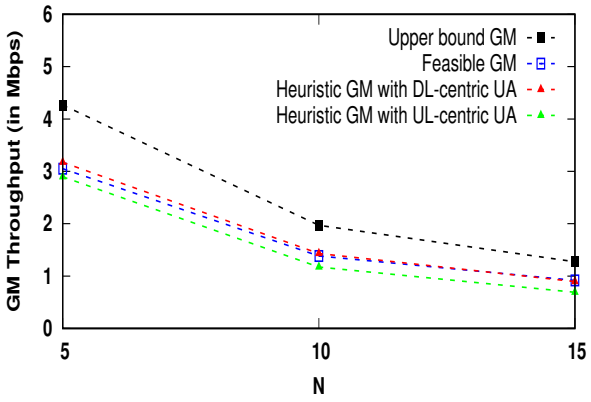

(d) Cell Layout 2: Downlink

Figure 4.4: Scenario 2: Average GM throughput over Ω vs the number of users in the macro cell.

4.6 Conclusions

In this chapter, we investigated the joint user scheduling (US) and user association (UA) problem for OFDMA based networks, which is nonetheless computationally intractable in its exact form. We transformed this problem into a corresponding upper bound problem with the help of a novel continuous rate function. The resulting problem could be solved efficiently in a C-RAN setting with inter-BBU coordination, after converting it into an equivalent convex optimization problem via geometric programming (GP). Furthermore, the solutions of the upper bound problem were mapped into the solution space of the original joint US and UA problem with a small gap. As a practically implementable solution to the original problem, heuristic-based schedulers were proposed to obtain quasi-optimal UA and US solutions for both uplink (UL) and downlink (DL) transmissions with decoupled UL-centric and DL-centric local UA rules, respectively. Extensive numerical simulations were conducted to verify the performance of the proposed heuristic based schedulers, which can achieve very close performance to the benchmark derived by solving the upper bound problem for either a homogeneous or a heterogeneous C-RAN. Our results for homogenous C-RAN demonstrate the performance gains for the local schedulers (one per RRU) through inter-BBU-coordination.

Chapter 5

Resource Allocation for Flexible HetNets

5.1 Introduction

In Chapter 4, we presented a joint US and UA problem along with its heuristic based quasi-optimal solution, which can be obtained under a CRAN setting. Further, we assumed that the RRUs in the underlying C-RAN are synchronized in terms of their UL and DL frames by using either TDD or FDD mode of transmission; where, the RRUs were in co-channel (*i.e.*, CCD) with each other for accessing the underlying spectrum. Under these assumptions, the joint US and UA problems for UL and DL can be decoupled into two problems. This is indeed true for conventional cellular networks, which were initially deployed for fixed and symmetric bandwidth requirements. Note that in these conventional networks the sub-channel allocations are statically provisioned across multiple cells, for the UL and the DL traffic, consequently, the sub-channels could only be allocated using either static FDD or static TDD based spectrum sharing techniques.

With the emergence of new mobile applications and Internet usage scenarios, such as, the ones that have emerged with interactive gaming, social media, cloud storage, and, nonetheless, with IoT, it is expected that the traffic demands on both UL and DL will

vary significantly from one macro/small cell to another and these asymmetries will further increase in the future [1, 2]. It is anticipated that during a short span of time the DL traffic volume would be several times larger than that of the UL and vice versa [4]. As a countermeasure, flexible spectrum sharing techniques have been advocated recently to meet the asymmetric bandwidth demands on the UL and DL of OFDMA-based networks. Specifically, flexible duplexing has been considered as a new promising technique to improve the spectral efficiency of the underlying network by handling asymmetric UL and DL traffic flows flexibly, unlike TDD and FDD that requires fixed time or frequency splitting between UL and DL.

Flexible spectrum sharing is indeed becoming more viable with time as many network operators have both unpaired as well as paired spectrum, therefore, an ability to aggregate the two types of spectrum could bring a number of potential benefits. For example, TDD spectrum could be used to supplement FDD spectrum to provide additional throughput and capacity on the DL. Conversely, FDD spectrum, which is generally at lower frequencies than TDD spectrum, could be used to achieve greater range on a TDD UL, which is often the limiting factor for TDD coverage. Further, the static spectrum sharing techniques do not consider a scenario common in today's cellular networks, in which a macro cell may support multiple DL and UL FDD carriers due to exploding wireless traffic. With a paired UL carrier for each DL carrier, the FDD spectrum has symmetric time/frequency resources that are not well suited for asymmetric traffic scenarios, in such cases, it is beneficial to serve DL traffic on a subset of the FDD UL carriers and vice versa.

Our Objective:

Apparently, it seems simple to share the underlying communication channel flexibly as and when needed, however, the flexible spectrum sharing techniques yield numerous technical challenges notably for multi-tier networks[1] due to the presence of inter-tier interference. Traditionally, with static FDD/TDD based spectrum sharing techniques, the RA process between multiple tiers was simple; due to the lack of inter-tier interference, it was decoupled

[1]We use the term multi-tier network for generalization, in which case a network could either be homogeneous or heterogeneous. However, in this chapter, we discuss the case of a HetNet only.

into two separate RA schemes, i.e., one for the DL and the other one for the UL. With the growing interest in flexible duplexing for allocating asymmetric time/frequency resources, depending on the statistics of the prevailing traffic in each macro cell, there is a need to analyze the jointly optimal RA schemes, for UL and DL, that would essentially minimize the inter-tier interference across the entire network in order to maximize the network-wide throughput gains.

In this chapter[2], we investigate the benefits of flexible duplexing after being motivated by its potential gains. We study and analyze the joint RA and US problem for a multi-tier multi-cell network from a link-layer's perspective only. The main purpose is to benchmark the performance gains that should be expected from flexible HetNets, which has not been done yet due to the complexity of coordination between different macro cells for interference mitigation. Our main contributions in this chapter can be summarized as follows:

1. We propose a reasonable benchmark for flexible FDD/TDD based multi-cell multi-tier networks by jointly optimizing the RA and US process across multiple macro cells. The joint problem provides proportional fairness by maximizing the sum of the logarithm of the achievable rates on both UL and DL while provisioning asymmetric traffic flows, DUD, and multiple BS associations.

2. The complicated UL-to-DL and DL-to-UL interference scenarios yield additional integer variables, which make the joint RA and US problem a large scale Mixed Integer Non-Linear Programming (MINLP) problem that is also non-convex in nature. However, we are interested in solving this problem to deal with the interferences exactly and also to compute a reasonable off-line benchmark. Therefore, we formulate a large scale convex upper bound problem by replacing these integer variables through a smart transformation that can only be solved off-line.

3. The benchmark problem is used as a framework for solving the joint RA and US problems in Reverse-FDD and Static FDD based HetNets, where extensive numerical results are obtained for the benchmark problem and compared with that of the existing RA schemes.

[2]Some of the results presented in this chapter have been submitted to IEEE Transactions [50].

5.1.1 Related Work

For multi-tier networks, small-cell (SC) deployments have been identified as a primary means to enhance network capacity and to address the asymmetric traffic issue by using flexible FDD/TDD[3] for SCs [51]; mainly, because, the coverage areas are smaller (in SCs) and the SC tiers do not cause significant interference to the nearby SCs when placed at the right distance. Based on this decoupling, cell-specific TDD pattern selection became feasible through ICI coordination between the SC tiers [52–54], as there are relatively fewer UEs associated with each SC, thus, the changes in the traffic could be dealt at a faster time scale, thereby, increasing the potential benefit of flexible TDD. Although, this scheme appears to be very attractive considering the typically small number of simultaneously active UEs in a SC, its efficacy has been studied in [52, 54] within a limited environment only, i.e., with only SC tiers. Note that the SCs cannot provide coverage to a large number of users and reducing their inter-site distances would lead to an increase in inter-SC interference. Hence, the macro-BSs (MBSs) need to be co-located and connected with a sparse number of SCs for providing coverage and backhaul connectivity in flexible FDD/TDD based networks. Nonetheless, there is a need to study the efficacy of using flexible FDD/TDD in such a network where MBSs are sharing the time/frequency resources along with the SCs. The resulting trade-off needs to be analyzed carefully as the UL SINR, under PSD or CCD, suffer significantly from severe performance degradation due to the strong DL-to-UL interference from an MBS to a SC tier and vice versa.

Motivated by the promising benefits of dynamic TDD, the authors in [53] have investigated the technical implementation issues for applying dynamic TDD in homogeneous SC networks and the feasibility of introducing dynamic TDD in HetNets; where, the users are associated using different cell range expansion (CRE) biases and almost blank subframe (ABS) has been used as a given RA scheme to study the efficacy of the proposed traffic-adaptive DL and UL schedulers. It was shown that SC-DL to MBS-UL interference cancellation is indispensable for the macro cells to achieve reasonable UL performance. Moreover, it has been noted that the DL-to-UL interference cancellation in the SC tier is required to mitigate the inter-link interference among SCs, particularly when the traffic

[3]We use the terms "flexible FDD/TDD" and "dynamic FDD/TDD" interchangeably.

load is medium or high. Nonetheless, the performance of the proposed schedulers has been benchmarked using system-level simulations for a few RA schemes, whose performance might not be close to the globally optimal one.

A joint UL and DL user association problem with provisioning for decoupled associations (DUD) has been proposed in [55] for a single macro cell based flexible FDD HetNet that maximizes the sum-rate of all users on the UL as well as the DL, thus it does not guarantee fairness. Due to complicated UL-to-DL and DL-to-UL interferences and integer optimization variables, the formulated problem has been relaxed and the intra-tier interferences have been estimated to convert the problem into a convex GP problem under high SINR assumptions. Similarly, a joint load balancing and interference mitigation problem in FD based HetNets, subject to wireless backhaul constraints, has been studied in [56] for a single macro cell.

The feasibility of a multi-cell flexible FDD based HetNet has been studied in [57, 58], where it has been shown that the inter-tier interference may be mitigated with DL power management, antenna tilt, and link-layer based interference cancellation. Some factors, such as, limitations in the RA granularity and the constraints to avoid full duplex challenge, were reported that could prevent ideal fairness, nevertheless, the potential performance improvements were shown to be significant. In contrast, a multi-cell homogeneous network has been considered in [59], where the available resources per cell and per TDD frame are freely allocated to both UL and DL transmission depending on traffic demand and user distribution within the network. The numerical results demonstrate significant gains with dynamic UL/DL mode selection as compared to the conventional TDD with fixed mode assignment.

In this chapter, we also consider the performance of a potential RA scheme, i.e., *Reverse FDD* (R-FDD), that is similar to the reverse mode in TDD (also known as R-TDD). R-TDD has been proposed in the past, mainly for enhancing spectrum sharing within a HetNet by deliberately introducing inter-tier interference between an MBS and its SC tiers; where, the MBS is in the DL mode of transmission when the SCs are operating on the UL and vice versa. In addition, it also leverages the channel reciprocity of the TDD protocol for providing an implicit coordination between the two tiers without the need of exchanging the channel state information (CSI).

The authors in [60] analyzed the performance of R-TDD using one macro cell with one MBS and numerous SCs. They considered a simple and coupled user association rule (CUD); where, the low mobility UEs were associated with the SCs, while those with medium-to-high mobility were served by the MBS. This study has been limited to static spectrum sharing schemes only with a single cell analysis. We want to study Reverse FDD as a potential RA scheme for flexible FDD networks as the underlying complex interference scenarios in R-FDD and R-TDD are quite similar to the case of flexible FDD and TDD, respectively.

The rest of this chapter is organized as follows: We discuss the RA process and our system model in Section 5.1.2 and 5.2. The joint RA and US problem along with its relaxed upper bound problem has been formulated in Section 5.3. We formulate a similar problem for some existing RA schemes in Section 5.4. The numerical results are presented in Section 5.5.

5.1.2 Resource Allocation with OFDMA

Resource allocation (RA) is a fundamental process for allocating different resources to different BSs in a multi-tier network. In OFDMA based networks, these resources are referred to as a set of OFDM symbols that are grouped together to constitute *sub-channels* in the frequency-domain and *time-slots* in the time-domain; where, one sub-channel in a given time-slot is known as a physical resource blocks (PRB)[4]. RA in OFDMA based networks is performed on a per *frame* basis after optimizing one or more RA parameters; where, each frame is composed of multiple PRBs and a subset of these PRBs, based on a RA parameter, are allocated to a BS that can be fully (CCD) or partially (PSD) or non overlapping (OD) with the subsets allocated to other BSs. In PSD, power on the shared sub-channels is another RA parameter that needs to be optimized. Once the PRBs are allocated to the BSs, they can schedule their users on the subsets of PRBs that are allocated to them through a user scheduler.

[4]Note that the use of TDD in flexible FDD allows the RA scheme to match the resources to either UL or DL at a finer granularity, since, it can occur at the PRB level as opposed to the sub-channel level for flexible FDD without TDD.

The RA process in a macro cell along with the underlying scheduler is simplified under static FDD or TDD based spectrum sharing techniques, because the interfering macro cells are synchronized, therefore, the RA/US process can be decoupled into UL-only and DL-only processes. Nonetheless, the decoupled RA/US schemes based on either UL-only or DL-only traffic cannot be extended for flexible FDD or TDD based networks, where the ratio of UL to DL traffic can vary significantly from one cell to another. Note that for static spectrum sharing the RA process can be further decoupled into local RA processes (one per macro cell) under certain conditions on the US process, for example, by estimating interference exactly. This has been discussed in [9] for the case of DL. In contrast, the RA process on the UL has not been studied explicitly, however, it can also be decoupled into local RA processes by using a local US process with interference estimation at the cost of significant performance degradations.

Ideally, each macro cell should be able to employ flexible duplexing by matching time/frequency resources, locally and independently, according to the prevailing traffic. Nonetheless, this is possible only if the interference from other cells could be measured exactly. In practice, this interference cannot be measured exactly, but it can be estimated beforehand to design local US schemes that are far from the optimal. Since, the multi-cell multi-tier networks are inherently limited by intra-cell and inter-cell interference, a local RA scheme in a macro cell, based on its local performance with an estimate on inter-cell interference, might not be optimal for the entire network consisting of multiple macro cells operating on the same spectrum.

The main purpose of this chapter is to provide a benchmark for RA for multi-cell multi-tier networks by jointly optimizing the RA process for different UL and DL traffic scenarios. Note that achieving optimal performance in such networks is not trivial, but necessary to benchmark the performance of different RA schemes and a comparative study in this context is also important, because it provides valuable insights on full duplex (FD) transmission, which has been identified as one of the candidate technologies for 5G; where, a BS can simultaneously transmit to and receive from different user equipments (UEs), thus enhancing spectrum reuse, but creating (i) *inter-cell inter-link interference*, (ii) *intra-cell inter-link interference*, and (iii) *self-interference*. Note that the main difference between FD and flexible FDD is that self-interference does not exist in the later one.

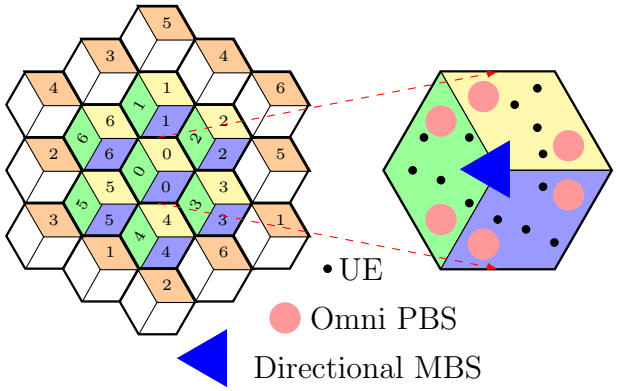

Figure 5.1: A multi-cell heterogeneous network (HetNet).

5.2 System Model

We consider a HetNet (as shown in Fig. 5.1) with a set of macro cells denoted by $\mathscr{K}$, which are using the same frequency spectrum and represented by yellow color. Note that in order to incorporate interference for the macro cells that are on the edge of the HetNet, we take a wrap-around technique which is recommended by 3GPP [36]; where, the adjacent macro cells that are operating on the same frequency band are filled with orange color. Each macro cell in $\mathscr{K}$ has one MBS and two outdoor pico-BSs (PBS), thus, altogether they constitute a set of BSs denoted by $\mathscr{B}$. These macro cells are operating on a set of sub-channels to serve a set of randomly distributed users with omni-directional antennas, identical antenna gains, and similar transmit power budgets (i.e., P_{UE}). All MBSs have tri-directional antennas with identical transmit power budgets (i.e., P_{MBS}) and unlimited back-haul capacities, whereas, all PBSs have omni-directional antennas with identical transmit power budgets (i.e., P_{PBS}) and unlimited front-haul capacities.

5.2.1 Channel Model, SINR, and Link Layer Rates

We study the joint RA and US process on a per frame basis by using a *realization*-based approach [37], where the duration of each realization (ω) is same as that of a frame. Recall that each frame corresponds to a set of sub-channels ($\mathscr{C}$) and time-slots ($\mathscr{T}$).

A realization ω is defined by a set of users (i.e., denoted by $U(\omega)$) and their channel gains. For mathematical simplicity, we assume that during each realization a user is either transmitting on the UL or receiving on the DL; without loss of generality, the users that are transmitting on both UL and DL can be considered as two separate users, consequently, $U(\omega)$ can be divided into a set of UL users (denoted by $U_{UL}(\omega)$) and a set of DL users (denoted by $U_{DL}(\omega)$).

Remark 5.1: *We assume that the user associations are under the DUD scenario, where a user can associate with different BS(s) on the UL as on the DL. In [55], DUD has been studied for flexible FDD based networks and it has been shown to perform better than the coupled UL and DL user association rules.*

Remark 5.2: *We consider a single half-duplex channel for both UL and DL transmissions; where, a BS can only serve one DL user at a given time (or PRB), similarly, an UL user can only transmit to one BS at a given time (or PRB). This is necessary to avoid self-interference scenarios.*

We define the following channel gains for this chapter that are also listed in Table 1:

1. A set of channel gains between the UL users and BSs, i.e., denoted by $\{G_{u,k,b}(\omega)\}_{u\in U_{UL}(\omega),k\in\mathscr{K},b\in\mathscr{B}}$; this set is required for the traditional UL channel gains or interference from UL users as seen by the BS (k,b).

2. A set of channel gains between the BSs and the DL users, denoted by $\{G_{k,b,d}(\omega)\}_{k\in\mathscr{K},b\in\mathscr{B},d\in U_{DL}(\omega)}$; this set is required for the traditional DL channel gains or interference from the BSs as seen by the DL user d.

3. A set of channel gains between different BSs, denoted by $\{G_{k',b',k,b}(\omega)\}_{k'\in\mathscr{K},b'\in\mathscr{B},k\in\mathscr{K},b\in\mathscr{B}}$; this set is required for the new DL-to-UL interference from other BSs as seen by the BS (k,b).

4. A set of channel gains between the UL and DL users, denoted by $\{G_{u,d}(\omega)\}_{u\in U_{UL}(\omega),d\in U_{DL}(\omega)}$; this set is required for the new UL-to-DL interference from UL users as seen by the DL UE d.

Table 5.1: List of Notations

Notation	Description
$\boldsymbol{G_{u,k,b}}$	Channel gain from UL user u to BS (k,b).
$\boldsymbol{G_{k,b,d}}$	Channel gain from BS (k,b) to DL user d.
$\boldsymbol{G_{k',b',k,b}}$	Channel gain from BS (k',b') to BS (k,b).
$\boldsymbol{G_{u,d}}$	Channel gain from UL user u to DL user d.
$\boldsymbol{P^{c,t}_{u,k,b}}$	Power on PRB (c,t) used by UL user u for BS (k,b).
$\boldsymbol{P^{c,t}_{k,d,b}}$	Power on PRB (c,t) used by BS (k,b) for DL user d.
$\boldsymbol{P_b}$	Total power budget for BS $b \in \mathscr{B}$, which is equal to P_{MBS} for all MBSs and P_{PBS} for all PBSs.
$\boldsymbol{I^{c,t}_{k,b}}$	UL interference seen by BS (k,b) on PRB (c,t).
$\boldsymbol{I^{c,t}_{d}}$	DL interference seen by the DL user d on PRB (c,t).
$\boldsymbol{\gamma^{c,t}_{u,k,b}}$	UL SINR on PRB (c,t) from UL user u to BS (k,b).
$\boldsymbol{\gamma^{c,t}_{k,b,d}}$	DL SINR on PRB (c,t) from BS (k,b) to user d.
$\boldsymbol{\lambda_{u,k}}$	Sum of CEs for UL user u from cell k.
$\boldsymbol{\lambda_{k,d}}$	Sum of CEs for DL user d from cell k.

Note that all channel gains listed in Table 5.1 depend on the location of the user/BS resulting in a path-loss, a large-scale slow fading coefficient (chosen at random) that remains constant during a frame, and a small-scale fast fading coefficient (chosen at random) that remains constant over each sub-channel of the given frame; we assume that the underlying radio channel exhibits large-scale slow fading as well as small-scale fast fading characteristics with coherence time greater than the duration of one frame:

$$\begin{aligned} G^{c}_{u,k,b}(\omega) &= G^{c,t}_{u,k,b}(\omega), \forall u, \forall k, \forall b, \forall c, \forall t \\ G^{c}_{k,b,d}(\omega) &= G^{c,t}_{k,b,d}(\omega), \forall d, \forall k, \forall b, \forall c, \forall t \end{aligned} \tag{5.1}$$

where, $u \in U_{UL}(\omega), d \in U_{DL}(\omega), k \in \mathscr{K}, b \in \mathscr{B}, c \in \mathscr{C}, t \in \mathscr{T}$.

Using the aforementioned channel gains, the UL SINR on PRB (c,t), from user u to BS (k,b), can be defined as follows:

$$\gamma^{c,t}_{u,k,b}(\omega) := \frac{P^{c,t}_{u,k,b} \times G^{c}_{u,k,b}(\omega)}{N_0 + I^{c,t}_{u,k,b}}, \forall u, \forall k, \forall b, \forall c, \forall t \tag{5.2}$$

Similarly, the DL SINR on PRB (c,t), from BS (k,b) to user u, can be defined as follows:

$$\gamma^{c,t}_{k,b,d}(\omega) := \frac{P^{c,t}_{k,b,d} \times G^{c}_{k,b,d}(\omega)}{N_0 + I^{c,t}_{k,b,d}}, \forall d, \forall k, \forall b, \forall c, \forall t \tag{5.3}$$

Here, $P^{c,t}_{u,k,b}$ and $P^{c,t}_{k,b,d}$ are the transmit powers chosen by BS (k,b) for user u and d, respectively. $I^{c,t}_{u,k,b}$ is the UL interference seen by BS (k,b) on PRB (c,t), $I^{c,t}_{k,b,d}$ is the DL interference seen by user d on PRB (c,t), and N_0 is the average noise power that is constant over all PRBs.

The exact UL interference on PRB (c,t) for UL user u, when it is transmitting to BS (k,b), can be computed as follows:

$$\begin{aligned} I^{c,t}_{u,k,b} = \sum_{k' \in \mathscr{K}} \sum_{b' \in \mathscr{B}} \Bigg(\sum_{u' \in U_{UL}(\omega)}^{u' \neq u} (P^{c,t}_{u',k',b} G^{c,t}_{u',k,b}(\omega)) + \\ \sum_{d' \in U_{DL}(\omega)} (P^{c,t}_{k',b',d'} G^{c,t}_{k',b',k,b}(\omega)) \Bigg), \forall k, \forall b, \forall c, \forall t \end{aligned} \tag{5.4}$$

Similarly, the exact DL interference on PRB (c,t) as seen by the DL user d, when it is receiving from BS (k,b), can be computed as follows:

$$\begin{aligned} I^{c,t}_{k,b,d} = \sum_{k' \in \mathscr{K}} \sum_{b' \in \mathscr{B}} \Bigg(\sum_{u' \in U_{UL}(\omega)} (P^{c,t}_{u',k',b'} G^{c,t}_{u',d}(\omega)) + \\ \sum_{d' \in U_{DL}(\omega)}^{d' \neq d} (P^{c,t}_{k',b',d'} G^{c,t}_{k',b',d}(\omega)) \Bigg), \forall d, \forall c, \forall t \end{aligned} \tag{5.5}$$

Remark 5.3: *In the equations (5.4) and (5.5), we take an implicit assumption that a BS cannot allocate a PRB to more than one users either on UL or DL. Therefore, there are no self-interference scenarios.*

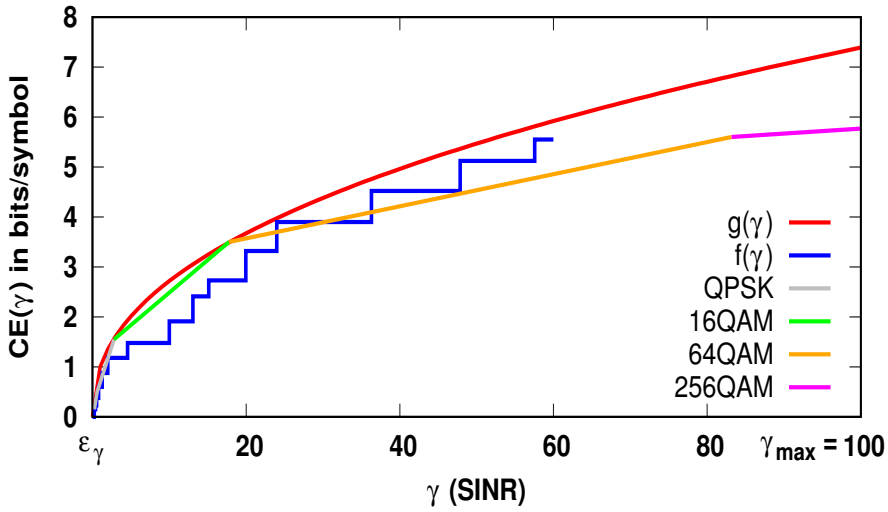

Figure 5.2: Continuous rate function $g(\gamma)$ as an upper bound for: (1) the discrete rate function $f(\gamma)$ from [23] and (2) the achievable CEs with BLER= 0.1 from [61].

In Chapter 4 and 5, we considered a continuous rate function (*i.e.*, $g(\gamma)$) that acted as a tight upper bound on the discrete rate function (*i.e.*, $f(\gamma)$) given in [23] when QPSK, 16QAM, and 64QAM based MCSs were considered. This continuous function can be extended (see Fig. 5.2) to envelop the achievable coding efficiencies (CEs), with BLER target equal to 0.1 as suggested by 3GPP [61], for 5G OFDMA networks. Note that the maximum link layer CE for 256QAM based MCS is approximately 7.4 bits/OFDM symbol as suggested by 3GPP in 2017 [62]. Therefore, $g(\gamma)$ can be extended to include 256QAM based MCSs that can be used in the high SINR region [63] and also within a slightly lower SINR region when combined with 8x8 MIMO techniques [64]. These 256QAM based MCSs highly depend on the SINR thresholds and the underlying physical layer techniques (e.g. MIMO), henceforth, no piece-wise discrete rate function has been proposed so far. Therefore, we need to use this function as is for computing an upper bound on the link layer CEs (in bits per OFDM symbol), knowing well that the actual set of CEs would be discrete in nature. We believe that this approach will give us a reasonable upper bound for an off-line study, since the resulting problem with discrete MCSs will be an intractable large scale MINLP problem.

The CEs using the suggested upper bound function can be computed as follows:

$$CE(\gamma) := \begin{cases} g(\epsilon_\gamma), & \gamma < \epsilon_\gamma \\ g(\gamma) = e^{(\log_{10}(e)\log_e(\gamma))}, & \epsilon_\gamma \leq \gamma \leq \beta_{max} \\ g(\beta_{max}), & \gamma > \beta_{max} \end{cases} \tag{5.6}$$

Here, ϵ_γ is a small positive value that acts as a lower bound on SINR, similarly, β_{max} is an upper bound on SINR. The corresponding data rate (in bits per second) on each PRB can be computed as follows by using the exact SINR (γ), $CE(\gamma)$, the total number of OFDM symbols (N_S), and the duration of each time-slot (T):

$$Rate(\gamma) := CE(\gamma) \times \frac{N_S}{T} \tag{5.7}$$

Note that we use a scheduler that schedule users on a per sub-channel basis, where the whole sub-channel is allocated to a user for the duration of a frame. Since, the channel gains are assumed to be constant over each sub-channel, the SINR and the corresponding link layer rate remains constant for each sub-channel of a given frame.

5.3 Joint RA and US for Flexible FDD

We want to study the performance of flexible FDD within a multi-tier multi-cell HetNet by formulating a joint RA and US problem that considers the exact inter-cell and intra-cell interferences. The RA process is optimized across multiple macro cells of the HetNet according to the ratio of UL and DL users in each macro cell. Without loss of generality, a similar problem can be formulated for flexible TDD. Since, the UL suffers from severe degradation on SINR due to the strong DL-to-UL interference, which is generated by MBS-DL to a SC-UL and vice versa, we use proportional fairness (PF) as our objective function for the joint problem, which maximizes the sum of the logarithm (with base e) of the total rates seen by each UL or DL user.

We consider a two-level UA process across the HetNet, i.e., one for determining the *cell-association* and the other for the *BS-association*. The cell-association for each user, either operating on the UL or the DL, is fixed and assumed to be known beforehand, i.e., denoted by $z_{v,k}(\omega)$, where $z_{v,k}$ is 1 if user v is associated with cell k and 0 otherwise. On the other hand, the BS-associations are unknown and need to be optimized for each network realization; where, we allow a user to transmit/receive data to/from multiple BSs, which is also known as *multi-BS-association*. However, the users cannot transmit/receive data to/from multiple BSs on the same PRB. Similarly, a BS cannot transmit/receive data to/from multiple users on the same PRB.

In addition to the variables and parameters defined in Table 5.1, we need the following additional variables for defining the joint RA and US problem:

- $\boldsymbol{x^{c,t}_{v,k,b}}$ is a PRB allocation indicator variable, which is 1 if user v is allocated PRB (c,t) by BS (k,b) and 0 otherwise. Note that the binary variables $x^{c,t}_{v,k,b}$ are essential for computing appropriate power on each PRB and then computing exact SINRs; whereas, the exact SINRs are necessary for computing the CEs using the continuous rate function $g(.)$.

5.3.1 The Joint RA and US Problem

Given a network realization ω, a set of cell-associations $(\{z_{v,k}(\omega)\})$, and the continuous rate function $g(.)$, we formulate the network-wide joint RA and US problem as follows:

$$\boldsymbol{P^{RA}_{Joint}(\omega)}: \underset{\{x^{c,t}_{v,k,b}\},\{P^{c,t}_{u,k,b}\},\{P^{c,t}_{k,b,d}\},\{I^{c,t}_{u,k,b}\},\{I^{c,t}_{k,b,d}\},\{\gamma^{c,t}_{u,k,b}\},\{\gamma^{c,t}_{k,b,d}\},\{\lambda_{u,k}\},\{\lambda_{k,d}\}}{\text{maximize}}$$

$$\sum_{u\in U_{UL}(\omega)} \log\Big(\sum_{k\in\mathscr{K}} \lambda_{u,k}\Big) + \sum_{d\in U_{DL}(\omega)} \log\Big(\sum_{k\in\mathscr{K}} \lambda_{k,d}\Big)$$

subject to: (5.4), (5.5), and

$$x^{c,t}_{v,k,b} \in \{0,1\}, \qquad \forall v, \forall k, \forall b, \forall c, \forall t \tag{5.8a}$$

$$x^{c,t}_{v,k,b} \leq z_{v,k}(\omega), \qquad \forall v, \forall k, \forall b, \forall c, \forall t \tag{5.8b}$$

$$\sum_{v \in U(\omega)} x^{c,t}_{v,k,b} \leq 1, \qquad \forall k, \forall b, \forall c, \forall t \tag{5.8c}$$

$$\sum_{b \in \mathscr{B}} x^{c,t}_{v,k,b} \leq 1, \qquad \forall v, \forall k, \forall c, \forall t \tag{5.8d}$$

$$\epsilon_p \leq P^{c,t}_{u,k,b} \leq x^{c,t}_{u,k,b} P_{UE} + (1 - x^{c,t}_{u,k,b})\epsilon_p, \forall u, \forall k, \forall b, \forall c, \forall t \tag{5.8e}$$

$$\epsilon_p \leq P^{c,t}_{k,b,d} \leq x^{c,t}_{d,k,b} P_b + (1 - x^{c,t}_{d,k,b})\epsilon_p, \quad \forall d, \forall k, \forall b, \forall c, \forall t \tag{5.8f}$$

$$\sum_{b \in \mathscr{B}} \sum_{c \in \mathscr{C}} P^{c,t}_{u,k,b} \leq P_{UE}, \qquad \forall u, \forall k, \forall t \tag{5.8g}$$

$$\sum_{d \in U_{DL}(\omega)} \sum_{c \in \mathscr{C}} P^{c,t}_{k,b,d} \leq P_b, \qquad \forall k, \forall b, \forall t \tag{5.8h}$$

$$\epsilon_\gamma \leq \gamma^{c,t}_{u,k,b} \leq \beta_{max}, \qquad \forall u, \forall k, \forall b, \forall c, \forall t \tag{5.8i}$$

$$\epsilon_\gamma \leq \gamma^{c,t}_{k,b,d} \leq \beta_{max}, \qquad \forall d, \forall k, \forall b, \forall c, \forall t \tag{5.8j}$$

$$P^{c,t}_{u,k,b} G^{c,t}_{u,k,b}(\omega) \geq \gamma^{c,t}_{u,k,b}(N_0 + I^{c,t}_{u,k,b}), \qquad \forall u, \forall k, \forall b, \forall c, \forall t \tag{5.8k}$$

$$P^{c,t}_{k,b,d} G^{c,t}_{k,b,d}(\omega) \geq \gamma^{c,t}_{k,b,d}(N_0 + I^{c,t}_{k,b,d}), \qquad \forall d, \forall k, \forall b, \forall c, \forall t \tag{5.8l}$$

$$\lambda_{u,k} = \sum_{c \in \mathscr{C}} \sum_{t \in \mathscr{T}} \sum_{b \in \mathscr{B}} g(\gamma^{c,t}_{u,k,b}), \qquad \forall u, \forall k \tag{5.8m}$$

$$\lambda_{k,d} = \sum_{c \in \mathscr{C}} \sum_{t \in \mathscr{T}} \sum_{b \in \mathscr{B}} g(\gamma^{c,t}_{k,b,d}), \qquad \forall d, \forall k \tag{5.8n}$$

where, $u \in U_{UL}(\omega), d \in U_{DL}(\omega), k \in \mathscr{K}, b \in \mathscr{B}, c \in \mathscr{C}, t \in \mathscr{T}$.

Note that the constraints (5.4) and (5.5) are for computing the UL and DL interference, respectively. The constraints (5.8c) are to ensure that only one user, either on UL or DL, would be scheduled on PRB (c,t) by BS (k,b) and the constraints (5.8d) ensure that a user will not receive/transmit data from/to more than one BS on each PRB. Here, ϵ_p and ϵ_γ are very small positive values that depend on the numerical values of P_{UE} and $\gamma^{c,t}_{u,k}$, respectively. The bilinear constraints (5.8k) and (5.8l) are for computing UL and DL SINR

on PRB (c,t), respectively; whereas, the constraints (5.8m) and (5.8n) are for computing the sum of the CEs seen by UL and DL users, respectively.

The joint RA and US problem ($\boldsymbol{P^{RA}_{Joint}(\omega)}$) is a large-scale optimization problem with both binary and continuous variables. Given the large number of mixed variables and non-convex constraints, such as (5.8k) and (5.8l), solving this problem is challenging even for a small number of users in each macro cell. Our goal is to solve this problem *exactly* in order to provide a benchmark solution that is essential for designing efficient on-line RA schemes for flexible FDD/TDD based HetNets. Next, we transform this problem into a relaxed problem that can be solved efficiently.

5.3.2 The Relaxed Problem

In this section, we transform $\boldsymbol{P^{RA}_{Joint}(\omega)}$ into a relaxed problem with continuous variables only. Our proposed transformation removes all the binary variables and the associated constraints (i.e., 5.8a to 5.8f) from $\boldsymbol{P^{RA}_{Joint}(\omega)}$. Note that the binary variables, i.e., $x^{c,t}_{v,k,b}$, are used to determine the BS-association for user v on PRB (c,t), and their removal will allow all users to transmit over the same PRB; this condition would lead to self interference scenarios, i.e., a user will be receiving/transmitting data from/to multiple BSs on a single PRB or multiple users will be scheduled by a BS on a single PRB. To avoid these scenarios and also to obtain a tight upper bound on $\boldsymbol{P^{RA}_{Joint}(\omega)}$, we need to add additional constraints to ensure that only one UE in each macro cell is transmitting with a considerable amount of power on PRB (c,t) of each BS. The corresponding upper bound joint RA and US problem is defined as follows:

$$\boldsymbol{P^{UB-RA}_{Joint}}: \underset{\{P^{c,t}_{u,k,b}\},\{P^{c,t}_{k,b,d}\},\{I^{c,t}_{u,k,b}\},\{I^{c,t}_{k,b,d}\},\{\gamma^{c,t}_{u,k,b}\},\{\gamma^{c,t}_{k,b,d}\},\{\lambda_{u,k}\},\{\lambda_{k,d}\}}{\text{maximize}}$$

$$\sum_{u\in U_{UL}(\omega)} \log\Big(\sum_{k\in\mathcal{K}} \lambda_{u,k}\Big) + \sum_{d\in U_{DL}(\omega)} \log\Big(\sum_{k\in\mathcal{K}} \lambda_{k,d}\Big)$$

$$\text{subject to}: \text{(5.4)}, \text{(5.5)}, \text{(5.8g)} \text{ to } \text{(5.8n)}, \text{ and}$$

$$\epsilon_p \leq P^{c,t}_{u,k,b} \leq z_{u,k}(\omega)P_{UE} + (1 - z_{u,k}(\omega))\epsilon_p, \qquad \forall u, \forall k, \forall b, \forall c, \forall t \tag{5.9a}$$

$$\epsilon_p \leq P^{c,t}_{k,b,d} \leq z_{d,k}(\omega)P_b + (1 - z_{d,k}(\omega))\epsilon_p \qquad \forall d, \forall k, \forall b, \forall c, \forall t \tag{5.9b}$$

$$P^{c,t}_{u,k,b}P^{c,t}_{u',k,b} \leq \epsilon_p, \qquad \forall u, \forall u', u \neq u', \forall k, \forall b, \forall c, \forall t \tag{5.9c}$$

$$P^{c,t}_{k,b,d}P^{c,t}_{k,b,d'} \leq \epsilon_p, \qquad \forall d, \forall d', d \neq d', \forall k, \forall b, \forall c, \forall t \tag{5.9d}$$

$$P^{c,t}_{u,k,b}P^{c,t}_{k,b,d} \leq \epsilon_p, \qquad \forall u, \forall d, \forall k, \forall b, \forall c, \forall t \tag{5.9e}$$

$$\prod_{b \in \mathscr{B}} P^{c,t}_{u,k,b} \leq \epsilon_p^{|\mathscr{B}|-1}, \qquad \forall u, \forall k, \forall c, \forall t \tag{5.9f}$$

$$\prod_{b \in \mathscr{B}} P^{c,t}_{k,b,d} \leq \epsilon_p^{|\mathscr{B}|-1}, \qquad \forall d, \forall k, \forall c, \forall t \tag{5.9g}$$

where, $u \in U_{UL}(\omega), d \in U_{DL}(\omega), k \in \mathscr{K}, b \in \mathscr{B}, c \in \mathscr{C}, t \in \mathscr{T}$.

Here, more constraints are added to achieve a one-to-one PRB mapping between different users and BSs of each macro cell without using any indicator variables. The bilinear constraints from (5.9c) to (5.9e) ensure that only one UE in each macro cell (either on UL or DL) is transmitting/receiving data to/from BS (k, b) with a considerable amount of power using PRB (c, t); whereas, the bilinear constraints (5.9f) and (5.9g) ensure that a user cannot send/receive data to/from more than one BSs on a single PRB.

Lemma 5.1: $\boldsymbol{P^{UB-RA}_{Joint}}$ *can be transformed into an equivalent convex problem, i.e.,* $\boldsymbol{P^{UB-RA'}_{Joint}}$ *by using GP transformation.*

Proof: See Appendix E.

5.4 Existing RA schemes

In this section, we formulate and solve a set of different joint RA and US problems which are corresponding to the existing RA schemes under static FDD/TDD scenarios (as shown in Fig. 5.3 and also enumerated in following paragraphs). The exact performance of these schemes can be compared with that of the proposed upper-bound RA problem, where we assume multi-BS-association for both UL and DL users. In addition, we also assume that all macro cells in the network are synchronized, i.e., they are using the same RA scheme.

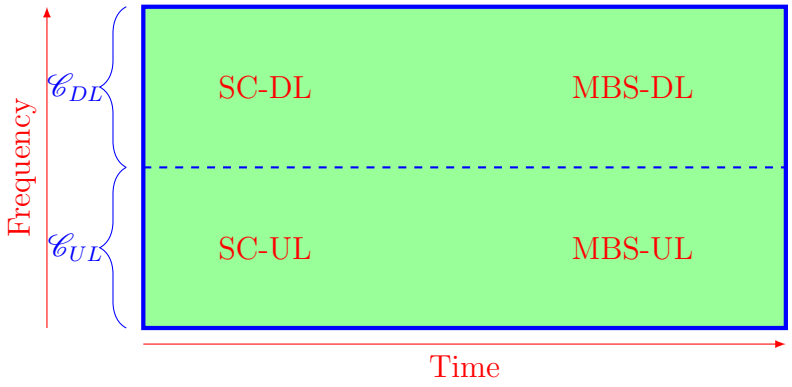

(a) Static FDD

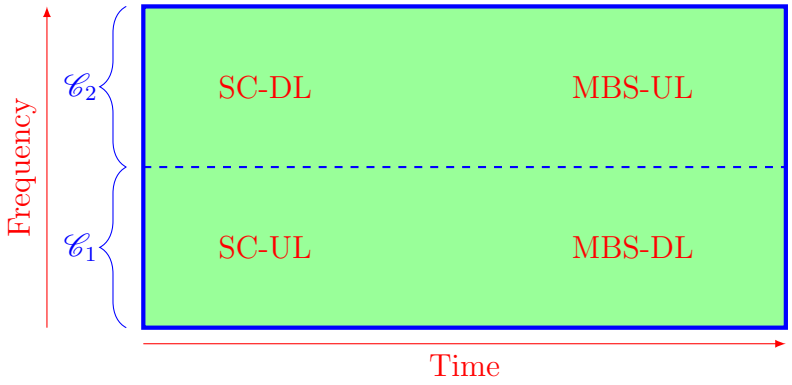

(b) Reverse FDD

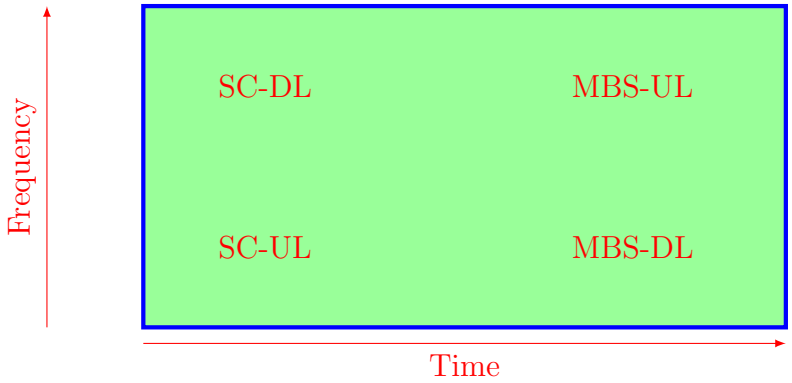

(c) Flexible FDD

Figure 5.3: Potential RA schemes for Flexible FDD based HetNets.

The following schemes have been considered, in this chapter, as the potential candidates for RA in flexible FDD/TDD based HetNets:

1. **Static FDD (S-FDD)**: In this RA scheme, the set of sub-channels are divided into two groups, namely, $\mathscr{C}_{UL}$ and $\mathscr{C}_{DL}$. The sub-channels in $\mathscr{C}_{UL}$ are shared between the MBS and the SCs for UL transmissions, while the sub-channels from $\mathscr{C}_{DL}$ are shared between the MBS and the SCs for the transmissions on DL.

2. **Reverse FDD (R-RDD)**: In this RA scheme, the set of sub-channels are divided into two sets, such that, when the MBS is operating on the UL then the SCs are operating on the DL and vice versa.

5.4.1 Joint RA and US Problem for Static FDD

Given a network realization ω, a set of cell-associations ($\{z_{v,k}(\omega)\}$), the continuous rate function $g(.)$, the sub-channel allocation parameter for the UL, i.e., $\alpha_{UL} \in \{1,..,|\mathscr{C}|\}$, and the sub-channel allocation parameter for the DL, i.e., $\alpha_{DL} = |\mathscr{C}| - \alpha_{UL} \in \{1,..,|\mathscr{C}|-1\}$, the network-wide joint RA and US problem for Static FDD can be formulated as follows:

$$\boldsymbol{P}^{\boldsymbol{S-FDD}}_{\boldsymbol{Joint}}(\boldsymbol{\omega}, \boldsymbol{\alpha_{UL}}) : \text{maximize} \sum_{u \in U_{UL}(\omega)} \log\big(\sum_{k \in \mathscr{K}} \lambda_{u,k}\big) + \sum_{d \in U_{DL}(\omega)} \log\big(\sum_{k \in \mathscr{K}} \lambda_{d,k}\big)$$

$$\text{subject to : (5.4), (5.5), (5.8g) to (5.8n), (5.9a) to (5.9g), and}$$

$$P^{c,t}_{k,b,d} = \epsilon_p, \forall d, \forall k, \forall b, \forall c \in \mathscr{C}_{UL}, \forall t \tag{5.10a}$$

$$P^{c,t}_{u,k,b} = \epsilon_p, \forall u, \forall k, \forall b, \forall c \in \mathscr{C}_{DL}, \forall t \tag{5.10b}$$

where, $u \in U_{UL}(\omega), d \in U_{DL}(\omega), k \in \mathscr{K}, b \in \mathscr{B}, c \in \mathscr{C}, t \in \mathscr{T}$, $\mathscr{C}_{UL} = \{1,..,\alpha_{UL}\}$, and $\mathscr{C}_{DL} = \{\alpha_{UL}+1,..,\alpha_{UL}+\alpha_{DL} = |\mathscr{C}|\}$. The set of constraints given by (5.10a) ensure that only UL users in each macro cell are transmitting data to BS (k,b) with a non-negligible amount of power over $\mathscr{C}_{UL}$, while, the set of constraints (5.10b) ensure that only DL users in each macro cell are receiving data from BS (k,b) with a non-negligible amount of power over $\mathscr{C}_{DL}$.

Note that when there are no DL users then $\alpha_{UL} = |\mathscr{C}|$ and $\alpha_{DL} = 0$, similarly, when there are no UL users then $\alpha_{DL} = |\mathscr{C}|$ and $\alpha_{UL} = 0$. In these scenarios, the static FDD problem becomes equivalent to the upper-bound problem, where SCs and the MBS in each cell are operating in the co-channel deployment (CCD) mode. For UL-only and DL-only traffic, we also consider partially-shared deployment (PSD) mode. The corresponding problem is denoted by $\boldsymbol{P}^{\boldsymbol{S-PSD}}_{\boldsymbol{Joint}}(\boldsymbol{\omega}, \boldsymbol{\alpha})$, where the set of sub-channels are divided into two sets using the sub-channel allocation parameter $\alpha \in \{1, .., |\mathscr{C}| - 1\}$, namely, the *shared* and the *non-shared* set of sub-channels. The non-shared sub-channels, i.e., denoted by $\mathscr{C}_\alpha \in \{1, .., \alpha\}$, are exclusively used by the MBS, whereas the shared sub-channels, i.e., denoted by $\mathscr{C}'_\alpha \in \{\alpha + 1, .., |\mathscr{C}|\}$, can be used by both SCs and the MBS.

Lemma 5.2: *The problems* $\boldsymbol{P}^{\boldsymbol{S-FDD}}_{\boldsymbol{Joint}}$ *and* $\boldsymbol{P}^{\boldsymbol{S-PSD}}_{\boldsymbol{Joint}}$ *can be transformed into equivalent convex problems, i.e.,* $\boldsymbol{P}^{\boldsymbol{S-FDD'}}_{\boldsymbol{Joint}}$ *and* $\boldsymbol{P}^{\boldsymbol{S-PSD'}}_{\boldsymbol{Joint}}$*, respectively, by using GP transformation.*

Proof: The problem $\boldsymbol{P}^{\boldsymbol{UB-RA}}_{\boldsymbol{Joint}}$ has been convexified in Appendix E. A similar approach can be used to obtain $\boldsymbol{P}^{\boldsymbol{S-FDD'}}_{\boldsymbol{Joint}}$ and $\boldsymbol{P}^{\boldsymbol{S-PSD'}}_{\boldsymbol{Joint}}$.

5.4.2 Joint RA and US Problem for Reverse FDD

Given a network realization ω, a set of cell-associations $(\{z_{v,k}(\omega)\})$, the continuous rate function $g(.)$, the sub-channel allocation parameter, i.e., $\alpha \in \{1, .., |\mathscr{C}| - 1\}$, the network-wide joint RA and US problem for R-FDD can be formulated as follows:

$$\boldsymbol{P}^{\boldsymbol{R-FDD}}_{\boldsymbol{Joint}}(\boldsymbol{\omega}, \boldsymbol{\alpha}) : \text{maximize} \sum_{u \in U_{UL}(\omega)} \log\big(\sum_{k \in \mathscr{K}} \lambda_{u,k}\big) + \sum_{d \in U_{DL}(\omega)} \log\big(\sum_{k \in \mathscr{K}} \lambda_{d,k}\big)$$

$$\text{subject to : (5.4), (5.5), (5.8g) to (5.8n), (5.9a) to (5.9g), and}$$

$$P^{c,t}_{u,k,b_m} = \epsilon_p, \forall u, \forall k, \forall b_m, \forall c_1, \forall t \tag{5.11a}$$

$$P^{c,t}_{u,k,b_s} = \epsilon_p, \forall u, \forall k, \forall b_s, \forall c_2, \forall t \tag{5.11b}$$

$$P^{c,t}_{k,b_m,d} = \epsilon_p, \forall d, \forall k, \forall b_m, \forall c_2, \forall t \tag{5.11c}$$

$$P^{c,t}_{k,b_s,d} = \epsilon_p, \forall d, \forall k, \forall b_s, \forall c_1, \forall t \tag{5.11d}$$

where, $u \in U_{UL}(\omega), d \in U_{DL}(\omega), k \in \mathscr{K}, b \in \mathscr{B}, c \in \mathscr{C}, t \in \mathscr{T}$, $c_1 \in \mathscr{C}_1 = \{1, .., \alpha\}$, $c_2 \in \mathscr{C}_2 = \{\alpha + 1, .., |\mathscr{C}|\}$, $b_m \in \{MBS\}$, and $b_s \in \mathscr{B}/\{MBS\}$.

We assume that all macro cells in the network are synchronized and they are sharing the same sub-channels for SC-UL and MBS-DL and vice versa. The constraints (5.11a) ensure that the UL users in each macro cell do not transmit data to the MBS on $\mathscr{C}_1$, while, the constraints (5.11c) ensure that the MBS in each macro cell do not transmit data to the DL users on $\mathscr{C}_2$. Likewise, the constraints (5.11b) ensure that the UL users in each macro cell do not transmit data to the SCs on $\mathscr{C}_2$, while, the constraints (5.11d) ensure that the DL users in each macro cell do not transmit data to the SCs on $\mathscr{C}_1$. Note that when there are only UL users or only DL users in the network, then R-FDD is equivalent to the case where the MBS and the SCs are operating in the orthogonal deployment (OD) mode.

Lemma 5.3: $\boldsymbol{P}_{\boldsymbol{Joint}}^{\boldsymbol{R-FDD}}$ *can be transformed into an equivalent convex problem* $\boldsymbol{P}_{\boldsymbol{Joint}}^{\boldsymbol{R-FDD'}}$ *by using GP transformation.*

Proof: The problem $\boldsymbol{P}_{\boldsymbol{Joint}}^{\boldsymbol{UB-RA}}$ has been convexified in Appendix E. A similar approach can be used to obtain $\boldsymbol{P}_{\boldsymbol{Joint}}^{\boldsymbol{R-FDD'}}$.

5.5 Numerical Results

We consider a scenario of multiple hexagonal cells ($|\mathscr{K}| = 7$) with an inter-site distance (ISD) of $500m$ (i.e., cell radius is $\frac{500}{\sqrt{3}}m$). As shown in Fig. 5.1, each macro cell $k \in \mathscr{K}$ has a directional MBS that is overlaid by 2 symmetrically placed PBSs at a distance of $200m$ from the MBS. All macro cells are operating on OFDMA-based frames, where each frame has $|\mathscr{C}| = 10$ sub-channels and $|\mathscr{T}| = 10$ time-slots. Our physical layer parameters are based on the 3GPP evaluation document [36] that are also shown in Table 5.2. The channel gains (i.e., listed in Table 5.1) account for antenna gain, directivity gain, path loss (given in Table 5.3), large-scale shadow fading coefficients, and small-scale fast fading coefficients; where, the directivity gain is a function of θ, i.e., the angle made by a user with the broadside direction of the MBS antenna. The shadow fading coefficients are modeled by a log-normal distribution that has zero mean and σ^2 variance (given in Table 5.3), whereas, the small-scale fast fading coefficients (due to multi-path propagation) are modeled by a normalized Rayleigh distribution.

Table 5.2: Physical Layer Parameters from [36]

N_S	12×14	T	$1ms$
Traffic Model	Full buffer	Penetration Loss	$20dB$
Subchannel BW	$180kHz$	Noise Power	$-174dBm/Hz$
UE Antenna Gain	$0dBi$	UE Noise Figure	$9dB$
PBS Antenna Gain	$5dBi$	Pico Noise Figure	$13dB$
MBS Antenna Gain	$15dBi$	MBS Noise Figure	$5dB$
MBS Directivity Gain	$\min(12(\frac{\theta}{65^o})^2, 20)$dB	UE Transmit Power	$24dBm$
MBS Transmit Power	$46dBm$	Pico Transmit Power	$24dBm$

Table 5.3: Path Loss and Shadow Fading Models from [36]

Path Loss (dB)		(σ)
MBS and UE	$131.1 + 42.8 \times log_{10}(d/1000), d \geq 35m$	8dB
MBS and MBS	$98.45 + 20 \times log_{10}(d/1000)$	8dB
MBS and Outdoor Pico	$125.2 + 36.3 \times log_{10}(d/1000), d \geq 75m$	6dB
Outdoor Pico and Outdoor Pico	$169.36 + 40 \times log_{10}(d/1000), d \geq 40m$	6dB
UE and Outdoor Pico	$145.4 + 37.5 \times log_{10}(d/1000), d \geq 10m$	10dB
UE and UE	$98.45 + 20 \times log_{10}(d/1000), d \leq 50m$ $175.78 + 40 \times log_{10}(d/1000), d > 50m$	12dB

We study the performance of the upper bound problem for joint RA and US along with the existing RA schemes by generating a set of 100 realizations (Ω) for symmetric as well as asymmetric UL/DL traffic scenarios. Each $\omega \in \Omega$ corresponds to the duration of one frame and a set of users ($U(\omega)$) including a set of UL users (i.e., $U_{UL}(\omega)$) and a set of DL users (i.e., $U_{DL}(\omega)$), which are distributed uniformly across all macro cells. We are interested in maximizing the geometric mean (GM) throughput of all users in the network that is equivalent to maximizing our objective function, i.e., $\sum_{u \in U_{UL}(\omega)} \log\big(\sum_{k \in \mathscr{K}} \lambda_{u,k}\big) + \sum_{u \in U_{DL}(\omega)} \log\big(\sum_{k \in \mathscr{K}} \lambda_{d,k}\big)$. Note that the GM throughput of all users in the network is defined as follows:

$$GM(\omega) := \sqrt[|U(\omega)|]{\prod_{u \in U(\omega)} \Big(\sum_{k \in \mathscr{K}} \frac{\lambda_{u,k}(\omega) \times N_S}{T \times |\mathscr{T}|}\Big)}, \forall \omega \in \Omega$$

where, N_S is the number of OFDM symbols in each PRB and T is the time duration for one PRB. Note that their numerical values are given in Table 5.2.

5.5.1 Performance Measures

The following measures have been computed for each realization (ω) using a non-linear programming solver SNOPT [39] before averaging them over Ω:

- The *Upper-bound GM* ($\boldsymbol{GM^{UB}(\omega)}$) is computed by solving $\boldsymbol{P_{Joint}^{UB-RA'}(\omega)}$, as discussed in Section 5.3.2.
- The *Static-FDD GM* ($\boldsymbol{GM^{S-FDD}(\omega, \alpha_{UL})}$) is computed by solving $\boldsymbol{P_{Joint}^{S-FDD'}(\omega, \alpha_{UL})}$ for each value of α_{UL}, as discussed in Section 5.4.1.
- The *Static-FDD GM Max* ($\boldsymbol{GM_{max}^{S-FDD}(\omega)}$) is computed by solving $\boldsymbol{P_{Joint}^{S-FDD'}(\omega, \alpha_{UL})}$ and the resulting GM is then maximized for all possible values of α_{UL}.
- The *Reverse-FDD GM* ($\boldsymbol{GM^{R-FDD}(\omega, \alpha)}$) is computed by solving $\boldsymbol{P_{Joint}^{R-FDD'}(\omega, \alpha)}$ for each value of α, as discussed in Section 5.4.2.
- The *Reverse-FDD GM* ($\boldsymbol{GM_{max}^{R-FDD}(\omega)}$) is computed by solving $\boldsymbol{P_{Joint}^{R-FDD'}(\omega, \alpha)}$ and the resulting GM is then maximized for all possible values of α.

- The *Static-PSD GM* ($\boldsymbol{GM^{S-PSD}(\omega, \alpha)}$) is computed by solving $\boldsymbol{P_{Joint}^{S-PSD'}(\omega, \alpha)}$ for each value of α, as discussed in Section 5.4.1.
- The *Static-PSD GM Max* ($\boldsymbol{GM_{max}^{S-PSD}(\omega)}$) is computed by solving $\boldsymbol{P_{Joint}^{S-PSD'}(\omega, \alpha)}$ and the resulting GM is then maximized for all possible values of α.

5.5.2 Comparison Results

To compare the efficacy of different CA schemes under varying traffic scenarios, we categorize our numerical results as follows:

- **DL-only traffic ($|U(\omega)| = |U_{DL}(\omega)| = 35$)**: In this scenario, R-FDD acts as an OD mode (i.e., the MBS is operating on $\mathscr{C}_1$ and the SCs are operating on $\mathscr{C}_2$ in each macro cell) and $\boldsymbol{GM^{UB}}$ acts as a CCD mode. The corresponding results are shown in Fig. 5.4, where we also computed the GM throughput for PSD mode (i.e., $\boldsymbol{GM^{S-PSD}}$). Clearly, this scenario can benefit from CCD mode (i.e., $\boldsymbol{GM^{UB}}$) that significantly outperforms the OD mode even when the CA parameters for R-FDD (i.e., α's are chosen to maximize the GM throughput of each realization), in contrast, PSD performs closely to the CCD mode when α's are maximized for each realization. In addition, choosing α independently for each realization in R-FDD (i.e., $\boldsymbol{GM_{max}^{R-FDD}(\omega)}$) can bring huge performance gains for DL users then the case when α's are constant for all realizations.
- **UL-only traffic ($|U(\omega)| = |U_{UL}(\omega)| = 35$)**: In this scenario, R-FDD acts as an OD mode (i.e., the SCs are operating on $\mathscr{C}_1$ and the MBS is operating on $\mathscr{C}_2$ in each macro cell) and $\boldsymbol{GM^{UB}}$ acts as a CCD mode. The corresponding results are shown in Fig. 5.5, where we see similar results as for the DL-only traffic scenario, i.e., the CCD mode (i.e., $\boldsymbol{GM^{UB}}$) outperform the OD and PSD modes even when the CA parameters for R-FDD and S-PSD (i.e., α's are chosen to maximize the GM throughput of each realization).
- **Symmetric UL and DL traffic ($|U(\omega)| = |U_{DL}(\omega)| + |U_{UL}(\omega)| = 35$)**: In this scenario, there are same number of UL and DL users in each macro cell. The cor-

responding results are shown in Fig. 5.6, 5.7, 5.8, and 5.9, which suggest that when there is disparity between the number of UL and DL users (Fig. 5.6 and 5.7) in each macro cell, S-FDD outperforms R-FDD, otherwise (Fig. 5.8 and 5.9), their performance gains remain quite similar to each other. Clearly, the solutions obtained for S-FDD are quasi-optimal as they are close to the upper bound ($\boldsymbol{GM^{UB}}$) under for different symmetric UL and DL traffic scenarios.

- **Asymmetric UL and DL traffic ($|U(\omega)| = |U_{DL}(\omega)| + |U_{UL}(\omega)| = 35$)**: the corresponding results, as shown in Fig. 5.10, suggest that when the number of UL and DL users in each macro cell are random (with at least one UL and one DL user in each macro cell), R-FDD outperforms S-FDD when α's are chosen to maximize the GM throughput of each realization. Hoever, in the case that α's cannot be adjusted on a per frame basis their performance is very far from the optimal.

Nonetheless, the purpose of this study is to benchmark the performance of the existing and/or yet-to-be designed RA schemes for flexible HetNets in an off-line manner. In practice the RA parameters, i.e., α_{UL} and α, could not be optimized on a per realization basis, since, it requires synchronization among all macro cells, which can be performed in a Centralized-Radio Access Network (C-RAN) scenario only, where the intra-cell and the inter-cell interferences can be measured exactly for each macro cell. In addition, within a C-RAN the RA parameters can also be adjusted periodically depending on the channel conditions and the UL/DL traffic scenario in each macro cell.

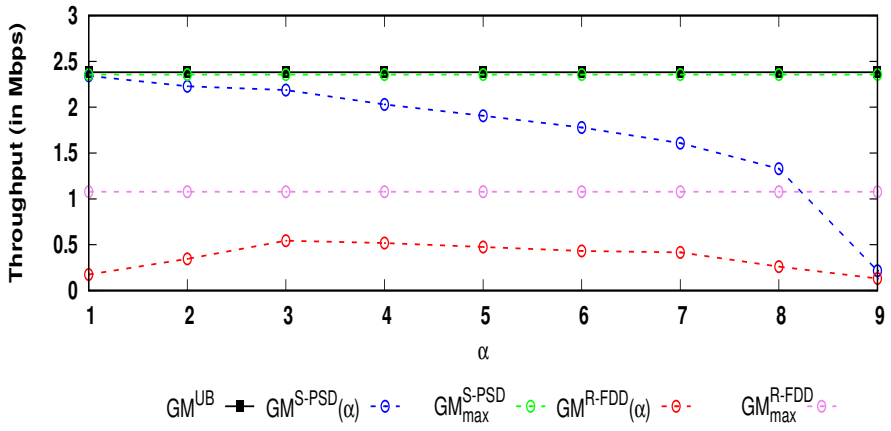

Figure 5.4: Symmetric UL/DL traffic (UL:DL=0:5): Average GM throughput over Ω

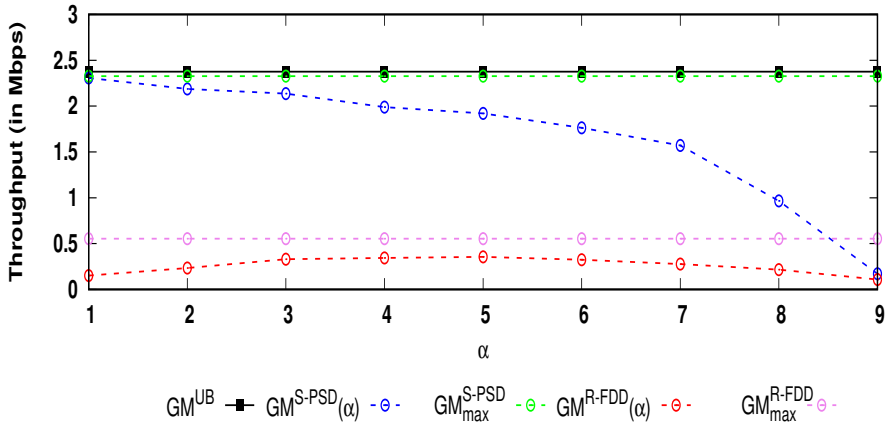

Figure 5.5: Symmetric UL/DL traffic (UL:DL=5:0): Average GM throughput over Ω

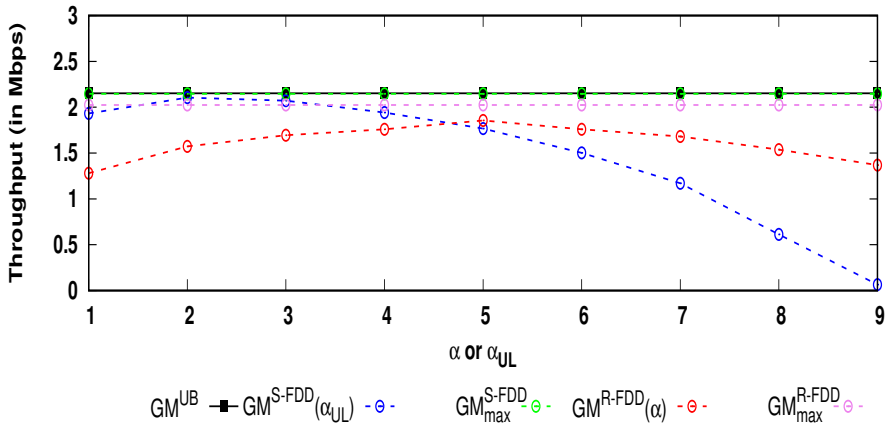

Figure 5.6: Symmetric UL/DL traffic (UL:DL=1:4): Average GM throughput over Ω

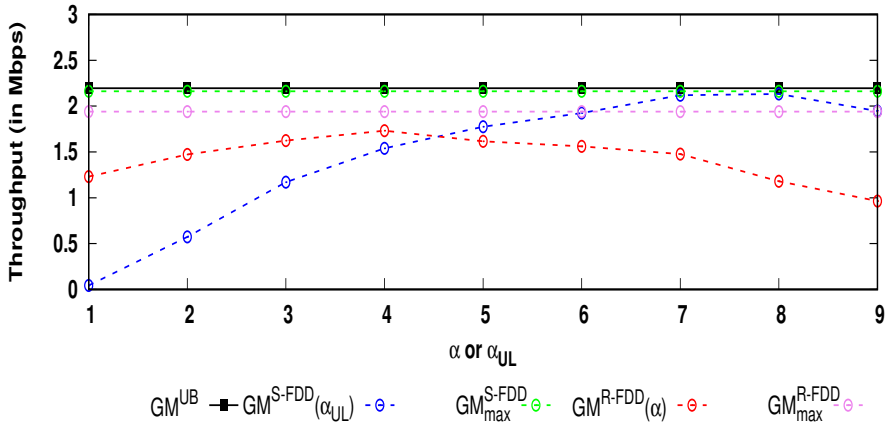

Figure 5.7: Symmetric UL/DL traffic (UL:DL=4:1): Average GM throughput over Ω

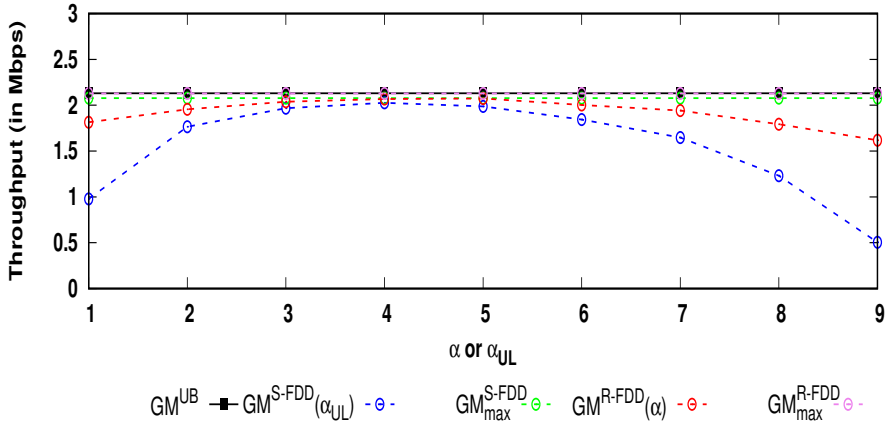

Figure 5.8: Symmetric UL/DL traffic (UL:DL=2:3): Average GM throughput over Ω

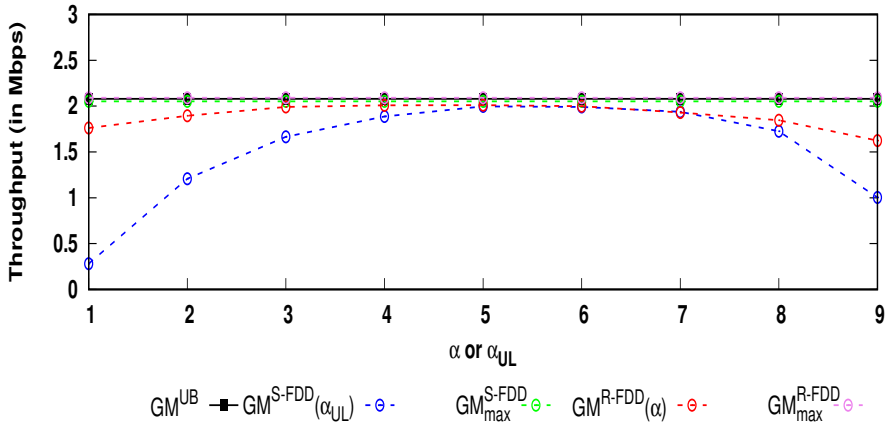

Figure 5.9: Symmetric UL/DL traffic (UL:DL=3:2): Average GM throughput over Ω

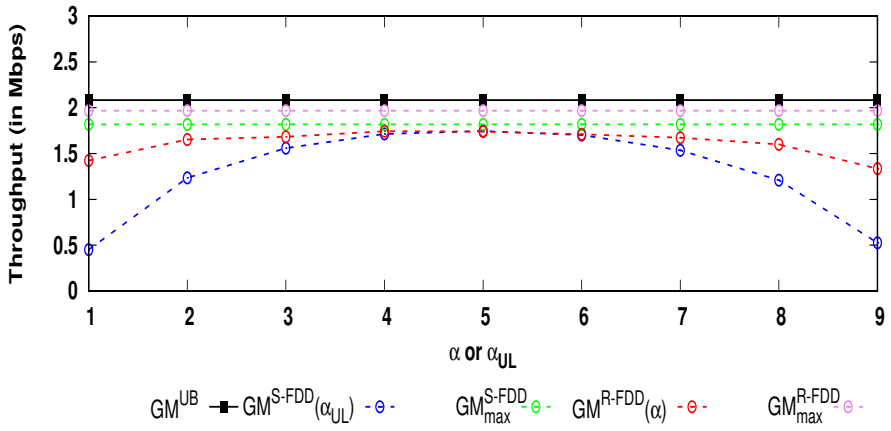

Figure 5.10: Asymmetric UL/DL traffic: Average GM throughput over Ω

5.6 Conclusions

In this chapter, we investigated the joint RA and US problem for a specific HetNet under various deployment choices, i.e., static, reverse, and flexible. We formulated the joint problems corresponding to each one of them, which are non-convex integer optimization problems that are, nonetheless, computationally intractable. We transformed them into convex problems by first removing the binary variables and then using GP transformation. Using this approach, we obtained upper bound solutions, which can serve as a benchmark to analyze the efficacy of existing or new RA schemes for flexible FDD based HetNets. These off-line solutions can also be used to propose engineering insights for designing future flexible HetNets. Through extensive numerical simulations, we demonstrated the performance of Static FDD and Reverse FDD for flexible FDD by comparing them with the proposed upper-bound solutions. It was observed that the Static FDD can outperform Reverse FDD for symmetric UL and DL traffic scenarios, whereas Reverse FDD achieves the closest performance with respect to the proposed upper-bound solutions under asymmetric UL/DL traffic scenarios. In general, it was observed that in order to achieve a quasi-optimal performance, either the RA parameters for R-FDD need to be adjusted for each network realization or new quasi-optimal RA schemes should be proposed for flexible HetNets to incorporate asymmetric UL/DL traffic scenarios.

Chapter 6

Cable based Front-hauls for C-RANs

6.1 Introduction

In recent years, different solutions, based on topological and architectural innovations of the current cellular networks, have been proposed to address the issues related to the increasing data requirements and asymmetries. In our previous chapters, we presented a detailed analysis of various RRM processes from a link-layer perspective only, where our main focus was on network densification, however, the current trends in cellular networks are to enhance the spectral efficiency of the currently available spectrum by using MIMO antennas or other related solutions which are based on enhanced physical layer techniques.

Note that these MIMO antennas are used on a large scale to further enhance the spectral efficiency of the underlying cellular network, nonetheless, at the cost of distributed signal processing operations that require strict synchronization/alignment of the cellular users with the MIMO antennas. Further, MU-MIMO have been proposed which adds multiple access (multi-user) capabilities to MIMO by leveraging multiple users as spatially distributed transmission resources, at the cost of somewhat more expensive signal processing operations. In contrast, single-user MIMO considers only local multiple antennas to serve each user, in particular, they are used to ensure outdoor coverage and to serve mobile UEs (allowing for handoff minimization), while MU-MIMO used within each SC can act as the main capacity-driver for indoor and outdoor UEs with low mobility.

Our Objective:

5G mobile networks are expected to support highly dynamic traffic and stringent delay requirements, therefore, pervasive deployment of a large number of low-power SCs with possibly overlapped radiation ranges appear to be the most viable solution to meet these requirements [65]. This is particularly the basis of achieving cost-effective indoor distribution systems for 5G indoor networks, since, each SC can exploit a low cost analog-fronthaul based DAU.

In this context, a low cost C-RAN architecture is necessary for handling the complex scenarios generated by the large number of SCs for indoor 4G/5G services. In conventional C-RANs, the front-haul link between a Base Band Unit (BBU) and a Remote Radio Unit (RRU) deploys digital baseband signaling using an optical fiber link; the optical fibers are used to transport data at a very high speed. Recently, copper-based all-analog front-hauls [66] have been proposed as a low cost alternative to the fiber optics based connections. These cable based fronthauls, also known as LTE over Cable (LoC) for 4G LTE, leverage the existing LAN cable based indoor architecture to meet the high bandwidth requirements with almost negligible cost.

This chapter presents a recently introduced novel distributed antenna access system [67] for indoor service provisioning, aiming to provide 5G indoor services with extremely low cost[1]. The proposed architecture is characterized by the fact that a DAU can be placed a few hundred meters from the BBU or RRU via a multi-segment front-haul, where the last hop is through a multi-pair LAN cable. This DAU architecture can provide a cost-effective alternative to the expensive fiber-optic based indoor solution(s), allow the antenna units to be distributed over a wide geographical area by using multi-pair LAN cables for transporting 4G LTE or 5G New Radio (NR) signals. However, the use of existing indoor cables has been limited because of the attenuation and the crosstalk among the twisted pairs of each cable. To realize the proposed system, we focus on the design, optimization, and implementation of a real-time scheduler for resource mapping between the Radio Frequency (RF) signals of the radio antennas and the sub-channels of a multi-pair LAN cable.

[1]Some of the figures and tables presented in this chapter have been published in [67] and [68].

The main contributions of this chapter are summarized as follows:

- We propose an optimization framework for an all-analog user scheduler for mapping 4G LTE or 5G NR signals from a DAU over a LAN cable. In particular, we propose a novel joint power allocation and sub-channel allocation problem, such that, the cable impairments are minimized before transporting the signals from each antenna unit onto the cable, this is also referred to as Multi-pair Air-to-Cable (MP-A2C) mapping problem. Based on the given DAU architecture, we introduce an optimal MP-A2C scheduler for mapping the antenna signals on the sub-channels of a multi-pair cable.
- The MP-A2C optimization problem is a MINLP problem whose feasible solution space is nonetheless non-linear and non-convex. To obtain optimal solutions for the MP-A2C problem, we propose a convex upper bound problem by exploiting GP. Through extensive numerical simulations, we show that the proposed framework can be used as a benchmark for evaluating the performance of any MP-A2C scheduler.
- We propose heuristic-based schedulers for the MP-A2C problem that allow us to decouple the joint power and sub-channel allocation problem (for mapping signals over the LAN cable) into two simple problems, which can be solved efficiently in real-time. By decoupling the power allocation process from the sub-channel allocation process over the LAN cable, we significantly reduce the computational complexity of the joint problem, *i.e.*, to polynomial time.
- We verify the performance of the heuristic-based schedulers via extensive simulation over a realistic 5G NR channel and a multi-pair cable channel (*i.e.*, with actual CAT-5 cable measurements) in terms of the optimal cable throughput of the radio users under the given rate requirements.

The rest of the chapter is organized as follows: Section 6.1.2 reviews the prior work on 5G indoor access systems. In Section 6.2, we present our system model along with the distributed antenna access architecture for 5G indoor service provisioning. Section 6.3 introduces the optimal MP-A2C scheduler and its feasible solutions through a novel upper bound problem. The proposed heuristic based MP-A2C scheduler and its performance evaluation is provided by Section 6.4 and 6.5, respectively.

6.1.1 Motivation

C-RANs have been considered as a promising solution for providing indoor services by centralizing the baseband units (BBUs) into a common BBU pool and geographically distributing the remote radio units (RRUs) over each indoor chamber (one per SC) for providing radio transmissions/receptions. One of the main considerations, for these indoor chambers is to achieve a cost-effective indoor distribution system for transporting RF signals between the BBU pool and each distributed RRU, also referred to as front-hauls. In this context, the current industry practice of indoor front-hauling is subject to various challenges for the 5G era, where much higher frequency bands and massive antenna arrays will be employed, as mentioned below:

1. Currently, the digital links are used for the transportation of the RF signals between the BBU and the RRU via the IEEE 802.3 Ethernet protocol and Common Public Radio Interface (CPRI), respectively, where A/D and D/A conversions are necessary at both ends. Note that a high-rise building may contain hundreds of deep-indoor chambers, and each chamber may require a DAU for broadband service provisioning.

2. The indoor front-hauls should be scalable to the number of antennas at each RRU. Optical fiber can provision a huge amount of bandwidth but is subject to high hardware complexity in achieving fine granularity. For example, a small indoor chamber just needs an antenna set with 4 radiation units that can provision a sum-rate of a few Gbps. In this case, using an optical module with CPRI based digital links is not cost-effective at all.

3. The reuse of existing infrastructure is highly desired for cost reduction and pervasive provisioning. Although optical fibers have been largely deployed in metropolitan areas, they may not reach every indoor femto/pico-cell as much as LAN cables. However, the digital link on LAN cables is subject to very low rates due to the need for A/D/A conversion as well as the waste of media spectrum due to frequency expansion.

4. The passive devices in the conventional system may not be able to support multiple high-frequency ranges of operation. The attenuation of a coaxial cable is significantly

more serious when signal frequency is in GHz. Further, a DAU with N_A antennas has to take N_A coaxial cables to feed it, which is not realistic in most cases.

6.1.2 Related Work

To the best of our knowledge, solutions for 5G indoor service provisioning that takes LAN cables and analog feeders to the antennas are seen in [66–73]. More specifically, [69, 70] suggested to directly launch analog radio signals over a twisted pair cable-based front-haul, also known as *Radio over cable (RoC)*, which has merits mostly due to the requirement of modest complexity for up conversion (from Baseband (BB) to RF) and down conversion (from RF to BB), also referred to as the analog-to-analog conversion (A/A) in the following context. Since, the latency of analog relaying at the RRUs is negligible and all latency is due to propagation, the 0.5 ms latency predicted in 5G NR [74] can be ensured.

The A/A operation is illustrated in Fig. 6.1, where the RF signal from a 5G user of 20 MHz band (with K sub-channels) is first received at an antenna and then mapped to the low frequency spectrum (below 500 MHz) of the cable with proper power shaping. Frequency down-conversion is performed before the RF signals are launched on the twisted pair LAN cable in order to avoid any further attenuation. An A/A operation is needed again at the other side where a frequency up-conversion is performed, so as to restore the original RF frequency. Note that crosstalk among bundled twisted pairs exists even if low frequency signals (0-500 MHz) are transported. This is also referred to as Far-end Crosstalk (FEXT). Note that an identical spectrum width is preserved during the frequency conversion with some power shaping, which is required to pre-compensate the attenuation with respect to the frequency over the LAN cable. The down-converted RF signal is then launched over the twisted pair using a predefined spectral mask as shown in Fig. 6.1. It is likewise but only reverse every step in the downlink direction.

A naive solution to mitigate the FEXT is to allow a single RF signal to be carried by a twisted pair, such as the one suggested by [69, 70]. However, in this scenario, we would be using the lowest possible band on the twist pair of the LAN cable to carry the frequency down-converted RF signal (at GHz carrier) with a small spectrum width ($\approx$ 20MHz). This naive mapping policy is feasible and can achieve a very low FEXT among

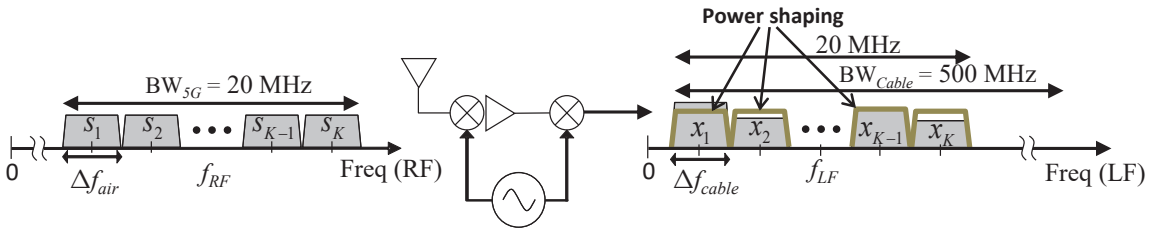

Figure 6.1: Air-to-Cable frequency translation [67].

the IF signals traveling on the cable. Nonetheless, such a policy casts a stringent constraint on the bandwidth usage of the twisted pair and the number of antennas at each RAU that has to be bounded by the number of twisted pairs to the RRU. For example, an RRU with a 16-antenna array would require 16 independent twisted pairs, which is not practical in most scenarios. Therefore, it is critical to have multiple antennas to be provisioned by a single twisted pair for the desired scalability, which can be achieved in the following two dimensions: one is to multiplex antenna signals in a single twisted pair (i.e., design in the frequency domain), and the other is to consider multiple twisted pairs accommodated in a single cable (i.e., design in the space domain). The resource of such a multi-pair cable is defined under the space-frequency (SF) domain, where the signal from/to each antenna is required to be mapped properly over a specific space frequency cable resource.

In [72], a scheduler has been proposed to achieve an efficient SF2SF mapping between the sub-channels of each antenna and the sub-channels of a certain twisted pair. Although feasible, it took an invalid/unrealistic assumption that each 22MHz of spectrum width has a flat channel response. In addition, it did not consider the fact that the multi-pair cable channel experiences insertion loss (IL) as well as far end crosstalk (FEXT) that are directly proportional to the frequency and the cable length. In [73], a similar scheduler was introduced and the scheduling problem was formulated into an Integer Linear Problem (ILP) problem, where one twisted-pair was allocated for analog baseband transmission while the rest of the twisted pairs were allocated to the Ethernet signals; such a setting may lead to higher crosstalk over the front-haul link as the transmit power spectrum density (PSD) of the Ethernet signals are significantly higher than the radio signals.

A similar analysis has been performed in [75] for a single UE based multiple-input single output (MISO) downlink scenario, which has been adopted to avoid the performance analysis to be affected by multi-user spatial multiplexing. Besides the technical issues presented in Section 6.1.1, all of the reported analog solutions for front-hauling have to modify the industry practice of using a digital optical link between the RRU and BBU, resulting in compatibility-issues.

6.2 System Model

In our previous chapters, we characterized and analyzed a HetNet consisting of a conventional macro-BS tier overlaid with a second tier of Pico-BSs considering uniformly distributed low mobility users. In general, the HetNets have non-uniformly distributed users that are endowed with a single antenna with different speeds. Those associated with the SCs (which acts as a HotSpot with a large number of users) are primarily static or have low mobility, while the medium-to-high mobility ones are served by the macro BS. Typically, the user association (UA) decisions are made locally, whereas we assume that the RRUs are connected to the DAUs through low cost and high capacity front-hauls, thus, both US and UA decisions can be taken by the RRU without any inter-BBU coordination.

In Fig. 6.2, we illustrate a scenario where an RRU is located at the top of the building and each floor is installed with a DAU. Different from distributed antenna systems with digital optical links, each DAU is connected to the RRU via a LAN cable. In particular, the DAU is assumed to be an all-analog device without any intelligent processing that is required to reduce its hardware cost. The DAU only performs simple tasks like frequency translation, amplification, and radiation/reception of radio frequency signals, and hosts an array of antennas. In Fig. 6.3, we present the functional diagram of the DAU system, which has been proposed in [67]. In line with the conventional C-RANs, the proposed DAU system has a CPRI-based optical link in between the BBU and RRU. The RRU supports two types of antenna units, one locally hosted at the RRU called local antenna units (LAUs), and the other referred to as DAUs which can be placed up to 200 meters away from the RRU.

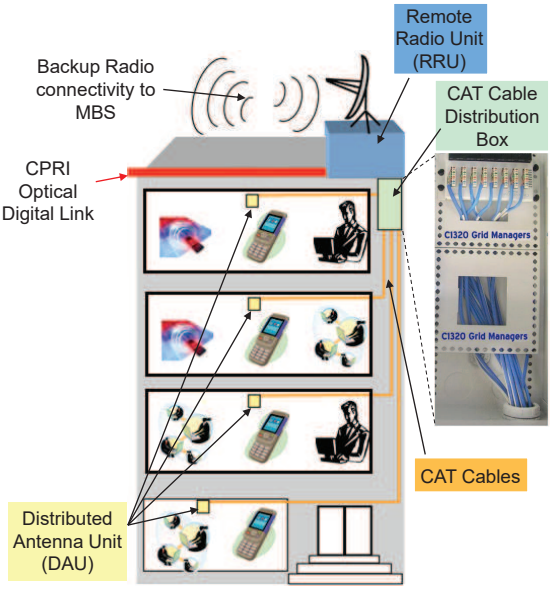

Figure 6.2: An example of a building with 5G indoor services [67].

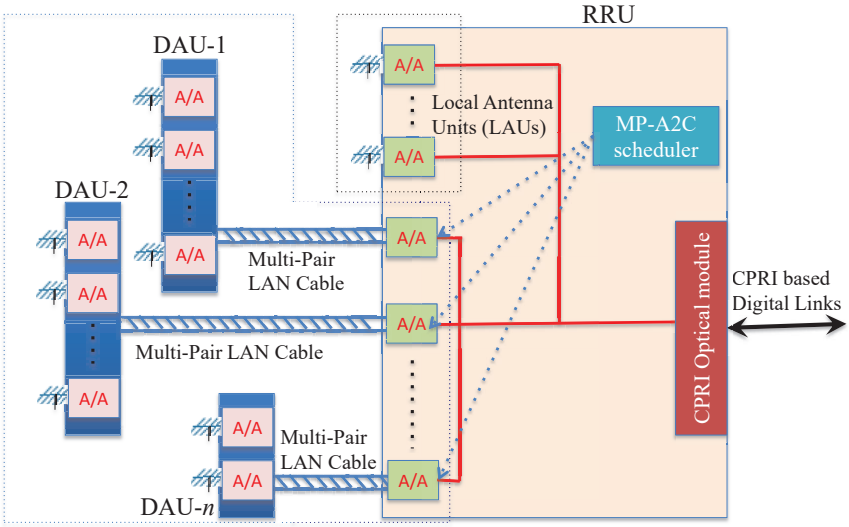

Figure 6.3: The functional diagram of the DAU system [67].

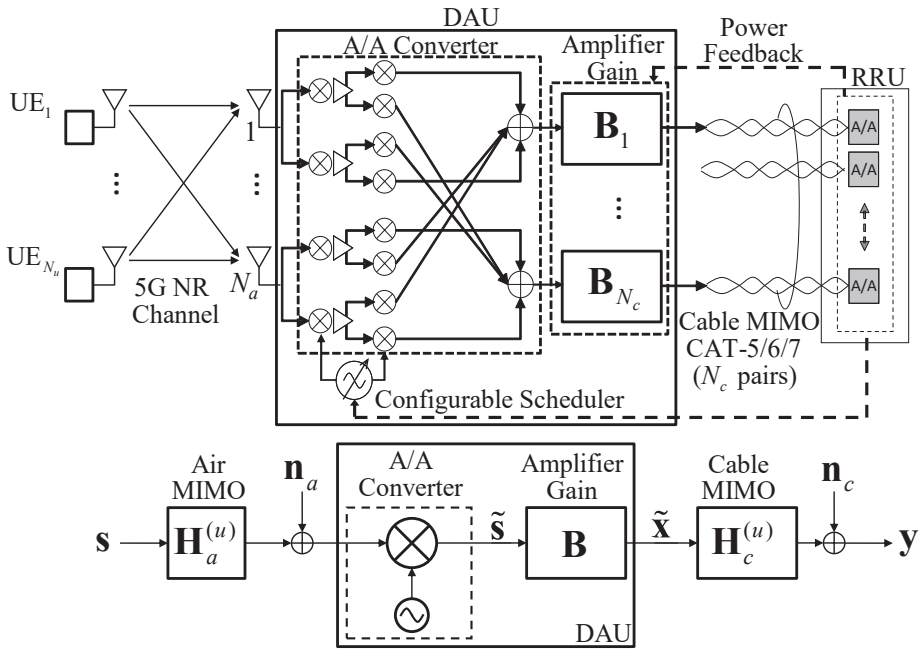

Figure 6.4: The block diagram of the proposed DAU system [67, 68].

The proposed architecture for 5G indoor services has the following merits: (i) the system is compatible with the conventional C-RAN front-hauls where CPRI based digital optical links are used to connect the BBU and RRUs, while the LAN cables are used to extend the DAUs away from the RRU. (ii) The DAU is a protocol-independent device that is transparent to the transmission rate. This leads to a fact that the DAU can incorporate with all possible wireless technologies and standards. (iii) Since, the LAN cables are pervasive in the indoor environment, using the LAN cables is very cost-effective compared with any other solution such as coaxial cable and optical fibers. Note that a multi-pair LAN cable contains at least 4 twisted pairs (i.e. CAT 5/6/7) bundled together to provide bandwidth up to 1 GHz/pair (depending on the cable type and length). Thus, by using such multi-pair LAN cables would enable the design of high-bandwidth, low-cost, and fine-granularity short distance interconnections (up to 200 meters) between the RRU and DAUs.

Notation: $[\mathbf{A}]_{ij} = a_{ij}$ denotes the ijth element of matrix $\mathbf{A}$ and $\text{diag}(\mathbf{A}_1, \ldots, \mathbf{A}_N)$ is a block-diagonal matrix. Letters $\mathbb{R}, \mathbb{C}$ refer to real and complex numbers, respectively. We denote matrix transposition and conjugate transposition as $(\cdot)^T$ and $(\cdot)^H$, respectively.

The system model of the proposed distributed antenna access system is shown in Fig. 6.4, where, the DAU with N_A antennas are available to serve N_U users. Each DAU is connected to the RRU through a LAN cable with N_C twisted pairs, where each twisted pair has N_F sub-channels over the cable bandwidth BW_C. Each sub-channel is equally spaced in the frequency domain at intervals equal to $\triangle f_{cable}$ (*i.e.*, $N_F = \lfloor \text{BW}_C / \triangle f_{cable} \rfloor$). The coherence bandwidth is assumed to be equal to $\triangle f_{air}$ over the bandwidth BW_{5G}, where each user has N_R sub-channels (*i.e.*, $N_R = \lfloor \text{BW}_{5G} / \triangle f_{air} \rfloor$). Without loss of generality, we assume that the sub-channel width of air and cable is identical ($\triangle f_{cable} \approx \triangle f_{air} \approx \triangle f$).

In the uplink, the DAU needs to filter the received RF signals at $\triangle f$ intervals to extract the corresponding IF signals that are suitable for transmission over the cable. The downlink operations are similar but just reversed. For this purpose, the DAU contains analog-to-analog (A/A) converters that down-convert (or up-convert) the received antenna signals into IF signals for uplink and vice versa for the downlink. Note that this A/A device is designed to map these IF signals on the cable by means of analog and/or digital processing. We assume that the US decisions are made by a scheduler located inside each RRU and the A/A converter receives the scheduling decisions through a control channel between the RRU and the DAU (as shown in Fig. 6.4). The carrier frequency of the local oscillators (that are attached to each antenna) is set based on these scheduling decisions to ensure that each IF signal is mapped at the desired sub-channel over the cable.

The received signal vector after down-conversion in Fig. 6.4 is defined as follows:

$$\tilde{\mathbf{s}} = \mathbf{H}_A \mathbf{s} + \mathbf{n}_A \tag{6.1}$$

here, $\mathbf{H}_A \in \mathbb{C}^{N_A \times N_U}$ is the air channel matrix for uplink transmission from N_U users to the N_A antennas at the DAU (which will be discussed in Section 6.2.2), $\mathbf{s} \in \mathbb{C}^{N_U}$ are the transmitted signals (with unit power $\sigma_s^2 = 1$) from the 5G users, $\mathbf{n}_A \sim \mathcal{CN}(\mathbf{0}, \sigma_A^2 \mathbf{I}_A)$ is the AWGN at different antennas of the DAU with a flat PSD equal to σ_A^2.

The signal vector $\mathbf{y} \in \mathbb{C}^{N_U}$ received at the RRU can be defined as:

$$\mathbf{y} = \mathbf{H}_C \mathbf{B} \tilde{\mathbf{s}} + \mathbf{n}_C \tag{6.2}$$

here, $\mathbf{H}_C \in \mathbb{C}^{N_C \times N_C \times N_F}$ is the block diagonal cable MIMO channel with frequency dependent direct channels on the main diagonal ($[\mathbf{H}_C]_{i,i}$) and far-end crosstalk (FEXT) channels on the off-diagonals ($[\mathbf{H}_C]_{i,j}$), $\mathbf{B}$ is the amplifier gain that controls the transmitted power over the cable, and $\mathbf{n}_C \sim \mathcal{CN}(\mathbf{0}, \sigma_C^2 \mathbf{I}_{N_C})$ is the thermal noise within the cable with a flat PSD equal to σ_C^2 . Note that the amplifier gain $\mathbf{B}$ is required to minimize the FEXT due to capacitive and inductive coupling between different cable pairs.

6.2.1 Cable MIMO Channel

The cable channel capacity can be greatly enhanced by considering cable MIMO, which is possible by employing LAN cables that have multiple twisted pairs [69]. Since, the N_C pairs within a single LAN cable can support a large number of antennas when the N_R sub-channels of each antenna can be properly mapped onto the cable. Therefore, a key functional element of the proposed distributed antenna access architecture is the mapping of RF signals over different sub-channels of the multi-pair cable. The overall cable bandwidth required to transport data signals from N_A antennas at DAU should be at least $N_A \times BW_{5G}$, where BW_{5G} is the transmission bandwidth of each user that is considered to be 20 MHz in this thesis. Hence the capacity of the cable must be

$$\sum_{n=1}^{N_C} BW_{C,n} \geq N_A \times BW_{5G} \tag{6.3}$$

here, the achievable transmission bandwidth for n-th cable pair is $B_{C,n}$ and N_C is the number of twisted pairs in the multi-pair LAN cable. Using (6.3), the maximum number of antennas (N_U^{max}) for all 5G users connected to a single DAU can be expressed as:

$$N_U^{max} = \sum_{n=1}^{N_C} \left\lfloor \frac{BW_{C,n}}{BW_{5G}} \right\rfloor \tag{6.4}$$

The number of radio signals that could be mapped over the LAN cable depends on multiple practical factors such as LAN cable type, length and total transmission bandwidth over each twisted pair (*i.e.*, $BW_{C,n}$). The multi-pair cable characteristics vary with the shielding type and the twist density (i.e. number of twist/cm). The most affordable and commonly deployed LAN cable for data networks is unshielded twisted pair (UTP) CAT-5 cable. However, it results in low noise immunity at high frequencies. In contrast, the noise and interference immunity is improved in high grade UTP CAT-6 cable with the help of additional foil and also by increasing the twist density (which is > 2 twists/cm). Further noise and interference immunity is achieved in high grade shielded CAT-7 cables through extensive shielding over each twisted pair.

For a CAT cable with N_C twisted pairs, the channel can be modeled as a block-diagonal matrix to ensure orthogonality among multiple sub-channels

$$\mathbf{H}_C = \text{diag}\big[\mathbf{H}_1, \mathbf{H}_2, \ldots, \mathbf{H}_{N_F}\big] \tag{6.5}$$

where, the diagonal elements of the k-th sub-channel, i.e, $\mathbf{H}_k \in \mathbb{C}^{N_C \times N_C}, k \in \{1...N_F\}$, represent the direct link between the RRU and the DAU, and the off-diagonal terms show the crosstalk between different twisted cable pairs [66, 72].

Thus, the SINR on the kth sub-channel on nth twisted pair is defined as follows:

$$[\mathbf{SINR}_{Cable}]^{n,k} = \frac{|h_n^{n,k}|^2 P^{n,k}}{\sum_{n'}^{n' \neq n} |h_n^{n',k}|^2 P^{n',k} + \sigma_C^2}, \quad \forall n, \forall k \tag{6.6}$$

here, $h_n^{n,k}$ is the direct channel gain on the kth sub-channel of the nth cable pair, $h_n^{n',k}$ is the off-diagonal channel gain between the kth sub-channels of the nth and n'th cable pairs, σ_C^2 is the noise power for cable sub-channels, and $P^{n,k}$ is the power allocated on the kth sub-channel of the nth cable pair. The sum power of all the sub-channels for the pair n are constrained by the total transmit power of P_T (*i.e.*, $\sum_{k=1}^{N_F} P^{n,k} \leq P_T$). In addition, the maximum power of the transmitted signals over the cable are also constrained by the maximum power spectral density (*i.e.*, $P^{n,k} \leq P_{max}$).

6.2.2 Radio MIMO Channel

We consider an uplink MIMO system that has N_U single antenna UEs transmiting signals to the DAU, which is equipped with N_A antennas, simultaneously. When the Non-line of sight (NLoS) channel is assumed, the air channel model can be generalized by $\mathbf{H}_A = \mathbf{G}\mathbf{D}^{1/2}$, where $D = \text{diag}\big[\beta_1, \beta_2, \ldots, \beta_{N_U}\big]$ is the large-scale propagation matrix and $\mathbf{G} \in \mathbb{C}^{N_A \times N_U}$ is the fast fading matrix; here, $\beta_u\,[\text{dB}] = \alpha + \gamma \times 10 \times \log_{10}(d_u) + \xi_u$; d_u is the distance between the user u and the DAU, α is a constant related to the antenna gain and carrier frequency, γ is the path loss exponent, and ξ_u is the log-normal shadow fading coefficient with $10 \times \log_{10}(\xi_u) \in \mathcal{N}(0, \sigma^2)$.

For computing the fast fading matrix $\mathbf{G}$, we assume a correlation-based channel model [76, 77] to evaluate the performance of the proposed DAU with linear antenna array, where the fast fading channel vector of each user can be formed by the correlation matrix multiplied by a standard complex Gaussian vector:

$$\mathbf{G}_u = \mathbf{R}_u \mathbf{v}_u, u = 1, 2, \ldots, N_U \tag{6.7}$$

where, the steering matrix $\mathbf{R}_u \in \mathbb{C}^{N_A \times N_U}$ contains D_u steering vectors with different angles of arrival (AoAs) for user u and $\mathbf{v}_u \sim \mathcal{CN}(\mathbf{0}, \mathbf{I}_{D_u})$.

When the linear antenna array is assumed at the DAU, the steering matrix $\mathbf{R}_u$ can be computed as:

$$\mathbf{R}_u = \frac{1}{D_u} \begin{bmatrix} \mathbf{a}(\theta_{u,1}) & \mathbf{a}(\theta_{u,2}) & \ldots & \mathbf{a}(\theta_{u,D_u}) \end{bmatrix}, \forall u \tag{6.8}$$

here, $\theta_{u,i} \sim \mathcal{U}(0,\, 2\pi)$ is the ith AoA of user u and the steering vector $\mathbf{a}(\theta_{u,i}) \in \mathbb{C}^{N_A \times 1}$ is given by:

$$\mathbf{a}(\theta_{u,i}) = \begin{bmatrix} 1 & e^{j2\pi d/\lambda \sin(\theta_{u,i})} & \ldots & e^{j2\pi(N_A-1)d/\lambda \sin(\theta_{u,i})} \end{bmatrix}^T \tag{6.9}$$

here, d is the distance between the adjacent antennas and λ is the carrier wavelength.

This correlation-based channel model introduces the AoAs, which can be utilized to distinguish the UE and improve the accuracy of channel estimation [78]. When the UE is located at different orientations, the user channels can almost be separated by angle information, thereby alleviating the pilot contamination.

It is also helpful to analyze the inter-user or inter-cell interference and develop scheduling algorithms with/without RRU cooperation to alleviate the interference. Note that a minimum-mean-square-error (MMSE) receiver has been assumed at the RRU for interference mitigation on the UL. In contrast, a concatenated linear pre-coding technique employing either zero-forcing (ZF) or regularized ZF (RZF) can be used on the DL to satisfy the minimum transmission rate constraints and also to nullify interference.

6.2.3 5G Transmission Rates

C-RAN front-haul implementation for 5G [79] defines several functional split options (e.g. different signal processing capabilities at the BBU and RRU) to relax the latency and bandwidth requirements within conventional CPRI implementation. We employ 5G new radio (NR) specifications for computing the transmission rates in this chapter, where physical layer functionalities, such as, FFT/ IFFT, sub-carrier mapping/ de-mapping, signal equalization, and MIMO processing, are implemented at the RRU. We assume that the Error Vector Magnitude (EVM) of each user is estimated at the RRU during the initialization procedure between UE and RRU as mentioned in [80]. The EVM of each IF signal in Fig. 6.4 can be translated into the corresponding Signal-to-Noise Ratio (SNR) by using the techniques discussed in [81] (*i.e.*, $[\mathbf{SNR}_{5G}]_{u,r}, u = 1, \ldots, N_U, r = 1, \ldots, N_R$); where, sub-channel r in 5G corresponds to multiple OFDM symbols (N_S) with varying bandwidths Δf_S per PRB (of duration T). Since, we consider BW_{5G} to be flat across Δf, the corresponding bit rates ($\mathbf{R}_{5G} \in \mathbb{R}^{N_U \times N_R}$) are assumed to be quasi-constant within each sub-channel. Therefore, the data rate (in bits per second) on each sub-channel (Δf) can be computed as follows:

$$[\mathbf{R_{5G}}]_{u,r} = \Delta f \times \log_2 \left(1 + [\boldsymbol{SNR_{5G}}]_{u,r}\right), u = 1, \ldots, N_U, r = 1, \ldots, N_R \tag{6.10}$$

6.3 The Joint MP-A2C Optimization Problem

In this section, we formulate the optimal MP-A2C problem, which jointly determines the power and sub-channel allocation along the multi-pair (MP) cable when there are $N_U \leq N_A$ active users transmitting to the DAU. Each user/antenna has N_R radio sub-channels that needs to be mapped over N_C twisted pairs, each one with N_F sub-channels.

The following optimization variables are required for the joint MP-A2C problem:

- $\boldsymbol{x_{u,r}^{n,k}}$ is an assignment variable for one-to-one sub-channel mapping; it is equal to 1 if sub-channel $r \in \{1, \ldots, N_R\}$ of user $u \in \{1, \ldots, N_U\}$ is allocated to sub-channel $k \in \{1, \ldots, N_F\}$ of the twisted pair $n \in \{1, \ldots, N_C\}$ and 0 otherwise.
- $\boldsymbol{P_{u,r}^{n,k}}$ is for allocating power for rth sub-channel of uth user over kth sub-channel of nth cable pair.
- $\boldsymbol{\gamma_{u,r}^{n,k}}$ is for computing SINR for rth sub-channel of uth user over kth sub-channel of nth cable pair.
- $\boldsymbol{I^{n,k}}$ is for computing interference on kth sub-channel of nth cable pair.
- $\boldsymbol{\lambda_{u,r}}$ is the data rate seen by user u on sub-channel r.

The objective function of the joint MP-A2C problem is based on maximizing the AM throughput of all users along the multi-pair cable. Given the cable channel matrix (*i.e.*, $\mathbf{H}_C$ with $h_n^{n,k}$ as the direct channel gains and $h_n^{n',k}$ as the off-diagonal channel gains) and the set of data rates achievable by each radio sub-channel (*i.e.*, $[\boldsymbol{R}^{5G}]_{u,r}$), the MP-A2C optimization problem, denoted by $[\boldsymbol{P_{MP-A2C}}]$[2], can be defined as follows:

$$[\boldsymbol{P_{MP-A2C}}] : \underset{\{x_{u,r}^{n,k}\},\{P_{u,r}^{n,k}\},\{\gamma_{u,r}^{n,k}\},\{I^{n,k}\},\{\lambda_{u,r}\}}{\text{maximize}} \sum_{u=1}^{N_U} \sum_{r=1}^{N_R} \lambda_{u,r}$$

[2] Here the bracket signifies that this problem is dependent on the network realization/snapshot of 5G users for determining $[\boldsymbol{R}^{5G}]_{u,r}$.

subject to:

$$x_{u,r}^{n,k} \in \{0,1\}, \qquad \forall u, \forall r, \forall n, \forall k \tag{6.11a}$$

$$\sum_{u=1}^{N_U}\sum_{r=1}^{N_R} x_{u,r}^{n,k} \leq 1, \qquad \forall n, \forall k \tag{6.11b}$$

$$\sum_{n=1}^{N_C}\sum_{k=1}^{N_F} x_{u,r}^{n,k} \leq 1, \qquad \forall u, \forall r \tag{6.11c}$$

$$0 \leq P_{u,r}^{n,k} \leq x_{u,r}^{n,k} P_{max}, \qquad \forall u, \forall r, \forall n, \forall k \tag{6.11d}$$

$$\sum_{u=1}^{N_U}\sum_{r=1}^{N_R}\sum_{k=1}^{N_F} P_{u,r}^{n,k} \leq P_T, \qquad \forall n \tag{6.11e}$$

$$0 \leq \gamma_{u,r}^{n,k} \leq x_{u,r}^{n,k}\gamma_{max}, \qquad \forall u, \forall r, \forall n, \forall k \tag{6.11f}$$

$$P_{u,r}^{n,k}|h_n^{n,k}|^2 \geq \gamma_{u,r}^{n,k}\big(I^{n,k} + \sigma_C^2\big), \qquad \forall u, \forall r, \forall n, \forall k \tag{6.11g}$$

$$I^{n,k} = \sum_{n'=1, n' \neq n}^{N_C}\sum_{u'=1}^{N_U}\sum_{r'=1}^{N_R} P_{u',r'}^{n',k}|h_n^{n',k}|^2, \qquad \forall n, \forall k \tag{6.11h}$$

$$\lambda_{u,r} = \Delta f \times \log_2(1 + \sum_{n=1}^{N_C}\sum_{k=1}^{N_F}\gamma_{u,r}^{n,k}), \forall u, \forall r, \forall n, \forall k \tag{6.11i}$$

$$\lambda_{u,r} \geq [\boldsymbol{R}^{5G}]_{u,r}, \qquad \forall u, \forall r \tag{6.11j}$$

where, $u \in \{1,\ldots,N_U\}, r \in \{1,\ldots,N_R\}, n \in \{1,\ldots,N_C\}$, and $k \in \{1,\ldots,N_F\}$. The constraints (6.11a), (6.11b), and (6.11c) ensure that a single sub-channel over the cable will not be assigned to multiple radio sub-channels and vice versa. The constraints (6.11d), (6.11e), and (6.11f) ensure that the transmit power (as well as the SINR) over each cable sub-channel is not higher than the specified margins.

Note that in $[\boldsymbol{P_{MP-A2C}}]$ the sub-channel assignment variables, i.e., $x_{u,r}^{n,k}$ are binary and the constraints for computing SINR are bilinear in nature. This leads to a non-convex solution space, therefore, solving this problem exactly is computationally intractable. To solve problem efficiently, we propose a convex upper bound problem by exploiting GP along with some smart transformations.

6.3.1 The Upper Bound Problem

We want to transform the joint MP-A2C problem into a tractable problem that can be solved efficiently. This can be achieved by removing all binary variables from $[\boldsymbol{P_{MP-A2C}}]$. Note that the binary variables $x_{u,r}^{n,k}$ are required for achieving one-to-one mapping between radio sub-channels and cable sub-channels. Therefore, after removing these binary variables, we need to add more constraints to ensure that two radio sub-channels do not to get mapped to the same cable sub-channel and vice versa. Given these considerations, we formulate the *relaxed* joint MP-A2C problem as follows:

$$[\boldsymbol{P}_{\boldsymbol{MP-A2C}}^{\boldsymbol{UB}}] : \underset{\{P_{u,r}^{n,k}\},\{I_{u,r}^{n,k}\},\{\gamma_{u,r}^{n,k}\},\{\lambda_{u,r}\}}{\text{maximize}} \sum_{u=1}^{N_U}\sum_{r=1}^{N_R} \lambda_{u,r}$$

subject to (6.11e), (6.11g), (6.11h),
(6.11i),(6.11j), and:

$$P_{min} \leq P_{u,r}^{n,k} \leq P_{max}, \qquad \forall u, \forall r, \forall n, \forall k \qquad (6.12a)$$

$$P_{u,r}^{n,k} P_{u',r'}^{n,k} \leq \epsilon_p, \qquad \forall u, \forall r, \forall (u',r'), (u',r') \neq (u,r), \forall n, \forall k \qquad (6.12b)$$

$$P_{u,r}^{n,k} P_{u,r}^{n',k'} \leq \epsilon_p, \qquad \forall u, \forall r, \forall n, \forall k, \forall (n',k'), (n',k') \neq (n,k) \qquad (6.12c)$$

$$\sum_{u=1}^{N_U}\sum_{r=1}^{N_R} P_{u,r}^{n,k} \leq P_{max}, \qquad \forall n, \forall k \qquad (6.12d)$$

$$\epsilon_\gamma \leq \gamma_{u,r}^{n,k} \leq \gamma_{max}, \qquad \forall u, \forall r, \forall n, \forall k \qquad (6.12e)$$

$$\sum_{u=1}^{N_U}\sum_{r=1}^{N_R} \gamma_{u,r}^{n,k} \leq \gamma_{max}, \qquad \forall n, \forall k \qquad (6.12f)$$

$$\sum_{n=1}^{N_C}\sum_{k=1}^{N_F} \gamma_{u,r}^{n,k} \leq \gamma_{max}, \qquad \forall u, \forall r \qquad (6.12g)$$

where, $u \in \{1,\ldots,N_U\}, r \in \{1,\ldots,N_R\}, n \in \{1,\ldots,N_C\}$, and $k \in \{1,\ldots,N_F\}$. The constraints (6.12b) and (6.12c) ensure that each cable sub-channel is assigned to only one user with a considerable amount of power. Similarly, the constraints (6.12f) and (6.12g) ensure that the total SINR on each sub-channel does not exceed its maximum specified value, hence, forcing a sub-channel to be mapped to only one user with a considerable

amount of SINR. Note that P_{min}, ϵ_p, and ϵ_γ are very small positive values that depend on the numerical values of $P_{u,r}^{n,k}$ and $\gamma_{u,r}^{n,k}$, respectively.

The upper bound problem ($[\boldsymbol{P}_{\boldsymbol{MP-A2C}}^{\boldsymbol{UB}}]$) is non-linear and non-convex in nature that requires extensive computational resources; mainly, due to the presence of bilinear constraints for computing the SINR. However, it has been shown in [82] that when SINR is much larger than 0dB, the GP transformation [38] can be used to efficiently compute the globally optimal power in many of the non-linear convex problems. The key observations that despite the apparent non-convexity, through logarithmic change of variable the GP techniques can turn these constrained optimization of power control into convex optimization.

Lemma 6.1: *In the high-SINR region, the problem ($[\boldsymbol{P}_{\boldsymbol{MP-A2C}}^{\boldsymbol{UB}}]$) can be solved by GP, i.e., can be transformed into a convex optimization problem ($[\boldsymbol{P}_{\boldsymbol{MP-A2C}}^{\boldsymbol{UB'}}]$) with efficient algorithms to compute the globally optimal power vector.*
Proof: Please see Appendix F.

6.3.2 Feasible Solutions

For a given realization, an optimal solution for $[\boldsymbol{P}_{\boldsymbol{MP-A2C}}^{\boldsymbol{UB'}}]$ can be used to find a feasible solution for the original problem $[\boldsymbol{P}_{\boldsymbol{MP-A2C}}]$ using the method described in Algorithm 4; where, the feasible solution is computed from the optimal SINR values (i.e., $\boldsymbol{\gamma}_{\boldsymbol{u,r}}^{\boldsymbol{*'n,k}}$) obtained by solving $[\boldsymbol{P}_{\boldsymbol{MP-A2C}}^{\boldsymbol{UB'}}]$. Note that each $\boldsymbol{\gamma}_{\boldsymbol{u,r}}^{\boldsymbol{*'n,k}}$ needs to be transformed into the corresponding $\boldsymbol{\gamma}_{\boldsymbol{u,r}}^{\boldsymbol{*n,k}}$.

Algorithm 4 A Feasible Solution for[$\boldsymbol{P_{MP-A2C}}$] using $\{\boldsymbol{\gamma_{u,r}^{*n,k}(\omega)}\}_{\forall u,\forall r,\forall n,\forall k}$

for each $u \in \{1,\ldots,N_U\}, r \in \{1,\ldots,N_R\}$ **do**
  $maxN \leftarrow -1$, $maxK \leftarrow -1$, $maxSINR \leftarrow 0$
  for each $n \in \{1,\ldots,N_C\}, k \in \{1,\ldots,N_F\}$ **do**
    if $\gamma_{u,r}^{*n,k} \geq maxSINR$ **then**
      if $maxN \geq 0$ AND $maxK \geq 0$ **then** $P_{u,r}^{n,k} \leftarrow 0$
      end if
      $maxN \leftarrow n$, $maxK \leftarrow k$, $maxSINR \leftarrow \gamma_{u,r}^{*n,k}$
    else $P_{u,r}^{n,k} \leftarrow 0$
    end if
  end for
end for
Compute modified SINRs (*i.e.*,$\gamma_{u,r}^{**n,k}, \forall u \in \{1,\ldots,N_U\}, \forall r \in \{1,\ldots,N_R\}$)

6.4 Heuristic-based MP-A2C Scheduler

The proposed joint MP-A2C problem can be solved in the presence of a joint scheduler in the RRU, which has extensive computational resources. However, in practice the computational resources are limited thereby low complexity heuristic-based schedulers are preferred for real-time mapping from air to cable and vice versa. We propose simple, but efficient heuristics for solving the joint MP-A2C problem by dividing it into two smaller problems, namely *Power Allocation Problem* and *Sub-channel Mapping Problem*, which can be solved one after the other as follows:

- The **Power Allocation Problem** computes the optimal power on each individual sub-channel given the inter-pair crosstalk due to FEXT. More specifically, it determines the amount of power required on each sub-channel that will maximize the overall sum-rate throughput on the given LAN Cable. Once the power has been optimized and thereby fixed on each sub-channel, we can determine one-to-one mapping between the radio sub-channels and cable sub-channels in an efficient manner.

- The **Sub-channel Mapping Problem** allocates appropriate sub-channel to find which radio sub-channels will be assigned to which sub-channel, i.e., it determines the set $\{x_{u,r}^{n,k}\}_{\forall u,\forall r,\forall n,\forall k}$, where $x_{u,r}^{n,k} = 1$ when rth sub-channel of uth user has been allocated kth sub-channel of nth cable pair and is 0 otherwise.

6.4.1 Power Allocation Problem

Power allocation over sub-channels of each twisted pair bundled in a LAN cable directly affects the crosstalk (FEXT) among the twisted pairs. Therefore, the power on each sub-channel of the LAN cable must be selected in a way that the overall data rates, corresponding to the actual SINR with FEXT considerations, are maximized. This could be achieved by solving a power allocation problem, denoted by $\boldsymbol{P_C}$, with the following optimization variables:

- $\boldsymbol{P^{n,k}}$ is the power allocation on k^{th} sub-channel of nth cable pair.
- $\boldsymbol{\gamma^{n,k}}$ is the actual SINR with FEXT on k^{th} sub-channel of nth cable pair.
- $\boldsymbol{R^{n,k}}$ is the maximum data rate (in bits per second) that can be achieved on k^{th} sub-channel of nth cable pair.

The objective function of the AM-based power allocation problem is based on maximizing the AM throughput of all sub-channels across the multi-pair cable. Given the cable channel matrix (*i.e.*, $\mathbf{H}_C$ with $h_n^{n,k}$ as the direct channel gains and $h_n^{n',k}$ as the off-diagonal channel gains), the AM-based power allocation problem, denoted by $\boldsymbol{P_C^{AM}}$, can be defined as follows:

$$\boldsymbol{P_C^{AM}}: \underset{\{P^{n,k}\},\{I^{n,k}\},\{\gamma^{n,k}\},\{\lambda^{n,k}\}}{\text{maximize}} \sum_{n=1}^{N_C}\sum_{k=1}^{N_F}(\lambda^{n,k})$$

subject to:

$$P_{min} \leq P^{n,k} \leq P_{max}, \qquad \forall n, \forall k \tag{6.13a}$$

$$\sum_{k=1}^{N_F} P^{n,k} \leq P^T, \qquad \forall n \tag{6.13b}$$

$$\gamma_{min} \leq \gamma^{n,k} \leq \gamma_{max}, \qquad \forall n, \forall k \tag{6.13c}$$

$$P^{n,k}|h_n^{n,k}|^2 \geq \gamma^{n,k}\big(I^{n,k} + \sigma_C^2\big), \forall n, \forall k \tag{6.13d}$$

$$I^{n,k} = \sum_{n'=1, n' \neq n}^{N_C} P^{n',k}|h_n^{n',k}|^2, \qquad \forall n, \forall k \tag{6.13e}$$

$$\lambda^{n,k} = \Delta f \times \log_2(1+\gamma^{n,k}), \quad \forall n, \forall k \tag{6.13f}$$

where, $k \in \{1, ..., N_F\}$ and $n \in \{1, .., N_C\}$.

Lemma 6.2: *In the high-SINR region, the problem $\boldsymbol{P_C^{AM}}$ can be solved by GP, i.e., can be transformed into a convex optimization with efficient algorithms to compute the globally optimal power vector.*

Proof: Please see Appendix G.

The objective function of the GM-based power allocation problem is based on maximizing the GM throughput of all sub-channels across the multi-pair cable. Given the cable channel matrix (*i.e.*, $\mathbf{H}_C$ with $h_n^{n,k}$ as the direct channel gains and $h_n^{n',k}$ as the off-diagonal channel gains), the GM-based power allocation problem, $\boldsymbol{P_C^{GM}}$, can be defined as follows:

$$\boldsymbol{P_C^{GM}}: \underset{\{P^{n,k}\},\{I^{n,k}\},\{\gamma^{n,k}\},\{\lambda^{n,k}\}}{\text{maximize}} \sum_{n=1}^{N_C}\sum_{k=1}^{N_F}\log\left(\lambda^{n,k}\right)$$

subject to: (6.13a-f)

Lemma 6.3: *In the high-SINR region, the problem $\boldsymbol{P_C^{GM}}$ can be solved by GP, i.e., can be transformed into a convex optimization with efficient algorithms to compute the globally optimal power vector.*

Proof: Please see Appendix H.

Let the optimal power matrix be denoted by $\boldsymbol{P}_{\boldsymbol{C}}^{*} \in \mathbb{R}^{N_C \times N_F}$ and the corresponding optimal rate matrix be denoted by $\boldsymbol{R}_{\boldsymbol{C}}^{*} \in \mathbb{R}^{N_C \times N_F}$, which can be obtained by solving the above mentioned power allocation problems. Once the optimal power $\boldsymbol{P}_{\boldsymbol{C}}^{*}$ is known, the amplifier gain matrix $\mathbf{B}$ is simple a block diagonal matrix; $\mathbf{B} = \text{diag}(\mathbf{B}_1, \ldots, \mathbf{B}_{N_F})$ and it can be computed beforehand to allocate optimal transmit power to the signals $\mathbf{x}$ before transmitting them over the cable. The $N_C \times N_C$ amplifier gain matrix $\mathbf{B}_k$ for the k-th sub-channel is defined as:

$$\mathbf{B}_k = \text{diag}\left[\sqrt{[\boldsymbol{P}_{\boldsymbol{C}}^{*}]_{1,k}^{2}}, \ldots, \sqrt{[\boldsymbol{P}_{\boldsymbol{C}}^{*}]_{N_C,k}^{2}}\right] \tag{6.15}$$

Thus, the SINRs of the received signals, i.e., $\mathbf{y}$ at the RRU will correspond to the maximum rates that can be obtained over the cable on a particular sub-channel. Note that the MP-A2C scheduler in the RRU is also responsible for allocating sub-channels to each user as discussed in the next sub-section.

6.4.2 Sub-channel Mapping Problem

In this section, we define a sub-channel mapping problem to determine one-to-one mapping between the radio sub-channels and cable sub-channels, when the power ($\boldsymbol{P}_{\boldsymbol{C}}^{*} \in \mathbb{R}^{N_C \times N_F}$) and the corresponding rate ($\boldsymbol{R}_{\boldsymbol{C}}^{*} \in \mathbb{R}^{N_C \times N_F}$) has been allocated to each sub-channel of the LAN cable after solving either $\boldsymbol{P}_{\boldsymbol{C}}^{\boldsymbol{AM}}$ or $\boldsymbol{P}_{\boldsymbol{C}}^{\boldsymbol{GM}}$. More specifically, we need to determine the set $\{\boldsymbol{x}_{\boldsymbol{u,r}}^{\boldsymbol{n,k}}\}_{u \in \{1,\ldots,N_U\}, r \in \{1,\ldots,N_R\}, n \in \{1,\ldots,N_C\}, k \in \{1,\ldots,N_F\}}$, where $x_{u,r}^{n,k} = 1$ when rth sub-channel of uth user has been allocated kth sub-channel of nth cable pair and is 0 otherwise.

We assume that the mapping of the received radio signals at the DAU is based on a utility function that considers the transmission rates of the users corresponding to the LAN cable, i.e., denoted by $\boldsymbol{Rate}_{\boldsymbol{u,r}}, \forall u, \forall r$. If the sub-channel mapping is based on maximizing the arithmetic mean rate (AM) of the sub-channels allocated to each user on the cable, we define our utility function as follows:

$$U(\{Rate_{u,r}\}_{u\in\{1,\ldots,N_U\},r\in\{1,\ldots,N_R\}}) := \sum_{u=1}^{N_U}\sum_{r=1}^{N_R}(Rate_{u,r}), \tag{6.16}$$

For maximizing the geometric mean rate (GM), we define the utility function as follows:

$$U(\{Rate_{u,r}\}_{u\in\{1,\ldots,N_U\},r\in\{1,\ldots,N_R\}}) := \sum_{u=1}^{N_U} log(\sum_{r=1}^{N_R} Rate_{u,r}), \tag{6.17}$$

We ensure that two radio sub-channels do not get mapped over the same cable sub-channel and vice versa. In addition, we consider a one-to-one mapping of only those radio and cable sub-channels that have strictly positive bit rates, i.e., $[\mathbf{R_{5G}}]_{u,r} > 0, \forall u, \forall r$ and $[\mathbf{R_C^*}]^{n,k} > 0, \forall n, \forall k$, respectively.

According to the above considerations, the optimization problem for one-to-one mapping between radio and cable sub-channels, denoted by $[\boldsymbol{P_{US}}]$[3], is defined as follows:

$$[\boldsymbol{P_{US}}] : \underset{\{x_{u,r}^{n,k}\},\{Rate_{u,r}\}}{\text{maximize}} \; U(\{Rate_{u,r}\}_{u\in\{1,\ldots,N_U\},r\in\{1,\ldots,N_R\}})$$

subject to:

$$x_{u,r}^{n,k} \in \{0,1\}, \qquad \forall u, \forall r, \forall n, \forall k \tag{6.18a}$$

$$\sum_{u=1}^{N_U}\sum_{r=1}^{N_R} x_{u,r}^{n,k} \leq 1, \qquad \forall n, \forall k \tag{6.18b}$$

$$\sum_{n=1}^{N_C}\sum_{k=1}^{N_F} x_{u,r}^{n,k} \leq 1, \qquad \forall u, \forall r \tag{6.18c}$$

$$Rate_{u,r} = \sum_{n=1}^{N_C}\sum_{k=1}^{N_F} x_{u,r}^{n,k}[\mathbf{R_C^*}]^{n,k}, \qquad \forall u, \forall r \tag{6.18d}$$

$$Rate_{u,r} \geq [\mathbf{R}_{5G}]_{u,r}, \qquad \forall u, \forall r \tag{6.18e}$$

[3] Here the bracket signifies that this problem is dependent on the network realization/snapshot of 5G users for determining $[\boldsymbol{R}^{5G}]_{u,r}$.

Note that $[\boldsymbol{P_{US}}]$ becomes a large scale matching problem when Δf is relatively small. Therefore, we need to transform this problem into a weighted bipartite matching problem that can be solved efficiently using existing algorithms, such as, the Hungarian algorithm [83]. This transformation is possible if the cost matrix for the weighted bipartite matching problem is computed using Algorithm 5; where, $[\boldsymbol{W}]_u$ are the weights assigned to each user, i.e., $[\boldsymbol{W}]_u = 1$ and $[\boldsymbol{W}]_u = \frac{1}{\sum_{r=1}^{N_R} [\mathbf{R_G}]_{u,r}}$ for $[\boldsymbol{P_{US}^{AM}}]$ and $[\boldsymbol{P_{US}^{GM}}]$, respectively. When the cost associated with each assignment is known, the mappings can be obtained by solving the following pure assignment problem:

$$[\boldsymbol{P_{US}^{'}}] : \underset{\{x_{u,r}^{n,k}\}}{\text{maximize}} \sum_{u=1}^{N_U} \sum_{r=1}^{N_R} \sum_{n=1}^{N_C} \sum_{k=1}^{N_F} x_{u,r}^{n,k} [\mathbf{C}]_{u,r}^{n,k}$$

subject to:

$$x_{u,r}^{n,k} \in \{0,1\}, \forall u, \forall r, \forall n, \forall k \tag{6.19a}$$

$$\sum_{u=1}^{N_U} \sum_{r=1}^{N_R} x_{u,r}^{n,k} = 1, \qquad \forall n, \forall k \tag{6.19b}$$

$$\sum_{n=1}^{N_C} \sum_{k=1}^{N_F} x_{u,r}^{n,k} = 1, \qquad \forall u, \forall r \tag{6.19c}$$

Pure assignment problems can be solved efficiently using existing algorithms, such as, the Hungarian method with complexity $\mathcal{O}(N^3)$, where $N = N_U \times N_R$. A step by step algorithm and its complexity has been derived in [83], whereas a latest heuristic for the Hungarian method with time complexity $\mathcal{O}(N^2)$ has been proposed in [84].

Algorithm 5 Algorithm for Computing Cost Matrix

Input: $[\boldsymbol{W}]_u, [\mathbf{R_G}]_{u,r}, [\mathbf{R_C^*}]^{n,k}, N_U, N_R, N_C, N_F$

1: **for** each $u \in \{1...N_U\}, r \in \{1...N_R\}, n \in \{1..N_C\}, k \in \{1..N_F\}$ **do**
2: **if** $[\mathbf{R_C^*}]^{n,k} \geq [\mathbf{R_G}]_{u,r}$ **then** $[\mathbf{C}]_{u,r}^{n,k} = [\boldsymbol{W}]_u \big([\mathbf{R_C^*}]^{n,k} - [\mathbf{R_G}]_{u,r}\big)$
3: **else** $[\mathbf{C}]_{u,r}^{n,k} = -\infty$
4: **end if**
5: **end for**

Output: $\mathbf{C} \in \mathbb{R}^{N_U \times N_R \times N_C \times N_F}$

Table 6.1: 5G NR Physical Layer Parameters

Sub-carrier spacing parameter (μ)	2 (indoor propagation)
Sub-carrier spacing ($\Delta f_{SC} = 2^{\mu} \times 15\text{kHz}$)	60 kHz
Number of sub-carriers per PRB (N_{SC})	12
PRB bandwidth ($\Delta f_{PRB} = N_{SC} \times 2^{\mu} \times 15\text{kHz}$)	720 kHz
OFDM symbols per PRB (N_S)	$12 \times 4 \times 14$
PRB Duration (T)	1 ms
Number of radio sub-channels per antenna/user (N_R)	4
Sub-channel bandwidth ($\Delta f = 6 \times \Delta f_{PRB}$)	4.32MHz
5G Bandwidth ($BW_{5G} = N_R \times \Delta f$)	17.28MHz $<$ 20MHz
Path Loss Constant (α)	140.7
Path Loss Exponent (γ)	3.67
Shadow Fading Coefficient ($\xi_u \in \mathcal{N}(\mathbf{0}, \sigma^2)$)	$\sigma = 8$dB

6.5 Performance Evaluation

In this section, we analyze the performance of the Heuristic-based MP-A2C scheduler and examine its efficiency in supporting a single DAU with multiple antennas via a LAN cable, when the DAU is placed in the middle of a chamber (of radius 100m). The DAU is connected with the RRU via a multi-pair LAN cable (*i.e.*, CAT-5) with varying lengths (i.e., from 100m to 200m). We consider the actual channel measurements, i.e., Insertion Loss (IL) and Far-end Crosstalk (FEXT) for multi-pair CAT-5 cable as discussed in [66]. The radio channel under consideration is modeled by 5G NR physical layer and transmission parameters for indoor propagation environment, which are given in Table 6.1. The radio channel is assumed to be flat across each sub-channel bandwidth (*i.e.*, Δf).

Note that we consider a cable bandwidth of 500MHz, since, the longer LAN cables, i.e. larger than 100m, offer almost zero spectral efficiency after this frequency band [66].

Table 6.2: LAN Cable Physical Layer Parameters

Multi-pair Cable	CAT-5
Number of twisted pairs (N_C)	4
Cable lengths	100m, 125m, 150m, 175m, 200m
Cable bandwidth (BW_C)	500MHz
Sub-channel bandwidth (Δf)	4.32MHz
Sum Power per Line (P^T)	4dBm
Maximum Transmit PSD mask (P_{max})	-80dBm/Hz
Cable Noise PSD (σ_C)	-140dBm/Hz

6.5.1 Power Allocation over a LAN Cable

The resources on the cable channel can be evaluated in terms of different parameters, including the maximum achievable bandwidth BW_C over each twisted pair, the sum throughput over a single multi-pair cable, and the maximum number of users that can be supported. For multi-pair cable channels, the extended bandwidth beyond 1 GHz is foreseen in future broadband access networks [85], however, it is limited to 500MHz in this chapter, where we consider a CAT-5 cable with $N_C = 4$ twisted pairs and $BW_C = 500$MHz.

Table 6.2 provides the simulation parameters derived from the multi-pair multi-length CAT-5 cable measurements. Since, the multi-pair cable channel is considered to be flat within the interval Δf, the optimal power ($\boldsymbol{P_C^*} \in \mathbb{R}^{N_C \times N_F}$) and the corresponding rates ($\boldsymbol{R_C^*} \in \mathbb{R}^{N_C \times N_F}$), obtained by solving either $\boldsymbol{P_C^{AM}}$ or $\boldsymbol{P_C^{GM}}$, are considered to be quasi constant within each sub-channel (of duration Δf). The results of the power allocation problems, i.e., $\boldsymbol{P_C^{AM}}$ and $\boldsymbol{P_C^{GM}}$, for cable lengths 100m, 125m, 150m, 175m, and 200m, have been shown in Fig. 6.5, 6.6, 6.7, 6.8, and 6.9, respectively. Particularly, the parts (a) and (b) show the transmit signal power (in dBm per Δf) for all twisted pairs (i.e., $n = \{1, \ldots, N_C\}$) with $\boldsymbol{P_C^{AM}}$ and $\boldsymbol{P_C^{GM}}$, respectively. Clearly, the transmit signal power requirements over the LAN cable are significantly low for frequencies below 50MHz, due to fact that the far-end crosstalk (FEXT) is minimum over the lower frequency band.

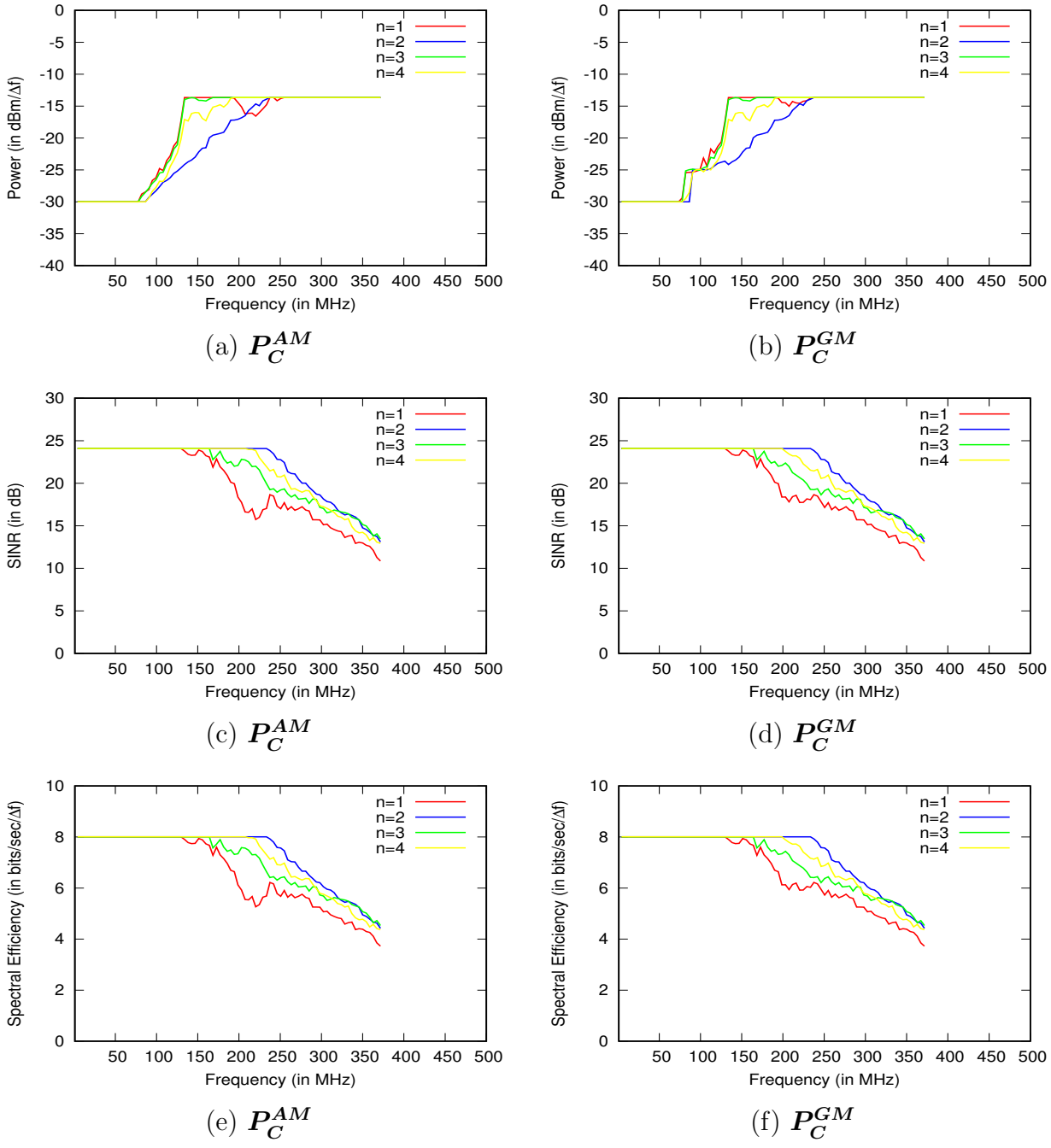

(a) $\boldsymbol{P_C^{AM}}$ (b) $\boldsymbol{P_C^{GM}}$

(c) $\boldsymbol{P_C^{AM}}$ (d) $\boldsymbol{P_C^{GM}}$

(e) $\boldsymbol{P_C^{AM}}$ (f) $\boldsymbol{P_C^{GM}}$

Figure 6.5: Power allocation problem for 100m long CAT-5 cable.

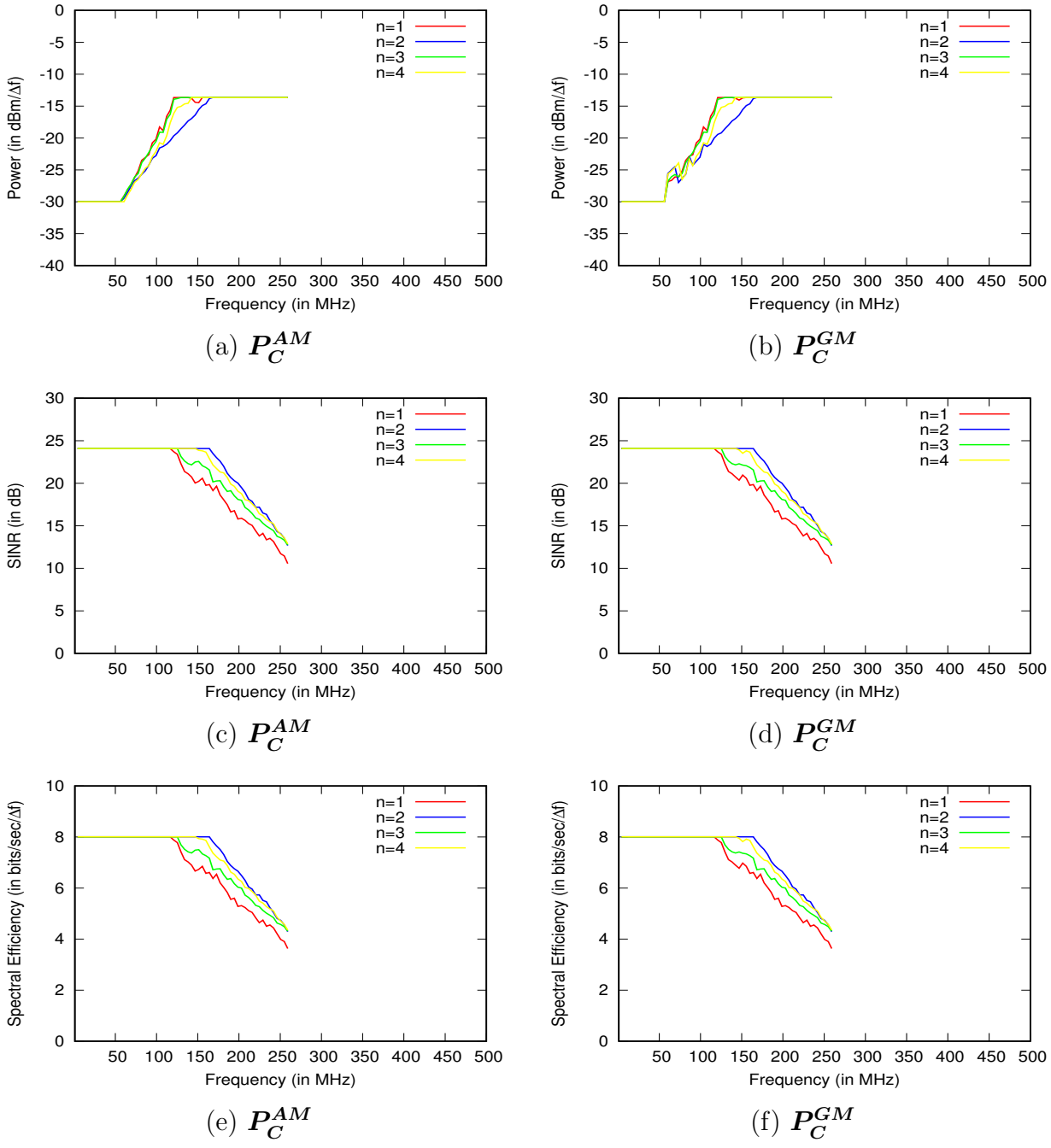

Figure 6.6: Power allocation problem for 125m long CAT-5 cable.

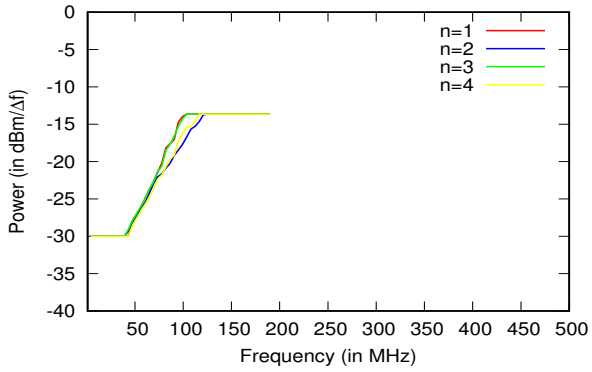

(a) $\boldsymbol{P_C^{AM}}$

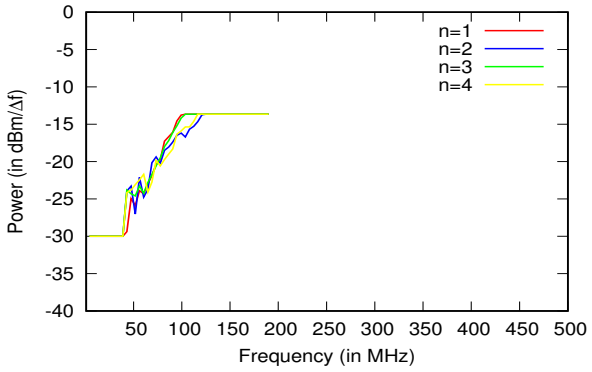

(b) $\boldsymbol{P_C^{GM}}$

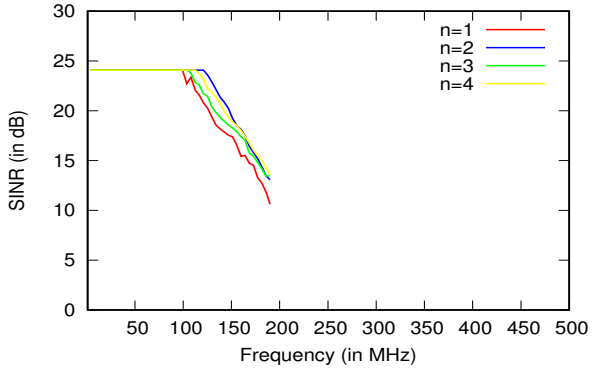

(c) $\boldsymbol{P_C^{AM}}$

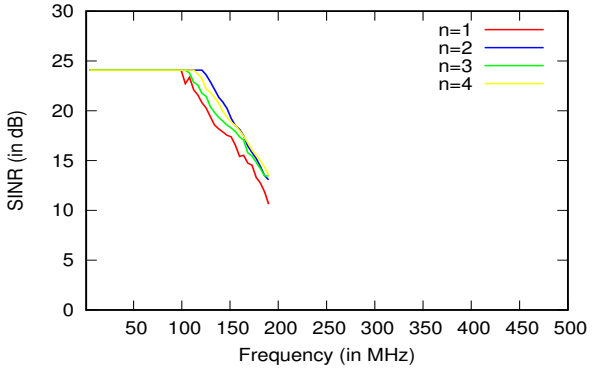

(d) $\boldsymbol{P_C^{GM}}$

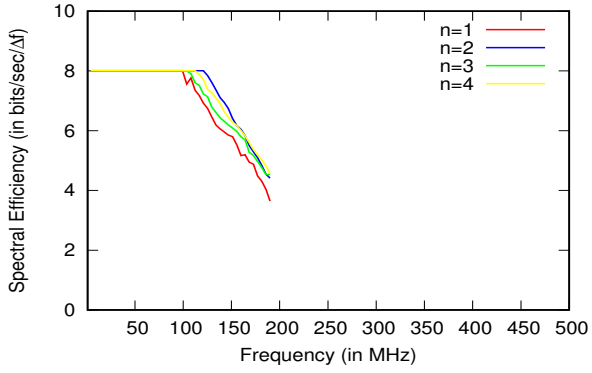

(e) $\boldsymbol{P_C^{AM}}$

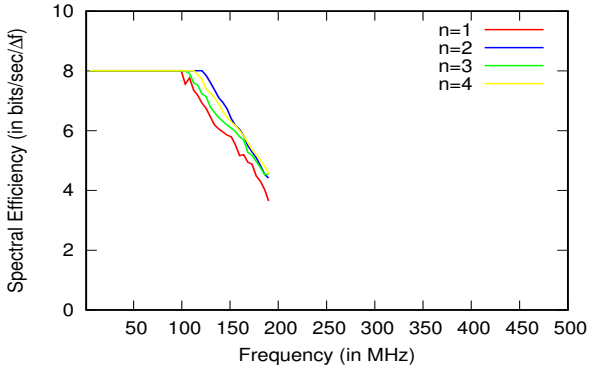

(f) $\boldsymbol{P_C^{GM}}$

Figure 6.7: Power allocation problem for 150m long CAT-5 cable.

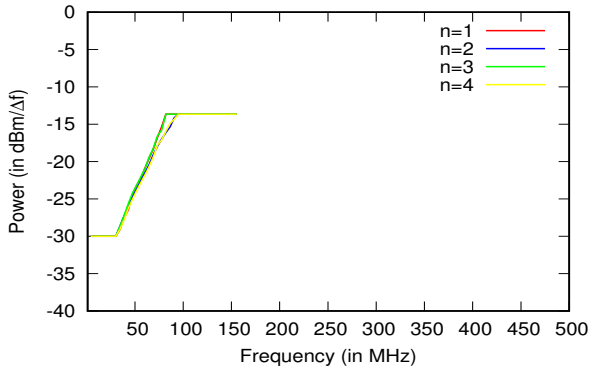

(a) $\boldsymbol{P_C^{AM}}$

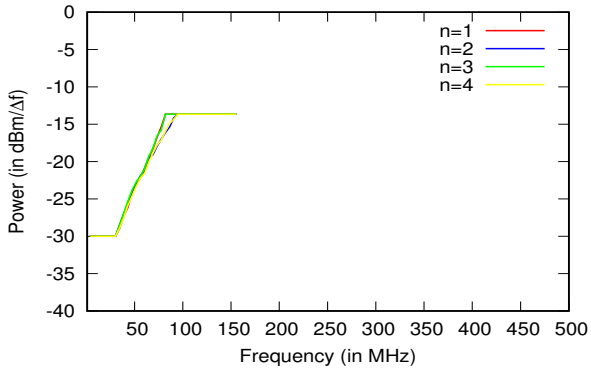

(b) $\boldsymbol{P_C^{GM}}$

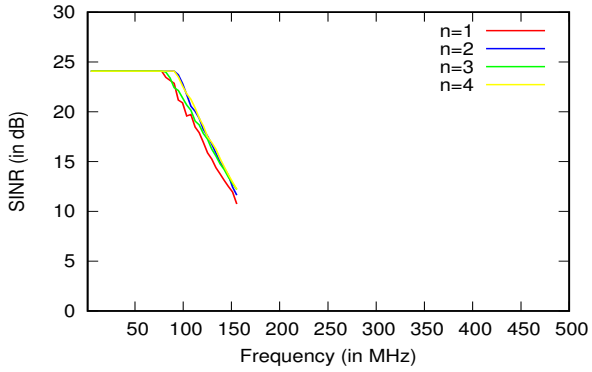

(c) $\boldsymbol{P_C^{AM}}$

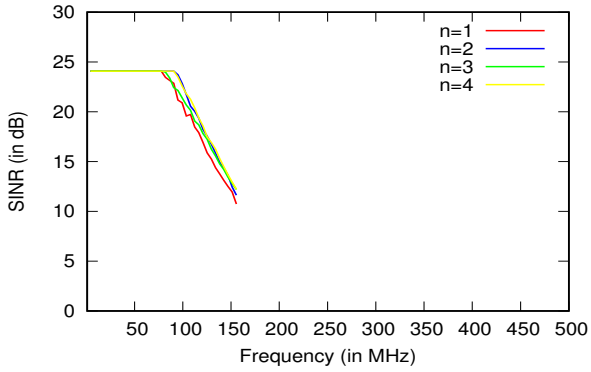

(d) $\boldsymbol{P_C^{GM}}$

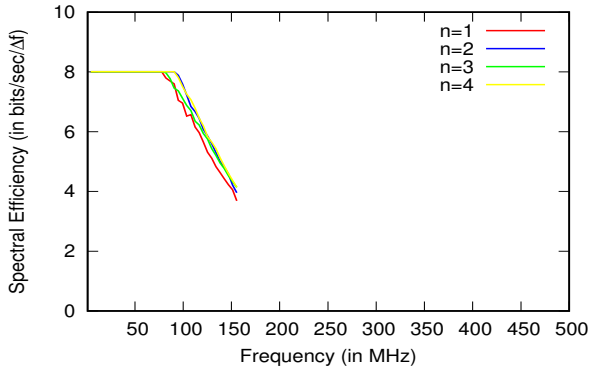

(e) $\boldsymbol{P_C^{AM}}$

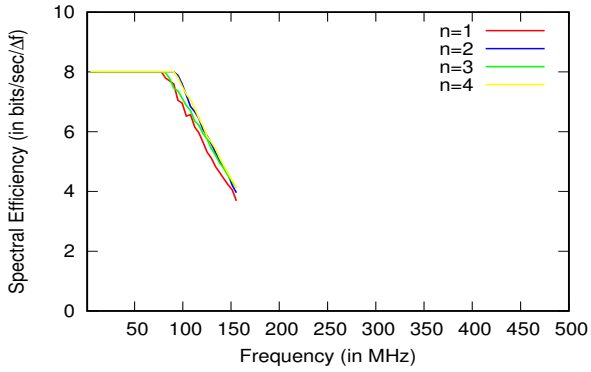

(f) $\boldsymbol{P_C^{GM}}$

Figure 6.8: Power allocation problem for 175m long CAT-5 cable.

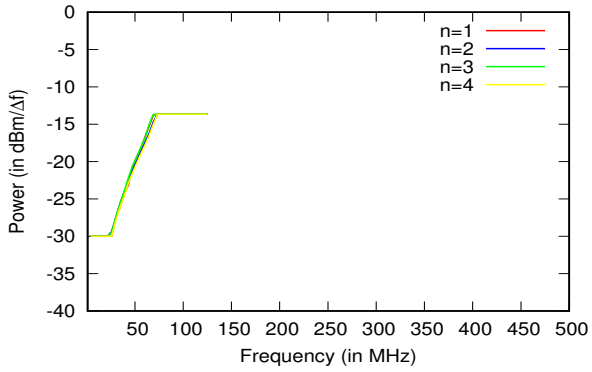

(a) $\boldsymbol{P_C^{AM}}$

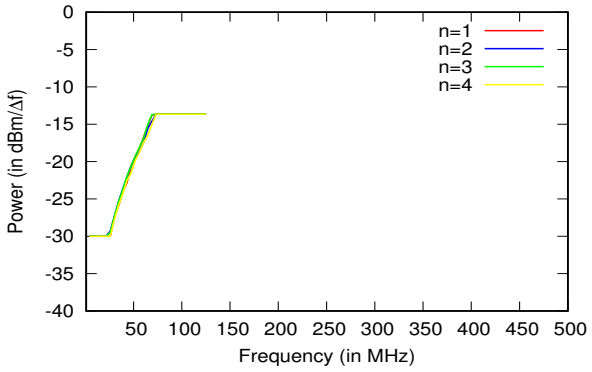

(b) $\boldsymbol{P_C^{GM}}$

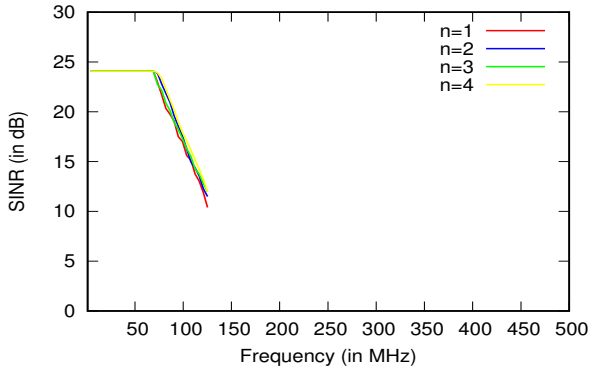

(c) $\boldsymbol{P_C^{AM}}$

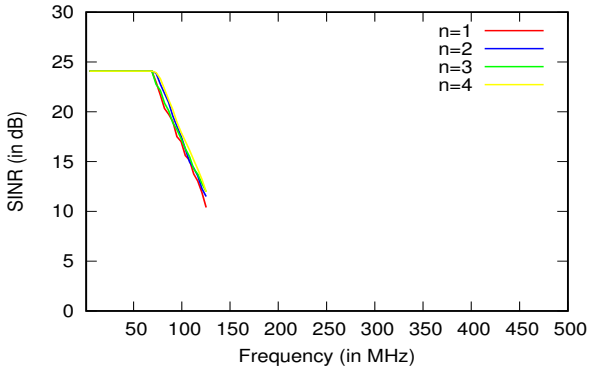

(d) $\boldsymbol{P_C^{GM}}$

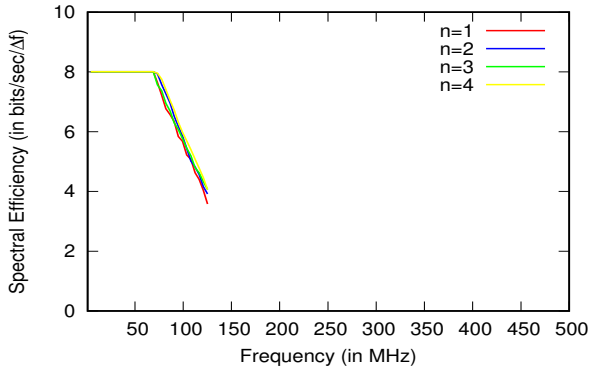

(e) $\boldsymbol{P_C^{AM}}$

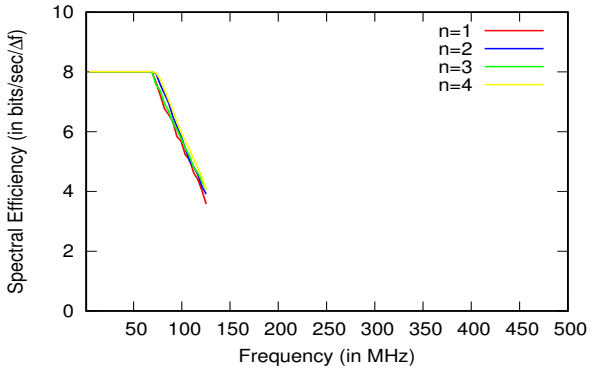

(f) $\boldsymbol{P_C^{GM}}$

Figure 6.9: Power allocation problem for 200m long CAT-5 cable.

The parts (c) and (d) show the SINR (in dB) for all twisted pairs (i.e., $n = \{1, \ldots, N_C\}$) with $\boldsymbol{P_C^{AM}}$ and $\boldsymbol{P_C^{GM}}$, respectively. Note that we used a high SINR assumption of 10dB for solving these power allocation problems, hence, we see results for only those cable frequencies/sub-channels that can satisfy the minimum SINR assumption. The parts (e) and (f) show the spectral efficiency (in bits per sec per Δf) for all twisted pairs (i.e., $n = \{1, \ldots, N_C\}$) with $\boldsymbol{P_C^{AM}}$ and $\boldsymbol{P_C^{GM}}$, respectively. It can be noted that the spectral efficiency of 8bps (corresponding to 256-QAM) can be guaranteed for a 100m long CAT-5 cable over the frequencies upto 150MHz, while this band is reduced to approximately 75MHz for a 200m long CAT-5 cable. Thus, the sum throughput and total number of sub channels that can be allocated over the LAN cable, are observed to be inversely proportional to the cable length.

6.5.2 Sub-channel Mapping over a LAN Cable

We evaluate the performance of the heuristic-based MP-A2C scheduler by generating a set of different radio network realizations denoted by Ω_{N_U} (with $|\Omega_{N_U}| = 100$). Each realization ($\omega \in \Omega_{N_U}$) corresponds to a set of N_U users (with $N_U \leq N_A$) that are distributed uniformly within the 100m radius chamber. The sub-channel mappings over the CAT-5 cable are obtained by maximizing the AM or the GM of user throughput allocations over the cable, i.e., by solving $\boldsymbol{P_{US}^{AM}}(\omega)$ and $\boldsymbol{P_{US}^{GM}}(\omega)$, respectively, via the modified problem $\boldsymbol{P'_{US}}(\omega)$. The corresponding AM and GM throughputs for each realization are defined as follows:

$$AM(\omega) := \frac{(\sum_{u=1}^{N_U} \sum_{r=1}^{N_R} Rate_{u,r})}{N_U}, \omega \in \Omega_{N_U} \tag{6.20}$$

$$GM(\omega) := \sqrt[N_U]{\prod_{u=1}^{N_U} (\sum_{r=1}^{N_R} Rate_{u,r})}, \omega \in \Omega_{N_U} \tag{6.21}$$

The numerical results are averaged after computing the AM as well as GM throughput over the CAT-5 cable for all realizations $\omega \in \Omega_{N_U}$, as shown in Fig. 6.10 and 6.11, respectively.

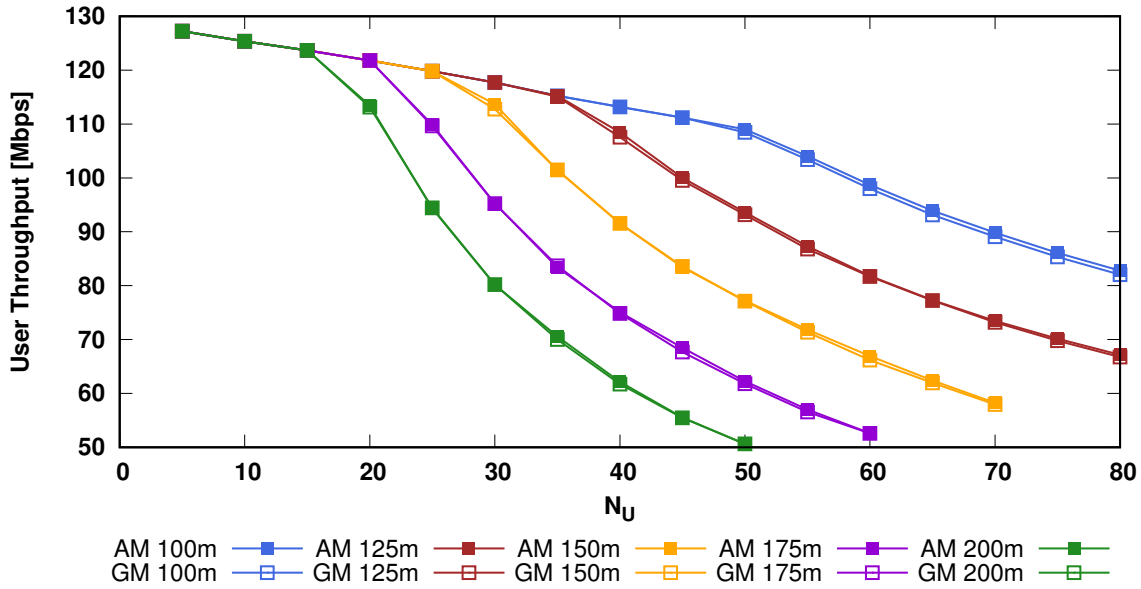

Figure 6.10: Average AM throughput over the CAT-5 cable: solving $\boldsymbol{P_C^{AM}}$ followed by $\boldsymbol{P_{US}^{\prime AM}}(\omega), \forall \omega \in \Omega_{N_U}$ vs solving $\boldsymbol{P_C^{GM}}$ followed by $\boldsymbol{P_{US}^{\prime GM}}(\omega), \forall \omega \in \Omega_{N_U}$.

The AM and GM throughput of these AM and GM based MP-A2C schedulers significantly degrades when the number of users exceeds a certain limit. This limit appears to be equal to 50, 35, 25, 20, and 15 for the cable lengths 100m, 125m, 150m, 175m, and 200m, respectively. Note that the MP-A2C schedulers can support more users beyond this limit, but this will result in some unallocated sub-channels, which are shown in Fig. 6.12. This is due to the inability of the cable channel to satisfy the 5G rate constraints for all users. Thus, the number of un-allocated sub-channels increases significantly when the number of users exceeds a certain limit (based on the network realization ω). Consequently, the user throughputs decrease significantly after a limit; mainly, the GM throughput, since, it offers proportional fairness by allocating "good" sub-channels to the antennas with "poor" user rates, leaving slightly more un-scheduled sub-channels over the cable as shown in Fig. 6.12. Fig. 6.10 shows the average AM throughput over the CAT-5 cable when power is allocated by solving $\boldsymbol{P_C^{AM}}$ and the sub-channel mappings are obtained by solving $\boldsymbol{P_{US}^{\prime AM}}(\omega), \forall \omega \in \Omega_{N_U}$ vs when the power is allocated by solving $\boldsymbol{P_C^{GM}}$ and the sub-

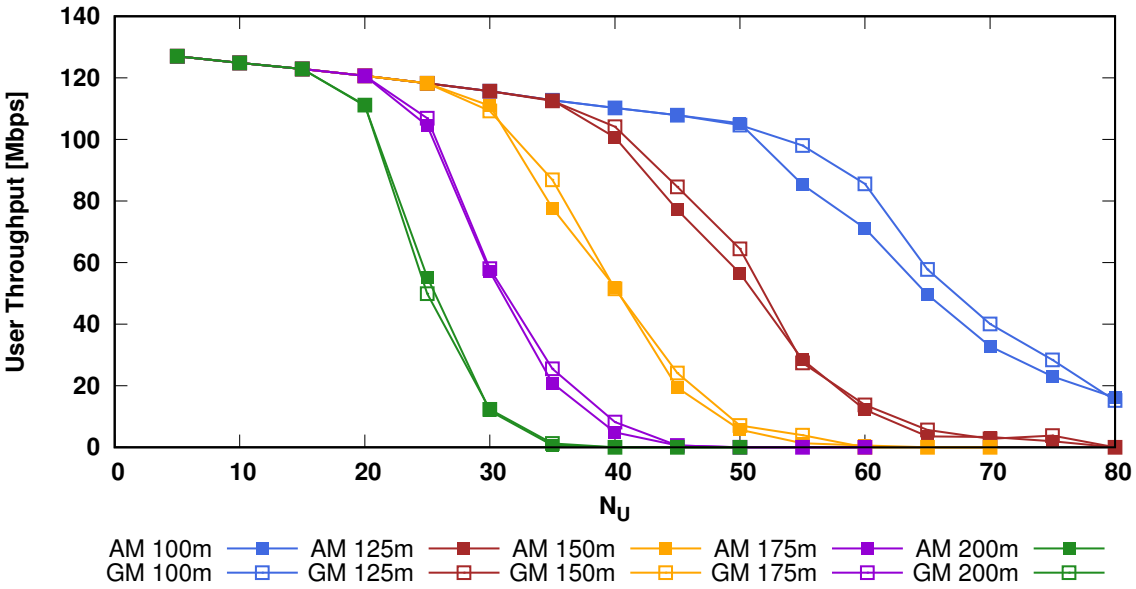

Figure 6.11: Average GM throughput over the CAT-5 cable when power is allocated by solving $\boldsymbol{P_C^{AM}}$ and the sub-channel mappings are obtained by solving $\boldsymbol{P_{US}^{\prime AM}}(\omega), \forall \omega \in \Omega_{N_U}$ vs when the power is allocated by solving $\boldsymbol{P_C^{GM}}$ and the sub-channel mappings are obtained by solving $\boldsymbol{P_{US}^{\prime GM}}(\omega), \forall \omega \in \Omega_{N_U}$.

channel mappings are obtained by solving $\boldsymbol{P_{US}^{\prime GM}}(\omega), \forall \omega \in \Omega_{N_U}$. Clearly, when the power is allocated through $\boldsymbol{P_C^{AM}}$, the AM throughput is slightly better than the case when it is allocated through $\boldsymbol{P_C^{GM}}$.

Fig. 6.11 shows the average GM throughput over the CAT-5 cable when power is allocated by solving $\boldsymbol{P_C^{AM}}$ and the sub-channel mappings are obtained by solving $\boldsymbol{P_{US}^{\prime AM}}(\omega), \forall \omega \in \Omega_{N_U}$ vs when the power is allocated by solving $\boldsymbol{P_C^{GM}}$ and the sub-channel mappings are obtained by solving $\boldsymbol{P_{US}^{\prime GM}}(\omega), \forall \omega \in \Omega_{N_U}$. Clearly, when the power is allocated through $\boldsymbol{P_C^{GM}}$, the GM throughput is significantly better than the case when it is allocated through $\boldsymbol{P_C^{AM}}$.

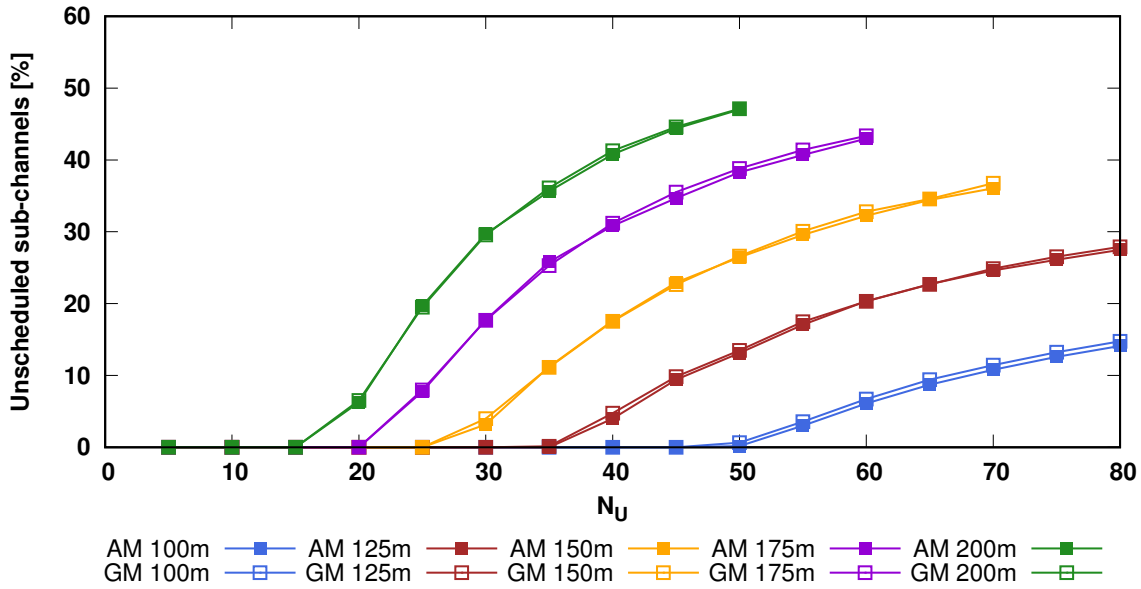

Figure 6.12: Average number of un-scheduled sub-channels over the CAT-5 cable.

Fig. 6.12 shows the average number of un-allocated sub-channels over the CAT-5 cable when power is allocated by solving $\boldsymbol{P_C^{AM}}$ and the sub-channel mappings are obtained by solving $\boldsymbol{P_{US}^{\prime AM}}(\omega), \forall \omega \in \Omega_{N_U}$ vs when the power is allocated by solving $\boldsymbol{P_C^{GM}}$ and the sub-channel mappings are obtained by solving $\boldsymbol{P_{US}^{\prime GM}}(\omega), \forall \omega \in \Omega_{N_U}$. Clearly, when the power is allocated through $\boldsymbol{P_C^{GM}}$, the un-allocated sub-channels are slightly more than the case when it is allocated through $\boldsymbol{P_C^{AM}}$. Since, the GM-based MP-A2C scheduler offers proportional fairness by allocating "good" sub-channels to the antennas with "poor" user rates, leaving slightly more un-scheduled sub-channels over the cable.

Since, some of the cable resources are still unused after allocation of the radio sub-channels, it gives an opportunity to use these leftover cable resources for duplicate transmissions of the antenna signals with bad channel quality to achieve diversity gain at the RRU.

6.6 Conclusions

This chapter introduced a distributed antenna unit (DAU) architecture for 5G indoor service provisioning, which has been proposed recently to provide a cost-effective alternative to the expensive fiber-optic based indoor solutions. This indoor architecture allows the antenna units to be distributed over a wide geographical area by using multi-pair LAN cables for transporting 5G (LTE or NR) signals. However, the use of existing indoor cables has been limited because of the attenuation and the crosstalk among the twisted pairs of each cable.

Based on the proposed DAU architecture, a novel multi-pair air-to-cable (MP-A2C) scheduler has been proposed in this chapter for joint allocation of power and sub-channels over a LAN cable. Since, the joint MP-A2C problem was a mixed-integer non-linear programming (MINLP) problem, with binary constraints, we used binary relaxations and Geometric Programming (GP) techniques to formulate a tractable upper bound problem. Through extensive numerical simulations, we show that the proposed framework can be used as a benchmark for evaluating the performance of existing MP-A2C schedulers.

Further, the joint MP-A2C problem was decoupled into two sub-problems, namely, power allocation problem and sub-channel mapping problem, which can be solved one after the other in real-time. The simulation results demonstrated that the performance of the proposed MP-A2C scheduler under various scheduling policies, such as, AM or GM, are quasi-optimal.

Chapter 7

Summary and Future Work

7.1 Summary

The work presented in this thesis has been mainly based on optimizing different network processes, such as, user scheduling, user association, and resource allocation, in a multi-tier network to find optimal uplink-centric as well as downlink centric network processes.

- We proposed globally optimal user scheduling solutions in Chapter 3, where our framework was based on optimizing the instantaneous network throughput per frame, while taking precise power and physical layer modulation and coding scheme (MCS) into consideration for joint optimization. To achieve the goal, we had to develop large-scale efficient optimization problems that can provide benchmark solutions for the considered framework.

- In the later part of Chapter 3, we demonstrated the trade-offs between inaccurate interference estimation and the instantaneous network throughput for a local user scheduling process within a BS. We found a huge gap between the performance of the local US process and the jointly optimal user scheduling process, which signified the importance of considering exact interference in the design of a local scheduler especially on the uplink.

- We proposed heuristic based joint user association and user scheduling solutions in Chapter 4 for maximizing instantaneous network throughput per frame in a C-RAN setting.

- We investigated an optimal resource allocation process in flexible FDD based multi-cell multi-tier networks in Chapter 5, for analyzing the performance of existing Static FDD or TDD based resource allocation schemes. Studying an optimal resource allocation process was necessary to benchmark the performance of existing schemes, but not trivial due to the high complexity of solving the joint problem; mainly because the formulated joint problem considered all types of interferences, including (i) inter-cell inter-link interference and (ii) intra-cell inter-link interference.

- In Chapter 6, we proposed a novel multi-pair air-to-cable (MP-A2C) scheduler for a distributed antenna unit (DAU) architecture, which can be used as a low cost alternative for front-hauling in C-RAN architectures. For obtaining solutions in real-time, the joint MP-A2C problem was decoupled into two sub-problems, which can be solved one after the other in real-time.

7.2 Future Research Direction

The current trends in cellular networks have brought a paradigm shift in the way the network processes have been run in the past. For example, the network operators now want to deliver more with less, e.g., more network throughput and better QoS with less energy for any of the underlying RAT. This is achievable if we can take full advantage of Machine Learning (ML) based solutions for providing wireless access, such as the ones discussed in [86–89].

We plan to take the advantage of the existing ML algorithms to come up with very fast distributed solutions that can minimize intra as well as inter cell interference in multi-tier multi-cell networks. Particularly, we want to develop efficient ML-based algorithms for enabling flexible spectrum allocation in each macro cell for both uplink and downlink based on instantaneous network load.

Further, the reinforcement-based ML algorithm can be used for estimating interference and thereby fine tuning the rate adaptation process, which is essential for selecting an appropriate modulation and coding scheme (MCS) for the underlying 4G LTE or 5G NR links. We strongly believe that an interference estimation process is at the heart of all network processes, therefore, they can be decoupled from each other if an appropriate interference estimation process is in place.

The autonomous ML-based UL and DL interference models, such as the one given in [89], will facilitate the working of other network processes. Note that it is necessary for all of them to optimize their long-term or instantaneous objectives without worrying much about the underlying dependence on the interference estimation process. An example would be the link selection process (i.e., 4G LTE or 5G NR), which depends on the amount and type of user traffic (including uplink and downlink) that has been sent on each link in the past, can benefit from the interference estimates for selecting the appropriate links for each user. Perhaps it would be able to assign the links with lesser interference to the users with poor channel gains given that an efficient ML-based interference estimation process is in place.

APPENDICES

Appendix A

Proof of Lemma 3.1

A.1 Proof for Upper bound

In the following, we show that the set of feasible solutions to $\boldsymbol{P^{UL}_{Global}(\omega)}$ is a subset of the set of feasible solutions for $\boldsymbol{P^{UB-UL}_{Global}(\omega)}$.

Let $F^{UB}(\omega)$ denote a feasible solution for $\boldsymbol{P^{UL}_{Global}(\omega)}$. If $F^{UB}(\omega)$ is a feasible solution for $\boldsymbol{P^{UL}_{Global}(\omega)}$ then it should satisfy all constraints defined by $\boldsymbol{P^{UL}_{Global}(\omega)}$. We show that $F^{UB}(\omega)$ will be able to satisfy all of them as follows:

1. After merging the constraints (3.9e) into (3.9f), the constraints for computing SINR in $\boldsymbol{P^{UB-UL}_{Global}(\omega)}$ impose that $F^{UB}(\omega)$ will satisfy

$$P^{c,t}_{u,k}G_{u,k}(\omega) \geq \gamma^{c,t}_{u,k}\big(N_0 + \sum_{k' \in \mathscr{K}}^{k' \neq k} \sum_{u' \in U(\omega)}^{u' \neq u} P^{c,t}_{u',k'}G_{u',k}(\omega)\big), \forall u, \forall k, \forall c, \forall t \tag{A.1}$$

   Therefore, by computing $x^{c,t,m}_{u,k} = 1$ when $\beta_m \leq \gamma^{c,t}_{u,k} < \beta_{m+1}, 1 \leq m < |\mathscr{M}|$, $F^{UB}(\omega)$ will be able to satisfy these constraints from $\boldsymbol{P^{UL}_{Global}(\omega)}$:

$$P^{c,t}_{u,k}G_{u,k}(\omega) \geq x^{c,t,m}_{u,k}\beta_m(N_0 + \sum_{k' \in \mathscr{K}}^{k' \neq k} \sum_{u' \in U(\omega)}^{u' \neq u} P^{c,t}_{u',k'}G_{u',k}(\omega)), \forall u, \forall k, \forall c, \forall t, \forall m \tag{A.2}$$

2. All other constraints except for the ones for computing rate, which are a part of the objective function, will be satisfied by $F^{UB}(\omega)$ as these constraints are a subset of the corresponding constraints in $\boldsymbol{P^{UB-UL}_{Global}(\omega)}$.

Since, $F^{UB}(\omega)$ satisfy all constraints for $\boldsymbol{P^{UB-UL}_{Global}(\omega)}$, there exists an *onto* mapping between the feasible solutions of $\boldsymbol{P^{UB-UL}_{Global}(\omega)}$ and $\boldsymbol{P^{UL}_{Global}(\omega)}$; different feasible solutions for $\boldsymbol{P^{UB-UL}_{Global}(\omega)}$ can be mapped on to the same feasible solution for $\boldsymbol{P^{UL}_{Global}(\omega)}$ and the reverse is not true. However, the objective value for the corresponding feasible solution for the original problem will be equal even though the objective values for the upper bound solutions (i.e., $F^{UB}(\omega)$) will vary depending on the values of $\gamma^{c,t}_{u,k}$. Since, $g(\gamma)$ is always greater than $f(\gamma)$, the objective value for any feasible solution of the upper bound problem (i.e., $F^{UB}(\omega)$) will always return an objective value that is greater than or equal to the objective value for the original problem.

Next we transform the upper bound problem into a convex problem to find a globally optimal solution, which will serve as an upper bound solution for the original problem. Nonetheless, the global optimal solution for $\boldsymbol{P^{UL}_{Global}(\omega)}$ lies in-between this feasible solution and the optimal solution obtained by solving $\boldsymbol{P^{UB-UL}_{Global}(\omega)}$.

A.2 Convexity of the Upper bound Problem

A Monomial Function

Let $x_1, ..., x_n$ denote n real positive variables, and $x = (x_1, ..., x_n)$ a vector with components x_i. A real valued function f of x, with the form $f(x) = cx_1^{a_1}x_2^{a_2}\dots x_n^{a_n}$, where $c > 0$ and $a_i \in \boldsymbol{R}$, is called a Monomial function.

A Posynomial Function

A sum of one or more monomials, i.e., a function of the form $f(x) = \sum_{k=1}^{k=K} c_k x_1^{a_{1k}}x_2^{a_{2k}}\dots x_n^{a_{nk}}$, where $c_k > 0$, is called a posynomial function with K terms.

Geometric Programming Transformation

Geometric programs are not in general convex optimization problems, but they can be transformed to convex problems by a change of variables and a transformation of the objective and constraint functions. In particular, after performing the change of variables and taking the log of the objective and constraint functions, the posynomial functions, are transformed into log-sum-exp functions, which are convex, and the monomial functions become affine. Hence, this transformation transforms every GP into an equivalent convex program. We show that the upper bound problem is a GP problem, by writing all constraints in the form of monomial and posynomial functions as follows:

$$\boldsymbol{P}^{\boldsymbol{UB-UL}}_{\boldsymbol{Global}}(\boldsymbol{\omega}) : \underset{\{P^{c,t}_{u,k}\},\{\gamma^{c,t}_{u,k}\}}{\text{maximize}} \sum_{u\in U_{UL}(\omega)} \log\Big(\sum_{c\in\mathscr{C}}\sum_{t\in\mathscr{T}}(\gamma^{c,t}_{u,k})^{\alpha}\Big)$$

subject to:

$$\epsilon_p (P^{c,t}_{u,k})^{-1} \leq 1, \qquad \forall u, \forall k, \forall c, \forall t \qquad \text{(A.3a)}$$

$$\frac{P^{c,t}_{u,k}}{P_{UE}} \leq 1, \qquad \forall u, \forall k, \forall c, \forall t \qquad \text{(A.3b)}$$

$$\frac{\sum\limits_{c\in\mathscr{C}} P^{c,t}_{u,k}}{P_{UE}} \leq 1, \qquad \forall u, \forall k, \forall t \qquad \text{(A.3c)}$$

$$\frac{P^{c,t}_{u,k} P^{c,t}_{u',k}}{\epsilon_p} \leq 1, \qquad \forall u, \forall u', u' \neq u, \forall k, \forall c, \forall t \qquad \text{(A.3d)}$$

$$\epsilon_\gamma (\gamma^{c,t}_{u,k})^{-1} \leq 1, \qquad \forall u, \forall k, \forall c, \forall t \qquad \text{(A.3e)}$$

$$\frac{\gamma^{c,t}_{u,k}}{\beta_{max}} \leq 1, \qquad \forall u, \forall k, \forall c, \forall t \qquad \text{(A.3f)}$$

$$\gamma^{c,t}_{u,k}\frac{N_0}{(P^{c,t}_{u,k}G_{u,k}(\omega))} + \gamma^{c,t}_{u,k}\sum_{k'\in\mathscr{K}}^{k'\neq k}\sum_{u'\in U(\omega)}^{u'\neq u}\left(\frac{P^{c,t}_{u',k'}G_{u',k}(\omega)}{P^{c,t}_{u,k}G_{u,k}(\omega)}\right) \leq 1, \forall u, \forall k, \forall c, \forall t \qquad \text{(A.3g)}$$

where, $\alpha = \log_{10}(e), u \in U_{UL}(\omega), k \in \mathscr{K}, c \in \mathscr{C}, t \in \mathscr{T}$.

Note that the objective function is a concave function because: (1) $(\gamma_{u,k}^{c,t})^{\alpha}$ on $\boldsymbol{R}_{++}$ is a concave function when $0 \leq \alpha \leq 1$ (with $\alpha = \log_{10}(e)$), (2) the sum of two concave functions is itself concave, and (3) every concave function that is non-negative on its domain is log-concave. In addition, the left hand side of the constraints (A.3a-f) are monomial functions, whereas the left hand side of (A.3g) is a posynomial function when we rearrange and substitute equation (3.9f) into (3.9e).

By making a logarithmic change of the variables and a logarithmic transformation of the objective and the constraints, we can convert the upper bound problem into a a GP problem. For consistency, we use the same notation to represent the transformed variables but with a prime symbol, i.e., $\boldsymbol{P_{u,k}^{'c,t} = \log(P_{u,k}^{c,t})}$ and $\boldsymbol{\gamma_{u,k}^{'c,t} = \log(\gamma_{u,k}^{c,t})}$. For simplicity of notation, we use $\boldsymbol{LSE(\{x\})}$ to denote the logarithm of the sum of exponentials over the set $\{x\}$.

Using these transformations, we re-formulate the upper bound problem as a GP problem as follows:

$$\boldsymbol{P_{Global}^{UB-UL'}(\omega)}: \underset{\{P_{u,k}^{'c,t}\},\{\gamma_{u,k}^{'c,t}\}}{\text{maximize}} \sum_{u \in U_{UL}(\omega)} LSE\big(\{\alpha\gamma_{u,k}^{'c,t}\}_{k\in\mathscr{K},c\in\mathscr{C},t\in\mathscr{T},}\big)$$

subject to:

$$\log(\epsilon_p) \leq P_{u,k}^{'c,t} \leq z_{u,k}(\omega)\log(P_{UE}) + (1 - z_{u,k}(\omega))\log(\epsilon_p), \forall u, \forall k, \forall c, \forall t \tag{A.4a}$$

$$LSE(\{P_{u,k}^{'c,t}\}_{c\in\mathscr{C}}) \leq \log(P_{UE}), \forall u, \forall k, \forall t \tag{A.4b}$$

$$P_{u,k}^{'c,t} + P_{u',k}^{'c,t} \leq \log(\epsilon_p), \forall u, \forall u', u \neq u', \forall k, \forall c, \forall t \tag{A.4c}$$

$$\log(\epsilon_\gamma) \leq \gamma_{u,k}^{'c,t} \leq \log(\beta_{max}), \forall u, \forall k, \forall c, \forall t \tag{A.4d}$$

$$log\Bigg(\exp\left(\gamma_{u,k}^{'c,t} - P_{u,k}^{'c,t} + \log(N_0) - \log(G_{u,k}(\omega))\right) + \tag{A.4e}$$

$$\sum_{k'\in\mathscr{K}}^{k'\neq k} \sum_{u'\in U(\omega)}^{u'\neq u} \exp\left(\gamma_{u,k}^{'c,t} + P_{u',k'}^{'c,t} - P_{u,k}^{'c,t} + \log(G_{u',k}(\omega)) - \log(G_{u,k}(\omega))\right)\Bigg) \leq 0, \forall u, \forall k, \forall c, \forall t \tag{A.4f}$$

where, $\alpha = \log_{10}(e), u \in U_{UL}(\omega), k \in \mathscr{K}, c \in \mathscr{C}, t \in \mathscr{T}$.

Appendix B

Global User Scheduling Problem for Downlink

B.1 The Global User Scheduling Problem

Given a set of macro cells $\mathscr{K}$, a set of sub-channels $\mathscr{C}$, a set of sub-frames $\mathscr{T}$, a network realization ω, a set of user associations ($\{z_{k,d}(\omega)\}_{d\in U_{DL}(\omega),k\in\mathscr{K}}$), and a set of pre-defined SINR thresholds (i.e., $\{\beta_m\}_{m\in\mathscr{M}}$), we define the following optimization variables for the global US problem:

- $\boldsymbol{x_{k,d}^{c,t,m}}$ is a binary variable for assigning discrete rates; it is equal to 1 if user d is allocated MCS m by the MBS k on PRB (c,t) and 0 otherwise.
- $\boldsymbol{P_{k,d}^{c,t}}$ is for allocating DL power on PRB (c,t).
- $\boldsymbol{I_{k,d}^{c,t}}$ is for computing DL interference on PRB (c,t) at user d for MBS k.
- $\boldsymbol{\lambda_{k,d}}$ is the total coding rate seen by user d from MBS k

The system-wide global US problem for DL is defined as follows:

$$\boldsymbol{P}^{\boldsymbol{DL}}_{\boldsymbol{Global}}(\boldsymbol{\omega}) : \underset{\{x^{c,t,m}_{k,d}\},\{P^{c,t}_{k,d}\},\{I^{c,t}_{k,d}\},\{\lambda_{k,d}\}}{\text{maximize}} \sum_{d\in U_{DL}(\omega)} \log\big(\sum_{k\in\mathscr{K}} \lambda_{k,d}\big)$$

subject to:

$$x^{c,t,m}_{k,d} \in \{0,1\}, \qquad \forall d,\forall k,\forall c,\forall t,\forall m \tag{B.1a}$$

$$P^{c,t}_{k,d} \geq 0, \qquad \forall d,\forall k,\forall c \tag{B.1b}$$

$$x^{c,t,m}_{k,d} \leq z_{k,d}(\omega), \qquad \forall d,\forall k,\forall c,\forall t,\forall t,\forall m \tag{B.1c}$$

$$\sum_{d\in U_{DL}(\omega)} \sum_{m\in\mathscr{M}} x^{c,t,m}_{k,d} \leq 1, \qquad \forall k,\forall c,\forall t \tag{B.1d}$$

$$\sum_{d\in U_{DL}(\omega)} \sum_{c\in\mathscr{C}} P^{c,t}_{k,d} \leq P_{MBS}, \qquad \forall k,\forall t \tag{B.1e}$$

$$P^{c,t}_{k,d} \leq P_{MBS} \sum_{m\in\mathscr{M}} x^{c,t,m}_{k,d}, \qquad \forall d,\forall k,\forall c,\forall t \tag{B.1f}$$

$$P^{c,t}_{k,d} G_{k,d}(\omega) \geq \beta_m(N_0 + I^{c,t}_{k,d}) - (1 - x^{c,t,m}_{k,d})\boldsymbol{B}, \qquad \forall d,\forall k,\forall c,\forall t,\forall m \tag{B.1g}$$

$$I^{c,t}_{k,d} = \sum_{k'\in\mathscr{K}}^{k'\neq k} \sum_{d'\in U_{DL}(\omega)}^{d'\neq d} P^{c,t}_{k',d'} G_{k',d}(\omega), \qquad \forall d,\forall k,\forall c,\forall t \tag{B.1h}$$

$$\lambda_{k,d} = \sum_{c\in\mathscr{C}} \sum_{t\in\mathscr{T}} \sum_{m\in\mathscr{M}} x^{c,t,m}_{k,d} f(\beta_m), \qquad \forall d,\forall k \tag{B.1i}$$

where, $d \in U_{DL}(\omega), k \in \mathscr{K}, c \in \mathscr{C}, t \in \mathscr{T}, m \in \mathscr{M}$, and $\boldsymbol{B}$ is a very large number.

The constraint (B.1d) ensures that only one MCS is assigned to a user on each PRB. It also ensures that only one user is scheduled on a PRB in each macro cell. The constraints (B.1e) and (B.1f) are for assigning power on each PRB. The constraints (B.1h) and (B.1i) are for computing DL interference and coding rates, respectively. $\boldsymbol{P}^{\boldsymbol{DL}}_{\boldsymbol{Global}}$ is also a large-scale linear problem with binary and continuous variables and solving it is challenging even for very small number of users in each macro cell. To solve $\boldsymbol{P}^{\boldsymbol{DL}}_{\boldsymbol{Global}}$, we need to transform it into a relaxed problem that can be solved efficiently and that can provide a tight upper bound to the original problem. In the next section, we transform the system-wide global US problem into a tractable upper bound problem that can be solved efficiently.

B.2 The Upper Bound Problem

Using the same approach that was discussed in Section 3.4.1, we formulate the upper bound problem for the DL as follows:

$$\boldsymbol{P}^{\boldsymbol{UB-DL}}_{\boldsymbol{Global}}(\boldsymbol{\omega}): \underset{\{P^{c,t}_{k,d}\},\{I^{c,t}_{k,d}\},\{\gamma^{c,t}_{k,d}\}}{\text{maximize}} \sum_{d\in U_{DL}(\omega)} \log\big(\sum_{k\in\mathscr{K}} \lambda_{d,k}\big)$$

subject to:

$$\epsilon_p \leq P^{c,t}_{k,d} \leq z_{k,d}(\omega)P_{MBS} + (1 - z_{k,d}(\omega))\epsilon_p, \qquad \forall d, \forall k, \forall c, \forall t \tag{B.2a}$$

$$\sum_{d\in U_{DL}(\omega)} \sum_{c\in\mathscr{C}} P^{c,t}_{k,d} \leq P_{MBS}, \qquad \forall k, \forall t \tag{B.2b}$$

$$P^{c,t}_{k,d} P^{c,t}_{k,d'} \leq \epsilon_p, \qquad \forall d, \forall d', d' \neq d, \forall k, \forall c, \forall t \tag{B.2c}$$

$$\epsilon_\gamma \leq \gamma^{c,t}_{k,d} \leq \beta_{max}, \qquad \forall d, \forall k, \forall c, \forall t \tag{B.2d}$$

$$P^{c,t}_{k,d} G_{k,d}(\omega) \geq \gamma^{c,t}_{k,d}\big(N_0 + I^{c,t}_{k,d}\big), \qquad \forall d, \forall k, \forall c, \forall t \tag{B.2e}$$

$$I^{c,t}_{k,d} = \sum_{k'\in\mathscr{K}}^{k'\neq k} \sum_{d'\in U_{DL}(\omega)}^{d'\neq d} P^{c,t}_{k',d'} G_{k',d}(\omega), \qquad \forall d, \forall k, \forall c, \forall t \tag{B.2f}$$

$$\lambda_{k,d} = \sum_{c\in\mathscr{C}} \sum_{t\in\mathscr{T}} g(\gamma^{c,t}_{k,d}), \qquad \forall d, \forall k, \forall t \tag{B.2g}$$

where, $d \in U_{DL}(\omega), k \in \mathscr{K}, c \in \mathscr{C}, t \in \mathscr{T}$.

The upper bound problem $\boldsymbol{P}^{\boldsymbol{UB-DL}}_{\boldsymbol{Global}}$ is a non-linear non-convex continuous optimization problem that requires extensive computational resources; mainly, due to the presence of bilinear constraints for computing SINR. We can transform it into an equivalent convex problem by using geometric programming (GP) transformations given in [38].

The Convex Upper Bound Problem:

The GP transformation of a non-convex optimization problem is based on a logarithmic change of variables, and a logarithmic transformation of the objective and the constraints to form a convex problem; a convex optimization problem has a convex objective, convex inequality constraints, and linear equality constraints. We define the following additional optimization variables to state the convex problem:

- $\boldsymbol{R_{k,d}^{c,t}}$ is the DL coding rate from MBS k to user d on PRB(c,t)

For consistency, we use the same notation to represent the transformed variables but with a prime symbol. For example, $\boldsymbol{P_{k,d}^{'c,t}} = \boldsymbol{\log(P_{k,d}^{c,t})}$, $\boldsymbol{\gamma_{k,d}^{'c,t}} = \boldsymbol{\log(\gamma_{k,d}^{c,t})}$, and $\boldsymbol{R_{k,d}^{'c,t}} = \boldsymbol{\log(R_{k,d}^{c,t})}$. For simplicity of notation, we use $\boldsymbol{LSE(\{x\})}$ to denote the logarithm of the sum of exponentials over the set $\{x\}$. Using logarithmic transformation, the objective of the upper bound problem can be written as:

$$\begin{aligned}\sum_{d\in U_{DL}(\omega)} \log\big(\sum_{k\in\mathscr{K}} \lambda_{k,d}\big) &= \sum_{d\in U_{DL}(\omega)} \log\Big(\sum_{k\in\mathscr{K}}\sum_{c\in\mathscr{C}}\sum_{t\in\mathscr{T}} e^{R_{k,d}^{'c,t}}\Big) \\ &= \sum_{d\in U_{DL}(\omega)} LSE\big(\{R_{k,d}^{'c,t}\}_{k\in\mathscr{K},c\in\mathscr{C},t\in\mathscr{T}}\big)\end{aligned} \tag{B.3}$$

Before transforming the bilinear constraints given in (B.2e) into convex constraints, we need to rearrange and substitute equations (B.2f) in (B.2e) as follows:

$$\gamma_{k,d}^{c,t}\frac{N_0}{P_{k,d}^{c,t}G_{k,d}(\omega)} + \gamma_{k,d}^{c,t}\sum_{k'\in\mathscr{K}}^{k'\neq k}\sum_{d'\in U_{DL}(\omega)}^{d'\neq d}\left(\frac{P_{k',d'}^{c,t}G_{k',d}(\omega)}{P_{k,d}^{c,t}G_{k,d}(\omega)}\right) \leq 1, \forall d, \forall k, \forall c, \forall t \tag{B.4}$$

Note that the left hand side of the above inequality is a *posynomial* function that is non-convex in nature. However, we can apply a logarithmic transformation to a posynomial function, as described in [38], in order to convert it into an LSE function (which is convex):

$$\begin{aligned}&\log\Bigg(\exp\big(\gamma_{k,d}^{'c,t} - P_{k,d}^{'c,t} + \log(N_0) - \log(G_{k,d}(\omega))\big) + \\ &\sum_{k'\in\mathscr{K}}^{k'\neq k}\sum_{d'\in U_{DL}(\omega)}^{d'\neq d}\exp\big(\gamma_{k,d}^{'c,t} + P_{k',d'}^{c,t} - P_{k,d}^{'c,t} + \log(G_{k',d}(\omega)) - \log(G_{k,d}(\omega))\big)\Bigg) \leq 0, \forall d, \forall k, \forall c, \forall t\end{aligned} \tag{B.5}$$

Using the above transformations, we formulate the convex upper bound problem as follows:

$$\boldsymbol{P}^{\boldsymbol{UB-DL'}}_{\boldsymbol{Global}}(\boldsymbol{\omega}) : \underset{\{P^{'c,t}_{k,d}\},\{\gamma^{'c,t}_{k,d}\},\{R^{'c,t}_{k,d}\}}{\text{maximize}} \sum_{d\in U_{DL}(\omega)} LSE\big(\{R^{'c,t}_{k,d}\}_{k\in\mathscr{K},c\in\mathscr{C},\forall t\in\mathscr{T}}\big)$$

subject to (B.5) and:

$$\log(\epsilon_p) \leq P^{'c,t}_{k,d} \leq z_{d,k}(\omega)\log(P_{MBS}) + (1-z_{d,k}(\omega))\log(\epsilon_p), \forall d, \forall k, \forall c, \forall t \quad \text{(B.6a)}$$

$$LSE(\{P^{'c,t}_{k,d}\}_{d\in U_{DL}(\omega),c\in\mathscr{C}}) \leq \log(P_{MBS}), \quad \forall k, \forall t \quad \text{(B.6b)}$$

$$P^{'c,t}_{k,d} + P^{'c,t}_{k,d'} \leq \log(\epsilon_p), \quad \forall d, \forall d', d\neq d', \forall k, \forall c, \forall t \quad \text{(B.6c)}$$

$$\log(\epsilon_\gamma) \leq \gamma^{'c,t}_{k,d} \leq \log(\beta_{max}), \quad \forall d, \forall k, \forall c, \forall t \quad \text{(B.6d)}$$

$$R^{'c,t}_{k,d} = \log_{10}(e)\gamma^{'c,t}_{k,d}, \quad \forall d, \forall k, \forall c, \forall t \quad \text{(B.6e)}$$

where, $d \in U_{DL}(\omega), k \in \mathscr{K}, c \in \mathscr{C}, t \in \mathscr{T}$.

Computing Feasible Solutions:

Given an optimal solution for $\boldsymbol{P}^{\boldsymbol{UB-DL'}}_{\boldsymbol{Global}}(\boldsymbol{\omega})$, we can compute a feasible solution for $\boldsymbol{P}^{\boldsymbol{DL}}_{\boldsymbol{Global}}(\boldsymbol{\omega})$. This is achieved by computing the binary variables $x^{c,t,m}_{k,d}$ for each PRB (c,t); $x^{c,t,m}_{k,d}, \forall d,k,c,t,m$ can be computed by using the optimal value of $\gamma^{'c,t}_{k,d}$ from $\boldsymbol{P}^{\boldsymbol{UB-DL'}}_{\boldsymbol{Global}}(\boldsymbol{\omega})$ and mapping it to the highest SINR threshold with $\beta_m \leq \gamma^{'c,t}_{k,d}$, $m \in \mathscr{M}$. Since, $g(\gamma^{c,t}_{k,d})$ is always greater than or equal to $f(\gamma^{c,t}_{k,d})$, the optimal objective of $\boldsymbol{P}^{\boldsymbol{UB-DL'}}_{\boldsymbol{Global}}(\boldsymbol{\omega})$ will always be greater than or equal to the optimal objective of $\boldsymbol{P}^{\boldsymbol{DL}}_{\boldsymbol{Global}}(\boldsymbol{\omega})$. The optimal solution for $\boldsymbol{P}^{\boldsymbol{DL}}_{\boldsymbol{Global}}(\boldsymbol{\omega})$ lies in-between the feasible solution and the optimal solution from $\boldsymbol{P}^{\boldsymbol{UB-DL'}}_{\boldsymbol{Global}}(\boldsymbol{\omega})$. Hence, we have a method that delivers a feasible solution to the intractable system-wide global US problem on the DL.

Appendix C

Proof of Theorem 3.1

We prove that an optimal solution for the local sub-channel allocation problem, *i.e.*, given in Section 3.5.2, will allocate equal number of PRBs to the local users, given that the integer variables have been relaxed from $\boldsymbol{P_k^{DL}(\omega, \{I_{k,d}^{EP}(\omega)\})}$. The Lagrangian for the relaxed primal problem can then be computed as:

$$L(\mu_t, \gamma_d^t, n_{k,d}^t) = -\sum_{d \in U_{DL_k}(\omega)} log(\sum_{t \in \mathscr{T}} n_{k,d}^t \hat{R}_{k,d}(\omega))) + \mu_t(\sum_{d \in U_{DL_k}(\omega)} n_{k,d}^t - |\mathscr{C}|) - \gamma_d^t(n_{k,d}^t) \tag{C.1}$$

For dual and primal feasibility, we derive the following first-order necessary conditions for optimality along with the complementary-slackness conditions:

$$\begin{aligned} \frac{\partial L(\mu_t, \gamma_d^t, n_{k,d}^t)}{\partial n_{k,d}^t} &= -(\sum_{t \in \mathscr{T}} n_{k,d}^t)^{-1} + \mu_t - \gamma_d^t = 0, \quad \forall d, \forall t \\ \mu_t(\sum_{d \in U_{DL_k}(\omega)} n_{k,d}^t - |\mathscr{C}|) &= 0, \qquad \forall t \\ \gamma_d^t(n_{k,d}^t) &= 0, \qquad \forall d, \forall t \end{aligned} \tag{C.2}$$

Since, the primal problem involves maximization of a concave function over a convex set, hence any tuple of the primal and dual variables satisfying the KKT conditions given by (C.2) is optimal [38]. By substituting $\gamma_d^t = 0$ and $n_{k,d}^t = \frac{|\mathscr{C}|}{|U_{DL_k}(\omega)|}$, we can see that all of the KKT conditions are satisfied. Hence, the optimal solution for $\boldsymbol{P_k^{DL}(\omega, \{I_{k,d}^{EP}(\omega)\})}$ is the one that will allocate equal number of PRBs to the local users.

Appendix D

Proof of Lemma 4.1

We formulate a relaxed upper bound problem for $\boldsymbol{P^{UL}_{Joint}(\omega, c, t)}$ using GP transformation, where all variables are continuous and the constraints are convex. For consistency, we use the same notation to represent the transformed variables but with a prime symbol; for example, $\boldsymbol{P'^{c,t}_{u,r} = \log(P^{c,t}_{u,r})}$, $\boldsymbol{\gamma'^{c,t}_{u,r} = \log(\gamma^{c,t}_{u,r})}$, and $\boldsymbol{\lambda'^{c,t}_{u,r} = \log(\lambda^{c,t}_{u,r})}$.

$$\boldsymbol{P^{UL'}_{Joint}(\omega, c, t)}: \underset{\{P'^{c,t}_{u,r}\},\{\gamma'^{c,t}_{u,r}\},\{\lambda'^{c,t}_{u,r}\}}{\text{maximize}} \sum_{u\in U_{UL}(\omega,c,t)} \lambda'^{c,t}_{u,r}$$

subject to:

$$\log(\epsilon_p) \leq P'^{c,t}_{u,r} \leq \log(P^{EP}_{u,r}(\omega) + P^{unused}_{u,r}(\omega)), \qquad \forall u, \forall r \tag{D.1a}$$

$$\log(\epsilon_\gamma) \leq \gamma'^{c,t}_{u,r} \leq \log(\beta_{max}), \qquad \forall u, \forall r \tag{D.1b}$$

$$\log\Bigg(\exp\left(\gamma'^{c,t}_{u,r} - P'^{c,t}_{u,r} + \log(N_0) - \log(G_{u,r}(\omega))\right) + \sum_{r'\in\mathscr{R}}^{r'\neq r} \sum_{u'\in U(\omega,c,t)}^{u'\neq u} \exp\left(\gamma'^{c,t}_{u,r} + P'^{c,t}_{u',r'} - P'^{c,t}_{u,r} + \log(G_{u',r}(\omega)) - \log(G_{u,r}(\omega))\right)\Bigg) \leq 0, \qquad \forall u, \forall r \tag{D.1c}$$

$$\lambda'^{c,t}_{u,r} = \log_{10}(e)\gamma'^{c,t}_{u,r}, \qquad \forall u, \forall r \tag{D.1d}$$

where, $u \in U_{UL}(\omega, c, t)$ and $r \in \mathscr{R}$.

Appendix E

Proof of Lemma 5.1

The problem $\boldsymbol{P_{Joint}^{UB-RA}(\omega)}$, which is non-convex in nature, requires extensive computational resources. By making a logarithmic change of the variables and a logarithmic transformation of the objective and the constraints, the GP transformation (that is described in [38]) can convert this problem into an equivalent convex problem, i.e., $\boldsymbol{P_{Joint}^{UB-RA'}(\omega)}$. We define the following additional optimization variables for the GP transformation:

- $\boldsymbol{R_{u,k,b}^{c,t}}$ is the UL CE from user u to BS (k,b) on PRB(c,t)
- $\boldsymbol{R_{k,b,d}^{c,t}}$ is the DL CE from BS (k,b) to user d on PRB(c,t)

For consistency, we use the same notation to represent the transformed variables but with a prime symbol, i.e., $\boldsymbol{P_{u,k,b}^{'c,t}} = \mathbf{log}(\boldsymbol{P_{u,k,b}^{c,t}})$, $\boldsymbol{\gamma_{u,k,b}^{'c,t}} = \mathbf{log}(\boldsymbol{\gamma_{u,k,b}^{c,t}})$, and $\boldsymbol{R_{u,k,b}^{'c,t}} = \mathbf{log}(\boldsymbol{R_{u,k,b}^{c,t}})$. For simplicity of notation, we use $\boldsymbol{LSE(\{x\})}$ to denote the logarithm of the sum of exponentials over the set $\{x\}$. By using GP transformation, the objective of the problem $\boldsymbol{P_{Joint}^{UB-RA}(\omega)}$ can be written as a sum of LSE functions as follows:

$$
\begin{aligned}
&\sum_{u\in U_{UL}(\omega)} \log\big(\sum_{k\in\mathscr{K}} \lambda_{u,k}\big) + \sum_{d\in U_{DL}(\omega)} \log\big(\sum_{k\in\mathscr{K}} \lambda_{d,k}\big) \\
&\quad= \sum_{u\in U_{UL}(\omega)} \log\Big(\sum_{k\in\mathscr{K}}\sum_{c\in\mathscr{C}}\sum_{t\in\mathscr{T}}\sum_{b\in\mathscr{B}} e^{R^{'c,t}_{u,k,b}}\Big) + \sum_{d\in U_{DL}(\omega)} \log\Big(\sum_{k\in\mathscr{K}}\sum_{c\in\mathscr{C}}\sum_{t\in\mathscr{T}}\sum_{b\in\mathscr{B}} e^{R^{'c,t}_{k,b,d}}\Big) \\
&\quad= \sum_{u\in U_{UL}(\omega)} LSE\big(\{R^{'c,t}_{u,k,b}\}_{k\in\mathscr{K},b\in\mathscr{B},c\in\mathscr{C},t\in\mathscr{T},}\big) + \sum_{d\in U_{DL}(\omega)} LSE\big(\{R^{'c,t}_{k,b,d}\}_{k\in\mathscr{K},b\in\mathscr{B},c\in\mathscr{C},t\in\mathscr{T}}\big)
\end{aligned}
\tag{E.1}
$$

Before transforming the bilinear constraints given in (5.8k) into convex constraints, we need to rearrange and substitute (5.4) into (5.8k) as follows:

$$
\begin{aligned}
&\gamma^{c,t}_{u,k,b}\frac{N_0}{(P^{c,t}_{u,k,b}G_{u,k,b}(\omega))} + \gamma^{c,t}_{u,k,b}\sum_{k'\in\mathscr{K}}\sum_{b'\in\mathscr{B}}\sum_{u'\in U_{UL}(\omega)}^{u'\neq u}\left(\frac{P^{c,t}_{u',k',b'}G_{u',k,b}(\omega)}{P^{c,t}_{u,k,b}G_{u,k,b}(\omega)}\right)+ \\
&\gamma^{c,t}_{u,k,b}\sum_{k'\in\mathscr{K}}\sum_{b'\in\mathscr{B}}\sum_{d'\in U_{DL}(\omega)}\left(\frac{P^{c,t}_{k',b',d'}G_{k',b',k,b}(\omega)}{P^{c,t}_{u,k,b}G_{u,k,b}(\omega)}\right) \leq 1, \forall u, \forall k, \forall b, \forall c, \forall t
\end{aligned}
\tag{E.2}
$$

Note that the left-hand side of the above inequality is a *posynomial* function, however, we can apply a logarithmic transformation to this function in order to convert it into a corresponding LSE function, which is convex:

$$
\begin{aligned}
&\log\Bigg(\exp\big(\gamma^{'c,t}_{u,k,b} - P^{'c,t}_{u,k,b} + \log(N_0) - \log(G_{u,k,b}(\omega))\big)+ \\
&\sum_{k'\in\mathscr{K}}\sum_{b'\in\mathscr{B}}\sum_{u'\in U_{UL}(\omega)}^{u'\neq u}\exp\big(\gamma^{'c,t}_{u,k,b} + P^{'c,t}_{u',k',b'} - P^{'c,t}_{u,k,b} + \log(G_{u',k,b}(\omega)) - \log(G_{u,k,b}(\omega))\big)+ \\
&\sum_{k'\in\mathscr{K}}\sum_{b'\in\mathscr{B}}\sum_{d'\in U_{DL}(\omega)}\exp\big(\gamma^{'c,t}_{u,k,b} + P^{'c,t}_{k',b',d'} - P^{'c,t}_{u,k,b} + \log(G_{k',b',k,b}(\omega)) - \log(G_{u,k,b}(\omega))\big)\Bigg) \\
&\leq 0, \forall u, \forall k, \forall b, \forall c, \forall t
\end{aligned}
\tag{E.3}
$$

Similarly, before transforming the bilinear constraints given in (8l) into convex constraints, we need to rearrange and substitute equation (5) in (8l) as follows:

$$\gamma^{c,t}_{k,b,d}\frac{N_0}{P^{c,t}_{k,b,d}G_{k,b,d}(\omega)}+\gamma^{c,t}_{k,b,d}\sum_{k'\in\mathscr{K}}\sum_{b'\in\mathscr{B}}\sum_{u'\in U_{UL}(\omega)}\left(\frac{P^{c,t}_{u',k',b'}G_{u',d}(\omega)}{P^{c,t}_{k,b,d}G_{k,b,d}(\omega)}\right)+$$
$$\gamma^{c,t}_{k,b,d}\sum_{k'\in\mathscr{K}}\sum_{b'\in\mathscr{B}}\sum_{d'\in U_{DL}(\omega)}^{d'\neq d}\left(\frac{P^{c,t}_{k',b',d'}G_{k',b',d}(\omega)}{P^{c,t}_{k,b,d}G_{k,b,d}(\omega)}\right)\leq 1,\forall d,\forall k,\forall b,\forall c,\forall t \tag{E.4}$$

Now, we can apply the logarithmic transformation of the variables as follows:

$$\begin{aligned}&\log\Bigg(\exp\left(\gamma^{'c,t}_{k,b,d}-P^{'c,t}_{k,b,d}+\log(N_0)-\log(G_{k,b,d}(\omega))\right)+\\&\sum_{k'\in\mathscr{K}}\sum_{b'\in\mathscr{B}}\sum_{u'\in U_{UL}(\omega)}\exp\left(\gamma^{'c,t}_{k,b,d}+P^{'c,t}_{u',k',b'}-P^{'c,t}_{k,b,d}+\log(G_{u',d}(\omega))-\log(G_{k,b,d}(\omega))\right)+\\&\sum_{k'\in\mathscr{K}}\sum_{b'\in\mathscr{B}}\sum_{d'\in U_{DL}(\omega)}^{d'\neq d}\exp\left(\gamma^{'c,t}_{k,b,d}+P^{c,t}_{k',b',d'}-P^{'c,t}_{k,b,d}+\log(G_{k',b',d}(\omega))-\log(G_{k,b,d}(\omega))\right)\Bigg)\\&\leq 0,\forall d,\forall k,\forall b,\forall c,\forall t\end{aligned} \tag{E.5}$$

Using the above transformations, we formulate the convex upper-bound problem as follows:

$$\boldsymbol{P^{UB-RA'}_{Joint}(\omega)}:\underset{\{P^{'c,t}_{u,k,b}\},\{\gamma^{'c,t}_{u,k,b}\},\{R^{'c,t}_{u,k,b}\}}{\text{maximize}}$$
$$\sum_{u\in U_{UL}(\omega)}LSE\left(\{R^{'c,t}_{u,k,b}\}_{k\in\mathscr{K},b\in\mathscr{B},c\in\mathscr{C},\forall t\in\mathscr{T}}\right)+\sum_{d\in U_{DL}(\omega)}LSE\left(\{R^{'c,t}_{k,b,d}\}_{k\in\mathscr{K},b\in\mathscr{B},c\in\mathscr{C},\forall t\in\mathscr{T}}\right)$$

subject to (E.3), (E.5), and:

$$\log(\epsilon_p)\leq P^{'c,t}_{u,k,b}\leq z_{u,k}(\omega)\log(P_{UE})+(1-z_{u,k}(\omega))\log(\epsilon_p),\forall u,\forall k,\forall b,\forall c,\forall t \tag{E.6a}$$
$$\log(\epsilon_p)\leq P^{'c,t}_{k,b,d}\leq z_{d,k}(\omega)\log(P_b)+(1-z_{d,k}(\omega))\log(\epsilon_p),\quad \forall d,\forall k,\forall b,\forall c,\forall t \tag{E.6b}$$
$$LSE(\{P^{'c,t}_{u,k,b}\}_{b\in\mathscr{B},c\in\mathscr{C}})\leq\log(P_{UE}),\qquad \forall u,\forall k,\forall t \tag{E.6c}$$
$$LSE(\{P^{'c,t}_{k,d,b}\}_{d\in U_{DL}(\omega),c\in\mathscr{C}})\leq\log(P_b),\qquad \forall k,\forall b,\forall t \tag{E.6d}$$

$$P^{'c,t}_{u,k,b} + P^{'c,t}_{u',k,b} \leq \log(\epsilon_p), \qquad \forall u, \forall u', u \neq u', \forall k, \forall b, \forall c, \forall t \tag{E.6e}$$

$$P^{'c,t}_{k,b,d} + P^{'c,t}_{k,b,d'} \leq \log(\epsilon_p), \qquad \forall d, \forall d', d \neq d', \forall k, \forall b, \forall c, \forall t \tag{E.6f}$$

$$P^{'c,t}_{u,b,d} + P^{'c,t}_{k,b,d} \leq \log(\epsilon_p), \qquad \forall u, \forall d, \forall k, \forall b, \forall c, \forall t \tag{E.6g}$$

$$P^{'c,t}_{u,k,1} +, ..., + P^{'c,t}_{u,k,|\mathscr{B}|} \leq (|\mathscr{B}| - 1)\log(\epsilon_p), \qquad \forall u, \forall k, \forall c, \forall t \tag{E.6h}$$

$$P^{'c,t}_{k,1,d} +, ..., + P^{'c,t}_{k,|\mathscr{B}|,d} \leq (|\mathscr{B}| - 1)\log(\epsilon_p), \qquad \forall d, \forall k, \forall c, \forall t \tag{E.6i}$$

$$\log(\epsilon_\gamma) \leq \gamma^{'c,t}_{u,k,b} \leq \log(\beta_{max}), \qquad \forall u, \forall k, \forall b, \forall c, \forall t \tag{E.6j}$$

$$\log(\epsilon_\gamma) \leq \gamma^{'c,t}_{k,b,d} \leq \log(\beta_{max}), \qquad \forall d, \forall k, \forall b, \forall c, \forall t \tag{E.6k}$$

$$R^{'c,t}_{u,k,b} = \log_{10}(e)\gamma^{'c,t}_{u,k,b}, \qquad \forall u, \forall k, \forall b, \forall c, \forall t \tag{E.6l}$$

$$R^{'c,t}_{k,b,d} = \log_{10}(e)\gamma^{'c,t}_{k,b,d}, \qquad \forall d, \forall k, \forall b, \forall c, \forall t \tag{E.6m}$$

Appendix F

Proof of Lemma 6.1

The problem $[\boldsymbol{P^{UB}_{MP-A2C}}]$ requires extensive computational resources, by making a high SINR assumption, we can convert it into an equivalent convex problem ($[\boldsymbol{P^{UB'}_{MP-A2C}}]$) using the techniques given in [82]. We take the high SINR assumption on the sum of the SINR variables, which leads to the following approximation of the constraints (6.11i) and (6.11j):

$$\begin{aligned} \lambda_{u,r} \approx \Delta f \times \log_2(\sum_{n=1}^{N_C}\sum_{k=1}^{N_F}\gamma_{u,r}^{n,k}) = \Delta f \times \frac{\log(\sum_{n=1}^{N_C}\sum_{k=1}^{N_F}\gamma_{u,r}^{n,k})}{\log(2)} \geq [\boldsymbol{R}^{5G}]_{u,r} \\ \implies \log(\sum_{n=1}^{N_C}\sum_{k=1}^{N_F}\gamma_{u,r}^{n,k}) \geq \frac{\log(2)\times[\boldsymbol{R}^{5G}]_{u,r}}{\Delta f} \end{aligned} \tag{F.1}$$

By making a logarithmic change of the variables, a logarithmic transformation of the objective and the constraints, the GP transformation (*i.e.*, described in [38]) can convert this problem into an equivalent convex problem using the high SINR approximation. For consistency, we use the same notation to represent the transformed variables but with a prime symbol; for example, $\boldsymbol{P'^{n,k}_{u,r}} = \boldsymbol{\log(P^{n,k}_{u,r})}$ and $\boldsymbol{\gamma'^{n,k}_{u,r}} = \boldsymbol{\log(\gamma^{n,k}_{u,r})}$. For simplicity of notation, we use $\boldsymbol{LSE(\{x\})}$ to denote the logarithm of the sum of exponentials over the set $\{x\}$.

By using GP transformation, the objective of the problem $[\boldsymbol{P^{UB}_{MP-A2C}}]$ can be reformulated as follows:

$$\begin{aligned}\sum_{u=1}^{N_U}\sum_{r=1}^{N_R}\lambda_{u,r} &= \sum_{u}\sum_{r}\Delta f \times \frac{\log(\sum_{n=1}^{N_C}\sum_{k=1}^{N_F}\gamma_{u,r}^{n,k})}{\log(2)} \\ &= \sum_{u=1}^{N_U}\sum_{r=1}^{N_R}\frac{\Delta f}{\log(2)} \times LSE(\{\gamma_{u,r}^{'n,k}\}_{n\in\{1,\ldots,N_C\},k\in\{1,\ldots,N_F\}})\end{aligned} \tag{F.2}$$

Before transforming the bilinear constraints given in (6.11g) into convex constraints, we need to rearrange and substitute (6.11g) into (6.11h) as follows:

$$\begin{aligned}&\gamma_{u,r}^{n,k}\frac{\sigma_C^2}{(P_{u,r}^{n,k}|h_n^{n,k}|^2)} + \gamma_{u,r}^{n,k}\sum_{n'=1,n'\neq n}^{N_C}\sum_{u'=1}^{N_U}\sum_{r'=1}^{N_R}\frac{P_{u',r'}^{n',k}|h_n^{n',k}|^2}{P_{u,r}^{n,k}|h_n^{n,k}|^2} \leq 1, \forall u, \forall r, \forall n, \forall k \\ &\implies \log\Bigg(\exp\left(\gamma_{u,r}^{'n,k} - P_{u,r}^{'n,k} + \log(\sigma_C^2) - \log(|h_n^{n,k}|^2)\right) + \\ &\sum_{n'=1,n'\neq n}^{N_C}\sum_{u'=1}^{N_U}\sum_{r'=1}^{N_R}\exp\left(\gamma_{u,r}^{'n,k} + P_{u',r'}^{'n',k} - P_{u,r}^{'n,k} + \log(|h_n^{n',k}|^2) - \log(|h_n^{n,k}|^2)\right)\Bigg) \\ &\leq 0, \forall u, \forall r, \forall n, \forall k\end{aligned} \tag{F.3}$$

Note that we applied a logarithmic transformation to the above constraint and converted its left hand side into a corresponding LSE function which is convex.

Using the above transformations, we can formulate the convex optimization problem as follows:

$$[\boldsymbol{P}^{\boldsymbol{UB'}}_{\boldsymbol{MP-A2C}}]: \underset{\{P^{'n,k}_{u,r}\},\{\gamma^{'n,k}_{u,r}\}}{\text{maximize}} \sum_{u=1}^{N_U}\sum_{r=1}^{N_R} \frac{\Delta f}{\log(2)} \times LSE(\{\gamma^{'n,k}_{u,r}\}_{n\in\{1,\ldots,N_C\},k\in\{1,\ldots,N_F\}})$$

subject to (F.3) and:

$$\log(P_{min}) \leq P^{'n,k}_{u,r} \leq \log(P_{max}), \qquad \forall u,\forall r,\forall n,\forall k \tag{F.4a}$$

$$P^{n,k}_{u,r} + P^{n,k}_{u',r'} \leq \log(\epsilon_p), \forall (u',r'),(u',r') \neq (u,r), \qquad \forall u,\forall r,\forall n,\forall k \tag{F.4b}$$

$$P^{'n,k}_{u,r} + P^{'n',k'}_{u,r} \leq \log(\epsilon_p), \forall (n',k'),(n',k') \neq (n,k), \qquad \forall u,\forall r,\forall n,\forall k \tag{F.4c}$$

$$LSE(\{P^{'n,k}_{u,k}\}_{u\in\{1,\ldots,N_U\},r\in\{1,\ldots,N_R\}}) \leq \log(P_{max}), \qquad \forall n,\forall k \tag{F.4d}$$

$$LSE(\{P^{'n,k}_{u,k}\}_{u\in\{1,\ldots,N_U\},r\in\{1,\ldots,N_R\},k\in\{1,\ldots,N_F\}}) \leq \log(P_T), \qquad \forall n \tag{F.4e}$$

$$\log(\epsilon_\gamma) \leq \gamma^{'n,k}_{u,r} \leq \log(\gamma_{max}), \qquad \forall u,\forall r \tag{F.4f}$$

$$LSE(\{\gamma^{'n,k}_{u,k}\}_{u\in\{1,\ldots,N_U\},r\in\{1,\ldots,N_R\}}) \leq \log(\gamma_{max}), \qquad \forall n,\forall k \tag{F.4g}$$

$$LSE(\{\gamma^{'n,k}_{u,k}\}_{n\in\{1,\ldots,N_C\},k\in\{1,\ldots,N_F\}}) \leq \log(\gamma_{max}), \qquad \forall u,\forall r \tag{F.4h}$$

$$LSE(\{\gamma^{'n,k}_{u,k}\}_{n\in\{1,\ldots,N_C\},k\in\{1,\ldots,N_F\}}) \geq \frac{\log(2)\times[\boldsymbol{R}^{5G}]_{u,r}}{\Delta f}, \qquad \forall u,\forall r \tag{F.4i}$$

where, $u \in \{1,\ldots,N_U\}, r \in \{1,\ldots,N_R\}, n \in \{1,\ldots,N_C\}$, and $k \in \{1,\ldots,N_F\}$.

Appendix G

Proof of Lemma 6.2

The problem $\boldsymbol{P_C^{AM}}$ requires extensive computational resources, by making a high SINR assumption, we can convert it into an equivalent convex problem ($\boldsymbol{P_C^{AM'}}$) using the techniques given in [82]. We take the high SINR assumption on the sum of the SINR variables, which leads to the following approximation of the constraints (6.13f):

$$\lambda^{n,k} = \Delta f \times \log_2(1+\gamma^{n,k}) \approx \Delta f \times \log_2(\gamma^{n,k}) = \Delta f \times \frac{\log(\gamma^{n,k})}{\log(2)}, \quad \forall n, \forall k \tag{G.1}$$

By making a logarithmic change of the variables, a logarithmic transformation of the objective and the constraints, the GP transformation (*i.e.*, described in [38]) can convert this problem into an equivalent convex problem using the high SINR approximation. For consistency, we use the same notation to represent the transformed variables but with a prime symbol; for example, $\boldsymbol{P'^{n,k}} = \mathbf{log}(\boldsymbol{P^{n,k}})$ and $\boldsymbol{\gamma'^{n,k}} = \mathbf{log}(\boldsymbol{\gamma^{n,k}})$. For simplicity of notation, we use $\boldsymbol{LSE(\{x\})}$ to denote the logarithm of the sum of exponentials over the set $\{x\}$.

By using GP transformation, the objective of the problem $\boldsymbol{P_C^{AM}}$ can be written as follows:

$$\sum_{n=1}^{N_C}\sum_{k=1}^{N_F}\lambda^{n,k} = \sum_{n=1}^{N_C}\sum_{k=1}^{N_F}\left(\Delta f \times \frac{\log(\gamma^{n,k})}{\log(2)}\right) = \sum_{n=1}^{N_C}\sum_{k=1}^{N_F}\left(\frac{\Delta f \times \gamma'^{n,k}}{\log(2)}\right) \tag{G.2}$$

Before transforming the bilinear constraints given in (6.13d) into convex constraints, we need to rearrange and substitute (6.13e) into (6.13d) as follows:

$$\gamma^{n,k}\frac{\sigma_C^2}{(P^{n,k}|h_n^{n,k}|^2)}+\gamma^{n,k}\sum_{n'=1,n'\neq n}^{N_C}\frac{P^{n',k}|h_n^{n',k}|^2}{P^{n,k}|h_n^{n,k}|^2}\leq 1, \qquad \forall n,\forall k$$

$$\implies \log\Bigg(\exp\left(\gamma^{'n,k}-P^{'n,k}+\log(\sigma_C^2)-\log(|h_n^{n,k}|^2)\right)+ \tag{G.3}$$

$$\sum_{n'=1,n'\neq n}^{N_C}\exp\left(\gamma^{'n,k}+P^{'n',k}-P^{'n,k}+\log(|h_n^{n',k}|^2)-\log(|h_n^{n,k}|^2)\right)\Bigg)\leq 0, \quad \forall n,\forall k$$

Note that we applied a logarithmic transformation to the above constraint and converted its left hand side into a corresponding LSE function which is convex.

Using the above transformations, we can formulate the convex optimization problem as follows:

$$\boldsymbol{P_C^{AM'}}: \underset{\{P^{'n,k}\},\{\gamma^{'n,k}\}}{\text{maximize}} \sum_{n=1}^{N_C}\sum_{k=1}^{N_F}\left(\frac{\Delta f\times\gamma^{'n,k}}{\log(2)}\right)$$

subject to (G.3) and:

$$\log(P_{min})\leq P^{'n,k}\leq\log(P_{max}),\forall n,\forall k \tag{G.4a}$$

$$LSE(\{P^{'n,k}\}_{k\in\{1,\ldots,N_F\}})\leq\log(P^T), \qquad \forall n \tag{G.4b}$$

$$\log(\gamma_{min})\leq\gamma^{'n,k}\leq\log(\gamma_{max}),\ \forall n,\forall k \tag{G.4c}$$

where, $n\in\{1,\ldots,N_C\}$, and $k\in\{1,\ldots,N_F\}$.

Appendix H

Proof of Lemma 6.3

The problem $\boldsymbol{P_C^{GM}}$ requires extensive computational resources, by making a high SINR assumption, we can convert it into an equivalent convex problem ($\boldsymbol{P_C^{GM'}}$) using the techniques given in [82]. We take the high SINR assumption on the sum of the SINR variables, which leads to the following approximation of the constraints (6.13f):

$$\lambda^{n,k} = \Delta f \times \log_2(1+\gamma^{n,k}) \approx \Delta f \times \log_2(\gamma^{n,k}) = \Delta f \times \frac{\log(\gamma^{n,k})}{\log(2)}, \quad \forall n, \forall k \tag{H.1}$$

By making a logarithmic change of the variables, a logarithmic transformation of the objective and the constraints, the GP transformation (*i.e.*, described in [38]) can convert this problem into an equivalent convex problem using the high SINR approximation. For consistency, we use the same notation to represent the transformed variables but with a prime symbol; for example, $\boldsymbol{P'^{n,k}} = \mathbf{log}(\boldsymbol{P^{n,k}})$ and $\boldsymbol{\gamma'^{n,k}} = \mathbf{log}(\boldsymbol{\gamma^{n,k}})$. For simplicity of notation, we use $\boldsymbol{LSE(\{x\})}$ to denote the logarithm of the sum of exponentials over the set $\{x\}$.

By using GP transformation, the objective of the problem $\boldsymbol{P_C^{GM}}$ can be written as follows:

$$\begin{aligned}\sum_{n=1}^{N_C}\sum_{k=1}^{N_F}\log(\lambda^{n,k}) &= \sum_{n=1}^{N_C}\sum_{k=1}^{N_F}\log\left(\Delta f \times \frac{\log(\gamma^{n,k})}{\log(2)}\right) = \sum_{n=1}^{N_C}\sum_{k=1}^{N_F}\log\left(\frac{\Delta f \times \gamma^{'n,k}}{\log(2)}\right) \\ &= \sum_{n=1}^{N_C}\sum_{k=1}^{N_F}\left(\log\left(\frac{\Delta f}{\log_2(2)}\right) + \log(\gamma^{'n,k})\right)\end{aligned} \tag{H.2}$$

Using these transformations, we can formulate the convex optimization problem as follows:

$$\boldsymbol{P_C^{GM'}}: \underset{\{P^{'n,k}\},\{\gamma^{'n,k}\}}{\text{maximize}} \sum_{n=1}^{N_C}\sum_{k=1}^{N_F}\left(\log\left(\frac{\Delta f}{\log_2(2)}\right) + \log(\gamma^{'n,k})\right)$$

subject to (G.3) and:

$$\log(P_{min}) \leq P^{'n,k} \leq \log(P_{max}), \forall n, \forall k \tag{H.3a}$$

$$LSE(\{P^{'n,k}\}_{k\in\{1,\ldots,N_F\}}) \leq \log(P^T), \quad \forall n \tag{H.3b}$$

$$\log(\gamma_{min}) \leq \gamma^{'n,k} \leq \log(\gamma_{max}), \ \forall n, \forall k \tag{H.3c}$$

where, $n \in \{1,\ldots,N_C\}$, and $k \in \{1,\ldots,N_F\}$.

Bibliography

[1] Ericsson. *Ericsson Mobility Report*. [Online]. 2017. URL: https://www.ericsson.com/assets/local/mobility-report/documents/2017/ericsson-mobility-report-november-2017-middle-east-and-africa.pdf.

[2] Red Mobile Consulting. *Study of Future Demand for Radio Spectrum in Canada 2011-2015*. [Online]. 2012. URL: https://www.ic.gc.ca/eic/site/smt-gst.nsf/eng/sf10253.html.

[3] Nokia Solutions and Networks. *Nokia Solutions and Networks TD-LTE Frame Configuration Primer*. [Online]. 2013. URL: http://www.networks.nokia.com/system/files/document/nsn_td_lte_frame_configuration_wp.pdf.

[4] B. Yang, W. Guo, Y. Jin, and S. Wang. "Smartphone Data Usage: Downlink and Uplink Asymmetry". In: *Electronics Letters* 52.3 (2016), pp. 243–245.

[5] 3GPP-TSG-RAN-WG1. *Evolved Universal Terrestrial Radio Access (E-UTRA)*. 3GPP, Tech. Rep. TR 36.814. 2010.

[6] Huwawei. *The Second Phase of LTE-Advanced*. [Online]. URL: http://www.huawei.com/ilink/en/download/HW_259010.

[7] Ping Wang, Hai Jiang, Weihua Zhuang, and H Vincent Poor. "Redefinition of max-min Fairness in Multi-hop Wireless Networks". In: *IEEE Transactions on Wireless Communications*, 7.12 (2008), pp. 4786–4791.

[8] Frank Kelly. "Charging and Rate Control for Elastic Traffic". In: *European Transactions on Telecommunications* 8.1 (1997), pp. 33–37.

[9] Dariush Fooladivanda and Catherine Rosenberg. "Joint Resource Allocation and User Association for Heterogeneous Wireless Cellular Networks". In: *IEEE Transactions on Wireless Communications* 12.1 (2013), pp. 248–257.

[10] Jagadish Ghimire. "Heterogeneous Cellular Networks: From Resource Allocation To User Association". PhD thesis. University of Waterloo, 2015.

[11] Abhinav Kumar and Catherine Rosenberg. "Energy and Throughput Trade-offs in Cellular Networks using Base Station Switching". In: *IEEE Transactions on Mobile Computing* 15.2 (2016), pp. 364–376.

[12] Elias Yaacoub and Zaher Dawy. "A Game Theoretical Formulation for Proportional Fairness in LTE Uplink Scheduling". In: *IEEE Wireless Communications and Networking Conference*. 2009.

[13] Elias Yaacoub, Ahmad M El-Hajj, and Zaher Dawy. "Weighted Ergodic sum-rate Maximisation in Uplink Orthogonal Frequency Division Multiple Access and its Achievable Rate Region". In: *IET Communications* 4.18 (2010), pp. 2217–2229.

[14] David NC Tse and Stephen V Hanly. "Multiaccess Fading Channels. I. Polymatroid Structure, Optimal Resource Allocation and Throughput Capacities". In: *IEEE Transactions on Information Theory* 44.7 (1998), pp. 2796–2815.

[15] Jianwei Huang, Vijay G Subramanian, Rajeev Agrawal, and Randall Berry. "Joint Scheduling and Resource Allocation in Uplink OFDM systems for Broadband Wireless Access Networks". In: *IEEE Journal on Selected Areas in Communications* 27.2 (2009), pp. 226–234.

[16] Andreas Muller and Philipp Frank. "Cooperative Interference Prediction for Enhanced Link Adaptation in the 3GPP LTE Uplink". In: *IEEE Vehicular Technology Conference*. 2010.

[17] Elias Yaacoub and Zaher Dawy. "Proportional Fair Scheduling with Probabilistic Interference Avoidance in the Uplink of Multicell OFDMA Systems". In: *IEEE Global Communications Workshop*. 2010.

[18] K. Shen and W. Yu. “A Coordinated Uplink Scheduling and Power Control Algorithm for Multicell Networks”. In: *Asilomar Conference on Signals, Systems, and Computers*. 2015.

[19] G. Y. Li, J. Niu, D. Lee, J. Fan, and Y. Fu. “Multi-Cell Coordinated Scheduling and MIMO in LTE”. In: *IEEE Communications Surveys Tutorials* 16.2 (2014), pp. 761–775.

[20] W. Yu, T. Kwon, and C. Shin. “Multicell Coordination via Joint Scheduling, Beamforming, and Power Spectrum Adaptation”. In: *IEEE Transactions on Wireless Communications* 12.7 (2013), pp. 1–14.

[21] Erik Dahlman, Stefan Parkvall, and Johan Skold. *4G: LTE/LTE-Advanced for Mobile Broadband*. Academic Press, 2013.

[22] D. López-Pérez, Á. Ladányi, A. Jüttner, H. Rivano, and J. Zhang. “Optimization method for the joint allocation of modulation schemes, coding rates, resource blocks and power in self-organizing LTE networks”. In: *2011 Proceedings IEEE INFOCOM*. 2011, pp. 111–115.

[23] Christian Mehlfuhrer, Martin Wrulich, Josep Colom Ikuno, Dagmar Bosanska, and Markus Rupp. “Simulating the Long Term Evolution Physical Layer”. In: *IEEE European Signal Processing Conference*. 2009.

[24] S. Fu, H. Wen, and B. Wu. “Power-Fractionizing Mechanism: Achieving Joint User Scheduling and Power Allocation via Geometric Programming”. In: *IEEE Transactions on Vehicular Technology* 67.3 (2018), pp. 2025–2034.

[25] A. Khandekar, N. Bhushan, J. Tingfang, and V. Vanghi. “LTE-Advanced: Heterogeneous networks”. In: *2010 European Wireless Conference (EW)*. 2010, pp. 978–982.

[26] A. Mesodiakaki, F. Adelantado, L. Alonso, and C. Verikoukis. “Joint uplink and downlink cell selection in cognitive small cell heterogeneous networks”. In: *2014 IEEE Global Communications Conference*. 2014, pp. 2643–2648.

[27] N. Sapountzis, T. Spyropoulos, N. Nikaein, and U. Salim. "Optimal downlink and uplink user association in backhaul-limited HetNets". In: *IEEE INFOCOM 2016 - The 35th Annual IEEE International Conference on Computer Communications*. 2016, pp. 1–9.

[28] H. Elshaer, F. Boccardi, M. Dohler, and R. Irmer. "Downlink and Uplink Decoupling: A disruptive architectural design for 5G networks". In: *2014 IEEE Global Communications Conference*. 2014, pp. 1798–1803.

[29] K. Smiljkovikj, L. Gavrilovska, and P. Popovski. "Efficiency analysis of downlink and uplink decoupling in heterogeneous networks". In: *2015 IEEE International Conference on Communication Workshop (ICCW)*. 2015, pp. 125–130.

[30] K. Smiljkovikj, P. Popovski, and L. Gavrilovska. "Analysis of the Decoupled Access for Downlink and Uplink in Wireless Heterogeneous Networks". In: *IEEE Wireless Communications Letters* 4.2 (2015), pp. 173–176.

[31] S. Jabeen and P. Ho. "Joint User Scheduling for ODFMA-Based Multi-Cell Networks". In: *2018 International Conference on Networking and Network Applications (NaNA)*. 2018, pp. 232–236.

[32] S. Jabeen and P. Ho. "Joint User Scheduling and RRU Association for ODFMA-based Networks with Inter-BBU Coordination". In: *Accepted for publication in IEEE Transactions on Communications* (2018).

[33] I. C. Wong, O. Oteri, and W. Mccoy. "Optimal resource allocation in uplink SC-FDMA systems". In: *IEEE Transactions on Wireless Communications* 8.5 (2009), pp. 2161–2165.

[34] M. Kalil, A. Shami, and A. Al-Dweik. "QoS-Aware Power-Efficient Scheduler for LTE Uplink". In: *IEEE Transactions on Mobile Computing* 14.8 (2015), pp. 1672–1685.

[35] F. Wang, W. Chen, H. Tang, and Q. Wu. "Joint Optimization of User Association, Subchannel Allocation, and Power Allocation in Multi-Cell Multi-Association OFDMA Heterogeneous Networks". In: *IEEE Transactions on Communications* 65.6 (2017), pp. 2672–2684.

[36] Tech. Rep. TR 36.828 3GPP. *E-UTRA: Further Enhancemenets to TDD for DL-UL Interference Management and Traffic Adaptation*. [Online]. 2012.

[37] D. P. Palomar and Mung Chiang. "A tutorial on decomposition methods for network utility maximization". In: *IEEE Journal on Selected Areas in Communications* 24.8 (2006), pp. 1439–1451.

[38] Stephen Boyd and Lieven Vandenberghe. *Convex optimization*. Cambridge university press, 2004.

[39] Philip E. Gill, Walter Murray, and Michael A. Saunders. "SNOPT: An SQP algorithm for large-scale constrained optimization". In: *SIAM Rev.* 47 (2005), pp. 99–131.

[40] Tobias Achterberg. "SCIP: Solving Constraint Integer Programs". In: *Springer Mathematical Programming Computation* 1.1 (2009), pp. 1–41.

[41] Aleksandra Checko, Henrik L Christiansen, Ying Yan, Lara Scolari, Georgios Kardaras, Michael S Berger, and Lars Dittmann. "Cloud RAN for mobile networks: A technology overview". In: *IEEE Communications surveys and tutorials* 17.1 (2015), pp. 405–426.

[42] Y. Shi, J. Zhang, and K. B. Letaief. "Group Sparse Beamforming for Green Cloud-RAN". In: *IEEE Transactions on Wireless Communications* 13.5 (2014), pp. 2809–2823.

[43] B. Dai and W. Yu. "Energy Efficiency of Downlink Transmission Strategies for Cloud Radio Access Networks". In: *IEEE Journal on Selected Areas in Communications* 34.4 (2016), pp. 1037–1050.

[44] C. Pan, H. Zhu, N. J. Gomes, and J. Wang. "Joint Precoding and RRH Selection for User-Centric Green MIMO C-RAN". In: *IEEE Transactions on Wireless Communications* 16.5 (2017), pp. 2891–2906.

[45] M. A. Marotta, N. Kaminski, I. Gomez-Miguelez, L. Z. Granville, J. Rochol, L. DaSilva, and C. B. Both. "Resource sharing in heterogeneous cloud radio access networks". In: *IEEE Wireless Communications* 22.3 (2015), pp. 74–82.

[46] Mohammed S. Al-Abiad, Ahmed Douik, Sameh Sorour, and Md Jahangir Hossain. *Throughput Maximization in Cloud-Radio Access Networks using Rate-Aware Network Coding*. 2018. arXiv: 1806.08230 [cs.IT].

[47] Y. Qi and H. Wang. "Interference-aware User Association under Cell Sleeping for Heterogeneous Cloud Cellular Networks". In: *IEEE Wireless Communications Letters* 6.2 (2017), pp. 242–245.

[48] J. Wu, Z. Zhang, Y. Hong, and Y. Wen. "Cloud radio access network (C-RAN): a primer". In: *IEEE Network* 29.1 (2015), pp. 35–41.

[49] P. Gupta, A. Vishwanath, S. Kalyanaraman, and Y. H. Lin. "Unlocking wireless performance with co-operation in co-located base station pools". In: *International Conference on Communication Systems and Networks*. 2010.

[50] S. Jabeen and P. Ho. "A Benchmark for Joint Channel Allocation and User Scheduling in Flexible Heterogeneous Networks". In: *Submitted to IEEE Transactions on Vehicular Technology* (2018).

[51] S. Goyal, P. Liu, S. Panwar, R. A. DiFazio, R. Yang, J. Li, and E. Bala. "Improving small cell capacity with common-carrier full duplex radios". In: *2014 IEEE International Conference on Communications (ICC)*. 2014, pp. 4987–4993.

[52] V. Pauli, Y. Li, and E. Seidel. "Dynamic TDD for LTE-A and 5G". In: *Nomor Research* (2015). [Online].

[53] M. Ding, D. López-Pérez, R. Xue, A. V. Vasilakos, and W. Chen. "On Dynamic Time-Division-Duplex Transmissions for Small-Cell Networks". In: *IEEE Transactions on Vehicular Technology* 65.11 (2016), pp. 8933–8951.

[54] B. Yu, L. Yang, H. Ishii, and S. Mukherjee. "Dynamic TDD Support in Macrocell-Assisted Small Cell Architecture". In: *IEEE Journal on Selected Areas in Communications* 33.6 (2015), pp. 1201–1213.

[55] S. Sekander, H. Tabassum, and E. Hossain. "Decoupled Uplink-Downlink User Association in Multi-Tier Full-Duplex Cellular Networks: A Two-Sided Matching Game". In: *IEEE Transactions on Mobile Computing* 16.10 (2017), pp. 2778–2791.

[56] Trung Kien Vu, Mehdi Bennis, Sumudu Samarakoon, Merouane Debbah, and Matti Latva-aho. "Joint Load Balancing and Interference Mitigation in 5G Heterogeneous Networks". In: *IEEE Transactions on Wireless Communications* 16.9 (2017), pp. 6032–6046.

[57] S. Lembo, O. Tirkkonen, M. Goldhamer, and A. Kliks. "Coexistence of FDD flexible duplexing networks". In: *European Conference on Networks and Communications (EuCNC)*. 2017, pp. 1–6.

[58] K. Balachandran, J. H. Kang, K. Karakayali, and K. M. Rege. "Flexible duplex in FDD spectrum". In: *2017 IEEE International Conference on Communications Workshops (ICC Workshops)*. 2017, pp. 296–301.

[59] A. Tölli, J. Kaleva, G. Venkatraman, and D. Gesbert. "Joint UL/DL mode selection and transceiver design for dynamic TDD systems". In: *2016 IEEE Global Conference on Signal and Information Processing (GlobalSIP)*. 2016, pp. 630–634.

[60] L. Sanguinetti, A. Moustakas, and M. Debbah. "Interference management in 5G reverse TDD HetNets with wireless backhaul: A large system analysis". In: *IEEE Journal on Selected Areas Communication* 33.6 (2015), pp. 1187–1200.

[61] CCSA. *3GPP R12 related research and standardaization in China*. [Online]. 2012.

[62] 3GPP-TSG-RAN-WG1. *3GPP TSG RAN WG1 Meeting no 91*. [Online]. 2017.

[63] T. Nakamura, S. Nagata, A. Benjebbour, Y. Kishiyama, T. Hai, S. Xiaodong, Y. Ning, and L. Nan. "Trends in small cell enhancements in LTE advanced". In: *IEEE Communications Magazine* 51.2 (2013), pp. 98–105.

[64] E. Basar. "Index modulation techniques for 5G wireless networks". In: *IEEE Communications Magazine* 54.7 (2016), pp. 168–175.

[65] Federico Boccardi, Robert W Heath, Angel Lozano, Thomas L Marzetta, and Petar Popovski. "Five disruptive technology directions for 5G". In: *IEEE Communications Magazine* 52.2 (2014), pp. 74–80.

[66] Syed Hassan Raza Naqvi, Andrea Matera, Lorenzo Combi, and Umberto Spagnolini. "On the transport capability of LAN cables in all-analog MIMO-RoC fronthaul". In: *IEEE Wireless Communications and Networking Conference (WCNC)*. 2017, pp. 1–6.

[67] S. H. R. Naqvi, P. H. Ho, and S. Jabeen. "A Novel Distributed Antenna Access Architecture for 5G Indoor Service Provisioning". In: *IEEE Journal on Selected Areas in Communications* 36.11 (2018), pp. 2518–2527.

[68] S. H. Raza Naqvi, S. Jabeen, and P. H. Ho. "Low-complexity Optimal Scheduler for LTE Over LAN Cable". In: *2018 International Conference on Networking and Network Applications (NaNA)*. 2018, pp. 36–41.

[69] Jonathan Gambini and Umberto Spagnolini. "Wireless over cable for femtocell systems". In: *IEEE Communications Magazine* 51.5 (2013), pp. 178–185.

[70] Chenguang Lu, Miguel Berg, Elmar Trojer, Per-Erik Eriksson, Kim Laraqui, OV Tridblad, and H Almeida. "Connecting the dots: small cells shape up for high-performance indoor radio". In: *Ericsson Review* 91.2 (2014), pp. 38–45.

[71] Federico Tonini, Matteo Fiorani, Marija Furdek, Carla Raffaelli, Lena Wosinska, and Paolo Monti. "Radio and Transport Planning of Centralized Radio Architectures in 5G Indoor Scenarios". In: *IEEE Journal on Selected Areas in Communications* 35.8 (2017), pp. 1837–1848.

[72] Andrea Matera, Lorenzo Combi, Syed Hassan Raza Naqvi, and Umberto Spagnolini. "Space-frequency to space-frequency for MIMO radio over copper". In: *IEEE International Conference on Communications (ICC)*. 2017, pp. 1–6.

[73] Andrea Matera and Umberto Spagnolini. "On the optimal Space-Frequency to Frequency mapping in indoor single-pair RoC fronthaul". In: *IEEE Networks and Communications (EuCNC), 2017 European Conference on*. 2017, pp. 1–5.

[74] 3GPP. *5G; Study on Scenarios and Requirements for Next Generation Access Technologies*. Technical Report (TR) 38.913. Version 14.2.0. 3rd Generation Partnership Project (3GPP), May 2017.

[75] A. Matera and U. Spagnolini. "Analog MIMO-RoC Downlink with SF2SF". In: *IEEE Wireless Communications Letters* (2018), pp. 1–1.

[76] J. Hoydis, S. ten Brink, and M. Debbah. "Massive MIMO in the UL/DL of Cellular Networks: How Many Antennas Do We Need?" In: *IEEE Journal on Selected Areas in Communications* 31.2 (2013), pp. 160–171.

[77] Kan Zheng, Suling Ou, and Xuefeng Yin. "Massive MIMO channel models: A survey". In: *International Journal of Antennas and Propagation* (2014).

[78] H. Yin, D. Gesbert, M. Filippou, and Y. Liu. "A Coordinated Approach to Channel Estimation in Large-Scale Multiple-Antenna Systems". In: *IEEE Journal on Selected Areas in Communications* 31.2 (2013), pp. 264–273.

[79] ITU-T. *Transport network support of IMT-2020/5G*. Technical Report (TR). GSTR-TN5G. International Telecommunication Union (ITU), 2018.

[80] 3GPP. *LTE; Evolved Universal Terrestrial Radio Access (E-UTRA); Base Station (BS) radio transmission and reception*. ETSI Technical Specification (TS) 36.104. Version 9.4.0. 3rd Generation Partnership Project (3GPP), July 2010.

[81] R. A. Shafik, M. S. Rahman, and A. R. Islam. "On the Extended Relationships Among EVM, BER and SNR as Performance Metrics". In: *International Conference on Electrical and Computer Engineering*. 2006, pp. 408–411.

[82] M. Chiang, C. W. Tan, D. P. Palomar, D. O'neill, and D. Julian. "Power Control By Geometric Programming". In: *IEEE Transactions on Wireless Communications* 6.7 (2007), pp. 2640–2651.

[83] Harold W Kuhn. "The Hungarian method for the assignment problem". In: *Naval research logistics quarterly* 2 (1955), pp. 83–97.

[84] Peter Brown, Yuedong Yang, Yaoqi Zhou, and Wayne Pullan. "A heuristic for the time constrained asymmetric linear sum assignment problem". In: *Journal of Combinatorial Optimization* 33.2 (2017), pp. 551–566.

[85] Frank Effenberger. "Future broadband access networks [point of view]". In: *Proceedings of the IEEE* 104.11 (2016), pp. 2078–2081.

[86] K. I. Ahmed, H. Tabassum, and E. Hossain. *Deep learning for radio resource allocation in multi-cell networks*. 2018. arXiv: 1808.00667 [cs.NI].

[87] H. Sun, X. Chen, Q. Shi, M. Hong, X. Fu, and N. D. Sidiropoulos. "Learning to optimize: Training deep neural networks for wireless resource management". In: *2017 IEEE 18th International Workshop on Signal Processing Advances in Wireless Communications (SPAWC)*. 2017, pp. 1–6.

[88] Z. Xu, Y. Wang, J. Tang, J. Wang, and M. C. Gursoy. "A deep reinforcement learning based framework for power-efficient resource allocation in cloud RANs". In: *2017 IEEE International Conference on Communications (ICC)*. 2017, pp. 1–6.

[89] H. Ye, G. Y. Li, and B. Juang. "Power of deep learning for channel estimation and signal detection in OFDM systems". In: *IEEE Wireless Communications Letters* 7.1 (2018), pp. 114–117.